ACTA TECHNICA

ACADEMIAE SCIENTIARUM HUNGARICAE

EDITOR-IN-CHIEF: M. MAJOR

VOLUME 94
NUMBERS 1–2

AKADÉMIAI KIADÓ, BUDAPEST 1982

ACTA TECHNICA

A JOURNAL OF THE HUNGARIAN ACADEMY OF SCIENCES

Acta Technica publishes original papers, preliminary reports and reviews in English, which contribute to the advancement of engineering sciences.

Acta Technica is published by

AKADÉMIAI KIADÓ
Publishing House of the Hungarian Academy of Sciences
H-1450 Budapest, Alkotmány u. 21.

Subscription information

Orders should be addressed to

KULTURA Foreign Trading Company
H-1389 Budapest P.O.Box 149

or to its representatives abroad

Acta Technica is indexed in Current Contents

CONTENTS

Acta Technica Academiae Scientiarum Hungaricae, 94 (1—2), pp. 3—17 (1982)

ON THE "DUAL EXPONENTIALITY" OF THE STRESS LEVEL CROSS INTERSECTION NUMBERS IN ROAD VEHICLE VIBRATION SYSTEMS

E. JÁNOSDEÁK,** A. KERESZTES,* P. MICHELBERGER,* T. PÉTER***

[Manuscript received: 10 February, 1982]

On the basis of the calculation results can be stated that the endeavour of observing the timetable (which may be considered identic with the case of the running speed distribution determined only by the character of the traffic and independent of the road qualities) may cause really "dual exponentiality" concerning the stress level cross intersection expectation function. The "dual exponentiality" is particularly significant in the case occurring in practice with the greatest probability where along the longer section is the higher grade of road quality predominant, however, on some sections certain pavement deficiencies also occur. To the factors affecting the form of the level cross intersection curves the following conclusions may be drawn: 1. Dual exponentiality is caused by too large differences between road qualities and by a lower occurrence probability of the type of bad roads. 2. A form approximating pure exponentiality is called forth by very similar road qualities or by nearly identic encounter probability of road qualities. 3. The expectation function of the level cross intersection tends towards the Gaussian function if the road qualities only slightly differ or roads of low grade quality are predominant. An accessory achievement of the investigations has been attained: altering the expectation values of the zero level cross intersection numbers might be neglected in the course of mixing.

A comprehensive analysis of the statistics of the internal load induced in road vehicles pointed out the necessity of the simultaneous investigation of the interactions between vehicle and driver and other environmental interconnections [1], [2], [3].

On the basis of road measurement results may be established that the expectation value of the number of the stress level cross intersections, in most cases, might be described by two exponential functions partially overlapping each other in the physically real stress level region. This specific type of the stress level cross intersection distribution is called in the following "dual exponentiality". It is named specific because by representing the logarithms of the level cross intersection numbers graphically above the positive level region, with a close approximation, two adjoining straight segments of different slopes are obtained (Fig. 1).

Summarizing the achievements of [1] and [2], from the interrelation between the vehicle and driver might be pointed out that on the roads of different qualities, owing to the different schedules i.e., traffic constraints the low stress dispersions occur only with low probabilities, wherefore, in the proximity of the zero level of the dynamic stress a

* Prof. P. Michelberger, BME Közlekedésmérnöki Kar, Mechanikai Tanszék H-1114, Budapest 1521, Hungary

** E. Jánosdeák, AUTOKUT Budapest Csóka u. 4.

*** T. Péter, BME Közlekedésmérnöki Kar, Matematika Tanszék, H-1114 Budapest 1521, Hungary

degressive character differing from the exponential one develops. Nothing refers to the fact that the driver would endeavour to maintain the subjective vibration stress on a constant level but, from time to time, he selects also higher stress levels. The expectation functions of the stress level cross intersection of the processes taking place in the actual constructions became well known in an empirical way, from the results of road measurements.

In the course of the study in question empirical investigations have been carried out also further on by making use of a digital computer. Based on the measurement results has been assumed that the driver in achieving his transportation schedule task, even in case of periodic damages in the state of pavements strives to observe the

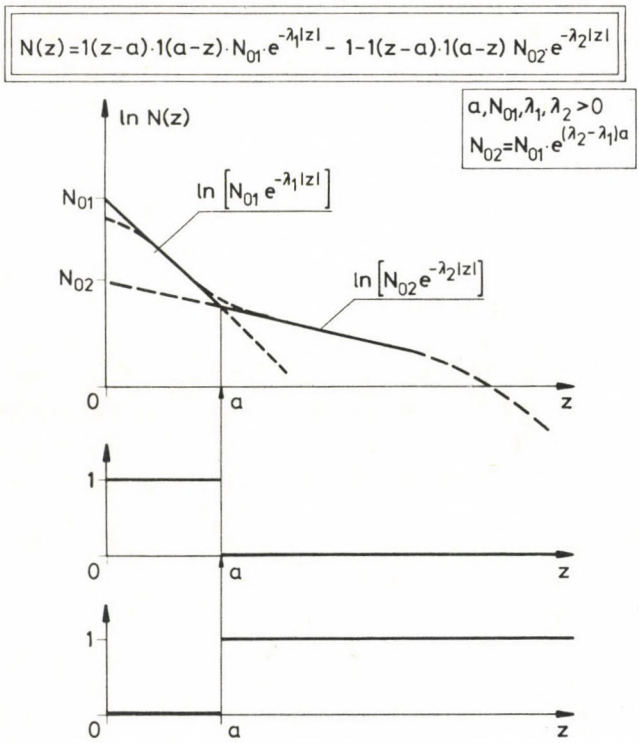

Fig. 1.

running speed distribution (average running speed) pre-established by himself, and this phenomenon may cause a "dual exponentiality" in connection with the stress level cross intersection function numbers.

Filtering out all disturbing circumstances in the course of the calculations, the effects of the distribution functions of the road grades and running speeds on the

evolution of the expectation values of the stress level cross intersection numbers may purely be observed, consequently, in this way, the above assumption becomes to be controllable.

1. Method of the investigations and certain assumptions

The evolution of the level cross intersection functions is defined by several parameters or, more precisely, by several random variables.

From [2] may be established that, for example, pure exponentiality might be called forth merely by several random variables themselves in case where each of them follows a separately determined distribution pattern. The distributions of these random variables (i.e., the running speed v of the vehicle, the categories of road u and the loading patterns m) calling forth separate pure exponentialities may be determined from the density function [1], [2] deduced to the variances σ_z of the dynamic stresses $z(t)$ of the vehicle vibration systems and from the empirical functional connections:

$$v \mapsto \sigma_z \quad | u, m = \text{const}, \qquad u \mapsto \sigma_z \quad | v, m = \text{const}. \qquad m \mapsto \sigma_z \quad | u, v = \text{const}.$$

This paper is primarily concerned with the further investigation of the phenomenon of the "dual exponentiality".

Let us start from the assumption that the driver riding with his vehicle on roads of high and medium grade, follows a certain running speed distribution.

In the opinion of the author this speed distribution is defined predominantly by the urgency of transportation to be fulfilled by the driver, as well as by the traffic conditions. Meanwhile for certain periods sometimes but for very short while and at another time for a longer duration, also the pavement on which the vehicle travels might be damaged. The vehicle runs to road sections of state of lower grade with a speed earlier used (with the experience of the driver on the developed speed distribution). According to [1] and [2] the driver, even at the cost of the vibration comfort strives to maintain the mean travelling speed in order to fulfil the transportation task to a given term. This phenomenon has been simulated simply in such a way that the running speed has been assumed to be of the very same distribution, independently of the road categories. The speeds developed on each of the road sections had been considered constant, i.e., the transient phenomena of short duration taking place due to the changes in speed, i.e., to the excitations of acceleration, have been neglected. For the purpose of the calculation a plane model of four degrees of freedom of rigid body of linear characteristics has been used (Fig. 2). For the short intervals where the speed and road quality do not change but between narrow limits, the Rice formula is valid, i.e., in each section the relationships

$$N(z) = N_0 \cdot \exp\left[-z^2/(2D_z^2)\right] \tag{1}$$

$$N_0 = N(0) = \frac{1}{\pi} \cdot \frac{D_{\dot{z}}}{D_z} \tag{2}$$

are to be used to the calculation of the stress level cross intersection numbers N depending on the stress level z related to the unit time (1 [s]). The meanings of the designations entering in Eqs (1) and (2) are as follows:

D_z – dispersion of signal $z(t)$ $(D_z = \sqrt{\sigma_z})$
$D_{\dot{z}}$ – dispersion of the derived signal $dz/dt = \dot{z}(t)$
N_0 – number of cross intersections of stress level $z = 0$ related to unit time (1 [s]).

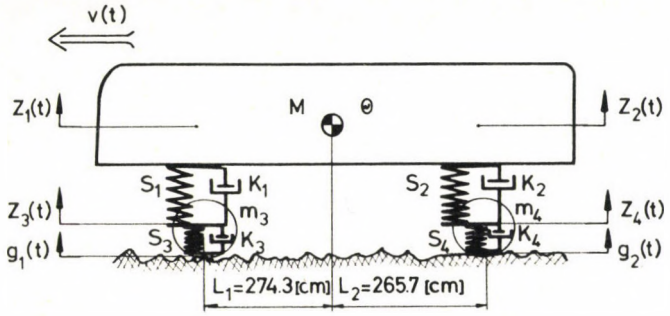

M = 7580 [kg], Θ = 60420 [kgm²], m_3 = 870 [kg], m_4 = 1550 [kg]
S_1 = 374, S_2 = 870, S_3 = 2800, S_4 = 5600 [daN/cm]
K_1 = 30, K_2 = 30, K_3 = 3.5, K_4 = 7 [daN/(cm/s)]

Fig. 2.

The dispersion of a certain output signal of a given vehicle vibration system in fulfilling the task of transportation is, as a matter of course, the function of the road categories, running speeds and loading patterns:

$$D_z = D_z(u, v, m)$$
$$D_{\dot{z}} = D_{\dot{z}}(u, v, m) \tag{3}$$

and on the basis of Eq. 2 also

$$N_0 = N_0(u, v, m)$$

is true.

Accordingly, it has been pointed out that in the Rice formula N is a four variable function depending beside the level value z also on the parameters u, v and m:

$$N(z, u, v, m) = N_0(u, v, m) \exp\left[-z^2/[2D_z^2(u, v, m)]\right] \tag{5}$$

wherein u, v and m are random variables. With the knowledge of the common density function $f(u, v, m)$ associated with the same transportation task of the random variables u, v, m the expectation density function of the level cross intersection belonging to the task of transportation:

$$M[N(z)] = \iiint_T N(z, u, v, m) \cdot f(u, v, m) \mathrm{d}u \, \mathrm{d}v \, \mathrm{d}m \tag{6}$$

might be determined.

In carrying out the measurements [1], [2], the loading has not been changed, therefore

$$P(m = m_0) = 1. \tag{7}$$

Also the investigations reported in the present paper have been performed at constant loading pattern. In consequence of that said above (the distribution of the speed v having been assumed to be independent of the road categories) the random variables have been assumed to be independent:

$$f(u, v) = f_1(u) \cdot f_2(v) \tag{8}$$

wherein: f_1 and f_2 being density functions of u and v respectively.

The calculation of multiple integral quickened by applying the simplifying assumption that the random variables were discrete:

$$\begin{aligned} &P(v = 10) = p_1, \qquad P(v = 20) = p_2, \ldots, \qquad P(v = 100) = p_{10}, \\ &P(u = 1) = p_1^*, \; P(u = 2) = p_2^*, \; \ldots, \qquad P(u = 6) = p_6^*. \end{aligned} \tag{9}$$

Thus, the calculations have been carried out by using 10 discrete

$$v_1 = 10 \ [\mathrm{km/h}], \ldots, \qquad v_{10} = 100 \ [\mathrm{km/h}]$$

and 6 discrete road category-related random variables and their distributions.

The actual calculations have been carried out by making use of a model of four degrees of freedom of the bus type IK 260 mentioned above.

Several different cases have been dealt with. In each case, the distribution of the road categories have been selected in such a way that the encounter probability of only two road categories for each case ought to differ from zero.

One of the two road categories was in each case the road No. 6 with concrete pavement, of a dispersion of $Dg = 1$ [cm].

The other categories in each case were as follows:

earth road	$D_g = 4$ [cm] (marked 1)
bad stone road	$D_g = 3$ [cm] (marked 2)
good stone road	$D_g = 2$ [cm] (marked 3)

square dressed road $D_g = 1.6$ [cm] (marked 4)
bituminous pavement $D_g = 1$ [cm] (marked 5)

(The dispersion and the spectral density function have been taken from the publication [4] widely known by the experts on the subject.)

Due to the introduction of the above simplifying condition, the effect of the approach of the road categories of lower quality to those of higher grade, on the stress level cross intersection functions may definitely be pointed out. Designating the encounter probability of the non-concrete road with the symbol p_i and that of the concrete road with the symbol p_6, the following three instances are dealt with in the investigations:

I. $p_i = 0.25$, $p_6 = 0.75$

II. $p_i = 0.50$, $p_6 = 0.50$

III. $p_i = 0.75$, $p_6 = 0.25$

The discrete distribution of the running speed of the road vehicle has been given in all cases with the following values:

$$P(v=10)=0.05, \quad P(v=20)=0.05, \quad P(v=30)=0.05,$$
$$P(v=40)=0.05, \quad P(v=50)=0.1, \quad P(v=60)=0.3,$$
$$P(v=70)=0.2, \quad P(v=80)=0.1, \quad P(v=90)=0.05,$$
$$P(v=100)=0.05.$$

The effort of the driver in fulfilling his transportation task at any means to the term given, has been simulated by this speed distribution being independent of the quality of the road.

2. The achievements of the investigations

The procedure of calculation of the integral (6) is called mixing of the stress level cross intersection functions.

The results are represented in Figs 3–17. In the figures for the different cases of mixing the expectation functions of the stress level cross intersections of each output signals are to be seen. On the axis of ordinates the natural logarithms of the level cross intersection numbers related to the unit time and on the x axis the level values of the stress investigated have been plotted where

$\ddot{z}_1$ [cm/s^2]-signal of exactly vertical vibration acceleration $z_1 - z_3$ [cm] of the body, over the front axle of the bus, and the stress signal of the front bearing spring $z_1 - g_1$ [cm] is the internal loading of the front wheels proportionate to the dynamic wheel load, the compression of the tyre.

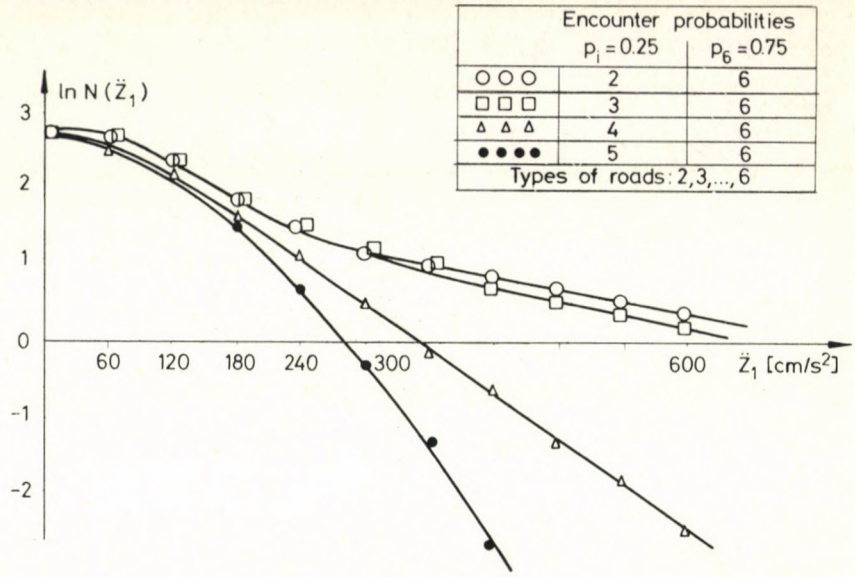
Encounter probabilities
$p_i = 0.25$ $p_6 = 0.75$
○ ○ ○ 2 6
□ □ □ 3 6
△ △ △ 4 6
● ● ● ● 5 6
Types of roads: 2,3,...,6
ln N ($\ddot{Z}_1$)
3
2
1
0
-1
-2
60 120 180 240 300 600 $\ddot{Z}_1$ [cm/s^2]

Fig. 3.

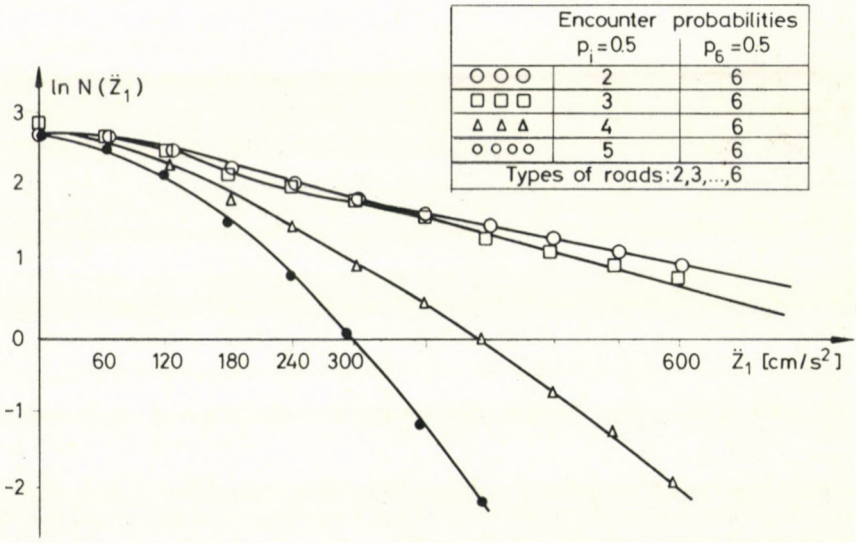
Encounter probabilities
$p_i = 0.5$ $p_6 = 0.5$
○ ○ ○ 2 6
□ □ □ 3 6
△ △ △ 4 6
○ ○ ○ ○ 5 6
Types of roads: 2,3,...,6
ln N ($\ddot{Z}_1$)
3
2
1
0
-1
-2
60 120 180 240 300 600 $\ddot{Z}_1$ [cm/s^2]

Fig. 4.

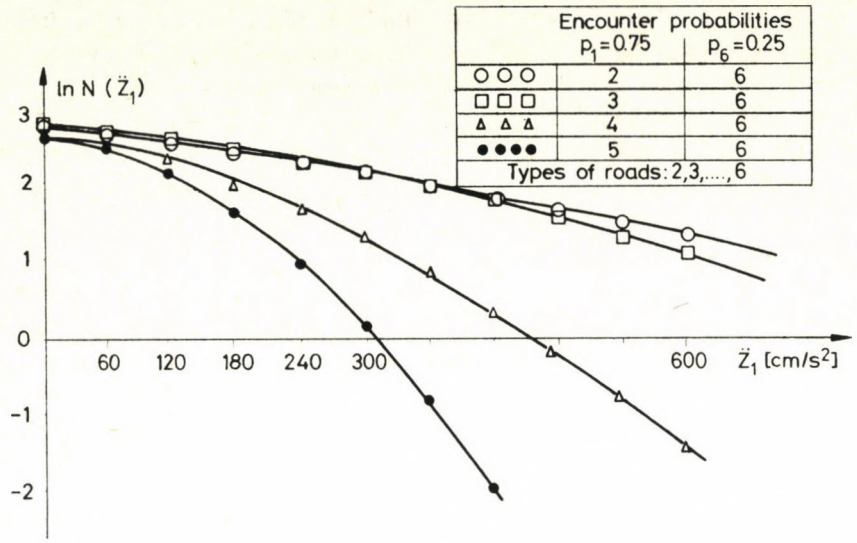
Encounter probabilities
$p_1 = 0.75$ $p_6 = 0.25$
2 6
3 6
4 6
5 6
Types of roads: 2,3,...., 6
ln N ($\ddot{Z}_1$)
3
2
1
0
-1
-2
60 120 180 240 300 600
$\ddot{Z}_1$ [cm/s^2]

Fig. 5.

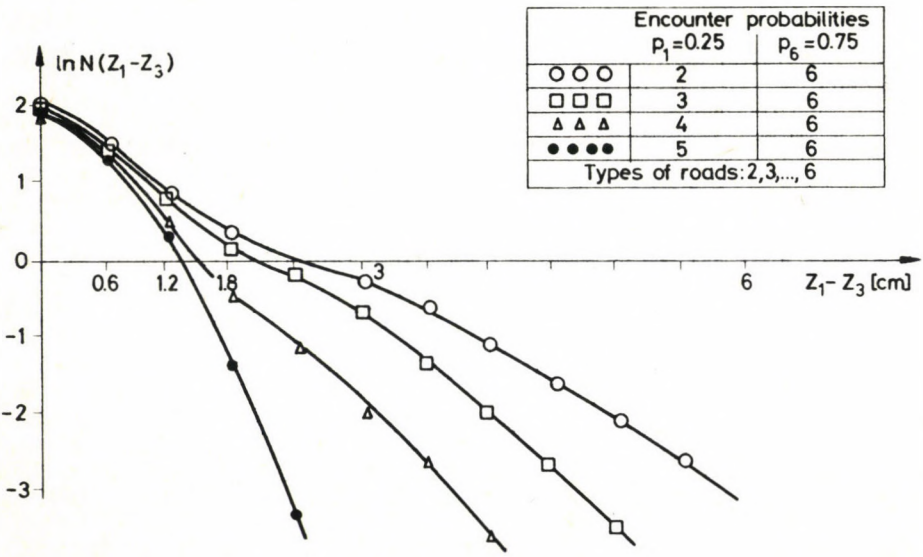
Encounter probabilities
$p_1 = 0.25$ $p_6 = 0.75$
2 6
3 6
4 6
5 6
Types of roads: 2,3,..., 6
ln N ($Z_1 - Z_3$)
2
1
0
-1
-2
-3
0.6 1.2 1.8 3 6
$Z_1 - Z_3$ [cm]

Fig. 6.

2.1. Effect of the different road qualities in mixing the stress level cross intersection functions in case where the encounter probability of the low grade road and the high grade road (i.e., pavement) of each case is not modified

It may be clearly observed that in case of mixing of road grades significantly differing from each other (Fig. 3. mix of bad stone pavement and concrete pavement: ○○○○○○, good stone pavement and concrete pavement □□□□□□) with a fairly good approximation the case of the "dual exponentiality" takes place.

Will the lower grade of road gradually replaced by a better one, so the mixed stress level cross intersection function shows, first in the physically realizable region, pure exponentiality (mixing of square-dressed pavement with a concrete one △△△△△△), thereafter, by upgrading further on the lower pavement quality, in case of road grades near to each other, the expectation function of the stress level cross intersection approaches more and more to the Gaussian character of the original Rice formula.

In case of mixing bituminous and concrete pavements similar conclusions may be drawn from the investigation of the level cross intersection functions characterizing the stress pattern of the front springs to be seen in Fig. 6, and also from the representation of the stress level cross intersection of the tyre compression depicted in Fig. 9.

1. On two roads of significantly differing qualities in case where the running speed distribution is the same on both of them, with a good approximation a "dual exponentiality" occurs.

2. In approximating the road qualities to each other, the slopes of the curves of both approximate exponentialities are approaching to each other, and their junction

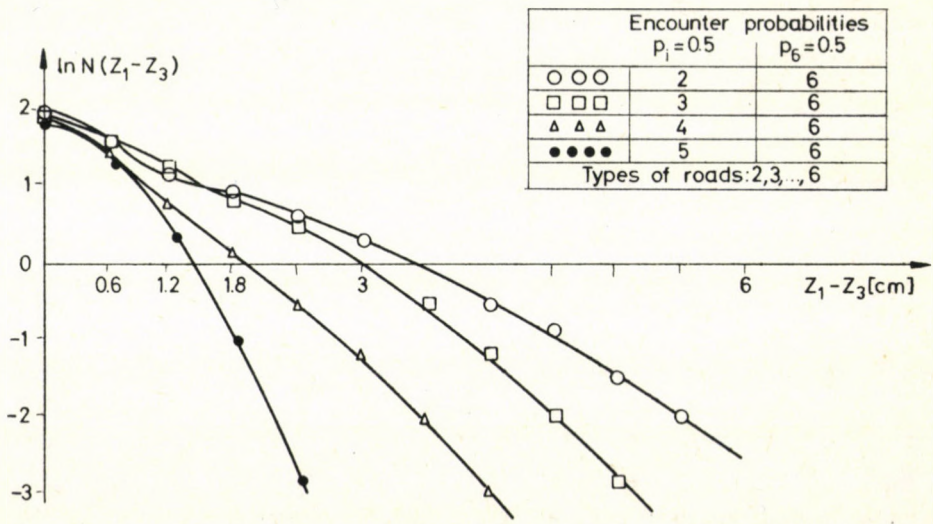

Fig. 7.

point is not displaced. Initially, the curves approximate the pure exponentiality, later, the stress level cross intersection curve familiar on the basis of the Rice relationship valid to the Gaussian signals.

3. In case of high stress level values, for all considered instances, $M[N(z)]$ is asymptotically parallel to the stress level cross intersection function of Gaussian character associated with the output signal of the largest dispersion.

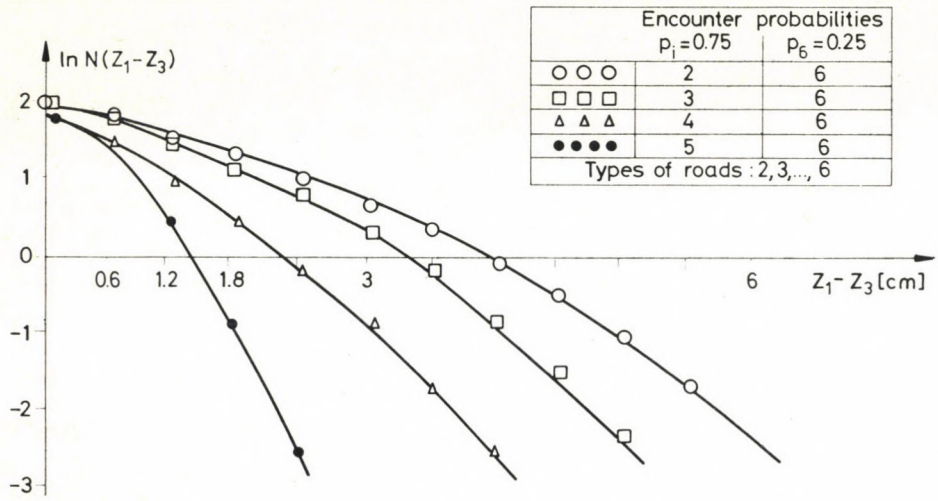

Fig. 8.

4. Mixing the different road categories, in case of a given fixed speed distribution does not significantly alter the zero-level cross intersection numbers $M[N_0]$. Keeping this statement in mind, the assumption of [1], [2] on the subject might now be considered to be proved.

2.2. *Effect of the encounter probability of the lower road qualities on the result of mixing*

1. Is the encounter probability of the lower road quality less than that of the higher and rides the driver in his vehicle at a constant speed distribution independently of the road qualities according to that mentioned above and is also the static load constant, so, in Figs 12–17 is to be seen that in the course of mixing the stress level cross intersection functions a "dual exponentiality" occurs. In the instances treated of the encounter probability of the bad road was $p_i = 0.25$ and that of the concrete road $p_i = 0.75$.

2. By gradually increasing the encounter probability of the bad road first to $p_i = 0.5$ and then to $p_i = 0.75$, might be experienced that the "dual exponentiality" tends

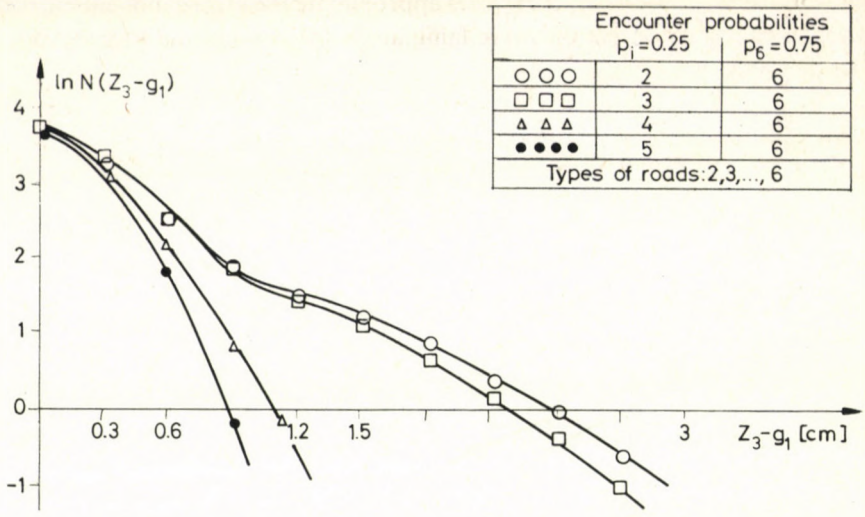

Fig. 9.

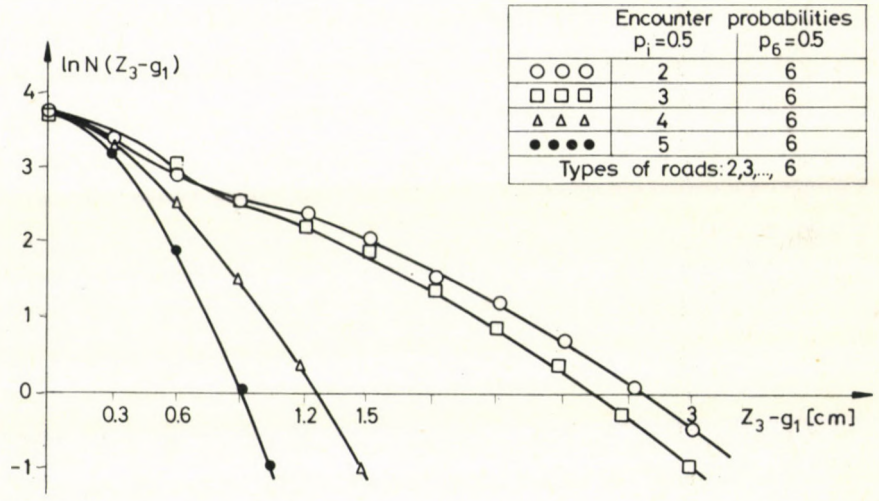

Fig. 10.

first towards the pure exponentiality and thereafter, towards the Gaussian type characterizing the lowest road quality.

In increasing the encounter probability of the bad road, the slopes of the two segments displaying approximate exponentialities coming near to each other, and the junction point tends to be displaced toward the axis of ordinates.

3. In case of high level values the curves are proceeding asymptotically parallel to the curve of the function mixed at the highest encounter probability of the bad road taking up the highest value.

4. The conclusion 4 of the subchapter *2.1* is true also for the above case.

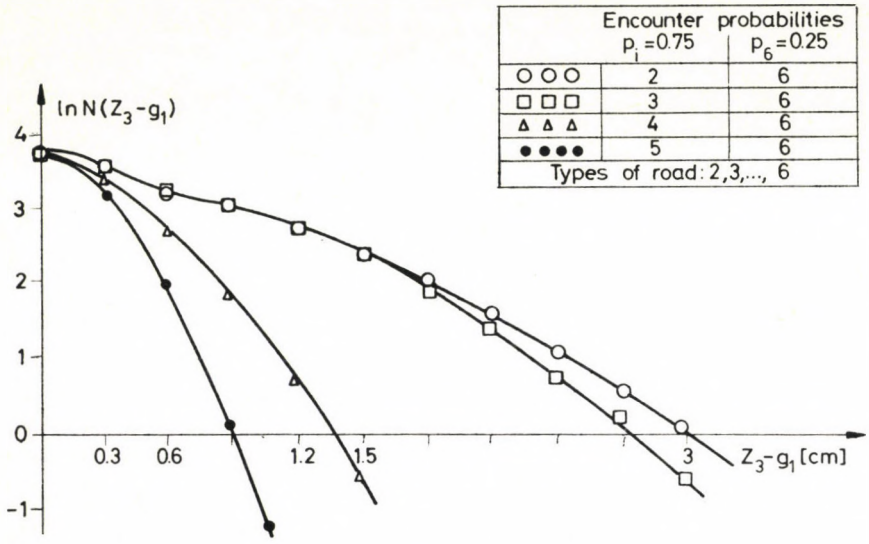

Fig. 11.

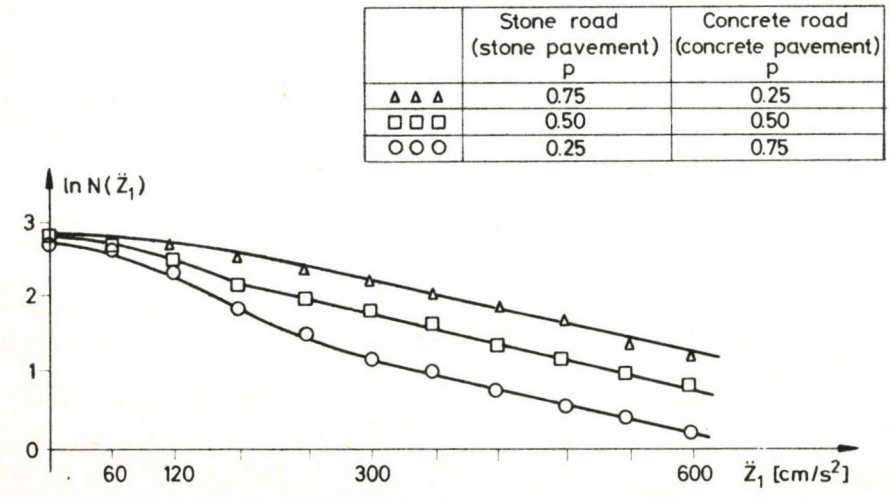

Fig. 12.

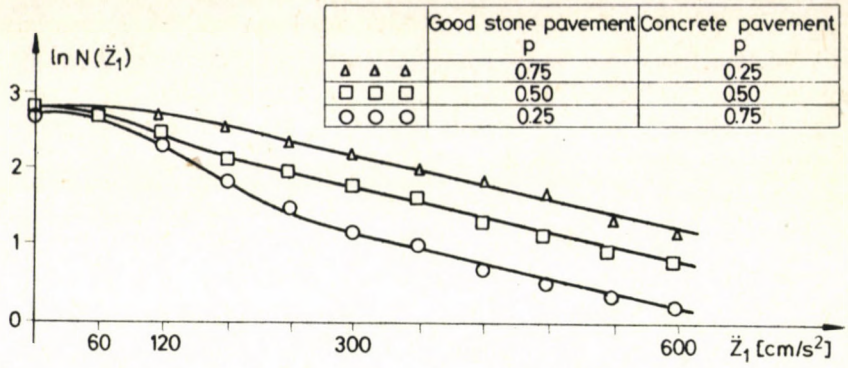

	Good stone pavement p	Concrete pavement p
△ △ △	0.75	0.25
□ □ □	0.50	0.50
○ ○ ○	0.25	0.75

Fig. 13.

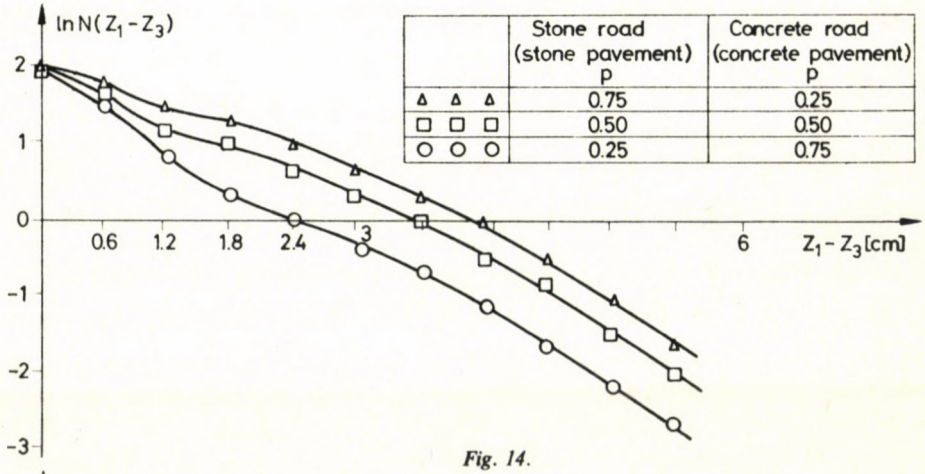

	Stone road (stone pavement) p	Concrete road (concrete pavement) p
△ △ △	0.75	0.25
□ □ □	0.50	0.50
○ ○ ○	0.25	0.75

Fig. 14.

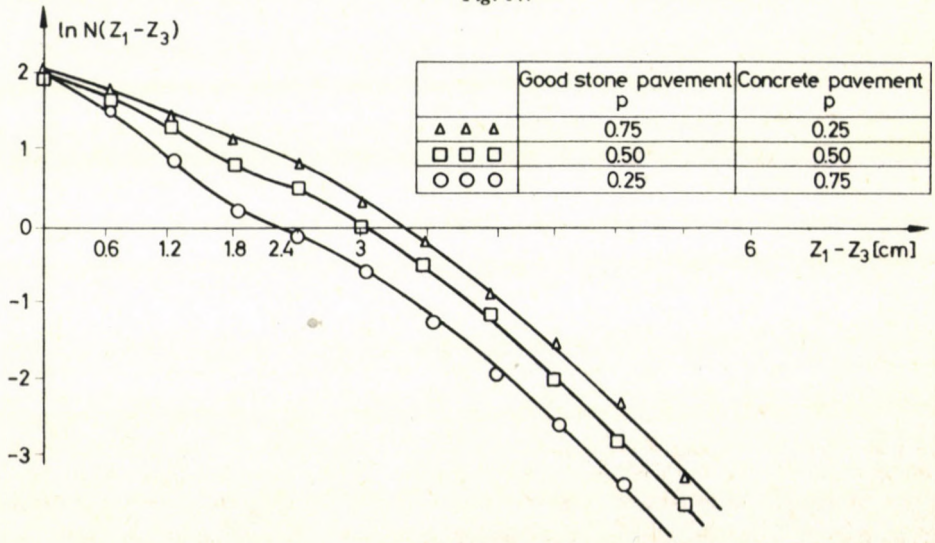

	Good stone pavement p	Concrete pavement p
△ △ △	0.75	0.25
□ □ □	0.50	0.50
○ ○ ○	0.25	0.75

Fig. 15.

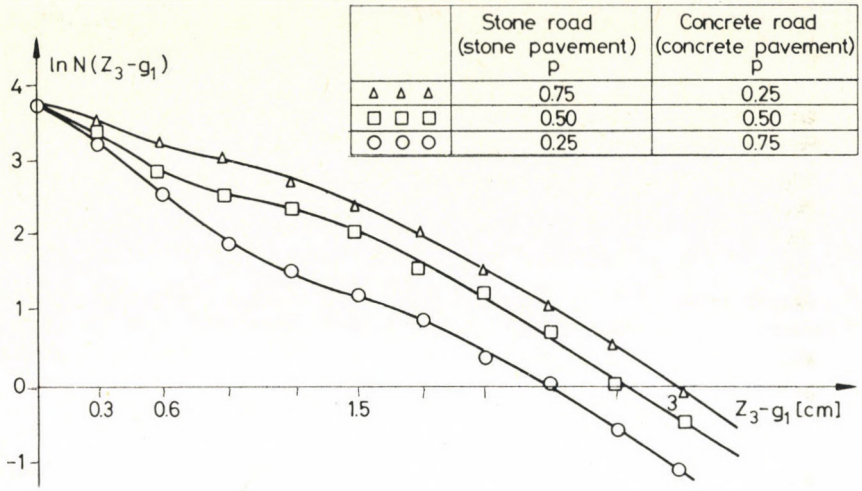

Fig. 16.

Fig. 17.

3. Summary

On the basis of the calculation results can be stated that the endeavour of observing the time-table (which may be considered identic with the case of the running speed distribution determined only by the character of the traffic and independent of road qualities) may cause indeed "dual exponentiality" for the stress level cross intersection expectation function. The "dual exponentiality" is particularly significant in the case occurring in practice with the greatest probability where along the longer

section is the higher grade of road predominant, however, on some sections pavement deficiencies also occur.

Concerning the factors affecting the history of the stress level cross intersection curves, the following conclusions may be drawn:

1. Dual exponentiality is caused

— by the too large differences between the road grades, as well as by the lower encounter probability of the type of bad roads.

2. A form approximate to the pure exponentiality is caused:

— by the road qualities being very similar to each other or

— by the nearly identic encounter probability of road qualities.

3. The expectation function of the stress level cross intersection tends towards the Gaussian function in case where:

—the road qualities only slightly differ from each other or

— the road qualities only slightly differ from each other or

An accessory achievement of the investigations has been attained:

4. Altering the expectation values of the zero level cross intersection numbers might be neglected in the course of mixing.

References

1. Jánosdeák E.: Vehicles, agricultural machines **24** (1977) 8.
2. Jánosdeák E.: *Acta Techn. Hung.* **89** (1–2) (1979), 145–148.
3. Jánosdeák E.—Keresztes A.—Michelberger P.: *Periodica Polytechnica* **9** (1981), 73–84.
4. Pevzner, J. M.–Tyihonov, A. A.: *Avtomobilnaja Promüslennoszty* (1964), 15–18.

Acta Technica Academiae Scientiarum Hungaricae, 94 (1—2), pp. 19—36 (1982)

FORECASTING FABRIC TENSILE STRENGTH FROM COVER FACTOR

B. GREGA* and M. G. ABDEL CHAFOUR

[Manuscript received 6 May, 1982]

The aim of the present work is to obtain a mathematical form which connects the tensile strength and the cover factor thus, if we know the yarn count of warp or weft in a cotton system and by measuring the number of threads per inch, we can obtain the cover factor and by the latter we can calculate the tensile strength by the equation we have obtained.

The work of Law [3] and Ashenhurst [1] on yarn diameter, they and other workers in the textile industry, used their estimates of yarn diameter as the basis for quite elaborate cloth-setting theories which were intended to help designers and cloth constructors to produce serviceable fabrics of the desired characteristics with a minimum of trial and error.

We have seen in Figure 1 that the ratio yarn diameter: yarn spacing, d/P, is a measure of the relative closeness of the yarns in the warp or weft of a woven fabric. This ratio also expresses the fraction of the area of the cloth covered by the warp or weft yarns. We may, therefore, call it the fractional cover [4].

$$\text{fractional cover} = d/P$$

Substituting Peirce's [5] estimate of yarn diameter, $d = 1/28\sqrt{N}$, we have

$$\frac{d}{P} = \frac{1}{28\sqrt{N}} \times \frac{1}{P}.$$

But $1/P = n$, where $n =$ threads/in., so

$$\frac{d}{P} = \frac{n}{28\sqrt{N}} \tag{1}$$

Now d/P has a value of 1.0 when the yarns are just touching.

Peirce multiplied Eq. (1) by 28 to eliminate the numerical constant, 28, and defined the result as the "cover factor", K.

$$\text{— cover factor, } K = \frac{n}{\sqrt{N}} \tag{2}$$

It will be recalled that the cover factor is the ratio of threads per inch to the square root of the yarn count (cotton system) [2].

* B. Grega, Németvölgyi út 22, H-1114 Budapest 1126, Hungary
M. G. Abdel Chafour, Cairo (Egypt), 259 Port-said Street, Sayida Zeinab

Just as twist factor enables us to compare the relative hardness of twist in yarns of different counts, so cover factor enables us to compare the relative closeness of the yarns in different fabrics. In practice, cover factors are calculated for warp and weft independently.

— warp cover factor, $$K_1 = \frac{n_1}{\sqrt{N_1}} \tag{3}$$

— weft cover factor, $$K_2 = \frac{n_2}{\sqrt{N_2}} \tag{4}$$

Fabric cover factor (K_c) is calculated from K_1 and K_2 as follows:

— Fabric cover factor, $$K_c = K_1 + K_2 \tag{5}$$

Therefore, the cover factor depends on the threads and the yarn count (cotton system).

Cover factors range from about 8 to 28 for most fabrics. A cover factor of 28 corresponds to threads which just touch, but higher values than 28 can be obtained when there is as lateral compression of the threads. It is usual to calculated separate cover factor for the warp and weft yarns and they show how closely each set of threads is woven [6].

The factors that determine the character of a particular cloth are its weave, threads per inch, count and twist of the warp and weft yarns, and the properties of the fibre from which the yarns have been spun.

There are, in addition, the conditions of spinning and weaving, the latter involving the types of loom, the loom settings, and the tension of warp and weft. If the cloth has been finished there are also the different effects of a large number of possible sequences of mechanical and chemical finishing processes and the conditions under which the processes are carried out.

It can been seen, therefore, that to describe a cloth fully is a very complicated business; indeed, the aim of a considerable branch of textile research is to measure properties that define the character of a cloth more precisely than does a statement of its structure and the processes that have been applied [6].

Therefore, this work aims to use the cover factor which is considered the more important formula in cloth geometry to forecast fabric tensile strength.

Experimental

A series of cloths was woven on Russia Loom AT 105. Six groups of fabrics were woven; the warp (50/1 metric) was common for all groups, but the weft was varied according to the scheme shown in Table I.

Within each group, five fabrics (*Z*, *E*, *I*, *N*), and four fabrics (*A*, *B*) with different number of picks/cm were woven according to the scheme shown in Table II.

Table I. Details of weft yarns used

Fabric group	Weft count (metric system)	Weft specification		Twist (turns/cm)
		Material	Spinning method	
Z	34/1	cotton	Not known	7.5
E	40/1	cotton	Not known	8.5
I	50/1	cotton	Not known	9.5
N	60/1	cotton	Not known	9.3
A	70/1	cotton	Not known	8.6
B	85/1	cotton	Not known	9.7

Table II. Details of fabric specifications

Fabric group	Fabric no.	Fabric construction	Warp and picks/cm	
			warp	picks
Z	1	1/1 plain	35.6	13.4
	2	1/1 plain	35.8	16.–
	3	1/1 plain	35.8	19.–
	4	1/1 plain	36.–	22.4
	5	1/1 plain	35.2	24.8
E	1	1/1 plain	35.2	13.–
	2	1/1 plain	36.4	16.3
	3	1/1 plain	36.9	19.2
	4	1/1 plain	37.7	23.9
	5	1/1 plain	37.5	26.6
I	1	1/1 plain	36.–	13.–
	2	1/1 plain	36.–	16.4
	3	1/1 plain	36.6	19.6
	4	1/1 plain	37.2	24.2
	5	1/1 plain	37.2	27
N	1	1/1 plain	37.3	13.4
	2	1/1 plain	37.8	16.7
	3	1/1 plain	38.5	19.7
	4	1/1 plain	38.6	25.2
	5	1/1 plain	38.5	30.6
A	1	1/1 plain	37.5	13.3
	2	1/1 plain	37.9	16.8
	3	1/1 plain	38.6	28.2
	4	1/1 plain	38.7	34.4
B	1	1/1 plain	36.8	16.–
	2	1/1 plain	38.8	28.–
	3	1/1 plain	38.8	30.–
	4	1/1 plain	38.4	35.6

Table III. Details of tensile strength of warp and weft

Fabric group	Fabric No.	Warp					Weft					Weight gr/m²
		Breaking load			Elongation		Breaking load			Elongation		
		$\bar{K}_g$	$\bar{N}$	cv %	%	cv %	$\bar{K}_g$	$\bar{N}$	cv %	%	cv %	
Z	1	44.53	436.9	3.91	8.49	4.36	20.–	195.8	10.61	13.64	5.71	108.20
	2	45.89	450.2	2.61	9.05	4.49	30.7	301.0	10.31	17.32	5.13	116.85
	3	45.55	446.9	3.43	10.61	6.78	37.2	364.5	5.13	19.31	5.23	128.13
	4	44.94	440.8	2.43	11.85	2.75	48.7	477.9	7.27	20.79	3.15	140.75
	5	43.78	429.5	3.01	12.75	7.57	53.9	528.4	3.93	19.95	4.90	149.68
E	1	45.2	443.4	2.12	7.53	9.15	19.2	188.1	3.48	13.77	2.56	99.30
	2	44.6	437.1	2.03	7.10	4.79	22.8	223.8	6.61	15.25	2.48	109.32
	3	45.0	441.5	2.22	8.52	14.62	28.9	283.9	4.81	20.29	4.18	117.54
	4	43.5	427.1	6.81	10.43	7.07	37.8	370.9	5.50	20.29	4.56	130.34
	5	44.7	438.6	5.25	10.42	5.89	41.6	407.9	6.92	23.79	5.98	142.07
I	1	44.3	434.8	1.04	6.74	3.38	13.6	133.3	7.78	12.35	5.03	93.06
	2	45.4	445.3	3.87	8.19	5.29	17.8	174.2	6.31	13.42	6.84	102.43
	3	45.3	444.1	3.39	8.57	11.82	23.3	228.2	6.03	17.55	4.20	109.96
	4	48.7	477.9	2.31	9.04	3.30	33.5	328.8	8.16	24.75	4.85	124.41
	5	44.9	441.1	1.07	7.47	4.68	34.9	342.0	5.34	25.17	6.06	127.42
N	1	42.02	412.2	6.38	4.95	19.74	10.1	99.4	6.72	12.59	11.10	88.07
	2	45.74	448.7	4.11	6.73	4.45	13.4	131.4	6.40	14.27	5.32	97.08
	3	45.94	450.7	5.48	6.64	9.35	18.6	182.2	6.91	18.53	5.68	102.75
	4	47.60	467.0	4.78	6.78	3.82	22.5	221.1	6.85	22.18	7.67	112.98
	5	42.79	419.8	3.25	8.33	6.22	32.1	314.9	3.36	25.77	1.67	123.41
A	1	41.9	410.9	3.28	6.48	3.72	16.2	158.7	6.90	13.06	9.36	86.59
	2	43.1	440.2	2.86	6.39	5.29	21.9	214.7	5.15	18.35	4.69	95.61
	3	44.7	438.9	3.42	8.04	4.34	43.4	426.2	3.60	26.36	6.32	117.89
	4	43.0	422.0	1.93	9.31	2.09	50.7	496.6	1.87	25.53	1.89	125.49
B	1	42.81	419.9	2.50	6.19	15.88	17.25	169.2	5.14	14.54	7.32	91.37
	2	43.78	429.5	4.68	7.32	5.37	36.86	361.6	3.31	23.58	4.64	111.49
	3	43.02	422.0	3.35	8.78	2.63	40.30	395.4	4.09	23.11	2.77	116.12
	4	43.4	409.9	8.21	8.05	7.99	49.68	487.4	1.69	27.46	2.59	124.04

The fabrics were scoured at 95 °C for one hour in a detergant and sodium carbonate.

The warp and weft threads in the fabrics were measured by counting the number of the threads in a 1 cm length of cloth.

Table IV. Details of warp, weft and cloth cover factor

Fabric group	Fabric No.	Cover factor		
		warp K_1	weft K_2	cloth $K_1+K_2=K_c$
Z	1	16.63	7.6	24.23
	2	16.73	9.1	25.83
	3	16.73	10.8	27.53
	4	16.82	12.7	29.52
	5	16.45	14.1	30.55
E	1	16.5	6.8	23.3
	2	17.–	8.5	25.5
	3	17.2	10.–	27.2
	4	17.2	12.5	29.7
	5	17.5	13.9	31.4
I	1	16.8	6.1	22.9
	2	16.8	7.7	24.5
	3	17.1	9.2	26.3
	4	17.4	11.3	28.7
	5	17.4	12.6	30.–
N	1	17.4	5.7	23.1
	2	17.7	7.1	24.8
	3	18.–	8.4	26.4
	4	18.–	10.8	28.8
	5	18.–	13.1	31.1
A	1	17.5	5.3	22.8
	2	17.7	6.6	24.3
	3	18.–	11.1	29.1
	4	18.1	13.6	31.1
B	1	17.2	5.7	22.9
	2	18.1	10.–	28.1
	3	18.1	10.8	28.9
	4	17.9	12.7	30.7

Tensile strength of the fabrics F was determined by extending the fabrics on ZT 100 Tensile Tester. Samples of size 25 cm × 5 cm were used in the tests, and the ZT 100 cross-head was driven at 30 ± 2 per second. The resulting of load and elongation to all groups is shown in Table III.

The warp and weft threads covered the factor for six group fabrics and were calculated according to formula (3), (4), (5) according to the scheme shown in Table IV.

Now having these results which connects the two factors:

1. tensile strength of the fabric F
2. the cover factor of the cloth K

we will try to get a mathematical form which describes this relationship.

Assuming that this form has that of a straight line:

$$F = a + bK,$$

with a and b are unknown real numbers.

These coefficients a and b must be determined under the following condition:

* the deviation of the given values (K, F) from this assumed equation as a function of the unknowns a and b must be a minimum value.

Thus we have the following:

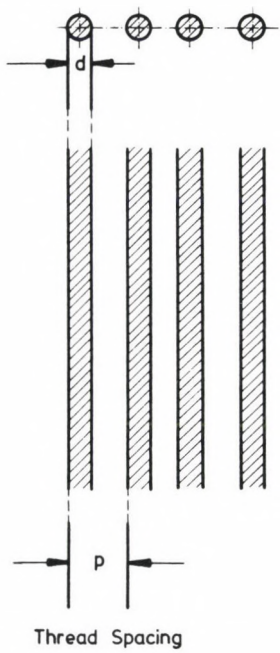

Fig. 1.

Considering the function

$$f(a, b) = \sum_{i=1}^{n} t_i^2$$

(Where n denotes the number of the given points.)

For $f(a, b)$ to be a minimum value, we must have:

(i) the first partial derivatives $\partial f/\partial a$ and $\partial f/\partial b$ must be zero;

(ii) the second partial derivatives

$$\frac{\partial^2 f}{\partial a^2} \quad \text{and} \quad \frac{\partial^2 f}{\partial b^2}$$

must be a positive value.

— the condition (ii) always holds depending on both a and b, so we only use condition (i) to get the following equations:

$$na + b \sum_{i=1}^{m} K_i = \sum_{i=1}^{m} F_i \qquad *$$

$$a \sum_{i=1}^{m} K_i + b \sum_{i=1}^{m} K_i^2 = \sum_{i=1}^{m} K_i F_i \qquad **$$

where (K_i, F_i) describes the given values $(i = 1, \ldots, m)$, with m denoting the number of testings.

Equations (*) and (**) determine the coefficients a and b (Fig. 16)

Now to be sure that really that relation between the factors F_k and F is linear, the ratio:

$$r = \sqrt{\frac{\sum_{i=1}^{n} (F_i - \bar{F}_1)^2}{\sum_{i=1}^{n} (F_{1i} - \bar{F}_1)^2}}$$

which describes the ratio of the deviation of the mathematic mean (K, F) of the given values from the straight line and its deviation from the given values, always satisfies the inequality:

$$0.5 \leqq r \leqq 1.$$

Now applying these methods to our experiments, we obtain the following results for the groups (Z, I, E, N, A and B).

The results (Figs 2, 5, 8, 11, 14, 17) show the relationship between tensile strength and the cover factor of the warps for the fabrics groups (Z, E, I, N, A, B) and the relationship between the parameters which can be described by the linear equation:

$$F_w = a + bK_w \qquad (6)$$

So:

$F_w = -33.45 + 4.70\, K_w$ ... group Z

$F_w = 56.755 - 0.712\, K_w$ ... group E

$F_w = -9.86 + 3.25\, K_w$ ... group I

$F_w = -41.94 + 4.87\, K_w$ ... group N

$F_w = -7.17 + 2.82\, K_w$ ... group A

$F_w = 31.25 + 0.67\, K_w$ ... group B

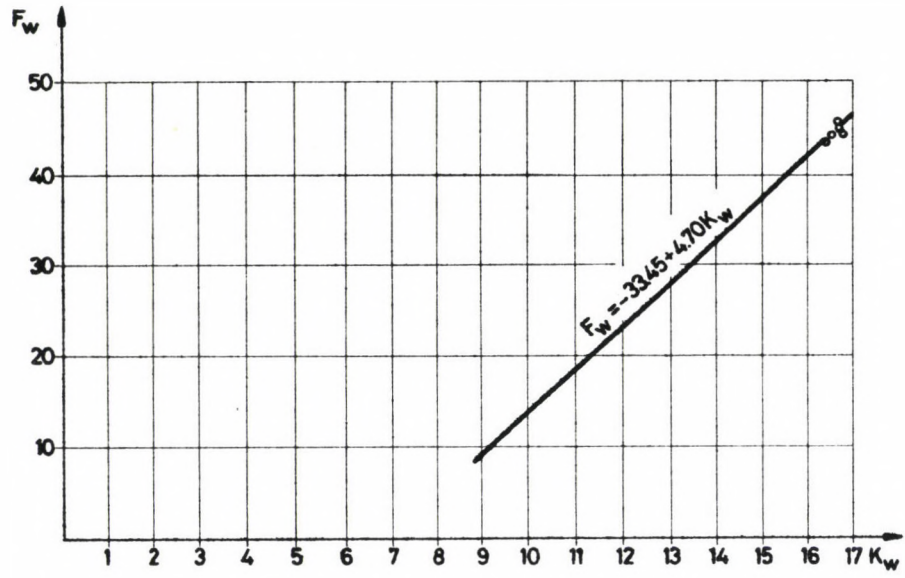
F_w
50
40
30
20
10
1 2 3 4 5 6 7 8 9 10 11 12 13 14 15 16 17 K_w
$F_w = -33.45 + 4.70 K_w$

Fig. 2.

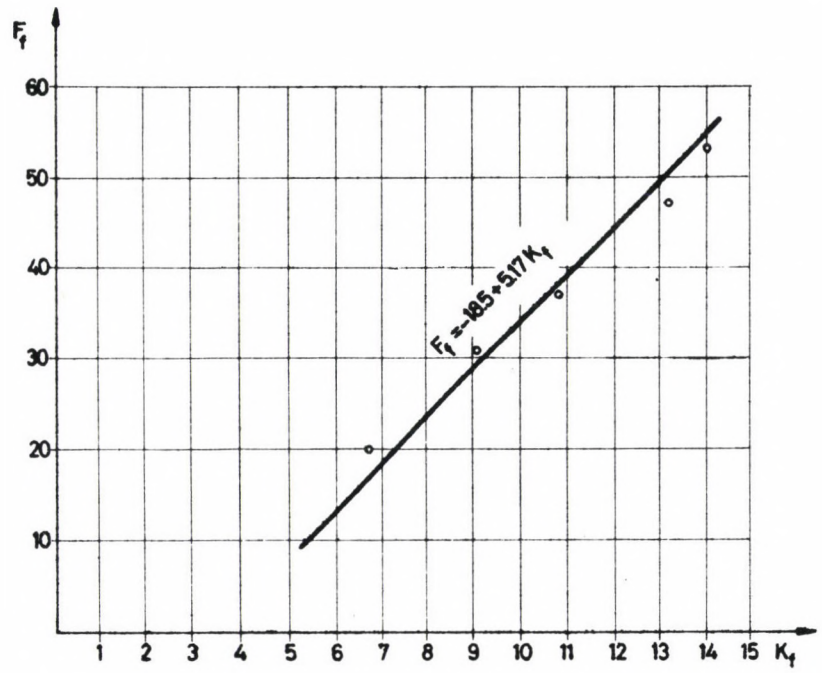
F_f
60
50
40
30
20
10
1 2 3 4 5 6 7 8 9 10 11 12 13 14 15 K_f
$F_f = -18.5 + 5.17 K_f$

Fig. 3.

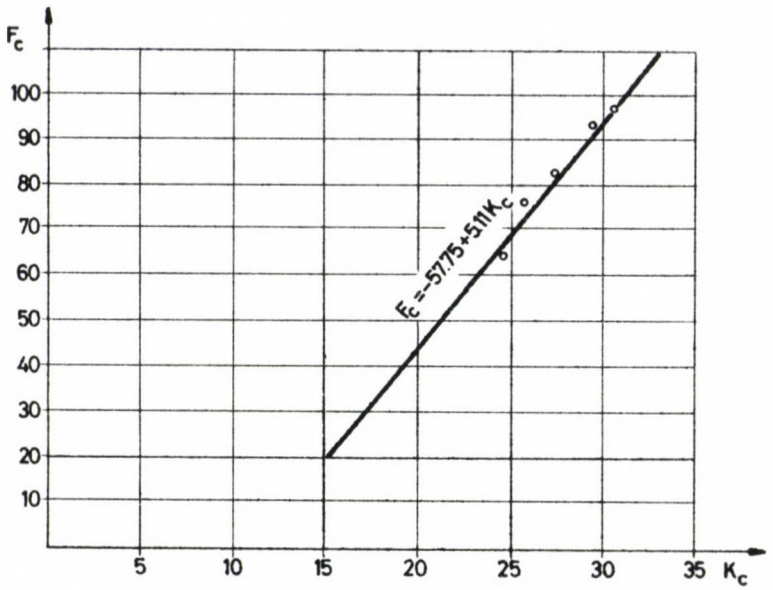
F_c
100
90
80
70
60
50
40
30
20
10
5
10
15
20
25
30
35
K_c
$F_c = -57.75 + 5.11 K_c$

Fig. 4.

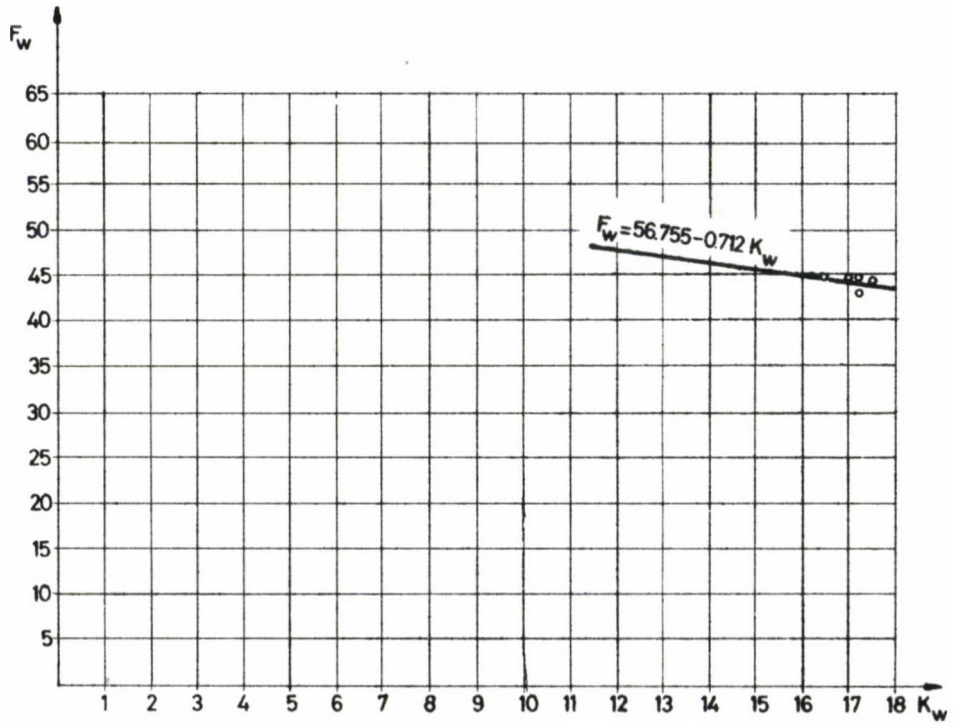
F_w
65
60
55
50
45
40
35
30
25
20
15
10
5
1
2
3
4
5
6
7
8
9
10
11
12
13
14
15
16
17
18
K_w
$F_w = 56.755 - 0.712 K_w$

Fig. 5.

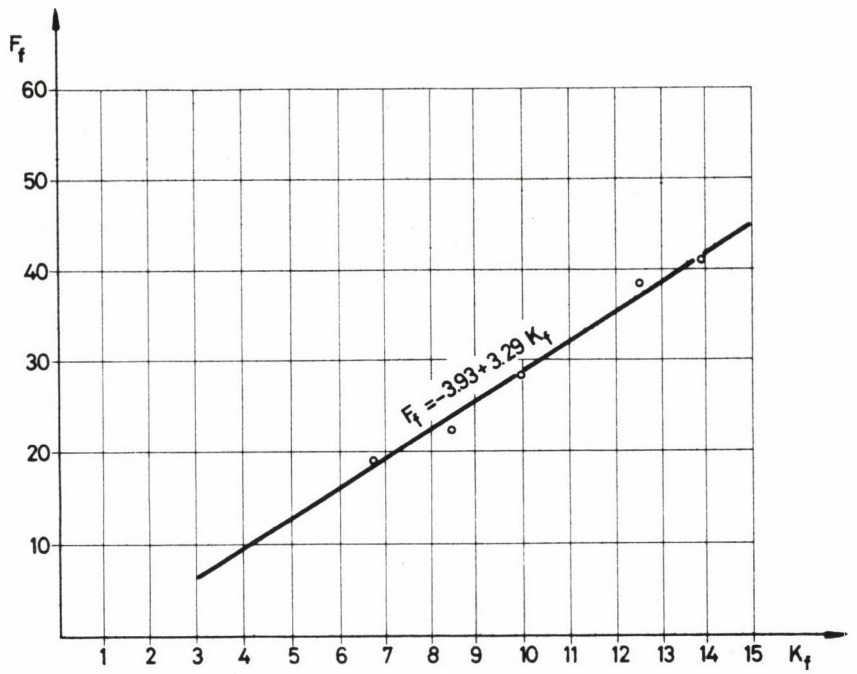
F_f
60
50
40
30
20
10
1 2 3 4 5 6 7 8 9 10 11 12 13 14 15 K_f
$F_f = -3.93 + 3.29\,K_f$

Fig. 6.

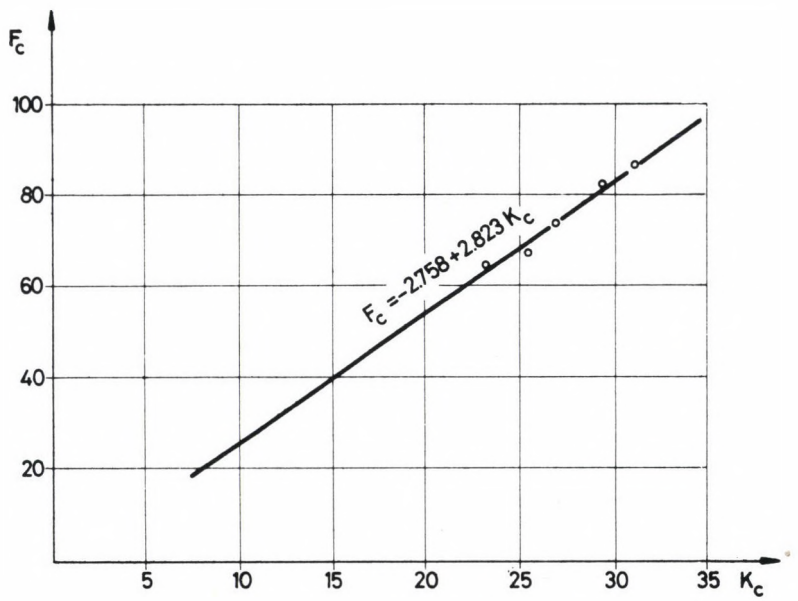
F_c
100
80
60
40
20
5 10 15 20 25 30 35 K_c
$F_c = -2.758 + 2.823\,K_c$

Fig. 7.

where:

F_w = warp tensile strength.

K_w = warp cover factor.

The results (Figs 3, 6, 9, 12, 15, 18) show the relationship between the tensile strength and the cover factor of the wefts for fabrics groups Z, E, I, N, A, B and relationship between the parameters can be described by the linear equation:

$$F_f = a + bK_f \tag{7}$$

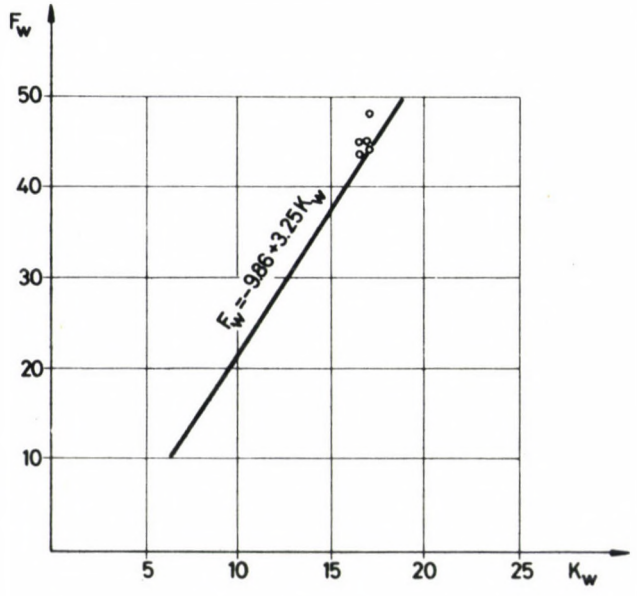

Fig. 8.

So:

$F_f = -18.05 + 5.17\,K_f$ ... group Z

$F_f = -3.93 + 3.29\,K_f$ ... group E

$F_f = -8.6 + 3.54\,K_f$ ... group I

$F_f = -6.56 + 2.87\,K_f$ ... group N

$F_f = -6.06 + 4.27\,K_f$ ... group A

$F_f = -9.141 + 4.608\,K_f$ ... group B

where:

F_f = weft tensile strength

K_f = weft cover factor.

The results (Figs 4, 7, 10, 13, 16, 19) show the relationship between tensile strength and the cover factor of the cloth for fabrics groups "*Z*, *E*, *I*, *N*, *A*, *B*" and the relationship between the parameters can also be described by the linear equation:

$$F_c = a + bK_c \tag{8}$$

So:

$$F_c = -57.75 + 5.11\,K_c \quad \ldots \text{ group } Z$$

$$F_c = -2.758 + 2.823\,K_c \quad \ldots \text{ group } E$$

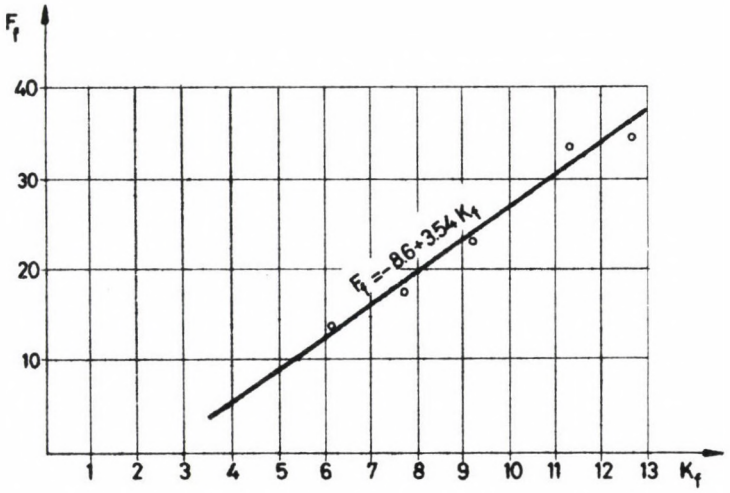

Fig. 9.

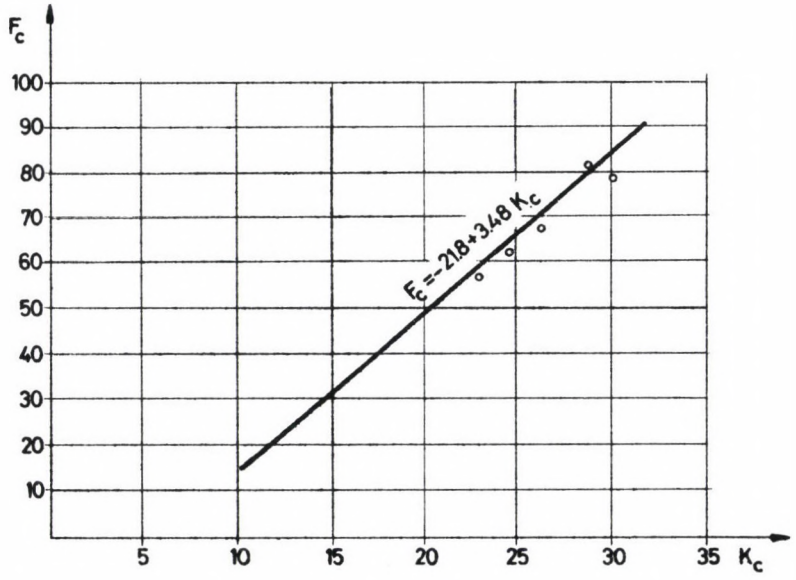

Fig. 10.

$F_c = -21.8 + 3.48\,K_c$ ... group *I*

$F_c = -10.73 + 2.79\,K_c$ ... group *N*

$F_c = -35.76 + 4.15\,K_c$ ... group *A*

$F_c = -35.87 + 4.17\,K_c$ ... group *B*

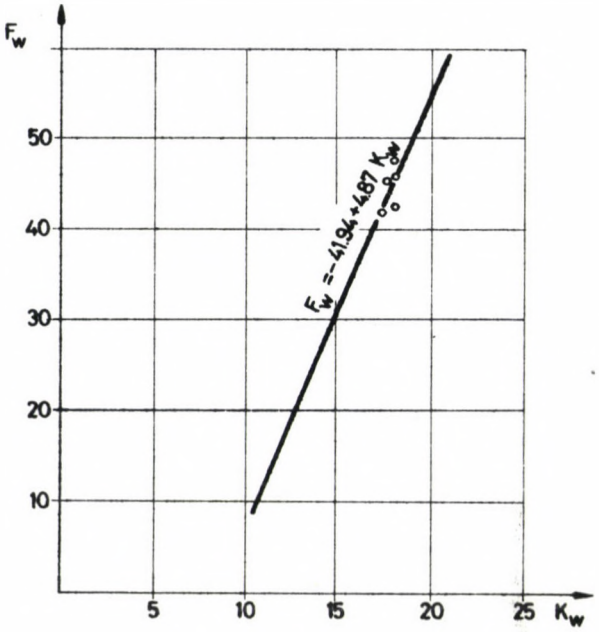

Fig. 11.

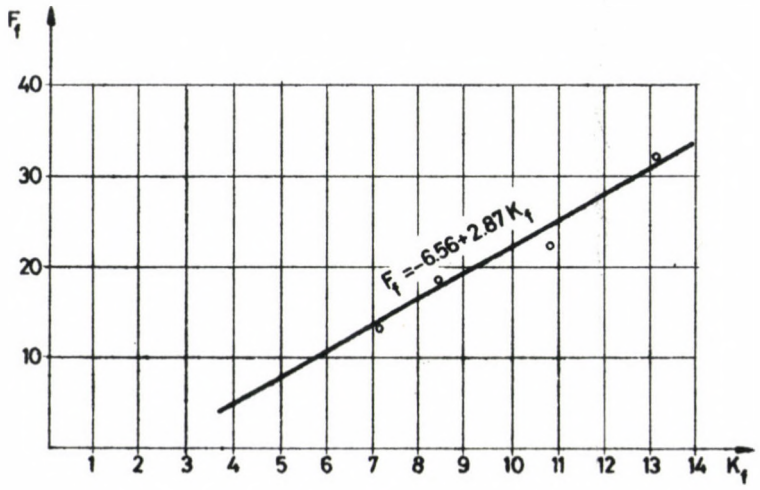

Fig. 12.

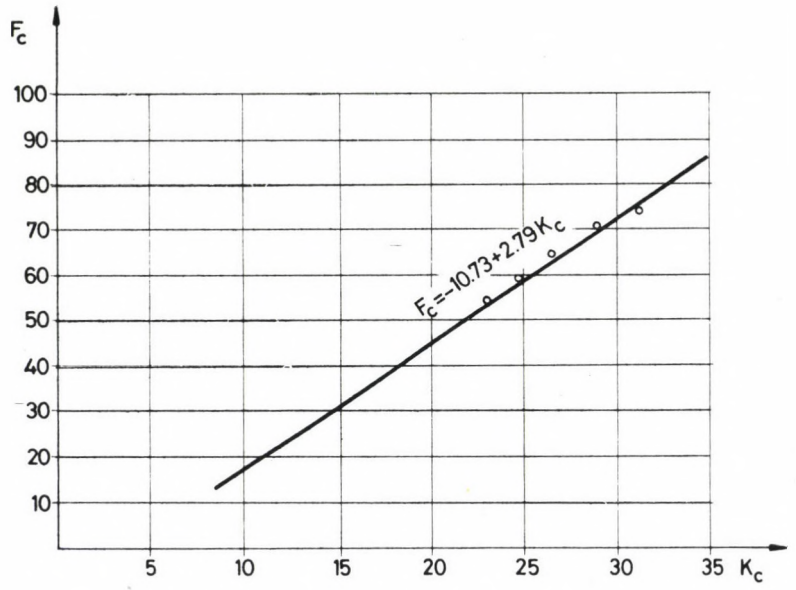
F_c
100
90
80
70
60
50
40
30
20
10
5
10
15
20
25
30
35
K_c
$F_c = -10.73 + 2.79 K_c$

Fig. 13.

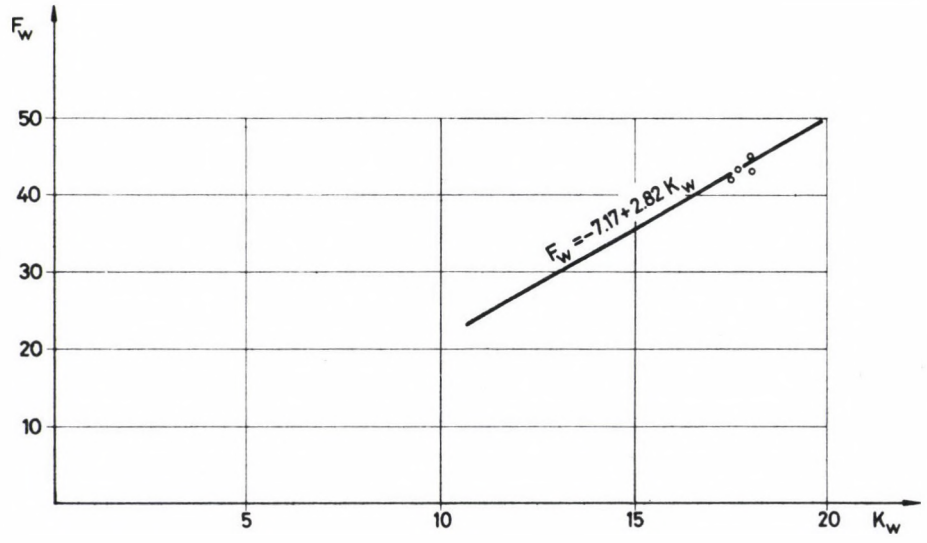
F_w
50
40
30
20
10
5
10
15
20
K_w
$F_w = -7.17 + 2.82 K_w$

Fig. 14.

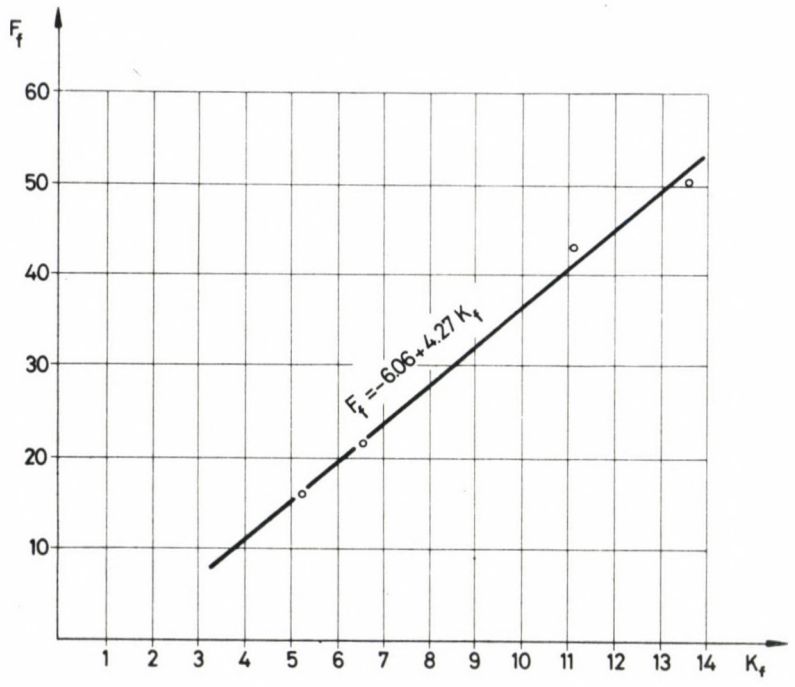
F_f
60
50
40
30
20
10
1 2 3 4 5 6 7 8 9 10 11 12 13 14 K_f
$F_f = -6.06 + 4.27\,K_f$

Fig. 15.

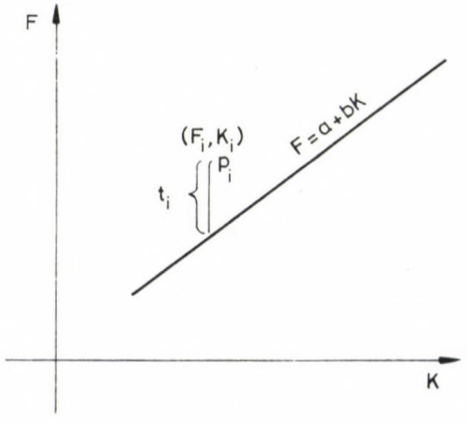
F
(F_i, K_i)
t_i
P_i
$F = a + bK$
K

Fig. 16.

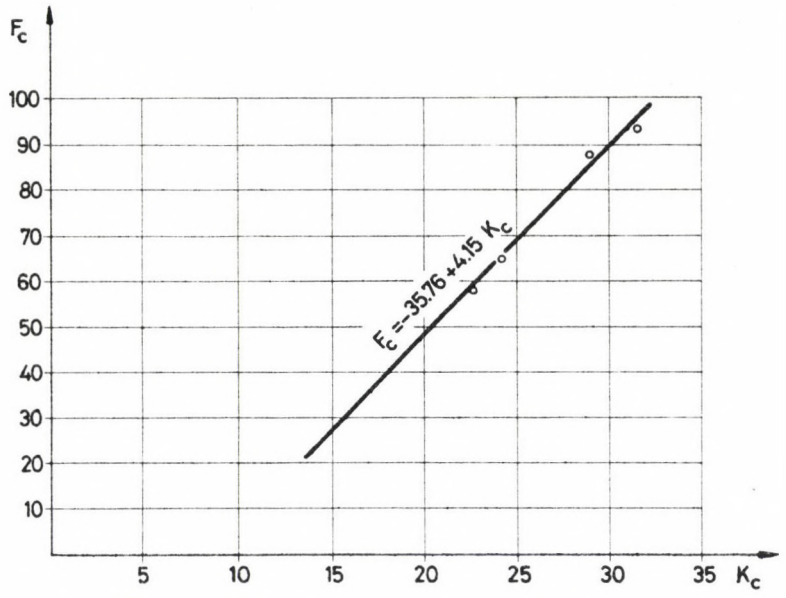
F_c
100
90
80
70
60
50
40
30
20
10
5
10
15
20
25
30
35
K_c
$F_c = -35.76 + 4.15\ K_c$

Fig. 17.

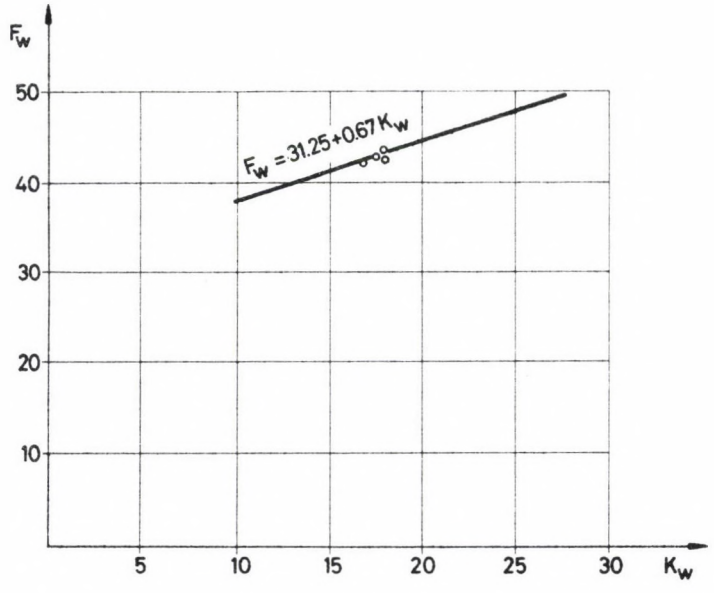
F_w
50
40
30
20
10
5
10
15
20
25
30
K_w
$F_w = 31.25 + 0.67\ K_w$

Fig. 18.

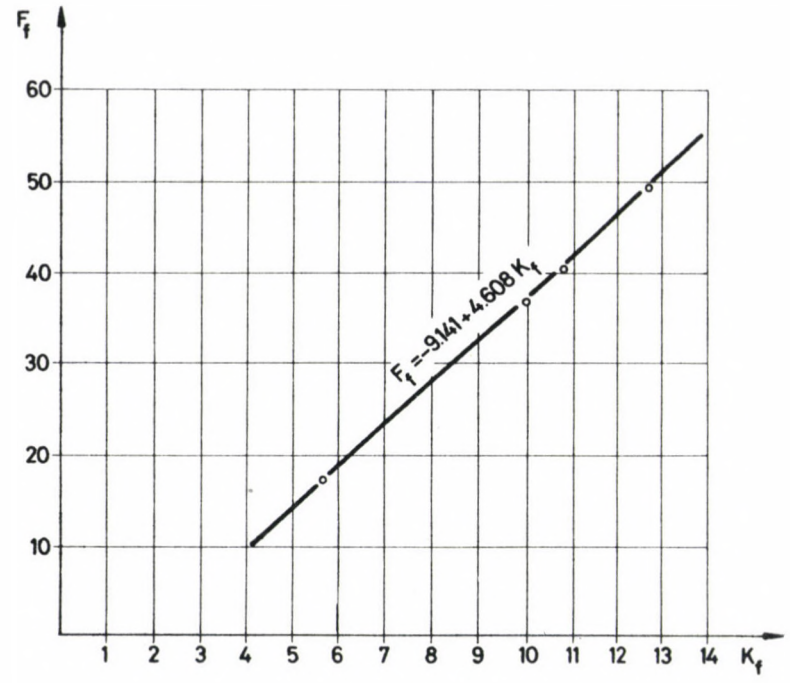
F_f
60
50
40
30
20
10
$F_f = -9.141 + 4.608\,K_f$
1 2 3 4 5 6 7 8 9 10 11 12 13 14 K_f

Fig. 19.

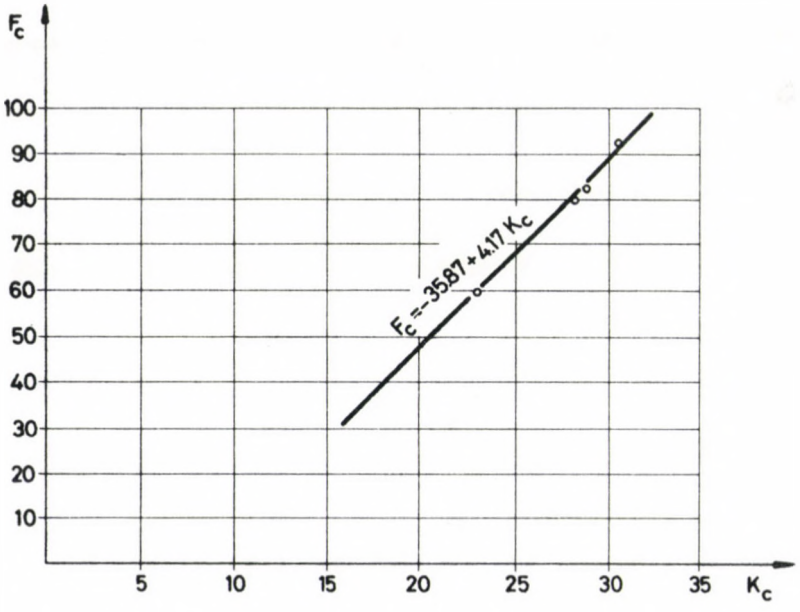
F_c
100
90
80
70
60
50
40
30
20
10
$F_c = -35.87 + 4.17\,K_c$
5 10 15 20 25 30 35 K_c

Fig. 20.

where:

F_c = cloth tensile strength

K_c = cloth cover factor.

References

1. Ashenhurst, T. R.: Text. Educator, 1888–89, 335.
2. Kaswell, E. R.: Textiles, Fibres, Yarns and Fabrics. Reinhold Publishing Corporation, New York 1953.
3. Law, W.: *Wool Rec. Text. Wld* No. 21 (1922), 968.
4. Robinson, A. T. C. and Mares, R.: Woven Cloth Construction. Manchester, Text. Inst. 1973.
5. Peirce, F. T.: The Geometry of Cloth Structure. *J. Text. Inst.*, Mar. 1937, 28, T45.
6. Pollitt, J.: The Geometry of Cloth Structure. *J. Text. Inst.*, **40** (1949).

Acta Technica Academiae Scientiarum Hungaricae, 94 (1—2), pp. 37—45 (1982)

LATERAL BUCKLING OF ELASTICALLY SUPPORTED ARCHES

L. KOLLÁR,* J. GYURKÓ**

[Manuscript received 9, November, 1982]

The paper develops the differential equations of buckling of arches with monosymmetric cross section, elastically supported in the lateral direction, and presents the solution for "fork-like" support.

1. Introduction

The problem of lateral (torsional) buckling of centrally compressed free arches has been solved for several cases, see e.g. in [1]. However, the main load-bearing elements of some recent structural types (e.g. tents stressed onto a row of arches, Fig. 1) can be modelled as having a continuous elastic lateral support, so that they necessitate to clarify the problem of lateral buckling of such arches. We intend to do that in the following.

2. Assumptions and approximations

Let us investigate an arch of constant cross section, made of homogeneous, isotropic and linearly elastic material, elastically supported in the lateral direction by a continuous medium equally resisting tension and compression. The axis of the arch should have the shape of a circular arc. The arch is subjected to central compression, i.e. the external forces q form a radially directed, uniformly distributed load system (Fig. 2), which is conservative, i.e. it maintains its direction during buckling.

The cross section of the arch has at least one axis of symmetry which lies in the plane of the arch. The cross section can also be thin-walled. The point of application of the external load should lie anywhere on the axis of symmetry, but its position should be the same for every cross section.

We apply the following approximate assumptions:

— The curvature of the arch is not very great, i.e. the ratio of the height of the cross section to the radius of curvature of the arch can be neglected in comparison to unity. Thus it follows that also all other vertical dimensions of the cross section are negligible in comparison to the radius of the arch:

$$1 \pm \frac{d}{R} \approx 1 , \tag{1}$$

* Dr. Kollár Lajos, Karap u. 9, H-1122 Budapest, Hungary
** Gyurkó János, Építéstudományi Intézet, Dávid Ferenc u. 6. H-1113 Budapest, Hungary.

where d is the height of the cross section and R is the radius of the arc passing through the centroids of the cross sections, see Fig. 2;

— The longitudinal fibres of the arch undergo during lateral buckling elongations which are antisymmetric with respect to the symmetry axis of the cross section. Hence only the fibre lying in the symmetry axis remains inextensional;

— The cross sections of the arch maintain their original form during buckling, except for their warping perpendicularly to their planes. We shall neglect the changes in the static characteristics of the cross sections occurring during buckling.

These assumptions are identical with those made in[1].

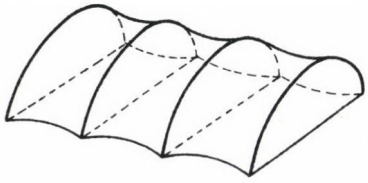

Fig. 1. Tent structure pitched on arches

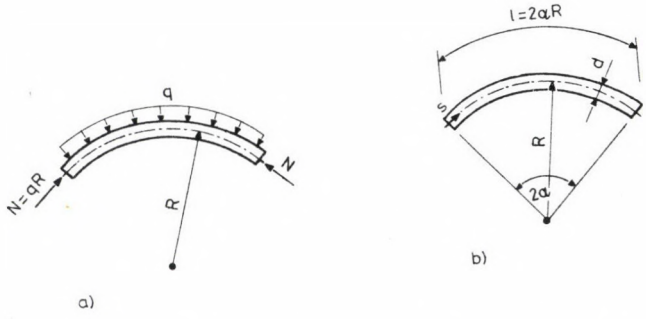

Fig. 2. The structure investigated: a) the loading; b) the arch

3. Notations

We introduce the following symbols (see also Fig. 3):

S	— centroid of the cross section;
T	— shear centre of the cross section;
e	— distance between T and S;
C	— point of application of the elastic support;
t_c	— distance between T and C;
P	— point of application of the external load q;
u_S, v_S, w_S	— displacements of the centroid S in three perpendicular directions;
$\varkappa_x$, $\varkappa_y$, φ	— rotations of the centroidal axes $\bar{x}$, $\bar{y}$, $\bar{z}$;

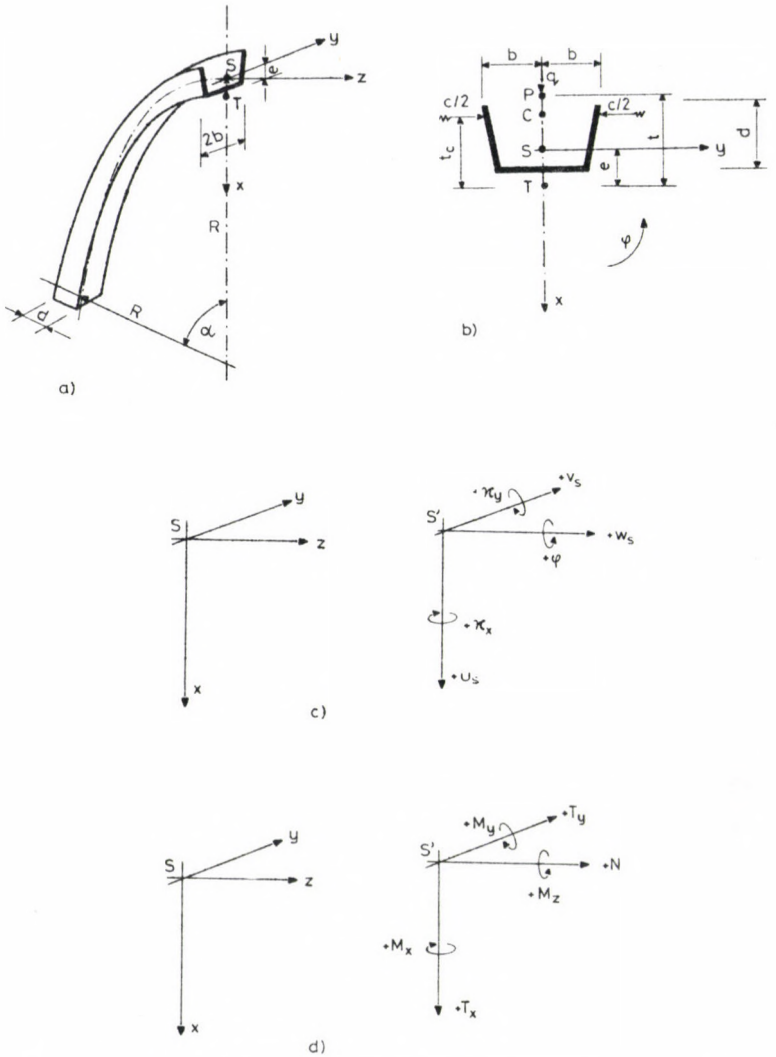

Fig. 3. Notations: a) the arch; b) the cross section; c) the displacement components of the centroid; the internal forces of the arch

M, T, N — internal forces (moment, shearing force, normal force);
s — arc length measured along the centroidal line of the arch;
$( )'$ — differentiation with respect to s;
c — constant of elastic support referred to unit length of the arc [N/m^2] or [kN/m^2];
α — half central angle of the arc;
l — length of the centroidal line of the arch (Fig. 2b);
t — distance between P and T.

4. Differential equations of lateral buckling

In the derivation we use the equilibrium method. The static equation system of the arch in the stage of bifurcation is [2]:

$$M_z' - \frac{M_x}{R} + \bar{m}_z = 0\,, \tag{2a}$$

$$T_y' + \bar{q}_y = 0\,, \tag{2b}$$

$$M_x' + \frac{M_z}{R} - T_y + \bar{m}_x = 0\,, \tag{2c}$$

Here M and T are internal forces arising during buckling, $\bar{m}$ and $\bar{q}$ are loading terms caused by buckling deformation, referred to unit arc length.

These loading terms are to be found in [1] for the case of unsupported arches [Eqs (3.120)–(3.123)]. We now have to complete them by the terms corresponding to the elastic support.

Let us express the y directed displacement v_C of point C with the aid of the displacement of the shear centre T:

$$v_C = v_T - t_c\varphi\,, \tag{3}$$

with v_T as the y directed displacement of T.

The specific load term $\bar{q}_y$ has thus to be completed, due to the elastic support, by the additional term:

$$\bar{q}_y^{\mathrm{III}} = -cv_C = -c(v_T - t_c\varphi)\,. \tag{4}$$

Similarly, we have to add the term

$$\bar{m}_z^{\mathrm{III}} = -\bar{q}_y^{\mathrm{III}} t_c = c(t_c - e)\,(v_T - t_c\varphi)\,, \tag{5}$$

due to the elastic support, to the specific twisting moment $\bar{m}_z$ turning around the axis z.

The loading term $\bar{m}_x$ will not be affected by the elastic support, hence its value remains zero.

Summing up, the load terms appearing in Eqs (2) take the form:

$$\bar{q}_y = -Nv_T'' + Ne\varphi'' - c(v_T - t_c\varphi)\,; \tag{6a}$$

$$\bar{m}_z = N\left[\frac{t-e}{R}\,\varphi - (i_x^2 + i_y^2)\varphi'' - \frac{i_x^2}{R^2}\,\varphi\right] + c(t_c - e)\,(v_T - t_c\varphi)\,; \tag{6b}$$

$$\bar{m}_x = 0\,; \tag{6c}$$

with i_x and i_y as the radii of gyration of the cross section.

We express the internal forces of the arch with the aid of the displacements of the shear centre:

$$N = qR = \mathrm{const}\,. \tag{7a}$$

$$T_y = N(v'_T - e\varphi') + c \int_{(s)} (v_T - t_c\varphi)\,\mathrm{d}s\,, \tag{7b}$$

$$M_x = EI_x\left(\frac{\varphi}{R} - v''_T\right), \tag{7c}$$

$$M_z = GI_T\left(\varphi' + \frac{v'_T}{R}\right) - EI_\omega\left(\varphi''' + \frac{v'''_T}{R}\right) + eT_y\,, \tag{7d}$$

where EI_x, GI_T and EI_ω are the lateral bending, the torsional and the warping rigidities, respectively.

We introduce Eqs (7) into (2a, b, c), differentiate (2c) according to s, and substitute the relation (2b) for T'_y:

$$EI_x\left(\frac{\varphi''}{R} - v''''_T\right) + \frac{GI_T}{R}\left(\varphi'' + \frac{v''_T}{R}\right) - \frac{EI_\omega}{R}\left(\varphi'''' + \frac{v''''_T}{R}\right) - N(v''_T - e\varphi'') - c(v_T - t_c\varphi) = 0\,. \tag{8a}$$

Eq. (2a), written in detail, becomes:

$$GI_T\left(\varphi'' + \frac{v''_T}{R}\right) - EI_\omega\left(\varphi'''' + \frac{v''''_T}{R}\right) + eN(v''_T - e\varphi'') - \frac{EI_x}{R}\left(\frac{\varphi}{R} - v''_T\right) - (i_x^2 + i_y^2)N\varphi'' + \left(\frac{t-e}{R} - \frac{i_x^2}{R^2}\right)N\varphi + ct_c(v_T - t_c\varphi) = 0\,. \tag{8b}$$

Eqs (8a, b), containing the unknown displacement functions v_T and φ, represent the differential equation system which governs lateral buckling of the arch corresponding to Sect. 2. They allow to calculate, according to the usual methods of elastic stability [3], the critical compressive force $N = N_{cr}$ for optional end supports.

For the sake of simplicity, we shall confine us in the following to the so-called "fork-like support", i.e. when the end cross sections are prevented from displacing laterally and from rotating about the axis z, but can freely rotate about the axis x and can freely warp:

$s = 0$: $s = l$:

$$v_T = 0\,, \tag{9a}$$

$$\varphi = 0\,, \tag{9b}$$

$$\frac{\varphi}{R} - v''_T = 0\,, \tag{9c}$$

$$\varphi'' + \frac{1}{R}v''_T = 0\,. \tag{9d}$$

5. Solution in the case of the "fork-like support"

We assume the unknown displacement functions in the form:

$$\varphi = \varphi_k \sin(\lambda_k s), \tag{10a}$$

$$v_T = v_k \sin(\lambda_k s), \tag{10b}$$

where

$$\lambda_k = k\frac{\pi}{l}; \tag{10c}$$

$k = 1, 2, 3, \ldots$ is the number of buckling half waves; φ_k and v_k are constants. Both functions satisfy the conditions (9a to d) of the fork-like support.

The derivatives of the functions (10a, b) have to be introduced into equation system (8a, b). Provided that $s \neq l$ and $s \neq 0$, we arrive at the following linear equation system for the coefficients v_k and φ_k:

$$\begin{bmatrix} a_{11} & a_{12} \\ a_{21} & a_{22} \end{bmatrix} \begin{bmatrix} v_k \\ \varphi_k \end{bmatrix} = \begin{bmatrix} 0 \\ 0 \end{bmatrix}. \tag{11}$$

The first matrix appearing in (11) is symmetric, i.e. $a_{12} = a_{21}$. Its elements are:

$$a_{11} = \lambda_k^2 \left[N - (GI_T + \lambda_k^2 EI_\omega)\frac{1}{R^2} - EI_x \lambda_k^2 \right] - c; \tag{12a}$$

$$a_{12} = a_{21} = -\lambda_k^2 \left[eN + (GI_T + \lambda_k^2 EI_\omega + EI_x)\frac{1}{R} \right] + ct_c; \tag{12b}$$

$$a_{22} = -\lambda_k^2 [-(e^2 + i_x^2 + i_y^2)N + GI_T + \lambda_k^2 EI_\omega] + \frac{1}{R}\left[N\left(t - e - \frac{i_x^2}{R}\right) - \frac{EI_x}{R} \right] - ct_c^2. \tag{12c}$$

The value of the critical compressive force $N = N_{cr}$ is to be calculated from the following equation:

$$a_{11}a_{22} - a_{12}^2 = 0, \tag{13}$$

since the condition for the existence of a solution of the equation system (11), which is different from zero, is that the determinant of the coefficient matrix be equal to zero.

Eq. (13) is of the second degree in N_{cr}:

$$K_2 N_{cr}^2 + K_1 N_{cr} + K_0 = 0; \quad \text{if} \quad \lambda_k \neq 0; \tag{14}$$

with

$$K_2 = (i_x^2 + i_y^2)\lambda_k^2 + \frac{t-e}{R} - \frac{i_x^2}{R^2}; \tag{15a}$$

$$K_1 = -EI_x \left[\frac{1}{R^2} + \lambda_k^4 (i_x^2 + i_y^2 + e^2) + \lambda_k^2 \left(\frac{e+t}{R} - \frac{i_x^2}{R^2} \right) \right] -$$

$$-(GI_T+\lambda_k^2 EI_\omega)\left[\lambda_k^2\left(1+\frac{i_x^2}{R^2}\right)+\frac{1}{R^2}\left(\frac{t-e}{R}-\frac{i_x^2}{R^2}\right)\right]-$$

$$-c\left[(e-t_c)^2+i_x^2+i_y^2+\frac{1}{\lambda_k^2}\left(\frac{t-e}{R}-\frac{i_x^2}{R^2}\right)\right]; \tag{15b}$$

$$K_0=EI_x(GI_T+\lambda_k^2 EI_\omega)\left(\lambda_k^2-\frac{1}{R^2}\right)^2+$$

$$+c\left[EI_x\left(\lambda_k t_c+\frac{1}{\lambda_k R}\right)^2+GI_T+EI_\omega\lambda_k^2\right]. \tag{15c}$$

Hence we obtained a closed formula for the critical compressive force of an arch with a fork-like support.

6. Numerical example

Let us show the influence of the elastic support on the critical compressive force of a simple arch shown in Fig. 4. The material of the arch is timber, it has a narrow rectangular cross section, and its centre line is a circular arc with a central angle $2\alpha=\pi/2$.

The dimensions of the structure are:
$R=15.0$ m,
$d=0.5$ m,
$2b=0.1$ m (the width of the cross section),
$l=23.6$ m
The cross sectional characteristics of the arch are (Fig. 4b):
$E=1.5\times10^7$ kN/m^2.
$G\approx0.4\ E=6\times10^6$ kN/m^2,
$EI_x=625$ kNm^2,
$GI_T=1000$ kNm^2
$EI_\omega\approx0$,
$t=e=t_c=0$,
$i_x^2\approx0$,
$i_y=0.144$ m.

Let us suppose that the lateral elastic support acts at the centroid of the cross section. Taking all these into account, Eq. (14) assumes the comparatively simple form:

$$N_{kr}^2 i_y^2\lambda_k^2+N_{kr}\left(-\frac{EI_x}{R^2}-EI_x\lambda_k^4 i_y^2-GI_T\lambda_k^2-ci_y^2\right)+EI_xGI_T\left(\lambda_k^2-\frac{1}{R^2}\right)^2+$$

$$+c\left(\frac{EI_x}{\lambda_k^2R^2}+GI_T\right)=0.$$

Let us assume the constant of the elastic support to be $c=68$ kN/m^2, which approximately corresponds to the stiffness exerted by the canvas of the structure shown in Fig. 1.

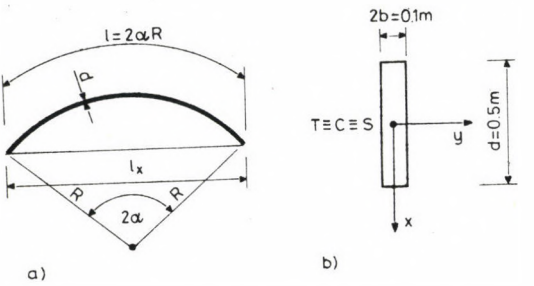

Fig. 4. The arch of the numerical example, a) elevation; b) cross section

Let us calculate the critical compressive force from the previous equation for the half wave numbers $k = 1, 2, 3, 4, 5$, and varying the value of c from 0 to 68 kN/m^2.

The numerical results are to be seen in Table I.

Table I

c	$k=1$	2	3	4	5
0.00	5.4	37.6	93.1	171.2	272.1
0.68	43.7	47.2	97.3	173.6	273.6
6.80	388.0	133.3	135.7	195.2	287.5
68.00	3830.9	994.6	518.9	411.1	426.0

In the table we framed the minimum values of the forces N, belonging to the same c, in each row. These minimum values give the critical forces belonging to every c. It is to be seen that even one tenth of the actual elastic support stiffness changes the buckling shape of the unsupported arch.

In our example the arch buckles in four half waves, under a critical stress of 8.2 MPa. That is, the lateral elastic support increases the critical load of the unsupported arch to about its 76-fold.

7. Two additional remarks

If we further simplify Eq. (14) by setting $R \to \infty$ and $GI_T \to \infty$, we obtain the critical compressive force of an elastically supported straight bar of the length l [3]:

$$N_{cr} = \frac{\pi^2 EI_x}{l^2}\left(k^2 + \frac{cl^4}{k^2\pi^4 EI_x}\right).$$

If we intend to apply the above results to canvas structures as that shown in Fig. 1, we also have to consider that the stiffness c of the elastic support exerted by the canvas also depends on the number k of buckling half waves [4]. Thus the critical force can be obtained by iteration in some steps.

References

1. Kollár, L.: Statik und Stabilität der Schalenbogen und Schalenbalken. W. Ernst und Sohn, Berlin — Akadémiai Kiadó, Budapest 1973
2. Love, A. E. H.: A Treatise on the Mathematical Theory of Elasticity. Dover Publ., New York, 1944
3. Timoshenko, S. P.–Gere, J. M.: Theory of Elastic Stability. McGraw-Hill, New York 1961
4. Gyurkó, J.–Kollár, L.: Problems of Canvas Structures (in Hungarian). In: *ÉTI Évkönyv* 1981, Budapest 1982

Acta Technica Academiae Scientiarum Hungaricae, 94 (1—2), pp. 47—62 (1982)

A RECENT METHOD FOR THE NUMERICAL SOLUTION OF ENGINEERING PROBLEMS. PART I.

E. BÉRES*

[Manuscript received: 31 May, 1982]

This method is featured partly by writing physical relationships directly in terms of finite elements, rather than to state and solve the problem in terms of differential equations; and partly, by applying an approximate function in the form (generally polynomial) of a function series valid for the entire domain, or at least for a group of elements. Physical conditions written either for elements or for boundary points or boundary domains equally lead to linear equations. Such equation systems are generally redundant hence with no exact solution. As an approximate solution that with the least square sum of equation errors will be taken. The change of this solution of the redundant equation system upon multiplying equations in the system by different constants may be utilized to find the solution where error maxima tend to a minimum.

The approximate polynomial at a sufficiently high power yields the exact load for the calculated deformation by resubstitution into the exact differential equation. Thereby a possibility results to exactly determine the error in terms of load.

1. Introduction

A calculation method advantageous in engineering problems or even in a wide field of physics will be presented. Reference to elasticity, a confined field of physics, is by no means to the detriment of general validity. At the same time it not only helps illustrativeness but it relates the notions to distinct physical magnitudes.

First, let us point to an essential difference between theoretically exact analytic methods, and approximate methods. Namely, much of misunderstanding and erroneous evaluation has resulted from the assumed validity for approximate methods of the statements on, and skills in, analytic methods. Though, recent computer facilities impose to revaluate and reformulate certain interpretations and principles, rather than to be simply means to extend the validity of theories. Such reinterpretations and reformulations include:

— Just the due respect to convergence demonstrations. For instance, convergence demonstration is needless for methods or cases where practical implication approximates by no means the critical range.

— Appointment of cases suiting an approximate solution exactly meeting one or several groups of conditions. One must be aware of the not absolute superiority of the method and solution exactly meeting one group of conditions, approximating the others, even, such a restriction is likely to impair the solution as a whole.

— Recognition of the excessive rigidity and erroneousness of the attitude to invariably consider the method and solution with regular equation systems as more

* Dr. E. Béres, Hunyadi János út 11, H-1011 Budapest, Hungary

concrete hence superior to those leading to redundant equation systems. The solution method applying redundant equation systems has its advantages.

— No optimum solution is possible by relying exclusively on principles to classify the methods. The optimum solution has to be found within the range of a given solution method — in particular, in complex problems.

In the following, first the suggested method will be presented, then its principal features analyzed, together with the problems arisen above.

2. Direct application of the physical model on finite elements

In most fields of physics — including elasticity — analytic methods, differential equations describing the problem were the first to be formulated. At present, exact theoretical relationships are known in most of the problems, at the same time, exact solutions of the established differential or integral equations can only be given — with a few exceptions — for special practically irrelevant problems, at most of educational interest. Obviously, earlier it was attempted to find some approximate solution for these equations, for the computing facilities of that time to cope with, it being no question of applying cumbersome numerical methods. The advent, however, of high-speed, program-controlled digital computers brought about radical changes.

Application of digital computers started by making programs for the known methods, much facilitating and even forwarding them. Problem volumes could significantly be increased, the accuracy improved by refining divisions and iterations. It became, however, soon clear that earlier methods developed for different tools failed to fully utilize possibilities offered by the new computing device, challenging to develop new methods suiting the new implement. In a meaning the finite element method can be classified as such, although it has inherited much of analytic methods (variation principle, meeting of boundary conditions, etc.).

Subsequently the case of elasticity problems where displacement components are considered as unknown will be concerned with. Three kinds of conditions are involved, namely:

equilibrium conditions;

dynamical boundary conditions;

geometrical boundary conditions.

Compared to differential equations of the analytic method, the simplest approximation is by writing the equilibrium equations directly for finite elements obtained by somehow dividing the solid; and the dynamical and geometrical boundary conditions partly for the corresponding boundary domains, and partly, for common points of the boundary and the dividing planes.

The simplest and most expedient method to divide the solid to elements is that by means of planes parallel to the coordinate planes, resulting in pyramids for most of the elements. More complex elements occur only in boundary domains where they are partly bounded by planes, and partly by domain boundary surfaces.

These elements are subject to mass forces and to surface stresses. Coordinates of the mass force resultants in tridimensional elements are given by triple integrals but since, in general, mass forces are constant, this integral simplifies to the product of the volume by a constant. Often even the effect of mass forces may be omitted.

Components of the resultant of element surface stresses can be obtained from double integrals. Division by planes parallel to the coordinate planes produces mostly rectangular integration domains, except boundary surfaces of elements adjacent to boundary domains. These double integrals prevail in solving equilibrium equations.

Dynamical boundary conditions are written for intersections of the domain boundary surfaces and the dividing planes, as well as for the boundary domains. The stress belonging to the displacement functions is equated to the given stress, and the force calculated for the boundary domain to the force acting there.

Geomatrical boundary conditions are still simpler handled. At the nodes defined above, displacement components are required to equal the given value. In exceptional cases, however, the displacement may be exactly specified for each boundary domain.

Of course, plane problems involve still simpler procedures and division. Now, elements inside the domain are rectangles, and its boundary is a plane curve. Resulting simplifications affect the calculation as a whole. To stress general validity, the subsequent theoretical discussion will refer to the spatial case, bidimensional problems being understood throughout as special cases with significant simplifications.

As to be detailed below, meeting the boundary conditions in this method involves twofold approximations. Namely, partly, displacement functions are replaced by approximate functions yielding but an approximation for the displacements of defined points, underlying interpolation resulting in further approximations. In general cases, this statement is valid for any approximate method, it can only be invalidated in special cases. The possibility of exactness at the defined points exists also in the presented method, but exact fulfilment of the boundary conditions will be seen later not to increase the accuracy, and even maybe to impair the solution as a whole, restricting this possibility to particular cases.

3. Polynomial approximation

First the simple, but practically most frequent case of applying a single approximate function for the entire domain will be considered. Such functions are written as finite function series:

$$u = \sum_{i=1}^{\alpha} a_i f_i(x, y, z);$$

$$v = \sum_{j=1}^{\beta} b_j g_j(x, y, z),$$

$$w = \sum_{k=1}^{\gamma} c_k h_k(x, y, z),$$

where f_i, g_j and h_k are arbitrary functions, a_i, b_j and c_k are wanted constants causing functions u, v and w to meet element equilibrium equations and boundary conditions at the defined points at the least error.

The simplest treatment is that where f_i, g_j and h_k are power functions, that is, displacement functions are polynomials of the form

$$u = \sum_{(i)} a_i x^{p_i} y^{q_i} z^{r_i},$$

$$v = \sum_{(j)} b_j x^{\bar{p}_j} y^{\bar{q}_j} z^{\bar{r}_j},$$

$$w = \sum_{(k)} c_k x^{\bar{\bar{p}}_k} y^{\bar{\bar{q}}_k} z^{\bar{\bar{r}}_k},$$

where $p_i, q_i, \ldots, r_k$ are positive integers or zero. The polynomial may comprise various numbers of terms as a function of u, v, w.

In other methods, e.g. that of finite elements, geometrical isotropy is required as a rule (see p. 134 in [1]). On the other hand, for an approximate polynomial affecting the entire domain, geometrical isotropy is irrelevant. The applied polynomial needs not be complete or symmetrical. Form of, and number of terms in, polynomials are arbitrarily chosen to cope with the type of the problem, excepted that the number of different

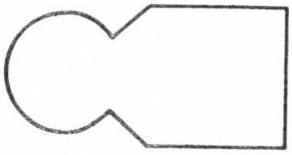

Fig. 1.

exponents of a variable must not exceed that of dividing points parallel to the variable axis. For instance, dividing a pyramid to 6 parts along x, to 10 parts along y, and to 5 parts along z, and having every variable at a lower power, too, the highest powers of variables x, y and z may be 6, 10 and 5, resp., hence the term at the highest power must not exceed $x^6y^{10}z^5$. Any variable at a higher power may induce a significant error inside the element even if the number of equations leads to a unique solution. This characteristic of approximate polynomials is, however, common knowledge.

4. Writing the equations

As concerns the approximation by polynomials, the method proceeds seemingly similarly to the finite element method. The essential change due to the higher-order approximation affecting the entire domain, and the error assessment possibilities it

offers will only be revealed later. Here simply the scheme of writing the equations will be presented and confronted to the same step in the finite element method. Namely, both methods yield linear equation systems, and both solutions consists of two parts: to write the equations, and to solve the system of equations.

Element equilibrium equations, and expressions for dynamical and geometrical boundary conditions at given points are in concise, vectorial form:

$$\iint_F \mathbf{s}\,\mathrm{d}F + \mathbf{f}V = 0\,,$$

$$\mathbf{s}_{p_i} = \mathbf{s}_{0i}$$

$$\mathbf{u}_{pj} = \mathbf{u}_{0j}\,,$$

respectively.

Coordinates of stress vector **s** in terms of stress tensor components are:

$$s_x = \sigma_x l + \tau_{yx} m + \tau_{zx} n\,,$$

$$s_y = \tau_{xy} l + \sigma_y m + \tau_{zy} n\,,$$

$$s_z = \tau_{xz} l + \tau_{yz} m + \sigma_z n\,,$$

where l, m, n are direction cosines of the surface normal.

Mass force vector **f** has been assumed as constant, thus, mass force acting on the element could be written as product of vector **f** by the element volume V. In the special case where mass force is place-dependent, mass force acting on the element is:

$$\iiint_V \mathbf{f}\,\mathrm{d}V$$

$\mathbf{s}_{0i}$ and $\mathbf{u}_{0j}$ are given boundary stress and displacement at P_i and P_j, respectively.

Since, however, as stated earlier, displacement components are approximated by polynomials, the stress components have to be substituted into the formulae in terms of displacement components, using well-known relationships:

$$\sigma_x = \frac{E}{(1+\nu)(1-2\nu)}\left[(1-\nu)\frac{\partial u}{\partial x} + \nu\left(\frac{\partial v}{\partial y} + \frac{\partial w}{\partial z}\right)\right],$$

$$T_{xy} = \frac{E}{2(1+\nu)}\left(\frac{\partial u}{\partial y} + \frac{\partial v}{\partial x}\right).$$

Actually, the unknowns are coefficients a_i, b_j, c_k of the polynomials, of a number independent of that of the elements. The relationship between unknowns and equations, will, however, be discussed only later. On element surfaces coincident with the domain boundary where surface stresses are given as boundary stresses, the integral value is constant, to be integrated with the right-hand-side constant of the equation system.

5. Solving the equations

Just as most of the usual approximate methods, the suggested one leads to a linear equation system to be solved. Even in this case, the equation system to be solved may be made regular, but the genuine method leads to a redundant system of equations. The number of equations and unknowns, advantages and inconvenients of redundant equation systems, and possibilities to improve the accuracy will be spent a deep-going analysis later. Here only essentials of the solution principle will be recapitulated.

The system of linear equations of n unknowns and a total of m equilibrium, dynamical and geometrical boundary conditions is, in general form:

$$\underset{(m\cdot n)}{\mathbf{A}}\ \underset{(n)}{\mathbf{x}} = \underset{(m)}{\mathbf{b}}\,,$$

solved according to the condition:

$$(\mathbf{Ax}-\mathbf{b})^2 = \min!$$

Difficulty with — and at the same time, interest in — the problem is that while the result of solving a regular equation system remains inaffected by multiplying its equations by different constants, and solving the resulting equation system, the result of a redundant equation system may be significantly altered by such multiplications.

This apparent instability is, however, not only an inconvenient but it permits at the same time to choose the most convenient one among solutions for the given type of function. Namely it will soon be clear that the idea of arbitrarily improving the accuracy by refining the division, hence increasing the number of elements has to be abandoned. It has to be examined instead, how to find the most convenient solution of a given type of function, e.g. tenth or twentieth-power polynomials. Development and progress impose this change of approach.

6. The problem of convergence

In mathematics, the first and most important requirement for approximation is generally the convergence of the procedure, hence decrease of the error with increasing number of terms, to tend to zero as limiting value; although series theoretically divergent but for an adequate number of terms yielding fair approximation in a given interval, have long been used in practical mathematics. But however selfintended the requirement of convergence is in theoretical analyses, it would be quite erroneous to prove applicability of an approximate method by its convergence in the case of a complex physical problem e.g. that of elasticity. Namely, on one hand, in approximating by a single-variable function, to achieve coincidence to 10, 12 or any digit is no problem, it can be achieved throughout, or at least in a part of the range of

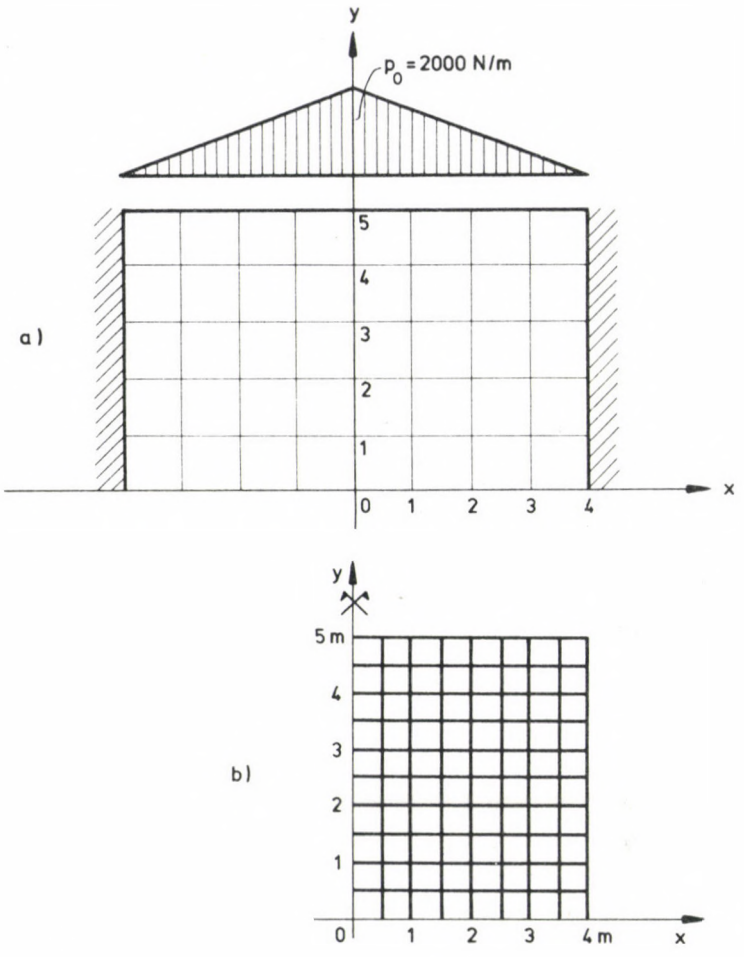

Fig. 2.

interpretation by means of polynomials of 10, 15, 20 or other, still maneuvrable power. The problem to be solved in practice is merely restriction of computation to the range where the desired accuracy can be achieved by means of the given computation tool. On the other hand, the error of results of some kinds of elasticity problems can hardly be diminished below 10, 20 or even 50 per cent. Namely refining the divisions or increasing the power have their limitations even for the actual high-capacity computers, because of an excessive number of unknowns beyond the storage capacity of the computer. To be illsutrative, let us take a simple example, determination of stress distribution in a rectangular prism. The prism is divided to elements by planes parallel to its sides, to ten parts in each direction, yielding 1000 elements and 1331 nodes. In the

simplest case where approximate functions are only fitted to the nodes, and specifying only C^0-order continuity of elements, thus, for each node, only three displacement components are unknown, the total number of unknowns is 3993. In the finite element method, this number is somewhat, but not significantly, reduced by specifying the displacement of some boundary points. Solution of equations with so many unknowns meets difficulties from several aspects, hence further increase of the number of unknowns would be practically meaningless. Namely halving the element edges would increase by about eight times the number of unknowns, and dividing to twenty parts, to 27,783. Neither the attempt to improve the accuracy by increasing the continuity order is luckier, namely in the bidimensional case, the number of unknowns assumed to provide for a continuity C^1 is at least four times that of the simplest case of continuity C^0.

For the tridimensional case there have not even practical elements been developed to provide continuity C^1 as stated by Huebner (p. 185 in [1]).

Obviously, refinement of division, hence increase of the number of elements has definite limitations. It is a serious problem, namely although often a division to 8 to 10 parts, underlying approximation, may lead to a result close to several digits, in certain — e.g. elasticity — problems of great many unknowns, such an approximation would produce an error of the result order.

Therefore it is quite wrong to evaluate the approximation result according to the theoretical behaviour at the limit.

All that means the practical irrelevance of theoretically proving the convergence. Safe evaluation of results cannot rely but on exact error calculus.

To avoid misunderstanding, it should stressed that the presented method is theoretically convergent. Thus, rather than as an apology for this inconvenient of the method, the sharp exposition of the problem has been intended to attribute the real value to the theoretical demonstration of convergence. Otherwise, so-called asymptotic or semiconvergent series have been used since Euler for calculating function values. These series do not convergent but the upper bound of calculation error is a calculable small value not to be made arbitrary small. For details see [2].

7. Bounds in the finite element method

In the finite element method, the system energy is known to be susceptible to an upper and a lower bound. This feature of the method is generally referred to, and even if it gives no rise to erroneous conclusions, eventual omission of evaluation may induce overestimation, misunderstanding. For instance, the sentence on p. 43 in [3]: "In the case of varieties $\pi_p = \min!$ and $-\pi_c = \min!$ of the principles of potential energy and of accessory energy, $\delta^2\pi_p$ and $\delta^2\pi_c$, respectively, can be affected by signs, that is, these two error principles yield bounds for the exact solution" makes it to seem as if the solution would be bounded. Though, there is no question about this, and a deeper-going study reveals it not to have been meant by the author.

Namely these solutions give no bound either for the stresses or for the displacements but only for the energy in the solid, and with these bounds tending to the common limit value, also solutions tend to the exact solution. Thus, also this possibility belongs rather to the problematic of limit value than to that of the practical evaluation of the approximate solution. Namely, even if two approximate solutions are known, with their respective potential energies, there is no proof that e.g. the maximum stress error is the less in the solution with the lesser potential energy.

The greatest convenience with the finite element method resides in the simple handling due to the linear approximation inside elements of the field of displacements, an approximation rather simple nevertheless with plenty of theoretical and practical difficulties. The impossibility to achieve other than C^0-order continuity by linearly approximating the field of displacements leads to a discontinuity of stress functions at element boundaries, not to be helped even by applying a higher-order approximation fitting to several points of the element, causing the function to result in a closer approximation inside the element but no higher-order continuity at element boundaries. Although theoretically a higher-order continuity can be provided at element boundaries, but no suitable practical method has yet been developed for tridimensional cases. Though, the theoretical possibility may raise better than real hopes by borrowing the air of simplicity from the linear approximation. Well, simplicity and generalizability are contradictory. But special cases permitting a higher-order fitting have been susceptible of development.

This is illustrated by [4] applying higher-order fitting elements for computing axisymmetrical deformations of shells of revolution showing the stress to be continuous if elements have at least twelve degrees of freedom. Application of such elements permits to reduce the number not only of elements but also of unknowns without reducing, but generally even increasing, the accuracy.

The strive to a higher-order continuity of elements corresponds to the attempt to handle the complete domain as a single element, realized by assuming the approximate function as a high-power polynomial.

8. Fulfilment of certain conditions

In developing the analytical methods, it was natural to seek solutions in the form of function series with terms meeting some of the conditional equations. If these functions make up a complete system then the exact solution can be produced as an infinite function series. Often, however, the complete system is even theoretically difficult to produce. In reality, always finite function series are encountered, preventing fulfilment of certain conditions.

At the first glance it may be misleading that in the finite element method the condition for the displacement of given boundary points is exactly met, while in the

presented method, an approximate solution is made up with even in this respect. The inessentiality of this difference is obvious by realizing that

— fulfilment of the boundary condition of displacement for given points means no fulfilment for every boundary point;

— continuity of displacements means no continuity of stresses and strains.

These considerations are, however, useless, since it is simple to prove theoretically, or to show by examples that a forcible exact meeting or close approximation of boundary conditions significantly impairs, rather than improves, the solution as a whole.

This statement will be theoretically proven as follows.

Be H the error function of arbitrary definition. Its minimum cannot be reduced for any by-condition, that is

$$\min H \leq \min H/F\,, \tag{1}$$

H/F denoting the error function meeting condition F. In a still more general way,

$$\min H/F_1 \leq \min H/F_2\,,$$

if condition F_2 comprises condition F_1.

Thus, by-conditions are seen to increase the error, or keep it at the same level provided the by-condition fits the solution for condition min H.

Thus, from the aspect of solution accuracy, application of functions meeting the boundary conditions (or a part of them, or the differential equations of equilibrium) is seen not only not to improve but even to impair reliability of the result.

At the first glance, the possibility to define an infinity of functions H may be embarrassing. But here the values of the same function H for different solutions, rather than comparison of different values of function H anyhow impossible to compare in merit, are spoken of.

For the redundant equation system

$$\mathbf{A}\mathbf{x} = \mathbf{b} \tag{2}$$

a simple numerical value, that is, however, typical of the error rate is simplest defined by

$$H = (\mathbf{A}\mathbf{x} - \mathbf{b})^2\,. \tag{3}$$

Concerning the defined error function, (1) has the following meaning. Having determined vector $\mathbf{x}$ with the least H value, then modifying equation system (2) by multiplying its equations by a constant each, and solving the obtained equation system $\tilde{\mathbf{A}}\tilde{\mathbf{x}} = \tilde{\mathbf{b}}$ relying on the condition of minimum error square sum, only to substitute resulting vector $\tilde{\mathbf{x}}$ into (3) yields an H value that is higher than or equal to the H value obtained for the original equation system, that is:

$$(\mathbf{A}\mathbf{x} - \mathbf{b})^2 \leq (\mathbf{A}\tilde{\mathbf{x}} - \mathbf{b})^2\,.$$

Analysis of numerical examples showed the effect to be significant, decisive for the computation result, rather than to be unimportant, only theoretically detectible.

Closer meeting the boundary conditions beyond a given limit was found to much impair the solution as a whole. The improvement for the boundary conditions is by orders less than the increase of errors elsewhere. It is obvious, since rather than to simply reduce the boundary error, to charge the forces correcting the error on the real boundary errors of the boundary condition are reduced on the condition of keeping the character of the approximate function (e.g. power of, and number of terms in, a polynomial) unaltered. Accordingly, this is the most apparent difference between the exact and the approximate methods.

The conception that in solving certain problems boundary conditions prevail can largely be attributed to the denomination arising from the mathematical solution method. The denomination "boundary value problem" is clearly seen in [5] to refer mainly to the solution method.

9. The number of unknowns

As mentioned above, division to elements is advisably made by planes parallel to coordinate planes. For the power of the approximate polynomial to be applied, only the upper bound was given so that the exponent of a variable must not exceed the number of divisions parallel to its axis. Under these conditions, writing equilibrium equations for each element and also dynamical or geometrical boundary conditions for each boundary node (assuming only dynamical or only geometrical boundary condition can be specified at a given node), there are more equations than unknowns. Without a deeper analysis, let us made some comments.

There is no theoretical or practical hindrance to equate numbers of unknowns and of equations. Retaining as many equations as there are unknowns (omitting the excess) provides a regular equation system and the usual unique solution. Beyond, however, the fact that this approximate solution fails equilibrium and/or boundary conditions even for the assumed elements and points, hence reducing the number of equations is to the detriment of uniform error distribution (irrespective of the close fulfilment of conditions for certain elements and points), in this case the solution is markedly affected by what equations have been retained or omitted. Even a slight change of the equation weight significantly affects the result, omission of some equations being an extreme case of changing the weight. Adding the impossibility to suggest a rule or even an advice of what equations to omit to the least detriment of the result makes it obvious to renounce of this possibility, and to be concerned with the solution by means of redundant equation systems.

Nevertheless let us point out that application of redundant equation systems is motivated by its convenients rather than the outlined difficulties. Namely, a redundant equation system comprising more equations than unknowns permits, on one hand,

more of conditions to be taken into consideration, on the other hand, by changing the weight of any equation permits to choose the most convenient from among functions of the given type. Remind the practical impossibility of an illimited refinement of divisions or illimited increase of the power of the approximate polynomial. Therefore the purpose of the problem has to be reformulated to yield the most convenient one of the given type functions — in general, polynomials of given power and number of terms.

In the presented method, only an upper bound can be given for the number of unknowns, even after divisions. In case of the suggested division to prismatic or rectangular domains, this upper bound is essentially the same as the lower bound in the finite element method. Namely dividing the prism to p, q and r parts by planes parallel to its sides results in $(p+1)(q+1)(r+1)$ nodes. In the simplest case of the finite element method where the displacement function is continuous of order C^0 and linear interpolation between nodes, the simplest approximation possible, is applied, the number of unknowns is less than $3(p+1)(q+1)(r+1)$ by not more than as many displacement components have been specified at boundary nodes. Again, at most $3(p+1)(q+1)(r+1)$ unknown coefficients may belong to polynomials approximating the displacement component functions. Within this range, both polynomial type and the number of unknowns can be arbitrarily assumed, to correspond to the kind of the problem.

It is essential to have not much more of unknowns, even in extreme cases than are contained in the simplest cases of the finite element method or in the finite difference method. But as soon as an approximation of higher order than that in the finite element method, for instance, a continuity of order C^1 between elements is specified, the number of unknowns is multiplied to become several times that in our case.

Realizing the number of unknowns to be quadrupled by ensuring continuity of order C^1 in bidimensional problems, providing e.g. continuity of the plate alone, rather than those of the stresses and of the load pertaining to the computed form, points out the difference between the finite element method providing a continuity C^0 or maybe C^1, and a method of higher-order continuity.

10. The number of equations

Writing only force equilibrium equations and boundary conditions arising from the division of a prismatic (or rectangular in the bidimensional case) domain, the number of equations can be demonstrated to exceed that of unknowns. Thus, writing all equations of the same value for a given division leads to a redundant equation system, to underlie the solution procedure.

Of course, also moment equilibrium equations can be written for these elements. Their consideration further refines the solution, unduly increasing, however, the number of equations and the encumbrance of the problem. Although the number of unknowns and the size of the regular equation system yielding the solution remain

unaltered but the work needed for writing the original redundant equation system and the storage capacity needed for the coefficients are much increased. Improvement of the results has been experienced not to be proportional to the labour spent, reducing the application of this means to improve the accuracy to exceptional cases.

11. The redundant equation system

Rather than only to illustrate the approximateness of the solution, the excess number of equations in the system over that of unknowns offers a direct possibility to error estimation. Namely whatever approximate solution result is utilized to examine the equilibrium of different elements and the fulfilment of boundary conditions, neither the equilibrium of the different elements, nor the boundary conditions are perfectly met. Here this unfulfilment is sensed directly in the elements, and although not even in dividing to congruent elements can it be said that the greatest equilibrium error is the possible greatest error of an element of this size and form, since even a greater one is possible for a different division, the error in each equation offers a true information on both equilibrium and boundary condition errors, to be used for improving the solution.

The lack of common parts of elements the equilibrium conditions are written for, so that each equation of boundary condition refers to another node or domain, ensures linear independence of the equations. This fact and the increased number of equations concludes on that the equation system has no solution in the traditional meaning of the word. This is why no solution meeting every equation is sought for, but one minimizing the error function established from the error of each equation. An arbitrary number of error functions can be established but here the general analysis will be omitted to restrict our considerations to the simplest case of defining the error function as square sum of the error of each equation. Thus, solution for the equation system with the minimum of equation error square sum is sought for.

Solution of redundant equation system (2)

$$\underset{(m,n)}{\mathbf{A}} \; \underset{(n)}{\mathbf{x}} = \underset{(m)}{\mathbf{b}} \qquad (m>n)$$

meeting the condition above is known to issue from the regular equation system

$$\mathbf{A^*Ax} = \mathbf{A^*b}\,.$$

For a fixed matrix **A** this procedure leads to a unique solution. But matrix **A** can be fixed in an infinity of forms. Namely, correctness of an equation is inaffected by multiplying it by any constant, while multiplying different equations by different constants leads to different matrices **A**. Denoting one by $\mathbf{A}_{(i)}$ and the other by $\mathbf{A}_{(j)}$, solutions of this equation system characterized by these two matrices will only be equal if

$$\mathbf{A}_{(i)} = \lambda \mathbf{A}_{(j)}\,.$$

At first glance, this flexibility involving an infinity of possibilities may seem rather strange. But at a closer consideration, it is what development may rely on. It is, however, connected with error calculation, with the concept of error, to be integrated with in the analysis. Still a possible interpretation of multiplying the equations, and a special case will be considered.

Multiplication of each equation by a different constant means to change its weight. The degree how the change of equation weights in a redundant system alters the result could be illustrated on hand of simple numerical examples. These solutions are felt, however, to be considered as outcomes of manipulated problems, and the phenomenon is underestimated. So no such a purely mathematical example will be

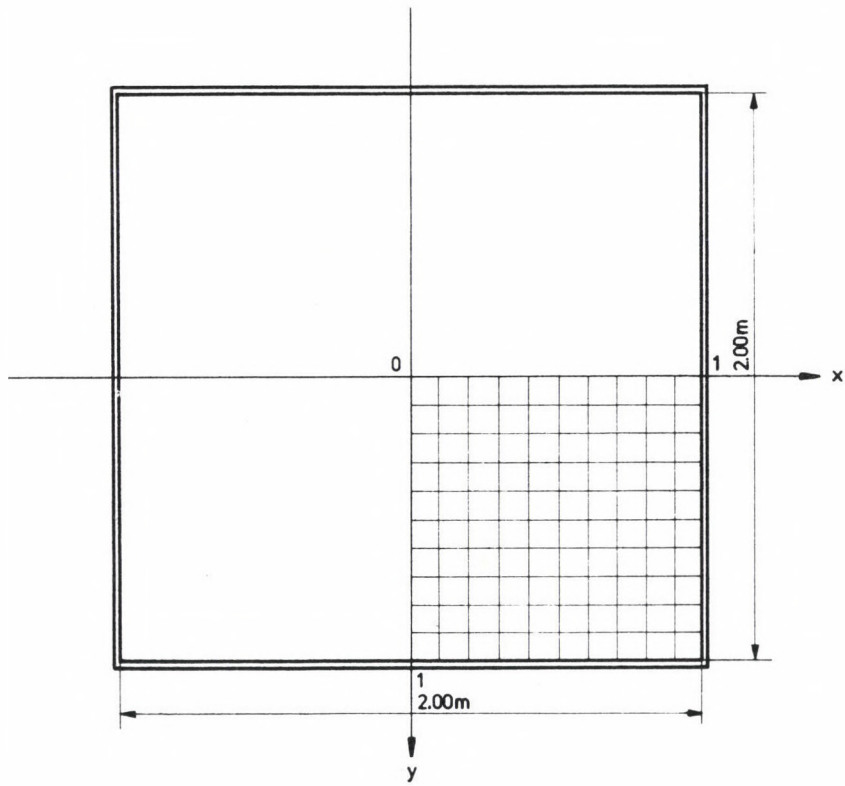

Fig. 2.

presented, the more so since this effect is decisive even in solving the simplest technical problems, as manifest from practical applications.

The extreme case of weighting the equations is that where certain equations are attributed as much weight as to cause their error to tend to zero. There are two simple

possibilities for it. Either these equations get multipled by a relatively high number, markedly increasing their weight. A suitably high factor may reduce the error practically to zero.

The other possibility — as against increasing the weight of the equation by multiplying by a constant, and to reduce its error in course of the numerical solution — is to find a solution exactly meeting the preferential equations hence of an also theoretically zero error.

Of course, beyond meeting the preferential equations, also the condition of minimum square sum of the errors of the other equations has to be met by the solution.

Let us rearrange equation system (2) to make quadratic matrix $\mathbf{A}_{22}$ of system

$$\begin{bmatrix} \mathbf{A}_{11} & \mathbf{A}_{12} \\ \mathbf{A}_{21} & \mathbf{A}_{22} \end{bmatrix} \begin{bmatrix} \mathbf{x}_1 \\ \mathbf{x}_2 \end{bmatrix} = \begin{bmatrix} \mathbf{b}_1 \\ \mathbf{b}_2 \end{bmatrix} \tag{4}$$

inversible, and to have matrices $\mathbf{A}_{21}$ and $\mathbf{A}_{22}$ arising from coefficients of those equations to be exactly met. Partitioned it means matrix equations

$$\mathbf{A}_{11}\mathbf{x}_1 + \mathbf{A}_{12}\mathbf{x}_2 = \mathbf{b}_1 ,$$

$$\mathbf{A}_{21}\mathbf{x}_1 + \mathbf{A}_{22}\mathbf{x}_2 = \mathbf{b}_2 .$$

Expressing from the second equation the vector $\mathbf{x}_2$ of unknowns

$$\mathbf{x}_2 = \mathbf{A}_{22}^{-1}(\mathbf{b}_2 - \mathbf{A}_{21}\mathbf{x}_1) \tag{5}$$

and substituting it into the first equation, then arranging, leads to

$$(\mathbf{A}_{11} - \mathbf{A}_{12}\mathbf{A}_{22}^{-1}\mathbf{A}_{21})\mathbf{x}_1 = \mathbf{b}_1 - \mathbf{A}_{12}\mathbf{A}_{22}^{-1}\mathbf{b}_2 , \tag{6}$$

to be solved under the condition of minimum error square sum. The resulting vector $\mathbf{x}_1$ includes part of the unknowns. The other unknowns make up vector $\mathbf{x}_2$ obtained by substituting $\mathbf{x}_1$ into (5). Perfect flexibility of this procedure results from the possibility of simultaneous application of weighing and exactly meeting the equations.

Acta Technica Academiae Scientiarum Hungaricae, 94 (1—2), pp. 63—72 (1982)

GEOMETRIC CONDITIONS OF HARMONIC DRIVES

J. PÉTER*

[Received April 10, 1982]

The normal operation of gearings may be disturbed by interference phenomena. The present paper investigates the possibility of the occurrence of internal tooth fillet interference, external tooth fillet interference and addendum interference in harmonic drives by taking the peculiar motion of the flex-spline into account.

1. Introduction

In the harmonic drive a pair of gears having external and internal toothing is integrated, toothed like a normal cylindrical wheel. Thus, the toothing of the pair of gears does not differ from the usual one. However, the teeth of the external gear are carried by a flexible wheel body which, during the working of the drive, suffers a wave-like deformation. The present paper deals with this particular case of the engagement and investigates the interference phenomena which may impede the normal working of the drive.

After a short survey of the calculation of the geometric data of the pair of gears, the work begun in [1] will be continued. In [1], the author summarizes the symbols and concepts needed for the investigation. By taking into accoun the peculiar motion of the flex-spline he considers the engagement of the teeth of the two wheels as that of a pair of wheels of variable angle of deflection and variable axle base and of internal-external toothing. Considering the small deflection angle of the axle, the problem is reduced to the simple engagement of a normal circular spline and a spur gear of displaced centre of rotation in relation to the centre of a circle, the axle base of the two wheels being variable.

For the purpose of the investigation the system of coordinates is fixed to the wave generator. Thus, such a pair of gears may be considered which, contrary to the customary arrangement are engaged at not only one, but at two zones. The two zones are assumed to be symmetrical, wherefore only one of them will be investigated.

2. Geometric basic data of the pair of gears

The distance between the centre O_3 or the circular spline and the centre O_2 associated with the investigated tooth of the flex-spline varies in dependence of their deflection as compared with the principal deformation axis ([1] Figs 6, 7). In case where

* Péter, J., Derkovits u. 54, I. 3., H-3529 Miskolc, Hungary

the symmetry axis f' of the investigated tooth of the flex-spline and the principal deformation axis are congruent (i.e., the tooth is situated on the crest of the wave of deformation), the distance between the centres $\overline{O_2O_3} = w_0$, which, as a matter of fact, is the displacement of the point A_0 of the middle surface K in the direction of the principal deformation axis (Fig. 3).

In this situation, the distance between the centres O_2 and O_3, similarly to the axle base of a normal pair of gears of internal-external toothing is

$$w_0 = \frac{z_3 - z_2}{2} m \frac{\cos \alpha_0}{\cos \alpha_g}, \tag{2.1}$$

wherein

z_2, z_3 — are the numbers of teeth,
m — module,
α_0 — base profile angle,
α_g — normal pressure angle defined on the principal deformation axis.

The difference between the coefficients of tool supply x_2, x_3 with the familiar relationship is as follows

$$x_3 - x_2 = \frac{\text{inv}\, \alpha_g - \text{inv}\, \alpha_0}{\tan \alpha_0} \frac{z_3 - z_2}{2}. \tag{2.2}$$

In case where the radii of the addendum circles are r_{f2} and r_{f3}, the common tooth height is

$$h_k = r_{f2} + w_0 - r_{f3}. \tag{2.3}$$

The other data of the pair of gears should be determined in the same way as in the case of the normal tooth wheels. After this short survey of the geometric data let us investigate the possibility of occurrence of the internal tooth fillet interference, the external tooth fillet interference and the addendum interference.

3. Internal tooth fillet interference

This phenomenon takes place when the circular spline ought to be engaged by the tooth-fillet rounding, built up from the relative path of the addendum point of the tool processing the spur gear.

The limiting instance of the internal tooth fillet interference is to be seen in Fig. 1:

$$\overline{O_3H_2} = r_{f3\min},$$

wherein

O_3 — centre of circular spline,
H_2 — limiting point of involute tooth profile of wheel 2.

The radius r_{H2} of the limit circle of the spur gear depends on whether the tooth cutting was carried out with the tool having tooth rack profile or a fellows cutter.

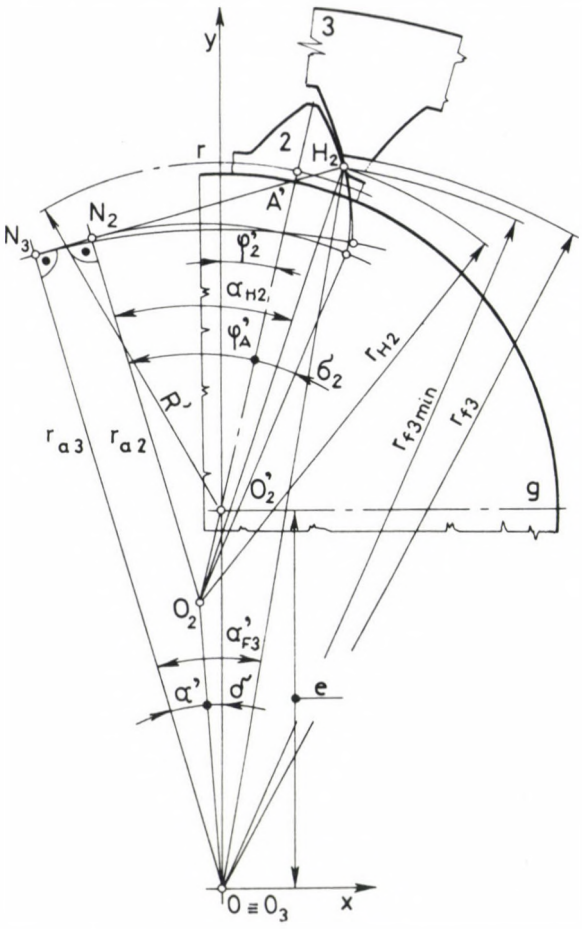

Fig. 1. Investigation of internal tooth fillet interference. O_2, O'_2 and H_2 are the centre, the centre of rotation and the limit point of the involute tooth profile, respectively, belonging to the investigated tooth of wheel *2*; O_3 is the centre and centre of rotation of wheel *3*. There is no internal tooth fillet interference in case where

$$r_{f3} > \overline{O_3 H_2}$$

In case of the tooth cutting with a tooth rack profile tool we have

$$r_{H2} = \sqrt{r_{a2}^2 + \left[r_{02} \sin \alpha_0 + \frac{(x_2 - f_0^*)m}{\sin \alpha_0} \right]^2}, \tag{3.1}$$

wherein:

r_{a2} and r_{02} — radius of base circle and pitch circle, respectively,
f_0^* — addendum factor.

In case of production with the aid of a fellows cutter

$$r_{H2}=\sqrt{r_{a2}^2+[a_{sz2}\sin\alpha_{sz2}-\sqrt{r_{fsz}^2-r_{asz}^2}]^2}\,, \tag{3.2}$$

wherein:

a_{sz2} and α_{sz2} — axle base and pressure angle of engagement, respectively, between wheel *2* and fellows cutter

r_{fsz} and r_{asz} — radius of addendum circle and base circle, respectively, of the tool.

By using the designations of Fig. 1 the distance between points O_3 and H_2 may be calculated with the formula

$$\overline{O_3H_2}=\sqrt{(\overline{H_2N_2}+\overline{N_2N_3})^2+r_{a3}^2}\,, \tag{3.3}$$

where:

$$\overline{H_2N_2}=r_{a2}\tan\alpha_{H2}\,, \tag{3.4}$$

α_{H2} — profile angle on the limit circle of radius r_{H2},

$$\overline{N_2N_3}=\sqrt{\overline{O_2O_3^2}+(r_{a3}-r_{a2})^2} \tag{3.5}$$

If the wave generator is of disc-type ([1] Chapter 4), the distance between the centres O_2 and O_3 is [1] (2):

$$\overline{O_2O_3}=\sqrt{e^2+(R_0-R')^2-2e(R_0-R')\cos\varphi_2'}\,.$$

Between the radii O_2N_2 and O_2A_2' the angle φ_A' may be calculated with the formula

$$\varphi_A'=\varphi_2'+\alpha'(\varphi_2')+\delta(\varphi_2')\,, \tag{3.6}$$

$\alpha'=f(\varphi_2')$, $\delta=f(\varphi_2')$ may be obtained from the relationships (3 and 4) of [1].

$$\alpha'=\arccos\frac{m(z_3-z_2)\cos\alpha_0}{2\overline{O_2O_3}}\,,$$

$$\delta=\arcsin\frac{(R_0-R')\sin\varphi_2'}{\overline{O_2O_3}}\,.$$

From the involute-geometry it is known that

$$\hat{\varphi}_A'=\tan\alpha_{H2}-\hat{\sigma}_2\,, \tag{3.7}$$

wherein σ_2 is the central angle associated with the half width of the circle-base tooth groove of wheel *2*.

With the knowledge of φ_A' (3.7) by making use of the relations (3.6), [1] (3 and 4) the value of φ_2' may be determined. Replacement of φ_2' into [1] (2) yields the distance between the centres O_2 and O_3. Knowing $\overline{O_2O_3}$ permits to calculate $\overline{N_2N_3}$ (3.5) which

replaced $\overline{H_2N_2}$ (3.4) determined earlier into (3.3) results in the distance between the centre O_3 and boundary point H_2.

There is no internal tooth fillet interference in the case where

$$\overline{O_3H_2} < r_{f3} . \tag{3.8}$$

4. External tooth fillet interference

This phenomenon occurs when the involute point on the addendum circle of the spur gear has to engage above the bound of the involute tooth profile of the circular spline with the tooth fillet determined by the addendum point of the tool processing the circular spline.

The limit case is to be seen in Fig. 2

$$\overline{O_2H_3} = r_{f2\max} ,$$

wherein

O_2 — centre, associated with the investigated tooth of wheel *2*
H_3 — limit point of involute tooth profile of wheel *3*.

In case where the circular spline is tootthed with a fellows cutter, the radius of the limit circle will be

$$r_{H3} = \sqrt{r_{a3}^2 + (a_{sz3} \sin \alpha_{sz3} + \sqrt{r_{fsz}^2 - r_{asz}^2})^2} , \tag{4.1}$$

wherein

r_{a3} — radius of base circle of wheel 3,
a_{sz3} and $sz3$ — axle base and pressure angle of engagement between wheel *3* and fellows cutter.

The distance between the centre O_2 and limit point H_3 may be calculated from the formula

$$\overline{O_2H_3} = \sqrt{r_{a2}^2 + \overline{N_2H_3^2}} , \tag{4.2}$$

wherein

$$\overline{N_2H_3} = (\hat{\varphi}'_A + \hat{\sigma}_2) r_{a2} . \tag{4.3}$$

φ'_A entering in *(4.3)* can be calculated with the aid of Eq. (3.6) which is the function of φ'_2 for the moment unknown.

In the triangle $O_3N_3H_3$

$$\overline{N_3H_3} = r_{a3} \tan \alpha_{H3} , \tag{4.4}$$

wherein α_{H3} is the profile angle on the circle of radius r_{H3}.

At the same time

$$\overline{N_3H_3} = \overline{N_3N_2} + \overline{N_2H_3} . \tag{4.5}$$

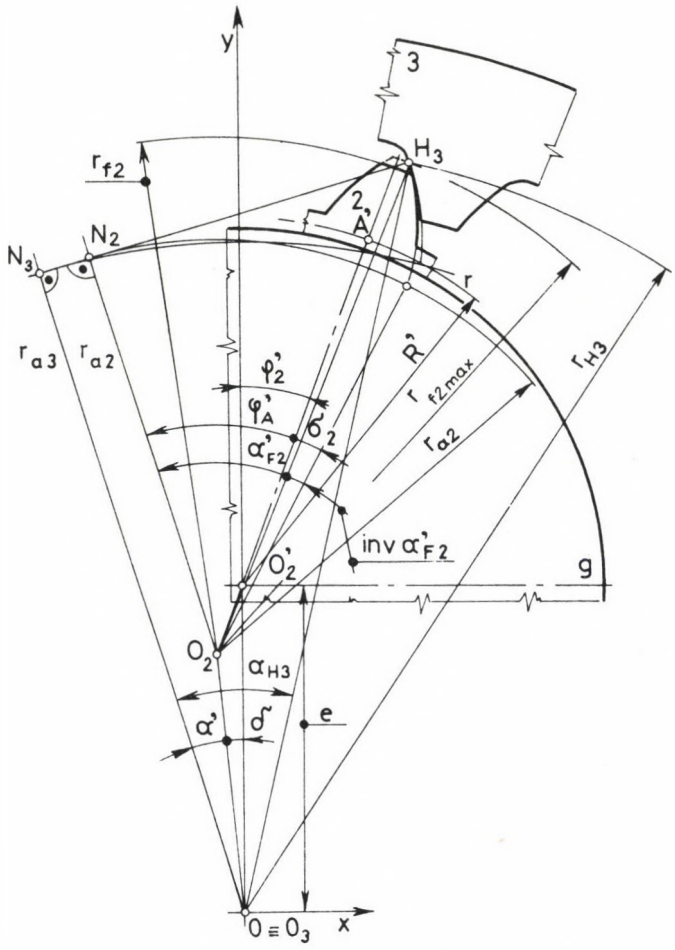

Fig. 2. Investigation of external tooth fillet interference. O_3 and H_3 is the centre of wheel *3* and limit point of the involute tooth profile, respectively; O_2 and O'_2 is the centre and the centre of rotation belonging to the investigated tooth of wheel *2*. There is no external tooth fillet interference if $r_{f2} < \overline{O_2H_3}$

Knowing $\overline{N_3H_3}$ (4.4) the value of φ'_2 may be determined by making use of the relationships (3.5), (4.3), (4.5) with whose knowledge $\overline{N_2H_2}$ (4.3), whereafter the distance between the centre O_2 and the limit point H_3 may be found.

There is no external tooth fillet interference in the case where

$$\overline{O_2H_3} > r_{f2}\,. \tag{4.6}$$

5. Addendum interference

The engagement of the pair of gears integrated into the harmonic drive is comparable to that of a pair of gears of low difference in number of teeth having internal-external toothings. In such drives it may occur that the points being on the tooth top of the spur gear are knocking against those being on the tooth top of the circular spline. This kind of jamming is called tooth fillet interference.

The tooth of the flex-spline positioned in the direction of the surface line (in Fig. 3, for example, a')of the flexible surface R, engages with the tooth of the circular spline in a similar way, like a pair of gears of external-internal toothing of variable axle deflection angle and variable axle base [1]. Contrary to the engagement zone (where the deflection of the axles is negligible) the deflections of the axles in the zones of engagement and disengagement of the teeth of the flex-spline into the tooth grooves of the circular spline should be taken into account. Due to the obliquity (Figs 3 and 4) of

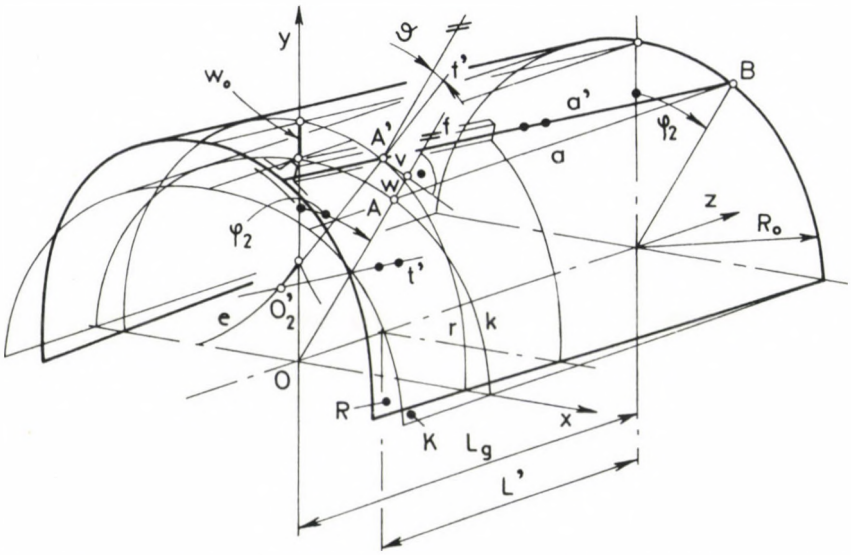

Fig. 3. Flexible surface R of the flex-spline with the tooth situated in the direction of the surface line a'

the teeth the corner of the tooth of the flex-spline may already knock at the moment when at a parallel tooth direction there is still a backlash.

The path curve of point F_2 of the tooth of the flex-spline intersects the tip cylinder of the circular spline at point M (Fig. 4). In case where the two wheels are deflected with an angle φ_2, i.e., φ_3 as compared with the principal axis to deformation, there is no addendum interference if the inequality

$$\varphi_M < \varphi_{F3}\,, \tag{5.1}$$

is true.

Herein:

φ_M and φ_{F3} are the polar coordinates associated with the point of intersection M and with the point F_3 on the tooth edge of wheel *3*, respectively.

The distance between point F_2 and the centre O_3, depending on the deflection (φ_2) of the flex-spline in relation to the principal deformation axis is

$$\overline{O_3 F_3} = \sqrt{Q}$$

with

$$Q = \left(R_0 + w' + h_{02} \cos \vartheta' - \frac{s_{f2}}{2} \sin \vartheta' \right)^2 + \left(v' + h_{02} \sin \vartheta' + \frac{s_{f2}}{2} \cos \vartheta' \right)^2, \quad (5.2)$$

wherein

R_0 — radius of central circle *k*,
h_{02} — distance between central circle and addendum circle of wheel *2*,
s_{f2} — width of tooth top of wheel 2.

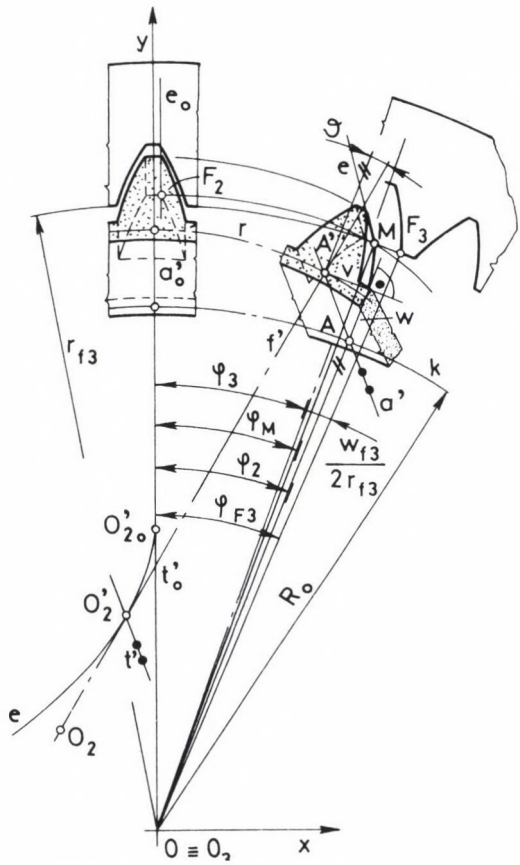

Fig. 4. One tooth of each of the wheels of the gear pair of variable axle deflection and variable axle base of internal-external toothing. There is no addendum interference if $\varphi_{F3} > \varphi_M$

In case where in the plane of the wave generator the radial displacement of point A of polar coordinate φ_2 is w, its tangential displacement is v, the normal rotation of f is ϑ, further, assuming that the displacements, i.e., rotation mentioned in approaching the end of wheel *2* decreases linearly in the plane belonging to the edge of the teeth (Fig. 3) are as follows

$$w' = w\frac{L'}{L_g}; \qquad v' = v\frac{L'}{L_g}; \qquad \vartheta' = \vartheta\frac{L'}{L_g}, \tag{5.3}$$

wherein:

L' — distance of tooth edges and
L_g — distance of plane of wave generator to the end of wheel *2*.

At point M:

$$\overline{O_3F_2} = r_{f3}\,. \tag{5.4}$$

By making use of Eqs (5.2), (5.4) the angle φ_2 might be found at which the path curve of point F_2 intersects the tip cylinder of wheel *3*.

$$\varphi_3 = \varphi_2\frac{1}{i^g_{23}} = \varphi_2\frac{z_2}{z_3}. \tag{5.5}$$

If the width of the tooth groove on the addendum circle of wheel *3* is w_{f3}, so

$$\varphi_{F3} = \varphi_3 + \frac{w_{f3}}{2r_{f3}}. \tag{5.6}$$

6. Example

Let us continue the work begun in [1] Chapter 5. The characteristics of major significance of the drive are as follows: $z_2 = 190$; $z_3 = 192$; $m = 1$ mm; $\alpha_0 = 20°$; $f^*_0 = 1.0$; $c^*_0 = 0.25$; $r_{f2} = 100{,}1$ mm; $r_{f2} = 99.95$ mm; $R_0 = 97.1$ mm; $L_g = 170$ mm; $L' = 155$ m; $e = 3.9$ mm; $w_0 = 1.2$ mm; the flex-spline is toothed with a tool of a tooth rack and the circular spline with a fellows cutter ($z_{sz} = 76$, $r_{fsz} = 39.88$ mm).

In case of toothing the flex-spline with a tool of a tooth rack $r_{H2} = 99.222$ mm, $\alpha_{H2} = 25.880\,478°$, $\sigma_2 = 2.359\,371°$, $\varphi'_A = 30.156\,961°$. In this case $\varphi'_2 = -2.75°$, $\overline{O_2O_3} = 1.210\,063$ mm, $\overline{N_2N_3} = 0.762\,384$ mm, $\overline{H_2N_2} = 43.310$ mm, $O_3H_2 = 100.400\,973$ mm. $\overline{O_3H_2} > r_{f3}$, therefore internal tooth fillet interference exists. The radius of the addendum circle *3* should be increased from 99.95 mm to 100.45 mm. In the present example $\overline{O_2O_3} - w_0 \approx 0.01$ mm; considering this very small value, the calculations may be carried out also in connection with a pair of gears of normal internal-external toothing ($\overline{O_3H_2} = 100.394$ mm).

The circular spline is toothed with a fellows cutter. The radius of the limit circle is $r_{H3} = 101.518$ mm. In this case, $\alpha_{H3} = 27.300\,236°$, $\varphi'_2 = -3.92°$, $O_2O_3 = 1.220\,357$ mm, $\overline{N_2N_3} = 0.778\,62$ mm; $\overline{N_3H_3} = 46.516\,577$ mm, $\overline{N_2H_3} = 45.782\,957$ mm, $\overline{O_2H_3} = 100.326\,241$ mm. $O_2H_3 > r_{f2}$, therefore there is no external tooth fillet interference. Considering the very small value $\overline{O_2O_3} - w_0 \approx 0.02$ mm, if one calculates with a pair of wheels of w_0 axle base, and of normal internal-external toothing, $\overline{O_2H_3} = 100.341$ mm.

The path curve of the point F intersects the tip cylinder of wheel *3* at $\varphi_2 = 49.45°$. The angle coordinate belonging to point M is $\varphi_M = 49.346\,665°$. $\varphi_3 = 48.934\,896°$, $w_{f3} = 2.018\,838$ mm. In this case, $\varphi_{F3} = 49.513\,54°$. There is no addendum interference, because $\varphi_{F3} > \varphi_M$.

7. Summary

The normal operation of harmonic drives might be impeded by interference phenomena similar to those of gear pairs of internal-external toothing. The investigation of the addendum interference may be performed on a tooth of each of the wheels of a normal gear pair of internal-external toothing of variable axle deflection and variable axle base.

In investigating the internal tooth fillet, interference and external tooth fillet interference, the axle deflection is assumed to be negligible and the problem is reduced to that of a simple investigation of a tooth of both a normal wheel of internal toothing and that of external toothing, however, of a displaced centre of rotation as compared to its centre.

References

1. Péter, J.: Investigation of the Engagement of Harmonic Drives-Part I
2. Szamosvölgyi O.: Geometric Conditions of Circular Spline Drives. Profile-Displacement Values Associated with Compensated Slip Conditions Retraining Institute for Engineers, Budapest 1960, pp. 88

Acta Technica Academiae Scientiarum Hungaricae, 94 (1—2), pp. 73—79 (1982)

THE ANALYSIS OF SPHERICAL AND PLANE GRIDS OF TRIANGULAR NETWORK WITH THE AID OF DUAL NETWORKS

I. HEGEDŰS*

[Manuscript received; 15 July, 1982]

The paper presents a method for analysing the bar forces of single-layer space grids of triangular network, constructed into a sphere and subjected to uniformly distributed radial load. The results of the analysis permit to state a necessary condition of macroscopically homogeneous isotropy of spherical and plane grids of triangular network.

Introduction

A variety of radiolariae (sphere-shaped unicellular deep-sea animals of the size of ~ 100 microns) has an external cellular skeleton of triangular network. The geometry of the skeleton suggests its being optimalized from the statical point of view. Some measurements have supported this conjecture with the discovery that the ratio of length of the longest and the shortest "bar" of the "structure" is closer to unity than that of engineering structures ostensibly having been optimalized from this point of view. [1, 2, 3]

To the author's knowledge until now also no investigations have been made on radiolaria skeletons for controlling the complementary conjecture that the ratios of "bar cross sections" show an optimalized structure too.

The subsequent analysis yields a simple rule for determining the optimal ratios of bar cross sections of grids of spherical triangular network subjected to uniformly distributed radial load. The results of the analysis can be used to give a similarly simple rule for assuming the ratios of cross sectional areas of bars in plane and spherical grids of triangular network in such a way that it results in the macrospically homogeneous isotropy of the grids.

1. The dual polyhedron of a triangular polyhedron constructed into a sphere

For the sake of brevity let us call the triangular polyhedron constructed into a sphere as primal polyhedron, its network as primal network, its elements — faces, edges and nodes — as primal faces, edges and nodes. The planes touching the circumscribed sphere of the primal polyhedron at the primal nodes form another polyhedron. Let it be defined as the dual polyhedron, corresponding to the primal one, and let us call its elements dual faces, edges and nodes (Fig. 1).

* Hegedűs István, Váci Mihály u. 10, 2083 Solymár, Hungary

The relations between the primal and dual elements are as follows:

I. Each dual face contains one primal node, thus the numbers of primal nodes and of dual faces are equal. The dual faces can be brought into correspondence with the primal nodes and vice versa.

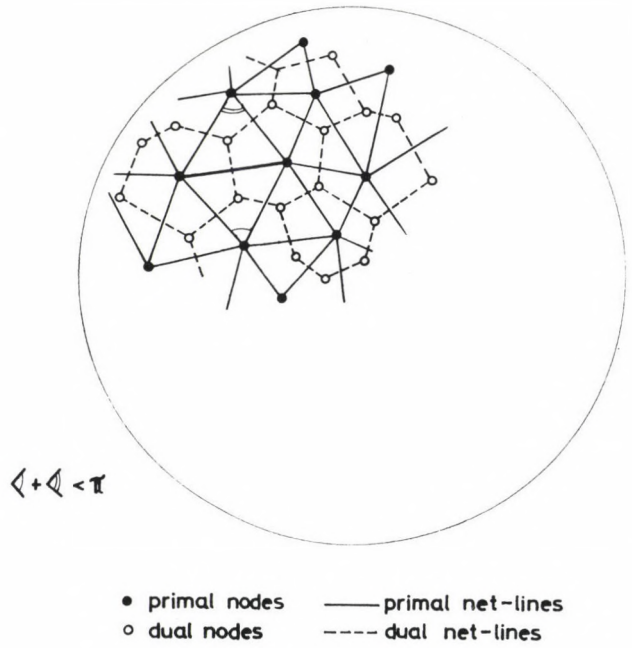

Fig. 1.

II. The neighbouring dual faces containing neighbouring primal nodes intersect each other along a dual edge perpendicular to the primal edge connecting the primal nodes lie on the intersecting dual faces, thus each dual edge can be brought into correspondence with a primal edge perpendicular to it and vice versa.

III. The number of dual nodes equals that of primal faces, the primal edges corresponding to the dual ones, intersecting each other in a dual node, form a triangle of the primal network.

IV. Each dual face is a polygon bordered by edges which are the duals of the primal edges intersecting each other at the primal node which lies on the dual face.

V. The angles enclosed by a primal edge and the adjacent dual faces are equal, thus the length of projections of this edge on the planes of both dual faces are equal.

VI. If the primal polyhedron is convex, its dual is also convex, or else among the faces of the dual polyhedron there are star-shaped polygons with self intersecting boundary lines (Fig. 2).

For the sake of continuity of the discussion, two well-known statements concerning the space grids, loaded at the joints by concentrated forces, are attached to the above ones.

VII. Each space grid of hinged joints, having a network forming a convex triangular polyhedron is internally statically determinate, i.e. each system of bar forces belongs to one equilibrium system of external loads acting on the joints of the grid and vice versa. (This statement is called Maxwell's or Föppl's theorem in the literature of statics.)

VIII. Let the forces acting at the same joint be projected to an arbitrary plane and to its normal line. If these projections yield zero sums for each joint, then the external

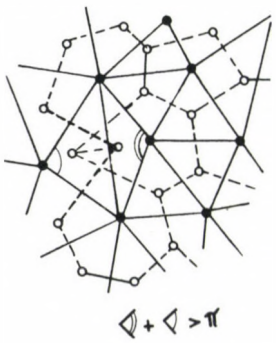

Fig. 2.

forces loading the grid at the joints form an equilibrium system, thus an arbitrarily taken system of the bar forces uniquely determines an equilibrium system of external forces, the elements of which can be separately computed at each joint.

All statements I to VIII may concern the investigated type of radiolaria skeletons.

2. The dual network as united diagram of bar forces

Let us stipulate that the primal polyhedron is convex. Since the polyhedron has a triangular network constructed into a sphere, the necessary and sufficient condition of its convexity is that no primal node lies inside any spherical calotte cut out by the planes of primal faces. Another condition, equivalent with the former one, is that the sum of the two angles of any pairs of neighbouring triangles which lie at the corners opposite to the common side of the triangles must be less than π, (see on Fig. 1.).

Statements II and IV yield a basis for the further statement that the boundary polygon of a dual face is a projection vector polygon of a properly chosen system of bar forces acting at the corresponding primal node, provided the vector polygon is rotated by $\pi/2$ in its plane.

Statement V permits to extend this interpretation simultaneously to all dual faces. That is, it also follows from the statement that the projections of bar forces on the adjecent dual faces are also equal.

Thus the common section of the boundaries of neighbouring dual faces can be considered as two projections of equal size of the same bar force which are rotated until they coincide. As a matter of course, the sense of rotation of the vector polygons has to be the same for all dual faces. Having stipulated this too, we can state that the dual network represents a system of bar forces which can be consistently determined by using the boundary polygons of the dual faces as vector polygons of the projected bar forces.

3. Determination of the internal and external forces belonging to the dual network

The corollary of Statement VII is that the structure has no self-stress state. As a consequence, the nodal resultants of the non-zero bar forces must not vanish. As was shown in the former section, the boundary polygons of the dual faces represent closed vector polygons of the projected bar forces. Since the lines of action of these bar forces have a common points of intersection at the joints, and the projected vector polygons which belong to the joints are closed, the resultant of the bar forces acting at any primal node has to be normal to the corresponding plane of projection, i.e. to the corresponding dual face. According to the equilibrium condition of internal and external forces, these nodal resultants have to be the opposites of nodal forces which constitute the load system.

Let the lengths of the primal edges, intersecting each other in the i-th node, be denoted with $s_{i1}, \ldots, s_{ik}, \ldots, s_{in}$, the lengths of the corresponding dual edges with $t_{i1}, \ldots, t_{ik}, \ldots, t_{in}$, the angles enclosed by the i-th dual face and the primal edges with $\varphi_{i1}, \ldots, \varphi_{ik}, \ldots, \varphi_{in}$, and the radius of the sphere with R. The relation between φ_{ik} and s_{ik} is given by the formula

$$\sin \varphi_{ik} = \frac{s_{ik}}{R}. \tag{1}$$

Let the bar force acting in the bar, which coincides with the primal edge of length s_{ik}, be denoted with N_{ik} and considered positive if it is tension, the external force acting at the i-th point denoted with P_i and considered positive if it points outwards.

From the fact that the dual network can be regarded as a unified vector diagram of the projection bar forces, it follows that these projections of bar forces are proportional to the lengths t_{ik} of the corresponding dual edges. Hence, by properly choosing a scale factor denoted by f, the projections of bar forces can be expressed according the formula

$$N_{ik} \cdot \cos \varphi_{ik} = f \cdot t_{ik}. \tag{2}$$

The equilibrium condition, written for the components of the nodal forces normal to the i-th dual face, yields the following equation:

$$P_i = \sum_{k=1}^{n_i} N_{ik} \cdot \sin \varphi_{ik}, \tag{3}$$

where n_i denotes the number of bars joining the i-th node. Introducing Eqs (1) and (2) into Eq (3), we obtain

$$P_i = \frac{f}{2R} \sum_{k=1}^{n_i} \frac{t_{ik} \cdot N_{ik}}{\cos \varphi_{ik}}. \tag{4}$$

According to Statement VIII, the nodal loads determined by Eq (4) constitute a force system being in equilibrium. Since we stipulated that the primal polyhedron is convex, the dual one is also convex. In consequence of the convexity, all dual edges represent bar force projections of the same sign.

The sum in Eq (4) geometrically means the quadruple of the area of i-th dual face. Neglecting for sake of simplicity that the centroids of the dual faces do not necessarily coincide with the corresponding primal nodes, the nodal forces can be regarded as the resultants of a uniformly distributed load of the intensity

$$p = \frac{2f}{R}, \tag{5}$$

acting perpendicularly to the dual faces.

Tarnai [6] have drawn the author's attention to the resemblance of the presented results to a not too much known principle of the equilibrium of polyhedral frames, which has been stated by Rankine [5] as follows: "If planes diverging from a point or line be drawn normal to the lines of resistance of the bars of a polyhedral frame, then the faces of a polyhedron whose edges lie on in those diverging planes (in such a manner that those faces together with the diverging planes which contain their edges form a set of continuous diverging pyramids or wedges) will represent, and be normal to a system of forces which, being applied to the summits of the polyhedral frame, will balance each other — each such force being applied to the summit of meeting of the bars whose lines of resistance are normal to the set of diverging planes that enclose that face of the polyhedron of forces which represents and is normal to the force in question. Also, areas of the diverging planes will represent the stresses along the bars to whose lines of resistance they are respectively normal."

Actually, if the polyhedral frame is constructed into a sphere, the planes in question are diverging from the centre of this sphere, and the bases of the diverging pyramids are touching this sphere (or another concentric sphere), then the connections between the geometric quantities permit to transform Rankine's principle into the form presented here in Sects. 2 and 3.

4. The geometric condition of uniform strength of radiolaria skeletons

Radiolaria skeletons — and engineering structures of similar forming — have a fine network, in which even the longest bar length is smaller by magnitudes than the radius of the circumscribed sphere. It follows from this, on the one hand, that all cosines in Eqs (2) and (4) are very close to and can be replaced by unity, and on the other hand, that the surfaces of the primal and the dual polyhedrons are very close to each other, and can be replaced by the surface of the sphere. Thus the bar forces of a sphere-shaped single-layer space grid of sufficiently fine and uniform triangular network, loaded by a pressure of intensity p, can be calculated using the formula, derived from Eqs (2) and (5), as follows:

$$N_{ik} = -\frac{p \cdot R}{2} t_{ik} . \tag{6}$$

The role of the radiolaria skeleton is to subtend the cellular membrane attached to it by short appendices of the nodes, thus the skeleton is subjected to a system of concentrated nodal loads, statically equivalent to a pressure on the surface, just like in our previously investigated case. It follows from this that — in knowledge of the data of network and pressure — the bar forces are to be calculated from Eq. (6).

In a grid of uniform strength the ratios of cross sectional areas have to be equal to those of bar forces. Consequently, in our problem they have to agree with the ratios of lengths of dual edges. According to the conjecture mentioned in the introduction, the "bar cross sections" of the radiolaria skeleton probably meet this condition of uniform strength. If the skeleton behaves as a structure of uniform strength, the uniform pressure does not cause any bending moments in the bars, even if the joints are not hinged ones.

5. The macroscopic homogeneous isotropy of single-layer spherical and plane grids of triangular network

If the spherical grid of uniform strength is subjected to an external load system statically equivalent to a uniform external pressure, its network deforms into an affine one in such a way that no marked points or directions of the deformation can be found, i.e. the deformation is macroscopically homogeneous.

The finer network we take, the closer the stress state and the strain state of the grid come to those of a plane grid having macroscopically homogeneous hydrostatic stress and strain states. While performing the $s_{max}/R \to 0$ limit transition, the primal network passes over to a general triangular plane network, and at the same time, the dual network becomes co-planar with the primal one so that the dual nodes coincide with the centres of circumscribed circles of the primal triangles (Fig. 3.).

Since, on the one hand, macroscopically homogeneous isotropy of a plane grid requires that homogeneous hydrostatic stress states belong to macroscopically

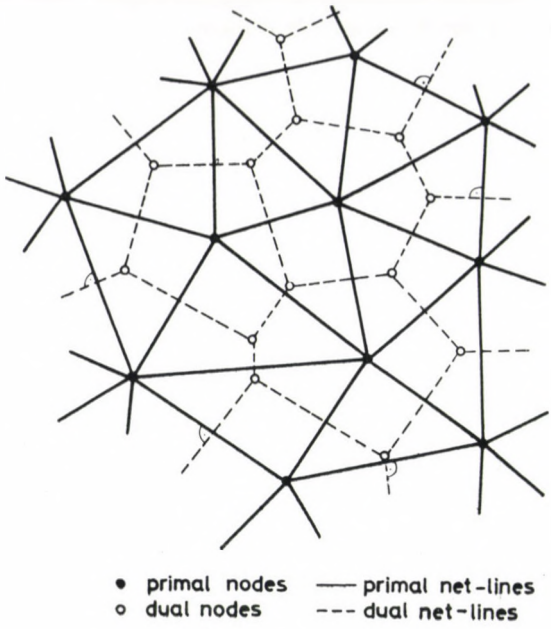

Fig. 3.

homogeneous strain states, and, on the other hand, only the derived ratios of cross sectional areas (more correctly: tensile rigidities) can furnish a grid with effective rigidities, which represent such connection between the stress and strain states, the equality of the ratios of the tensile rigidities to that of the lengths of the corresponding dual net lines is the necessary condition of macroscopically homogeneous isotropy of grids of triangular network.

The sufficiency of this condition does not follow from our analysis. Actually, the detailed analysis of grids of triangular network which consists of congruent scalane or isosceles triangles [4] shows that such grids cannot be made isotropic. However, if isotropy can exist, the above necessary condition adequately determines the ratios of tensile rigidities of the bars.

References

1. Makai, E. Jr.—Tarnai, T.: On the Morphology of Spherical Grids (in Hungarian), *Műszaki Tudomány* **51** (1976), 123–155
2. Makowski, Z. S.: Space Structures. A short review of their development. In: Space Structures. Ed. by R. M. Davies; Blackwell Sc. Publ., Oxford and Edinburgh 1967
3. Le Ricolais, R.: Essai sur des systèmes réticulés à 3 dimensions. *Annales des Ponts et Chaussées* (1940), VII. No. 4, 63–70; VIII. No. 11. 153–166.
4. Kollár, L.—Hegedűs, I.: Solution of Double-layer Space Trusses of General Triangular Grid by the Equivalent Continuum Method. *Acta Technica* Hung. **74,** (1972), 363–381
5. Rankine, W. J. M.: Principle of the Equilibrium of Polyhedral Frames. In: Miscellaneous Technical Papers; Ch. Griffin & Co. Stationers' Hall Court, London 1881. Ch. XXXVI
6. Tarnai, T.: Oral addendum to the referee's report written by him on this paper, 1982

Acta Technica Academiae Scientiarum Hungaricae, 94 (1—2). pp. 81—90 (1982)

POWER SYSTEM DYNAMIC EQUIVALENTS — A SURVEY

G. HORNIÁK,* A. Y. SALIB*

[Manuscript received: 6 May, 1982]

The field of dynamic equivalents of interconnected power systems has been rapidly developed during the past decade. Several techniques have been advanced for constructing power system dynamic equivalents in the off-line mode as well as in the on-line mode. A survey of such techniques is presented.

Introduction

Dynamic modelling is a necessary step for the solution of many practical problems in planning as well as operational applications. Among such problems: transient and dynamic stability studies, dynamic security analysis, dynamic identification, on-line control, etc. The use of an exact model for the analysis of such problems may be too complex to be conveniently handled, even by large computers, due to various factors such as: the growing size of interconnected power systems, the need for more detailed representation of system components, the analytical development, the computational effort, etc. It may also be inadequate due to: unavailability of data (parameters, structure, operating conditions), inaccuracy of available data, many details may not be relevant for the particular objective of a given study, and computing errors may be larger than by using a suitable simplified model. Therefore, suitable simplifications, with a certain accuracy, in power system dynamic models are usually needed. The accuracy requirements of a simplified model may be defined in terms of different targets, as: satisfactory reproduction of given selected variables for given time intervals, and satisfactory reproduction of some properties of the real system.

Several techniques have been advocated for constructing dynamic equivalents in planning (off-line) mode and in the operations (on-line) mode. In the off-line methods sufficient information about external systems is required to construct a complete dynamic model for both study and external systems. The most usual approaches in this mode are coherency analysis [1–15] and modal reduction [16–35] techniques. There are other methods [36–44] which use different criteria for constructing dynamic equivalents. The on-line methods are used if the direct information on the configuration, parameters or operating state of external systems are not available. In this mode identification techniques are used to identify external system parameters [45–51].

* G. Horniák, Villamosenergia Ipari Kutató Intézet, Zrínyi u. 1, 1051 Budapest, Hungary

In this paper, a survey of power system dynamic equivalents is given; detailed descriptions were given in reference [57]. The methods proposed to simplify dynamic systems in control theory, that unrelated to power systems and the static equivalents as used in steady-state power system analysis, are outside the scope of this paper. References on these topics can be found in the bibliography [56].

Coherency based dynamic equivalents have been tested, using a real system, for the purpose of measuring the accuracy of the simplified models as well as the computational requirements. The results of this procedure are deferred to a later paper.

1. Coherency based dynamic equivalents

The coherency analysis procedure is usually made for machines which can be represented by constant voltage behind transient reactance and which are remote from an initiating disturbance. The coherency approach reduces the order by lumping together groups of machines, in the external system, which tend to swing together when perturbed by distrubances in the internal system. The possibility of obtaining a simplified but still accurate representation of the system depends on the existence of nontrivial groups of generators oscillating coherently. The definition of an equivalent generator, for a given group, implies further simplification for deriving the equivalent network. Identification of groups of coherent generators is the essential step in developing coherency based dynamic equivalents. The proposed methods of coherency recognition are reviewed below.

(i) The Relaxed Definition of Coherency [1–6]

Two generators will be said to oscillate coherently if their angular difference is constant within a certain tolerance over a certain time interval. Based on this definition, several techniques have been proposed for constructing dynamic equivalents, such as: comparison of simulated responses [1, 4] and network structural [2, 3, 27, 28].

(ii) The Max-Min Coherency Measure [7]

It is defined to measure the difference between the maximum and minimum deviations in the rotor angles of two generators over a certain time interval.

(iii) The RMS Coherency Measure [7, 8]

It is defined to measure the expected value of a time average of differences in voltage angle deviations on generator buses for a probabilistically described disturbance. The generalized algebraic formula of this measure is derived in a way that relates it to both the parameters of the power system state model and the disturbance vector.

(iv) The Transient Coherency Measure [9]

It is defined as a Taylor series approximation of a mean square coherency measure, where the number of terms increases as the observation interval increases in order to keep the approximation error within some limits. The mean square coherency measure is equivalent and uniquely related to the RMS coherency measure.

(v) Coherency Indices Derived from Weighted Eigenvectors [10]

A closed form expression for the rotor angles and speeds of generators in the transient period is obtained in terms of weighted eigenvectors under the assumption of linearity. From these eigenvectors the coherency indices are derived. Two coherency indices are defined as the relative measures of the maximum deviations between the rotor angles of two generators in the faulted period and contributed by oscillatory and nonoscillatory modes. The corresponding degree of deviations in the post-fault period is defined in another two coherency indices.

(vi) The Pattern Recognition Method [11]

Coherency recognition is made by examining three factors. They are defined as: r_1 measures the spread of initial machine accelerations in the potentially coherent group, r_2 measures the ratio of maximum admittance distance between any two machines in the group to the minimum admittance distance from any machine in the group to the area of disturbance and r_3 measures the spread of machine inertias.

(vii) The Singular Points Method [12]

Two generators are said to oscillate coherently if the difference between the angle differences of the two generators is less than or equal to a certain tolerance. The angle difference of each generator is defined as the difference between the angle coordinates of the stable operating point and that of the singular point of the post-fault system which corresponds to the expected system instability.

(viii) The Lyapunov Function Method [13]

A group of generators whose partial Lyapunov function is of sufficiently small value, compared with that of the entire system, is thought to oscillate coherently.

(ix) The Slow Coherency Definition [14, 15]

Separating the slow and fast variables of the power system model, the notation of the slow coherency is expressed in the following way. If we consider the r is the slowest modes of the system's response to any fault, then two generators are slowly coherent if the difference of their angles contains non of the r slowest modes.

2. Modal analysis based on dynamic equivalents

Several methods have been proposed to derive reduced order models for external systems or the entire power system based on modal analysis criteria. The general aspect of these methods is the reduction of the eigenvalues of the original system and only significant eigenvalues are kept for the dynamic analysis. Rules for mode elimination of the nondominant modes were defined according to different criteria. The proposed dynamic equivalents may be classified as follows.

2.1. Modal Reduction Techniques

(i) Davison [16] proposes a method for simplifying dynamic systems which is based on neglecting eigenvalues of the original system that are farthest from the origin and retaining only dominant eigenvalues. An extension of this method was proposed [17, 18] in which the eigenvalues are divided into three groups, depending on their location in the complex plane, and theree simplified models can be evaluated for initial, intermediate and final stages of transient response. For this method the eigenvalues and eigenvectors of the overall system are to be computed. A decomposition-aggregation technique [19] can be used with this method offering the computation of eigenvalues and eigenvectors of subsystems instead of the overall system. Davison's method has been used [20] to form reduced order models of system components separately, and then combining these reduced models to obtain a dynamic equivalent of the overall system.

(ii) In contrast to the above method, a well defined criteria based on modal analysis technique has been proposed [21, 22, 23] for simplifying the model of any given area of the real system, viewed from its terminal nodes. Such criteria require the determination of dominant modes in the area response to small perturbation of a given form. The equivalent procedure produces three different forms of equivalents: linearized state equations, diagonalized state equations and reduced state equations. Several criteria were postulated for selecting modes which could be eliminated: very large eigenvalues, modes with very small rows in the input matrix and modes with very small columns in the output matrix. The reduced state equations can also be obtained [25, 26] by retaining only those modes of the external area which strongly interact with the states of the study area. The dynamic equivalent may be used for transient stability studies [25] with nonlinear representation of the study area. A link between this technique and coherency based reduction is established from the generalized algebraic formula of the RMS coherency measure [24].

(iii) Modal reduction technique was proposed [27, 28] to derive simplified models, for the whole system, by retaining some dominant modes and simplifying the remainders, in which case the modes of the simplified models come out as coincident with a subset of the original modes. The selection of dominant modes depends on the

observability conditions and the influence of the modes, in the output variables, on the input. Analysis was given to indicate cases when modal reduction is compatible with coherency based reduction.

2.2. Order Reduction Techniques

Some attempts have been made to put the form of system equations in a reduced order with comparison of the state space form, such as:

(i) A polynomial matrix form [29] of the differential equations describing the dynamics of the system. The retained variables are those appearing at the interface between generating units and transmission system.

(ii) An operational transfer matrix form [30, 31] of system equations between internal generator angles and input mechanical torques. The dimension of this matrix is equal to the number of system generators. Thus, significant eigenvalues can be obtained without calculating all the eigenvalues.

2.3. Physical Reduction Techniques

State variable grouping technique was used [18] to obtain simplified models of systems based on the speed of response of the variables. The model is obtained by the omission of the derivatives of state variables associated with small time constants. The omission of some states and state derivatives may be accomplished in their corresponding to some physical assumptions [32].

2.4. Different Methods of Modal Analysis

(i) A topological method of reduction [33, 34] in which the block diagrams and the interconnections that are to exist in the reduced model are chosen, and a set of desired eigenvalues with their eigenvectors is specified. The parameters of the reduced model are then computed so as to give a dynamic system with the desired eigenvalues and with the difference between the desired and specified eigenvectors minimized.

(ii) A diakoptically based eigenvalue method [35] which involves tearing the overall system into subsystems, formulating its characteristic equations and subsequently determining the eigenvalues. Eigenvalues are computed using a method that finds one eigenvalue at a time, offering the flexibility of computing some modes.

3. Dynamic equivalents based on different methods

Several procedures have been proposed to obtain dynamic equivalents for power system models using different criteria. These procedures are classified as follows, see [57] for detailed description.

(i) Dynamic equivalents developed in terms of equivalent circuits using distribution factors method [36], or by formulating an active network equivalent for the external area [37].

(ii) Dynamic equivalents based on different representations of system generators [38–40] according to their electrical distance from the fault location. Reference [40] proposes a factor that would give guidance to the choice of modelling accuracy required for each generator.

(iii) Dynamic equivalent based on the geometric properties of a quadratic type Lyapunov [41].

(iv) Dynamic equivalent based on multi-area dynamic energy balance technique [42, 43].

(v) Dynamic equivalent based on the theory of linear systems [44].

4. On-line dynamic equivalents

In the on-line mode, techniques are used to estimate equivalents of external systems using information on the present configuration of the study system and data telemetered to the control center from points within the study system, including boundary points. The best possibility for accomplishing this procedure seems to be in the application of identification techniques, which refer to the determination of the essential characteristics of the dynamic system by observing the response of system variables to random system inputs either natural or intentional. The proposed methods for on-line dynamic equivalents may be classified as given below. It will be noted that, many other procedures proposed concerning the development and applications of identification techniques to the estimation of unknown power system dynamics in neighbouring areas for various aims. C.f. [52–55].

4.1. Methods assume partial knowledge of external systems

In this case an off-line technique can be used to represent the steady-state performance of external systems, while an identification technique is used to represent their dynamics. These methods are:

(i) Coherent machine grouping is used [45] to form possible equivalents for various external system conditions, processing real-time measurements for these equivalents and computation of the likelihood functions. The true equivalent is the one that is the maximum of the likelihood function.

(ii) The generalized Thevenin's theory is used [46, 47] to represent static equivalent of the external system and stochastic linear difference equations to represent its dynamics. A recursive least-mean-square algorith is used to estimate the parameters of the stochastic model.

(iii) The REI (Radial, Equivalent, and Independent) approach is used [48] to determine the external system equivalent, together with a method for tracking on-line injection and network changes in the external system, by modifying the parameters of the equivalent.

4.2. Methods assume certain models for external systems and identification techniques are used to identify the parameters of such models

These methods are:

(i) Maximum likelihood technique is used [49] to identify parameter values for a specified equivalent structure of the external system. Measurements are made only within the study system without the intentional perturbation of the system.

(ii) An equivalent model with damping and inertia, explicity expressed, is chosen [50], an intentional disturbance of pulsed excitation is applied to generators of the study system and a least-squares algorithm is used to estimate the equivalent parameters.

(iii) A reduced order power system model consisting of two decoupled underdamped second order systems is assumed [51] whose damping factors and undamped natural frequencies are to be identified by a Model Adaptive Reference Control system.

Conclusions

In the previous sections different methods for simplifying power system dynamic models in the off-line mode as well as in the on-line mode have been mentioned. These methods are classified according to the basis of the techniques used for the construction of the dynamic equivalents.

The most usual approaches to power system dynamic equivalents in the off-line mode, are coherency analysis and modal reduction techniques. Coherency approach reduces the order by lumping together groups of machines, in the external system, which tend to swing together when perturbed by disturbances in the internal system. Most coherency studies are for linearized electromechanical models. This simplification has been justified by experimental evidence that coherency observed on linearized model is preserved for large disturbances of the nonlinear model [4, 14, 15]. By modal analysis techniques the number of eigenvalues of the original power system model is reduced according to certain criteria, and only significant eigenvalues are kept for the dynamic analysis. Coherency based dynamic equivalents have been compared with modal analysis based dynamic equivalents and it has been observed that either the physical variables or the modes retained by the two techniques do not necessarily coincide. Different attempts have been made to indicate cases when a modal reduction is compatible with coherency based reduction [7, 8, 27, 28]. Several discussions were given in literature concerning the applicability of the off-line methods for simplifying large scale power systems. Some of the predescribed methods have no such applicability due to some limitations of the techniques e.g., [18, 32, 33] or due to the lack of theoretical basis e.g., [36, 38, 39].

In the on-line mode, system identification techniques are used to estimate equivalents of neighbouring systems using information which can be obtained within

the study system. The proposed techniques are classified as: a — Methods assume partial knowledge of external systems [45–48]. In this case an off-line technique can be used to represent the steady-state performance of external systems, while an identification technique is used to represent their dynamics. b — Methods assume certain models for external systems and identification techniques are used to identify the parameters of such models [49–51].

References

1. Chang, A.—Adibi, M. M.: Power System Dynamic Equivalents. *IEEE Trans.*, Vol PAS-**89,** No. 8 Nov./Dec. (1970), 1737–1744
2. Marconato, R.—Mariani, E.—Saccomanno, F.: Application of Simplified Dynamic Models to the Italian Power System. *IEEE PICA Conf. Proc.* (1973), 118–126
3. Di Caprio, U.—Marconato, R.: A Novel Criterion for the Development of Multi-Area Simplified Models Oriented to the On-Line Evaluation of Power System Dynamic Security. *PSCC* (1975), Paper No. 3.2/3.
4. Podmore, R.: Identification of Coherent Generators for Dynamic Equivalents. *IEEE Trans.*, Vol. PAS-**97,** No. 4 July/August (1978), 1344–1354
5. Podmore, R.: A Comprehensive Program for Computing Coherency-Based Dynamic Equivalents. *IEEE PICA Conf. Proc.* (1979), 298–306
6. Hackett, D. L.: Coherency Based Dynamic Equivalent Application Experience-Eastern US Data Base. *IEEE PICA Conf. Proc.* (1979), 307–313
7. Schlueter, R. A.—Akhtar, H.—Modir, H.: An RMS Coherency Measure: A basis for Unification of Coherency and Modal Analysis Model Aggregation Techniques. Paper No. A 78 533–2, *IEEE PES Summer Meeting* (1978)
8. Lawler, J.—Schlueter, R. A.: Model-Coherent Equivalents Derived from an RMS Coherency Measure. *IEEE Trans.*, Vol. PAS-**99,** No. 4 July/Aug. (1980), 1415–1425
9. Schlueter, R. A.—Akhtar, H.: A Transient Coherency Measure and its Use to Analyze System Transient Response. Paper No. A 79 480-5, *IEEE PES Summer Meeting* (1979)
10. Pai, M. A.—Adgaonkar, R. P.: Identification of Coherent Generators Using Weighted Eigenvectors. Paper No. A 79 022-5, *M PES Winter Meeting* (1979)
11. Lee, S. T. Y.—Schweppe, F. C.: Distance Measures and Coherency Recognition for Transient Stability Equivalents. *IEEE Trans.*, Vol. PAS-**92,** No. 5 Sept./Oct. (1973), 1550–1557
12. Spalding, B. D.—Yee, H.—Goudie, D. B.: Coherency Recognition for Transient Stability Studies Using Singular Points. *IEEE Trans.*, Vol. PAS-**96,** No. 4 July/August (1977), 1368–1375
13. Ohsawa, Y.—Hayashi, M.: Coherency Recognition for Transient Stability Equivalents Using Lyapunov Function. *PSCC* (1978), 815–818.
14. Winkelman, J. R.—et al.: An Analysis of Interarea Dynamics of Multi-Machine Systems. *IEEE Trans.*, Vol. PAS-**100,** No. 2 Feb. (1981), 754–763
15. Avramovic, B.—et al.: Area Decomposition for Electromechanical Models of Power Systems. *Automatica,* **16,** (1980), 637–648
16. Davison, E. J.: A Method for Simplifying Linear Dynamic Systems. *IEEE Trans.*, Vol. AC-**11,** No. 1 January (1966), 93–101
17. Kuppurajulu, A.—Elangovan, S.: System Analysis By Simplified Models. *IEEE Trans.*, Vol. AC-**15,** April (1970), 234–237
18. Kuppurajulu, A.—Elangovan, S.: Simplified Power System Models for Dynamic Stability Studies. *IEEE Trans.*, Vol. PAS-**90,** No. 1 Jan./Feb. (1971), 11–23
19. Radhakrishna, C.—et al.: Simplified Modal Control for Dynamic Stability Studies. Paper No. A 78 609-0, *IEEE PES Summer Meeting* (1978)
20. Altalib, H. Y.—Krause, P. C.: Dynamic Equivalents By Combination of Reduced Order Models of System Components. *IEEE Trans.*, Vol. PAS-**95,** No. 5 Sept./Oct. (1976), 1535–1544
21. Undrill, J. M.—Turner, A. E.: Construction of Power System Electromechanical Equivalents By Modal Analysis. *IEEE Trans.*, Vol. PAS-**90,** No. 5 Sept./Oct. (1971), 2049–2059

22. Undrill, J. M.—et al.: Electromechanical Equivalents for Use in Power System Stability Studies. *IEEE Trans.*, Vol. PAS-**90,** No. 5 Sept./Oct. (1971), 2060–2071
23. Price, W. W.—et al.: Testing of the Modal Dynamic Equivalent Technique. *IEEE Trans.*, Vol. PAS-**97,** No. 4 July/August (1978), 1366–1372
24. Schlueter, R. A.—Ahn, U.—Modir, H.: Modal Analysis Equivalents Derived Based on the RMS Coherency Measure. Paper No. A 79 061-3, *IEEE PES Winter Meeting* (1979)
25. Spalding, B. D.—et al.: Use of Dynamic Equivalents and Reduction Techniques in Power System Transient Stability Computation. *PSCC* (1975), Paper No. 3.2/10
26. Spalding, B. D.—Goudi, D. B.: The Use of Dynamic Equivalents in the Analysis of Power System Steady State Stability. *IFAC Symposium on Automatic Control and Protection of Electric Power Systems,* Melbourne, 21–25 Feb. (1977), 119–124
27. Saccomanno, F.: Development and Evaluation of Simplified Models for Multimachine Electric Power Systems. *PSCC* (1972) Paper No. 3.1/22
28. Saccomanno, F.: Dynamic Modelling of Multimachine Electric Power System. *2nd Formator Symposium on Mathematical methods for the analysis of large systems.* Praga, 18–21 June (1974)
29. Van Ness, J. E.—Brasch Jr., F. M.: Polynomial Matrix Based Models of Power System Dynamics. *IEEE Trans.*, V10. PAS-**95,** No. 4 July/August (1976), 1465–1472
30. Okubo, S.—Suzuki, H.—Uemura, K.: Modal Analysis for Power System Dynamic Stability. *IEEE Trans.*, Vol. PAS-**97,** No. 4 July/August (1978), 1313–1318
31. Obata, Y.—Takeda, S.—Suzuki, H.: An Efficient Eigenvalue Estimation Technique for Multimachine Power System Dynamic Stability Analysis. *IEEE Trans.*, Vol. PAS-**100,** No. 1 January (1981), 259–263
32. Alden, R. T. H.—Nolan, P. J.: Evaluating Alternative Models for Power System Dynamic Stability Studies. *IEEE Trans.*, Vol. PAS-**95,** No. 2 March/April (1976), 433–440
33. Van Ness, J. E.—Zimmer, H.—Cultu, M.: Reduction of Dynamic Models of Power Systems. *IEEE PICA Conf. Proc.* (1973), 105–112
34. Van Ness, J. E.: Improving Reduced Dynamic Models of Power Systems. *IEEE PICA Conf. Proc.* (1975), 155–157
35. Nolan, P. J.–Janischewskyj, W.: A Diakoptical Approach to the Eigenvalue Problem in Power System Dynamic Stability Studies. *IEEE PICA Conf. Proc.* (1977), 211–219
36. Brown, H. E.—et al.: A Study of Stability Equivalents. *IEEE Trans.*, Vol. PAS-**88,** March (1969), 200–207
37. Roberge, R. M.—Etezadi-Amoli, M.: Active Network Equivalent of Large Scale Transient Stability Analysis. Paper No. A 76 420-0, *IEEE PES Summer Meeting* (1976)
38. Dandeno, P. L.—Kundur, P.: Simulation of the Non-Linear Dynamic Response of Interconnected Synchronous Machines. Part II- Network Solution Procedures and Comparisons of Particular Computational Methods. *IEEE Trans.*, Vol. PAS-**91,** No. 5 Sept./Oct. (1972), 2069–2077
39. Laha, A. K.—Bollinger, K. E.: Multi-Machine Modelling for Power System Generators. *IEEE PICA Conf. Proc.* (1973), 294–302
40. Ghafurian, A.—Cory, B. J.: Determination of Equivalents for Power System Transient Stability Studies. *PSCC* ?5), Paper No. 3.2/8
41. De Sarkar, A. K.—Rao, N. D.: Dynamic-System Simplification and an Application to Power-System-Stability Studies. *Proc. IEE* **119,** No 7 July (1972), 904–910
42. Stanton, K. N.: Power System Dynamic Energy Balance. pp. 147–167 of the book "Real Time Control of Electric Power Systems", Edited by H. Handschin, Elsevier 1972
43. Stanton, K. N.: Power System Dynamic Simulation Using Models With Reduced Dimensionality. *JACC* (1972), 415–419
44. Yamaguchi, T.—Takeda, S.: Derivation of Dynamic Equivalents for Power System Stability Studies. *PSCC* (1978), 807–814
45. Giri, J.—Bose, A.: Identification of Dynamic Equivalent for On-Line Transient Security Assessment. Paper No. A 77 514-3, *IEEE PES Summer Meeting* (1977)
46. Ibrahim, M. A. H.—Mostafa, O. M.—El-Abaid, A. H.: Dynamic Equivalents Using Operating Data and Stochastic Modeling. *M Trans.*, Vol. PAS-**95,** No 5 Sept./Oct. (1976), 1713–1722
47. Mostafa, O. M.: Partial Identification of Electric Power System Equivalents. *Proc. of the* 4th *IFAC Symposium on Identification and System Parameter Estimation* (Edited by N. S. Rajbman), Tibilisi, USSR 1976, 891–901
48. Dopazo, J. E.—Irisarri, G.—Sasson, A. M.: Real-Time External System Equivalent for On-Line Contingency Analysis. *IEEE Trans.*, Vol. PAS-**98,** No. 6 Nov./Dec. (1979), 2153–2171

49. Price, W. W.—et al.: Dynamic Equivalents from On-Line Measurements. *IEEE Trans.*, Vol. PAS-**94,** No. 4 July/August (1975), 1349–1357
50. Yu, Y. N.—El-Sharkawi, M. A.: Estimation of External Dynamic Equivalents of a Thirteen-Machine System. *IEEE Trans.*, Vol. PAS-**100,** No. 3 March (1981), 1324–1332
51. Grund, C. E.: Power System Modal Identification from Large Scale Simulations Using Model Adaptive Reference Control. *IEEE Trans.*, Vol. PAS-**97,** No. 3 May/June (1978), 780–788
52. Schwartz, M. W.—Park, G. L.—Schlueter, R. A.: Model Identification Using Tie Line Power and Frequency Measurements. *Automatica* **12,** (1976), 23–30
53. Yu, Y. N.—El-Sharkawi, M. A.—Wvong, M. D.: Estimation of Unknown Large Power System Dynamics. *IEEE Trans.*, Vol. PAS-**98,** No. 1 Jan./Feb. (1979), 279–289
54. Lequarre, J. Y.—Sen, A.: On-Line Model Identification as an Aid to Transient Stability Augmentation. Paper No. A 80 086-9, *IEEE PES Winter Meeting* (1980)
55. Lequarre, J. Y.—Sen, A.—Meisel, J.: Effectiveness of Local Control Schemes Using Model Identification for Transient Stability Augmentation. Paper No. A 80 087-7, *IEEE PES Winter Meeting* (1980)
56. Castro-Leon, E. G.—El-Abiad, A. H.: Bibliography on Power System Dynamic Equivalents and Related Topics. Paper No. A 80 034-9, *IEEE PES Winter Meeting* (1980)
57. Salib, A. Y.: A Survey of Simplified Power System Dynamic Models. Internal Report No. 52. 81-016-2, Institute for Electrical Power Research, Budapest — Hungary, October 1981.

Acta Technica Academiae Scientiarum Hungaricae, 94 (1—2), pp. 91—100 (1982)

INVESTIGATION OF THE ENGAGEMENT OF HARMONIC DRIVES. PART I.

J. PÉTER*

[Manuscript received: April 12, 1982]

In harmonic drives the teeth of one gear of a pair of gears are carried by a flexible gear body. During the running of the drive, the flexible wheel body suffers a wave-like deformation. The present paper deals with this particular case of the engagement of gears. The engagement of two gears is attributed to that of a pair of gears of a variable axle deflection and to a variable axle base of a spur gear and a circular spline, and the problem is reduced to the simple phenomenon of the engagement of a normal circular spline, and a spur gear the centre of rotation of which is displaced from its geometric centre.

1. Introduction

The harmonic drive is one of the varieties of the gear drives. A circular spline and a spur gear participate in the transformation of the motion. Dompared with the classic gear drives, the essential difference may be found in the fact that the teeth of the spur gear are carried by a flexible wheel body (Fig. 1. a). The circular spline does not differ from the usual one. The third central element is the wave generator, the function of

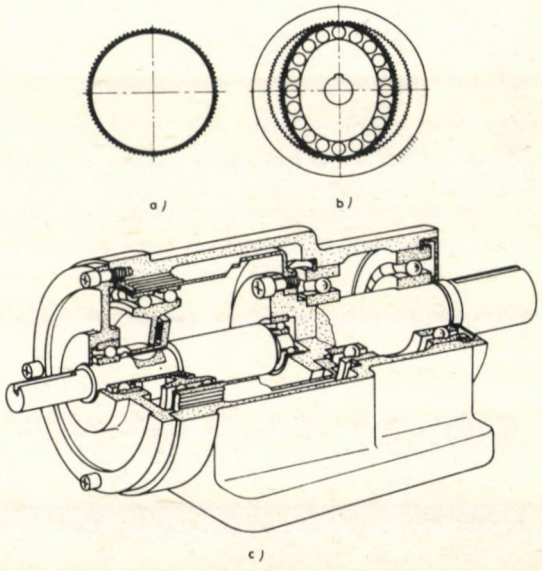

Fig. 1. Harmonic drive, type *bh*

* Péter, J., Derkovits u. 54, I. 3., H-3529 Miskolc, Hungary

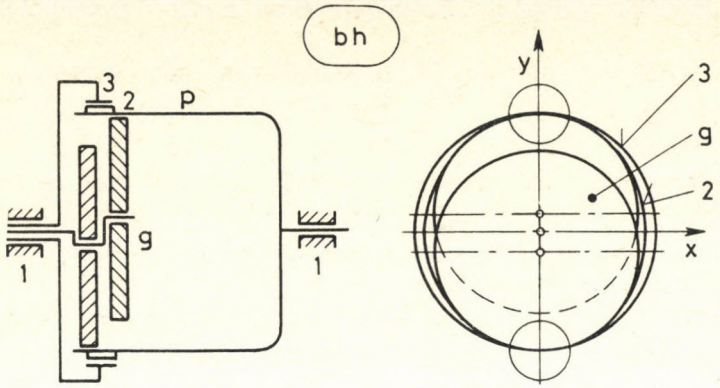

Fig. 2. Simplified scheme drawing of the harmonic drive type *bh*. *1*case; *2* flexible spur gear, wave wheel; *3* inflexible circular spline, ring wheel; *g* generator; *p* mantle

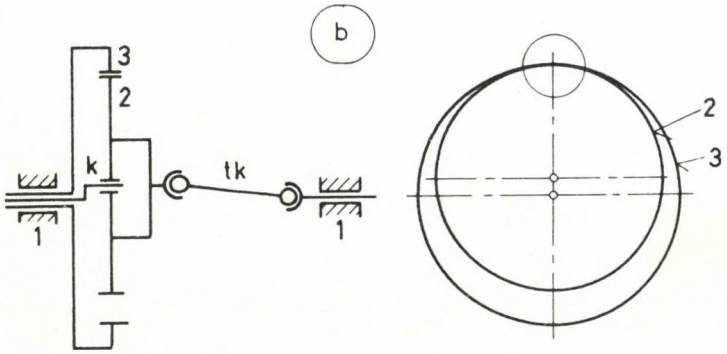

Fig. 3. Simplified scheme drawing of epicyclic train, type *b*. *1* case; *2* spur gear, satellite; *3* circular spline, ring wheel; *tk* coupling

which is to bring gears into engagement and to forward the zone of meshing (Fig. 1. b). The elements mentioned are comprised in a casing or stand (Fig. 1. c) [1].

The harmonic drive might be ranged among the family of the epicyclic train and might be compared to the simple *b*-type [3] planetary drive. The flexible satellite *2* (Fig. 2) of the harmonic drive does not engage at a single point, but at two points, to the circular spline. The function of the wave generator *g* is the same as that of the arm *k* (Fig. 3). The function of the casing *p* is similar to that of the coupling *tk*. This simple type of a harmonic drive comprising a spur gear and a circular spline meshing to each other in a wave-like way, may be called type *bh*.

2. The flex-spline

The flexspline is, prior to the assembling of the drive a cylindrical solid of revolution. It is assumed that

a) the middle surface K is a cylinder of radius R_0 (Fig. 4),

b) the generator g exerts effect upon the flexspline in a plane,

c) the middle surface K, after the wave generator having been slipped into the flexspline transits into the flexible surface R and an arbitrary generatrix a of the middle surface K transits into the surface line a',

d) the divergence of the surface line a' from the straight line may be neglected,

e) the displacement of the point A_0 lying on the middle surface K in the direction of the principal deformation axis is w_0 ($\overline{A_0 A_0'} = w_0$),

f) the plane of the generator (the plane x, y) intersects the middle surface K in the centre-line k and the flexible surface R in the flexible line r,

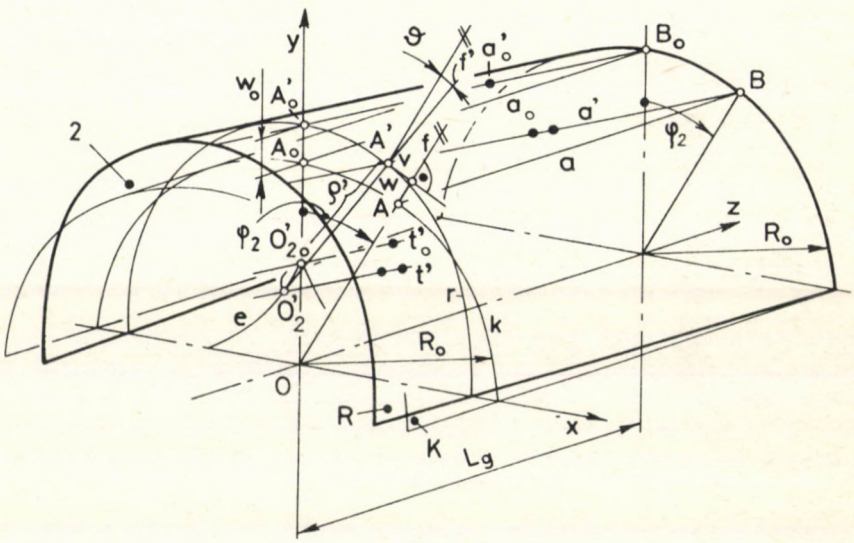

Fig. 4. Middle surface K and flexible surface R of the flexspline (due to symmetry only the half of them are investigated). k middle line; r flexible line; e evolute of the flexible line r; a generatrix of the middle surface K; a' surface line of the flexible surface R

g) the radial displacement w of an arbitrary point A of φ_2 angular coordinate of the centre-line k, its tangential displacement v, the normal f' of R at point A' forms an angle ϑ with the normal f of K at point A.

h) the radius of the osculatory circle associated with point A' of R is ρ', the centre of the osculatory circle is O_2',

j) the geometrical locus of the centres of the osculatory circles is the evolute e,

k) the flexspline is geared as a normal cylindrical wheel,

l) its teeth are situated, as compared with the middle surface K, in the direction of the generatrix and, as compared with the surface R in the direction of the surface line,

m) the deformation of the teeth in relation to the displacement of the points on the middle surface might be neglected; the teeth may be considered inflexible, in turn, the tooth groves may be taken as flexible (similarly to an endless chain: the teeth could be taken as chain links and the tooth grooves as hinges),

n) the axis of symmetry f of any arbitrary tooth transits into the plane of the wave generator, into f',

the symmetry axis f' of the tooth is the normal of r (Fig. 6),

p) the centre O_2 associated with the tooth on the axis of symmetry f' of the tooth as compared to the line r, may always be found to be at a distance R_0.

3. Engagement of the teeth of the harmonic drive

Prior to the investigations let us compare the satellite type b with the harmonic drive type bh. Stopping the arm k in the b-type epicyclic train (Fig. 3) the engagement of a spur gear and a circular spline may be investigated. Let us do the same with the harmonic drive; stop the wave generator g (Fig. 2). In this case, the teeth of the spur gear are moving on a path defined by the surface R (Figs 4 and 5) or by the linear r (Fig. 6) and are meshing at two points with the circular spline (Figs 1b and 2).

We assume that the two meshing zones are symmetrical, therefore, it is sufficient to investigate only one of them. The inflexible teeth situated in the direction of the surface lines of the surface R (Chapter 2) of the flexible wheel are engaging with the teeth of the circular spline like a pair of gears of a circular spline and a spur gear of a deflected axis. The angle of the axis deflection associated with each tooth as well as the axle base changes depending on the rotation (the angle φ_2) in relation to the principal deformation axis (Fig. 5). In the plane of the principal deformation axis (i.e. in the plane x, y) the axes intersect each other (Figs 4 and 5).

4. Investigation of the engagement in the plane of the wave generator

The zone of engagement is to be found in the proximity of the principal deformation axis. At the proximity of the principal deformation axis the angle of the axis deflection is neglectable. Neglecting the effect of the intersection of the axes exerted on the engagement, we may continue the investigations in the plane of the wave generator (Fig. 6). The centre and that of the rotation of the circular spline are at point O_3. The centre O_2 belonging to the investigated tooth of the spur gear is to be found on the axis of symmetry of tooth f' (at a distance R_0 from point A'), and the momentary point of rotation O_2' is on the involute e of line r.

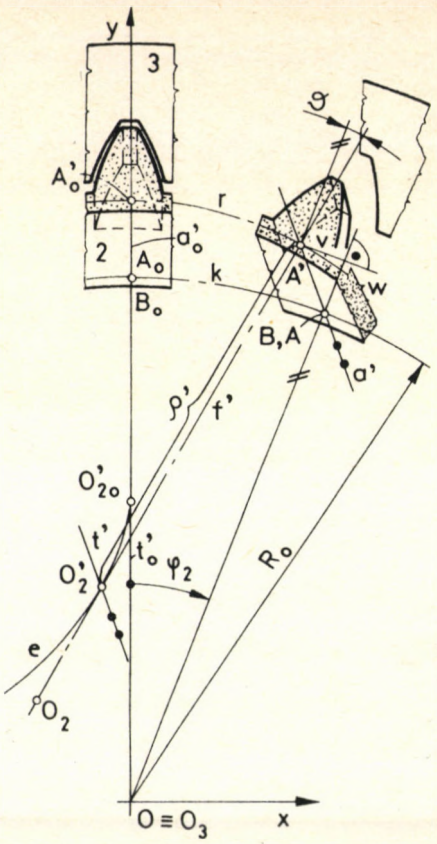

Fig. 5. Teeth of the pair of gears of internal and external toothings of variable axle deflection angle and variable axle base. t' is the momentary axis of rotation associated with the surface line a' of the flexible surface R

In case where the involute of the tooth profile (the radii of the basic circles being r_{a2} and r_{a3}), the momentary pole P' of the engagement is defined by the tooth normal $\vec{n}_{23}$ and by the straight line intersecting the centres of rotation O'_2, O_3.

The momentary transmission ratio is

$$i^g_{2'3} = \frac{\overline{O_3P'}}{\overline{O'_2P'}}, \tag{1}$$

where the superscript g of the transmission ratio designates the member which is at a standstill or to which the reference system is fixed, while the subscripts indicate the direction of drive 2→3.

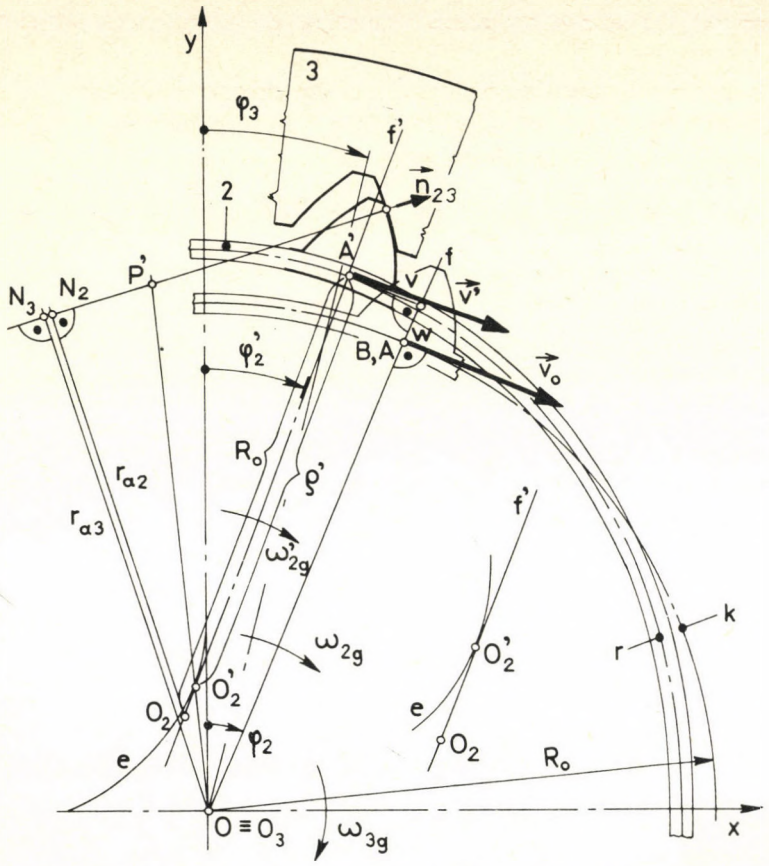

Fig. 6. Engagement of two teeth of a pair of gears of internal and external toothings of variable axle base. K middle line; r flexible line; f normal at the point A of the middle line k, symmetry axis of tooth which transits into the normal f'; O_2 centre associated with the tooth investigated of the flexspline, and O'_2 its momentary centre of rotation; O_3 is the centre and centre of rotation of the circular spline

Let us investigate how the transmission ratio of the tooth-pair changes if the generator is of disc design (Fig. 2). In case where the flexspline is deformed with two large diameter discs eccentrically supported in bearings, in dependence on the construction parameters, at the peak of the deformation wave, the flexspline closely osculates to the disc along the arc belonging to a central angle 35...60° [2]. Assuming that the zone of engagement is situated within the arc of the osculation of flexspline to the disc.

On the arc of osculation to the disc the radius of curvature of the elastic line r is constant, $\rho' = R'$. The axis of symmetry of the tooth f' is situated in the radial direction

of the disc while the momentary centre of rotation O'_2 is in the centre of rotation of the disc (Fig. 7).

The distance between the centre O_3 of the circular spline and the centre O_2 associated with the investigated tooth of the flexspline may be calculated as the function of the rotation φ'_2 from the relationship

$$\overline{O_2O_3} = a' = \sqrt{e^2 + (R_0 - R')^2 - 2e(R_0 - R')\cos\varphi'_2} \tag{2}$$

wherein

e = arm of eccentricity of disc generator,
R_0 = radius of central circle,
R' = radius of curvature of elastic line r along arc of osculation to disc,
φ'_2 = rotation of axis of symmetry of tooth investigated as compared to principal deformation axis.

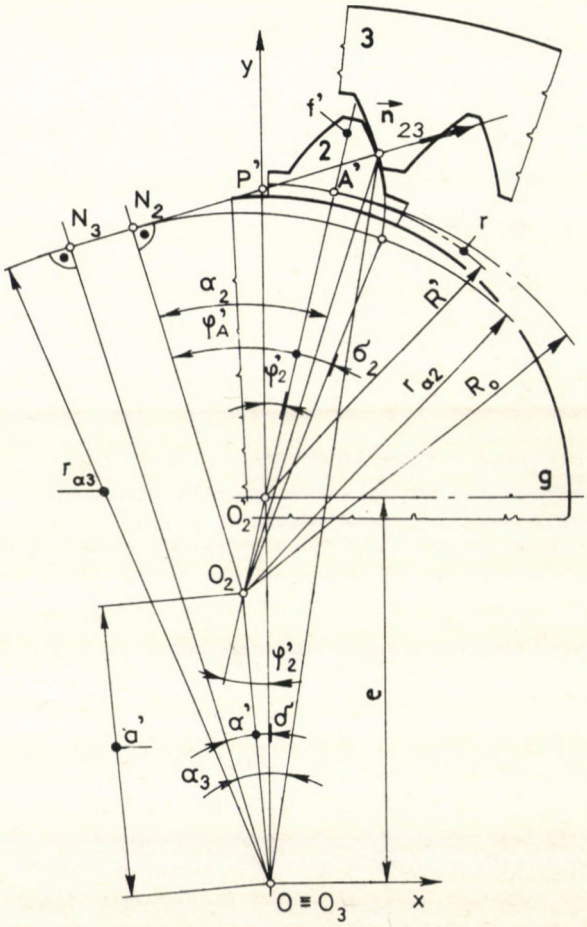

Fig. 7. Engagement of two teeth of a pair of gears of internal and external toothing. The generator is of disc-type. O_2 is the centre belonging to the investigated tooth of the flexible spline and O'_2 is the momentary centre of rotation, the centre of rotation of the disc

With the knowledge of a'

$$\alpha' = \arccos \frac{m(z_3 - z_2)\cos \alpha_0}{2a'}, \tag{3}$$

$$\delta = \arcsin \frac{(R_0 - R')\sin \varphi'_2}{a'}, \tag{4}$$

wherein

m = modul,
z_2 and z_3 = number of teeth,
α'_0 = basic profile angle.

With the knowledge of α' and δ, the momentary transmission ratio (1) is

$$i^g_{2'3} = \frac{\overline{O_3P'}}{\overline{O_3P'} - \overline{O'_2O_3}} = \frac{1}{1 - \dfrac{2e\cos(\alpha' + \delta)}{z_3 m \cos \alpha_0}}. \tag{5}$$

In describing the harmonic drives the great number of teeth simultaneously engaging is a stereotype attribute. At the nominal loading the 10...40 per cent of the teeth of the flexspline may be engaged. However, in an unloaded drive or at a fragmentary loading of the nominal one within the zones of engagement only the engagement of one or two pairs of teeth is typical. Let us investigate how the transmission ratio changes in case of individual engagement.

Assuming that the middle surface K is unstreachable. In such cases the absolute value of the velocity (Fig. 6) of point A' as well as the point A or B (Fig. 4) is the same: $|\vec{v}'| = |\vec{v}_0|$.

If at point $A'v' = \omega_{2'g}R'$, at point $Av_0 = \omega_{2g}R_0$, wherein $\omega_{2'g}$ is the angular velocity of the investigated tooth of the flexspline as compared with the generator, ω_{2g} is the angular velocity of the axle of the flexspline as compared with the wave generator.

Making use of the equality of the absolute values of the velocities of points A' and A results in

$$\omega_{2'g} = \omega_{2g} \frac{R_0}{R'}. \tag{6}$$

The momentary transmission ratio (1) with the angular velocities

$$i^g_{2'3} = \frac{\omega'_{2g}}{\omega_{3g}}, \tag{7}$$

wherein ω_{3g} is the angular velocity of wheel *3* as compared with the wave generator.

In case of two degrees of freedom the engagement between of the transmission ratios of the harmonic drive may be given with the relationship

$$i^g_{23}(i_{3g} - 1) = i_{2g} - 1 \tag{8}$$

where

$$i_{23}^{g} = \omega_{2g}(\omega_{3g}, i_{3g}) = \omega_3/\omega_g \text{ and } i_{2g} = \omega_2/\omega_g.$$

Let us fix the circular spline to the casing (Fig. 1c), be the driving element the wave generator and the driven one the flexspline (the direction of drive being $g \rightarrow 2$). From Eq. (8) the transmission ratio is

$$i_{g2}^{3} = \frac{1}{1 - i_{23}^{g}}. \tag{9}$$

Taking into account the relationships (6, 7, 9) within the individual engagement the transmission ratio changes according to the relationship

$$i_{g2}^{3} = \frac{1}{1 - \frac{R'}{R_0} i_{2'3}^{g}} = f(\varphi_2') \tag{10}$$

5. Example

Let us investigate how the transmission ratio of a drive gear changes if it is characterized by the data: $z_2 = 190$, $z_3 = 192$, $m = 1$ mm, $\alpha = 20°$, $e = 3.9$ mm, $R_0 = 97.1$ mm, $R' = 94.4$ mm.

The point at the tooth tip edge of the circular spline engages at $\varphi_2' = -4.83°$. At this moment $\alpha' = 40.226°$, $\delta = -10.644°$, $i_{2'3}^{g} = 1.039$, $i_{g2}^{3} = -98.296$. The point on the tooth tip edge of the flexspline engages at $\varphi_2' = -4.045°$, $\alpha' = 39.719°$, $\delta = -8.969°$, $i_{2'3}^{g} = 1.038\,6°$, $i_{g2}^{3} = -103.0025$. It is to be seen that while the pair of teeth engages in the interval $-4.045°$; $-4.83°$, the transmission ratio of the drive gear changes between $-98.296 \ldots -103.0025$ and, at the same time, the transmission ratio of the drive calculated on the basis of the number of teeth would be $i_{g2}^{3} = -95$. It is to be noted that beyond the given very small interval theoretically engaged by their edges (in practice along the tooth-profiles in the proximity of the tooth tip edges), and their transmission ratio fluctuates at about that calculated on the basis of the number of the teeth.

6. Summary

The engagement of the teeth of the harmonic drive my be investigated on the analogy of the epicyclic train type *b*. Instead of the arm, the generator is brought to a standstill, and such a pair of of gears is investigated where two zones of engagement are present. It is assumed that the engagement zones are symmetrical, wherefore, it is sufficient to investigate only one of them.

One assumes that the teeth of the flexspline are inflexible and are situated in the direction of the surface lines of the surface and the tooth-grooves are flexible.

Each of the teeth of the flexible spur gear and those of the inflexible circular spline is engaging like those of a pair of a spur gear and a circular spline of deflecting axle. The axle base and the angle of the axle deflection changes depending on their deflection related to the principal deformation axis.

By continuing the investigation in the plane of the generator, the problem will be reduced to the mere simple case of the engagement of a normal circular spline and a spur gear of a centre of rotation displaced in comparison to its centre. The transmission ratio of the "pair of wheels" is not constant.

References

1. Musser, C. W.: The Harmonic Drive. *Machine Design*, **32** (1960). 160–173
2. Шувалов, С. А.–Волков, А. Д.: Деформация гибкого колеса волновой передачи двумя дисками. *Известия ВУЗов. Машиностроение* (1971) 10, 44–49
3. Terplán, Z.–Apró, F.–Antal, M.–Döbröczöni, Á.: Epicyclic Trains. Műszaki Könyvkiadó, Budapest 1979, p. 258

Acta Technica Academiae Scientiarum Hungaricae, 94 (1—2), pp. 101 (1982)

BOOK REVIEW

G. FRANZ (Schriftleiter) *Beton-Kalender 1982*, Taschenbuch für Beton-, Stahlbeton- und Spannbetonbau sowie die verwandten Fächer.
Verlag von Wilhelm Ernst u. Sohn, Berlin—München 1982, Teil I: 1228 Seiten, Teil II: 1015 Seiten, Literaturnachweise, Stichwortverzeichnis.

Dieses Werk erscheint traditionsgemäß von Jahr zu Jahr wieder und bietet die Zusammenfassung der neuesten theoretischen und praktischen Kenntnisse des Beton- und Stahlbetonbaus in verjüngter Form. Professor Dr. Ing. Dr. Ing. E. h. G. Franz em. Professor der Technischen Universität Karlsruhe hat mit Hilfe der besten Kräfte des Faches den Stoff der verschiedenen Kapitel vorzüglich dargeboten. Sein Bestreben war es einen entsprechenden Überblick der aktuellen Fragen, besonders der neuesten Forschungsergebnisse des Betonfaches zu sichern und dadurch das zeitgemäße Bauen und die wirtschaftliche Anwendung und Ausnützung der geistigen, bzw. materiellen Werte zu fördern.

Der *erste Band* des Buches behandelt in 21 Kapiteln die bezeichnenden Eigenschaften der verschiedenen Baustoffe, und unterrichtet eingehend über die nötigen Kenntnisse der Konstruktionsplanung. In dem äußerst vielseitigen Stoff bedeuten eine besonders große Hilfe für den Entwurfsingenieur die von Prof. F. Czerny zusammengestellten Tafeln, welche die statischen Angaben für Rechteckplatten von verschiedenen Seitenverhältnissen bei gleichmäßig verteilter und nach Dreieckdiagramm veränderlicher Belastung enthalten.

Ein anderer ebenfalls sehr eingehend behandelter Teil des Buches — Verfasser: Proof. H. Duddeck und Prof. H. Ahrens — befaßt sich mit der Statik der Stabtragwerke und gibt einen verzüglichen Überblick von den verschiedenen genauen und annähernder Rechenverfahren. Sein reiches Tafelmaterial bietet eine außerordentlich nützliche Hilfe bei der Berechnung von Stabtragwerken und verschiedenen Rahmentragwerken. Besonders bedeutend ist die von Prof. N. Dimitrov geschriebene Zusammenfassung der Regel der Festigkeitslehre, sowie das Kapitel von Prof. E. Grasser über die Bemessung der Stahlbeton-Konstruktionselemente.

Der *zweite Band* des Buches behandelt hauptsächlich praktische Fragen. Das ausführliche Kapitel von G. Goffin teilt die gegenwärtig in der BRD gültigen Normen und Bestimmungen mit, welche sich auf die Planung und Ausführung von Beton-, Stahlbeton- und Spannbetonbauten beziehen. Nacher werden von Prof. H. Paschen die Bauverfahren mit Betonfertigteilen erörtert, mit der Betonung der Vorteile und Schwierigkeiten dieser Bauart. W. Klöckner und sene Mitverfasser behandeln die verschiedenen Gründungsmethoden, mit besonderer Hinsicht auf die Ausführungsprobleme. Schließlich werden die Abdichtungsfragen der Bauten von R. Linder mit besonderer Achtung auf die Grundwasserisolation erörtert.

Zusammenfassend kann festgestellt werden, daß der jüngste, 71. Jahrgang des Beton-Kalenders den vorhergehenden ähnlich — für die Fachkreise, die sich mit Beton-, Stahlbeton- und Spannbetonbau befassen, ein wertvolles Handbuch bedeutet und nicht nur im Verlagsland sondern auch weit über seine Grenzen auf allgemeines Interesse rechnen kann.

P. Csonka

ACTA OECONOMICA

Periodical
of the Hungarian Academy
of Sciences
Founded 1966

Editor: T. Földi

Acta Oeconomica publishes articles mainly on Hungary's economic development, economic policy and on some issues of economic management system and planning, on economic reforms and on mathematics applied in economics. Extra space is devoted to issues dealing with recent phenomena of world economy, East-West trade, socialist integration (place of Hungary in the international division of labour) and finally with developing countries. The journal contains reviews as well.

Papers mainly in English, some articles in German or Russian
Published in two volumes per year of 4 issues each
Subscription rate: $40.00 per volume

AKADÉMIAI KIADÓ
Publishing House
of the Hungarian Academy of Sciences
Budapest

Distributors:
KULTURA
Hungarian Foreign Trading Co.
P.O.B. 149
H-1389 Budapest

ACTA PHYSICA

ACADEMIAE SCIENTIARUM HUNGARICAE

EDITOR-IN-CHIEF

I. KOVÁCS

VOLUME 52 CONTENTS NUMBER 2

Papers in English. Published in two volumes (4 issues each) annually.
Subscription rate per vol ume: $40.00

AKADÉMIAI KIADÓ

Publishing House of the Hungarian Academy of Sciences

Budapest

Distributed by KULTURA, Hungarian Foreign Trading Co., P.O.B. 149, H-1389 Budapest

PRINTED IN HUNGARY
Akadémiai Kiadó és Nyomda, Budapest

NOTICE TO CONTRIBUTORS

Papers in English or in Hungarian are accepted to the condition that they have not been previously published or accepted for publication.

Manuscripts in two copies (the original type-written copy plus a clear duplicate one) complete with figures, tables, and references should be sent to

Acta Technica
Münnich F. u. 7.
Budapest, Hungary
H-1051

Although every effort will be made to guard against loss, it is advised that authors retain copies of all material which they submit. The editorial board reserves the right to make editorial changes.

Manuscripts should be typed double-spaced on one side of good quality paper with proper margins and bear the title of the paper and the name(s) of the author(s). The full postal address(es) of the author(s) should be given in a footnote on the first page. An abstract of 50 to 100 words should precede the text of the paper. The paper should not exceed 25 pages including tables and references. The approximate location of the tables and figures should be indicated on the margin. An additional copy of the abstract is needed. Russian words and names should be transliterated into English.

References. Only papers closely related to the author's work should be referred to. The citations should include the name of the author and/or the reference number in brackets. A list of numbered references should follow the end of the manuscript.

References to periodicals should mention: (1) name(s) and initials of the author(s); (2) title of the paper; (3) name of the periodical; (4) volume; (5) year of publication in parentheses; (6) number of the first page. Thus: 5. Winokur, A., Gluck, J.: Ultimate strength analysis of coupled shear walls. American Concrete Institute Journal 65 (1968), 1029.

References to books should include: (1) author(s)' name; (2) title; (3) publisher; (4) place and year of publication. Thus: Timoshenko, S., Gere, J.: Theory of Elastic Stability. McGraw-Hill Company, New York, Toronto, London 1961.

Illustrations should be selected carefully and only up to the necessary quantity. Black-and-white photographs should be in the form of glossy prints. The author's name and the title of the paper together with the serial number of the figure should be written on the back of each print. Legends should be brief and attached on a separate sheet. Tables, each bearing a title, should be self-explanatory and numbered consecutively.

Authors will receive proofs which must be sent back by return mail.

Authors are entitled to 50 reprints free of charge.

Periodicals of the Hungarian Academy of Sciences are obtainable at the following addresses:

AUSTRALIA
C.B.D. LIBRARY AND SUBSCRIPTION SERVICE
Box 4886, G.P.O., *Sydney N.S.W. 2001*
COSMOS BOOKSHOP, 145 Ackland Street
St. Kilda (Melbourne), Victoria 3182

AUSTRIA
GLOBUS, Höchstädtplatz 3, *1206 Wien XX*

BELGIUM
OFFICE INTERNATIONAL DE LIBRAIRIE
30 Avenue Marnix, *1050 Bruxelles*
LIBRAIRIE DU MONDE ENTIER
162 rue du Midi, *1000 Bruxelles*

BULGARIA
HEMUS, Bulvar Ruszki 6, *Sofia*

CANADA
PANNONIA BOOKS, P.O. Box 1017
Postal Station "B", *Toronto, Ontario M5T 2T8*

CHINA
CNPICOR, Periodical Department, P.O. Box 50
Peking

CZECHOSLOVAKIA
MAD'ARSKÁ KULTURA, Národní třida 22
115 66 Praha
PNS DOVOZ TISKU, Vinohradská 46, *Praha 2*
PNS DOVOZ TLAČE, *Bratislava 2*

DENMARK
EJNAR MUNKSGAARD, Norregade 6
1165 Copenhagen K

FEDERAL REPUBLIC OF GERMANY
KUNST UND WISSEN ERICH BIEBER
Postfach 46, *7000 Stuttgart 1*

FINLAND
AKATEEMINEN KIRJAKAUPPA, P.O. Box 128
SF-00101 Helsinki 10

FRANCE
DAWSON-FRANCE S. A., B. P. 40, *91121 Palaiseau*
EUROPÉRIODIQUES S. A., 31 Avenue de Versailles, *78170 La Celle St. Cloud*
OFFICE INTERNATIONAL DE DOCUMENTATION ET LIBRAIRIE, 48 rue Gay-Lussac
75240 Paris Cedex 05

GERMAN DEMOCRATIC REPUBLIC
HAUS DER UNGARISCHEN KULTUR
Karl Liebknecht-Straße 9, *DDR-102 Berlin*
DEUTSCHE POST ZEITUNGSVERTRIEBSAMT
Sraße der Pariser Kommüne 3–4, *DDR-104 Berlin*

GREAT BRITAIN
BLACKWELL'S PERIODICALS DIVISION
Hythe Bridge Street, *Oxford OX1 2ET*
BUMPUS, HALDANE AND MAXWELL LTD.
Cowper Works, *Olney, Bucks MK46 4BN*
COLLET'S HOLDINGS LTD., Denington Estate
Wellingborough, Northants NN8 2QT
WM. DAWSON AND SONS LTD., Cannon House
Folkstone, Kent CT19 5EE
H. K. LEWIS AND CO., 136 Gower Street
London WC1E 6BS

GREECE
KOSTARAKIS BROTHERS INTERNATIONAL BOOKSELLERS, 2 Hippokratous Street, *Athens-143*

HOLLAND
MEULENHOFF-BRUNA B.V., Beulingstraat 2,
Amsterdam
MARTINUS NIJHOFF B.V.
Lange Voorhout 9–11, *Den Haag*
SWETS SUBSCRIPTION SERVICE
347b Heereweg, *Lisse*

INDIA
ALLIED PUBLISHING PRIVATE LTD., 13/14
Asaf Ali Road, *New Delhi 110001*
150 B-6 Mount Road, *Madras 600002*
INTERNATIONAL BOOK HOUSE PVT. LTD.
Madame Cama Road, *Bombay 400039*
THE STATE TRADING CORPORATION OF INDIA LTD., Books Import Division, Chandralok 36 Janpath, *New Delhi 110001*

ITALY
INTERSCIENTIA, Via Mazzé 28, *10149 Torino*
LIBRERIA COMMISSIONARIA SANSONI, Via Lamarmora 45, *50121 Firenze*
SANTO VANASIA, Via M. Macchi 58
20124 Milano
D. E. A., Via Lima 28, *00198 Roma*

JAPAN
KINOKUNIYA BOOK-STORE CO. LTD.
17-7 Shinjuku 3 chome, Shinjuku-ku, *Tokyo 160-91*
MARUZEN COMPANY LTD., Book Department, P.O. Box 5050 Tokyo International, *Tokyo 100-31*
NAUKA LTD. IMPORT DEPARTMENT
2-30-19 Minami Ikebukuro, Toshima-ku, *Tokyo 171*

KOREA
CHULPANMUL, *Phenjan*

NORWAY
TANUM-TIDSKRIFT-SENTRALEN A.S., Karl Johansgatan 41–43, *1000 Oslo*

POLAND
WĘGIERSKI INSTYTUT KULTURY, Marszałkowska 80, *00-517 Warszawa*
CKP I W, ul. Towarowa 28, *00-958 Warszawa*

ROUMANIA
D. E. P., *Bucureşti*
ILEXIM, Calea Grivitei 64–66, *Bucureşti*

SOVIET UNION
SOJUZPECHAT – IMPORT, *Moscow*
and the post offices in each town
MEZHDUNARODNAYA KNIGA, *Moscow G-200*

SPAIN
DIAZ DE SANTOS, Lagasca 95, *Madrid 6*

SWEDEN
ALMQVIST AND WIKSELL, Gamla Brogatan 26
101 20 Stockholm
GUMPERTS UNIVERSITETSBOKHANDEL AB
Box 346, *401 25 Göteborg 1*

SWITZERLAND
KARGER LIBRI AG, Petersgraben 31, *4011 Basel*

USA
EBSCO SUBSCRIPTION SERVICES
P.O. Box 1943, *Birmingham, Alabama 35201*
F. W. FAXON COMPANY, INC.
15 Southwest Park, *Westwood Mass. 02090*
THE MOORE-COTTRELL SUBSCRIPTION AGENCIES, *North Cohocton, N. Y. 14868*
READ-MORE PUBLICATIONS, INC.
140 Cedar Street, *New York, N. Y. 10006*
STECHERT-MACMILLAN, INC.
7250 Westfield Avenue, *Pennsauken N. J. 08110*

YUGOSLAVIA
JUGOSLOVENSKA KNJIGA, Terazije 27, *Beograd*
FORUM, Vojvode Mišića 1, *21000 Novi Sad*

HU ISSN 0001—7035

Index: 26.025

ACTA TECHNICA

ACADEMIAE SCIENTIARUM HUNGARICAE

EDITOR: M. MAJOR

VOLUME 94
NUMBERS 3–4

AKADÉMIAI KIADÓ, BUDAPEST 1982

ACTA TECHNICA

A JOURNAL OF THE HUNGARIAN ACADEMY OF SCIENCES

Acta Technica publishes original papers, preliminary reports and reviews in English, which contribute to the advancement of engineering sciences.

Acta Technica is published by

AKADÉMIAI KIADÓ
Publishing House of the Hungarian Academy of Sciences
H-1450 Budapest, Alkotmány u. 21.

Subscription information

Orders should be addressed to

KULTURA Foreign Trading Company
H-1389 Budapest P.O.Box 149

or to its representatives abroad

Acta Technica is indexed in Current Contents

CONTENTS

BOOK REVIEWS

NEWS

Acta Technica Academiae Scientiarum Hungaricae, 94 (3—4), pp. 103–109 (1982)

NUMERICAL METHOD FOR SOLVING EIGENVALUE PROBLEMS OF LAMBDA-MATRICES OF DEGREE *m*

GY. POPPER*, ZS. GÁSPÁR**

[Manuscript received 10 July, 1980]

The present paper deals with a numerically efficient iteration method for computing the n smallest generalized eigenvalues in magnitude and the corresponding generalized eigenvectors of λ-matrices of degree m and order n. The conditions of convergence are given in the theorem. The method can be considered as an extension of the Bernoulli's method for matrix-polinomials.

1. Introduction

The numerical solution of mechanical problems often leads to the generalized eigenvalue problem of λ-matrices (see e.g.: [1], [2]). Vibration problems resulting λ-matrices of second degree are well-known. There are also stability and vibration problems which can be described by differential equations where the boundary conditions are functions of the eigenvalues. Finitization using the Galerkin's method can lead to the solution of the eigenvalue problem of a λ-matrix of higher degree.

In many cases we are interested only in the computing of some smallest (or largest) generalized eigenvalues in magnitude and the corresponding generalized eigenvectors.

The generalized eigenvalue problem of a λ-matrix of degree m always can be transformed to a special eigenvalue problem of a constant matrix of order mn, where n denotes the order of the original λ-matrix. However, this alternation is numerically fraught with difficulties because of the very high order.

In the present paper we consider a numerically very efficient iterative method for computing the first n smallest generalized eigenvalues in magnitude and the corresponding generalized eigenvectors of a λ-matrix of order n and degree m.

2. The method

Let us consider the generalized eigenvalue problem of a λ-matrix of degree m

$$(\mathbf{I}\lambda^m + \mathbf{A}_1\lambda^{m-1} + \ldots + \mathbf{A}_{m-1}\lambda + \mathbf{A}_m)\mathbf{v} = \mathbf{0}, \tag{1}$$

where $\mathbf{I}, \mathbf{A}_1, \ldots, \mathbf{A}_m$ denotes real matrices all of order n, $\mathbf{I}$ is the identity matrix and $\mathbf{A}_m$ is non-singular.

* Dr. Popper, Gy., Szirtes u. 28/A, H-1016 Budapest, Hungary
** Dr. Gáspár, Zs., Kapy u. 40/b, H-1025 Budapest, Hungary

Lemma. If the matrix $\tilde{\mathbf{Y}}$ is a solution of the matrix equation

$$\mathbf{Y}^m + \mathbf{A}_1 \mathbf{Y}^{m-1} + \ldots + \mathbf{A}_{m-1} \mathbf{Y} + \mathbf{A}_m = \mathbf{0} \tag{2}$$

then every eigenvalue and eigenvector of $\tilde{\mathbf{Y}}$ is generalized eigenvalue and eigenvector of problem (1).

This lemma follows from theorem 3.7. (i) p.5 and corrollary p. 49 in [3]. So, if an arbitrary solution (e.g. $\tilde{\mathbf{Y}}$) of Eq. (2) is known, solving the special eigenvalue problem of matrix $\tilde{\mathbf{Y}}$ we obtain n generalized eigenvalues and eigenvectors from the mn generalized eigenvalues and eigenvectors of problem (1).

This gives rise to concentrate on the solving Eq. (2). To solve it, let us apply the iteration formula

$$(\ldots((\mathbf{Y}_{k-m+2} + \mathbf{A}_1)\mathbf{Y}_{k-m+3} + \mathbf{A}_2) \ldots + \mathbf{A}_{m-1})\mathbf{Y}_{k+1} = -\mathbf{A}_m \tag{3}$$

$$(k = 0, 1, 2, \ldots)$$

with the starting matrices $\mathbf{Y}_0, \mathbf{Y}_{-1}, \ldots, \mathbf{Y}_{2-m}$.

The iteration (3) can be written in the form

$$\mathbf{A}\tilde{\mathbf{Z}}_{k+1} = \mathbf{Z}_k, \tag{4a}$$

$$\mathbf{Z}_{k+1} = \tilde{\mathbf{Z}}_{k+1}(\mathbf{R}\tilde{\mathbf{Z}}_{k+1})^{-1}, \tag{4b}$$

$$\mathbf{Y}_{k+1} = \mathbf{S}\mathbf{Z}_{k+1}, \tag{4c}$$

with

$$\mathbf{A} = \begin{bmatrix} -\mathbf{A}_1 & -\mathbf{A}_2 & \ldots & -\mathbf{A}_{m-1} & -\mathbf{A}_m \\ \mathbf{I} & \mathbf{0} & \ldots & \mathbf{0} & \mathbf{0} \\ \mathbf{0} & \mathbf{I} & \ldots & \mathbf{0} & \mathbf{0} \\ \vdots & \vdots & \ddots & \vdots & \vdots \\ \mathbf{0} & \mathbf{0} & & \mathbf{I} & \mathbf{0} \end{bmatrix}, \tag{5a}$$

$$\mathbf{Z}_k = \begin{bmatrix} \mathbf{Y}_{k-m+2} & \mathbf{Y}_{k-m+3} & \ldots & \mathbf{Y}_k \\ \mathbf{Y}_{k-m+3} & \mathbf{Y}_{k-m+4} & \ldots & \mathbf{Y}_{k+1} \\ & \vdots & & \\ & \mathbf{Y}_k & & \\ & \mathbf{I} & & \end{bmatrix}, \tag{5b}$$

$$\tilde{\mathbf{Z}}_{k+1} = \begin{bmatrix} \mathbf{Y}_{k-m+3} & \mathbf{Y}_{k-m+4} & \cdots & \mathbf{Y}_k \\ \mathbf{Y}_{k-m+4} & \mathbf{Y}_{k-m+5} & \cdots & \mathbf{Y}_k \\ & \vdots & & \\ & \mathbf{Y}_k & & \\ & \mathbf{I} & & \\ & \mathbf{Y}_{k+1}^{-1} & & \end{bmatrix},$$

$$\mathbf{R} = [\underset{(1)}{\mathbf{0}}, \underset{(2)}{\mathbf{0}}, \ldots, \underset{(m-2)}{\mathbf{0}}, \underset{(m-1)}{\mathbf{0}}, \underset{(m)}{\mathbf{I}}], \tag{6a}$$

$$\mathbf{S} = [\mathbf{0}, \mathbf{0}, \ldots, \mathbf{0}, \mathbf{I}, \mathbf{0}]. \tag{6b}$$

The equivalence of formula (3) with the inverse iteration (4) can be shown easily by the following. If we multiply from the right Eq. (3) by the inverse of $\mathbf{Y}_{k+1}$, we obtain the first equation in hyperequation (4a); the remaining equations of (4a) represent obvious equivalences. Because of

$$(\mathbf{R}\tilde{\mathbf{Z}}_{k+1})^{-1} = \mathbf{Y}_{k+1}$$

Eq. (4b) corresponding to a normalization means the remultiplication of Eq. (4a) by matrix $\mathbf{Y}_{k+1}$. Eq. (4c) is a formal extraction of block $\mathbf{Y}_{k+1}$.

The rewriting of the iteration (3) into form (4) is also very useful because of the followings:

a) The generalized eigenvalue problem (1) can always be reduced to the special eigenvalue problem

$$\mathbf{AX} = \mathbf{X}\boldsymbol{\Lambda}$$

where the matrix $\mathbf{A}$ of order mn was already introduced, $\boldsymbol{\Lambda}$ denotes a diagonal matrix composed of the mn generalized eigenvalues λ_i of the original problem,

$$\mathbf{X} = \begin{bmatrix} \mathbf{V}\boldsymbol{\Lambda}^{m-1} \\ \mathbf{V}\boldsymbol{\Lambda}^{m-2} \\ \vdots \\ \mathbf{V}\boldsymbol{\Lambda} \\ \mathbf{V} \end{bmatrix}, \tag{7}$$

and the i-th column of the $n \times mn$ matrix $\mathbf{V}$ is the generalized eigenvector $\mathbf{v}_i$ belonging to the generalized eigenvalue λ_i.

b) If the λ-matrix in (1) is a simple λ-matrix (i.e. to every generalized eigenvalue of multiplicity r there exist r linearly independent generalized eigenvectors),

then — as the consequence of Theorem 4.2. in [3] — the matrix $\mathbf{A}$ has a simple structure i.e. it can be written

$$\mathbf{A} = \mathbf{X}\Lambda\mathbf{X}^{-1}. \tag{8}$$

Assume the following ordering of the generalized eigenvalues:

$$|\lambda_i| < |\lambda_{i+1}|, \qquad i = 1, 2, \ldots, mn-1.$$

Denoting by Λ_1 and Λ_2 the diagonal matrices

$$\Lambda_1 = \langle \lambda_1, \ldots, \lambda_n \rangle, \qquad \Lambda_2 = \langle \lambda_{n+1}, \ldots, \lambda_{mn} \rangle,$$

and by $\mathbf{V}_1$ and $\mathbf{V}_2$ matrices having the corresponding generalized eigenvalues as columns, it can be written

$$\underset{n \times mn}{\mathbf{V}} = \underset{n \times n}{[\mathbf{V}_1,} \quad \underset{n \times (m-1)n}{\mathbf{V}_2]} \tag{9}$$

In the following it is supposed, that the λ-matrix in (1) is a simple λ-matrix. Then an arbitrary $mn \times n$ matrix $\mathbf{Z}_0$ can be written in a unique way in the form

$$\mathbf{Z}_0 = \mathbf{X}\mathbf{C} = \mathbf{X}\begin{bmatrix}\mathbf{C}_1\\ \mathbf{C}_2\end{bmatrix},$$

where $\mathbf{C}_1$ is quadratic matrix of order n and $\mathbf{C}_2$ is a $(m-1)n \times n$ matrix.

If the iteration (4a, b) is started with the matrix $\mathbf{Z}_0$, then

$$\mathbf{Z}_1 = \mathbf{A}^{-1}\mathbf{Z}_0(\mathbf{R}\mathbf{A}^{-1}\mathbf{Z}_0)^{-1},$$

$$\mathbf{Z}_2 = \mathbf{A}^{-2}\mathbf{Z}_0(\mathbf{R}\mathbf{A}^{-1}\mathbf{Z}_0)^{-1}[\mathbf{R}\mathbf{A}^{-2}\mathbf{Z}_0(\mathbf{R}\mathbf{A}^{-1}\mathbf{Z}_0)^{-1}]^{-1} = \mathbf{A}^{-2}\mathbf{Z}_0(\mathbf{R}\mathbf{A}^{-2}\mathbf{Z}_0)^{-1},$$

$$\vdots$$

$$\mathbf{Z}_k = \mathbf{A}^{-k}\mathbf{Z}_0(\mathbf{R}\mathbf{A}^{-k}\mathbf{Z}_0)^{-1}.$$

Using (4c), (8) and (10)

$$\mathbf{Y}_k = \mathbf{S}\mathbf{X}\Lambda^{-k}\mathbf{C}(\mathbf{R}\mathbf{X}\Lambda^{-k}\mathbf{C})^{-1}$$

holds.

Because of $\mathbf{S}\mathbf{X} = \mathbf{V}\Lambda$ and $\mathbf{R}\mathbf{X} = \mathbf{V}$ it follows

$$\mathbf{Y}_k = \mathbf{V}\Lambda^{1-k}\mathbf{C}(\mathbf{V}\Lambda^{-k}\mathbf{C})^{-1}. \tag{11}$$

Using the symbols introduced in (9) and (10)

$$\mathbf{Y}_k = (\mathbf{V}_1\Lambda_1^{1-k}\mathbf{C}_1 + \mathbf{V}_2\Lambda_2^{1-k}\mathbf{C}_2)(\mathbf{V}_1\Lambda_1^{-k}\mathbf{C}_1 + \mathbf{V}_2\Lambda_2^{-k}\mathbf{C}_2)^{-1}.$$

From the nonsingularity of $\mathbf{A}_m$ follows the nonsingularity of Λ_1. Suppose that neither $\mathbf{V}_1$ nor $\mathbf{C}_1$ are singular. Then $\mathbf{Y}_k$ can be written in the form

$$\mathbf{Y}_k = \mathbf{V}_1\Lambda_1^{1-k}\mathbf{C}_1(\mathbf{I} + \mathbf{C}_1^{-1}\Lambda_1^{k-1}\mathbf{V}_1^{-1}\mathbf{V}_2\Lambda_2^{1-k}\mathbf{C}_2)$$

$$(\mathbf{I} + + \mathbf{C}_1^{-1}\Lambda_1^{k}\mathbf{V}_1^{-1}\mathbf{V}_2\Lambda_2^{-k}\mathbf{C}_2)^{-1}\mathbf{C}_1^{-1}\Lambda_1^{k}\mathbf{V}_1^{-1}.$$

Each element in position (i, j) of matrix $\Lambda_1^k \mathbf{V}_1^{-1} \mathbf{V}_2 \Lambda_2^{-k}$ contains a coefficient of form $(\lambda_i/\lambda_{n+j})^k$.

If the inequality

$$|\lambda_n| < |\lambda_{n+1}| \tag{12}$$

holds, then

$$\mathbf{Y}_k \to \mathbf{V}_1 \Lambda_1^{1-k} \mathbf{C}_1 (\mathbf{I}+\mathbf{0})(\mathbf{I}+\mathbf{0})^{-1} \mathbf{C}_1^{-1} \Lambda_1^k \mathbf{V}_1^{-1} = \mathbf{V}_1 \Lambda_1 \mathbf{V}_1^{-1}$$

as $k \to \infty$.

It means that solving Eq. (2) by iteration (3) the process converges to that solution of Eq. (2), for which the eigenvalues and the eigenvectors coincide with the smallest generalized eigenvalues in magnitude and the corresponding generalized eigenvectors of problem (1).

On this basis we have proved the following convergence theorem.

Theorem. Suppose that

1) $\mathbf{I}\lambda^m + \mathbf{A}_1 \lambda^{m-1} + \ldots + \mathbf{A}_m$
is a simple λ-matrix,

2) for its generalized eigenvalues the
$$0 < |\lambda_1| \leqq |\lambda_2| \leqq \ldots \leqq |\lambda_n| < |\lambda_{n+1}| \leqq \ldots \leqq |\lambda_{mn}|$$
inequalities hold,

3) the matrix
$$\mathbf{V}_1 = [\mathbf{v}_1, \ldots, \mathbf{v}_n]$$
formed from the generalized eigenvectors associated with the generalized eigenvalues $\lambda_1, \ldots, \lambda_n$ respectively is nonsingular.

If the iteration (3) started with matrices $\mathbf{Y}_0, \mathbf{Y}_{-1}, \ldots, \mathbf{Y}_{2-m}$ for which the matrix $\mathbf{C}_1$ defined by the relations (5b) and (10) is nonsingular, then the iteration converges to matrix

$$\tilde{\mathbf{Y}} = \mathbf{V}_1 \langle \lambda_1, \ldots, \lambda_n \rangle \mathbf{V}_1^{-1}.$$

3. Remarks

1. For a non-singular matrix $\mathbf{V}_1$ condition $|\lambda_n| < |\lambda_{n+1}|$ indicates the matrix $\mathbf{V}_1 \Lambda_1 \mathbf{V}_1^{-1}$ to be real.

2. For $n = 1$ the iteration method (3) is identical with that variation of Bernoulli's method for computing of the smallest root in magnitude of polinomial equations, which overcomes the under- and overflow (see e.g.: [4] 8.10—52). An other extention of the Bernoulli's algorithm for computing of the dominant solution $\mathbf{Y}$ of the Eq. (2) was given by Lancaster in [5].

3. Analogously to the Bernoulli's method and the Mises's process the rate of convergence of the iteration (3) depends on the ratio $|\lambda_n|/|\lambda_{n+1}|$.

4. If we multiply Eq. (1) from left by the inverse of $\mathbf{A}_m$ and we denote $\tilde{\lambda} = 1/\lambda$, then we obtain a λ-matrix of identical form with the original one in Eq. (1). If the original λ-matrix is symmetric and $\mathbf{A}_m$ is positive definite, then the symmetric can be provided (see e.g. [1]). The iteration (3) with the new λ-matrix leads to the greatest generalized eigenvalues in magnitude and the corresponding generalized eigenvectors of the original problem.

5. Let us suppose, that using iteration (3) we have obtained a solution of Eq. (2) denoted by $\tilde{\mathbf{Y}}$. Then by the recursion

$$\mathbf{B}_0 = \mathbf{I},$$

$$\mathbf{B}_i = \mathbf{A}_i + \mathbf{B}_{i-1}\tilde{\mathbf{Y}}, \qquad (i = 1, 2, \ldots, m-1)$$

i.e. using the Ruffini—Horner's formula with the coefficients of (2), a λ-matrix of degree $m-1$ with coefficients $\mathbf{B}_i$ can be determined. The generalized eigenvalues of the new λ-matrix coincide with the generalized eigenvalues $\lambda_{n+1}, \ldots, \lambda_{mn}$ of the problem (1), and the generalized eigenvectors $\mathbf{v}_i$ of the original problem are given by the relation

$$\mathbf{v}_i = (\mathbf{I}\lambda_i - \tilde{\mathbf{Y}})^{-1}\tilde{\mathbf{v}}_i,$$

where $\tilde{\mathbf{v}}_i$ denotes the generalized eigenvectors of the new λ-matrix.

If the conditions in the previous theorem holds also for the λ-matrix of degree $m-1$, then the iteration (3) can be used for determination of the next n smallest generalized eigenvalues in magnitude and the corresponding generalized eigenvectors. In this sense the process can be continued.

6. An unreduced Hessenberg-matrix (i.e. there are no zero subdiagonal elements) of order mn always can be transformed into form (5a) using similarity transformations ([6]). In consequence the iteration process (3) can be applied to compute the n smallest eigenvalues in magnitude and the corresponding eigenvectors of a matrix of order mn.

4. Example

Consider the generalized eigenvalue problem

$$\left(\mathbf{I}\lambda^3 + \begin{bmatrix} -5 & 3 \\ -6 & -16 \end{bmatrix}\lambda^2 + \begin{bmatrix} 7 & -8 \\ 39 & 70 \end{bmatrix}\lambda + \begin{bmatrix} -24 & -24 \\ -54 & -84 \end{bmatrix}\right)\mathbf{v} = \mathbf{0}$$

with λ-matrix of 3rd degree. Its generalized eigenvalues are $\lambda_i = i$, $i = 1, 2, \ldots, 6$ and the corresponding eigenvectors are:

$$\mathbf{v}_1 = \begin{bmatrix} -29 \\ 21 \end{bmatrix}; \quad \mathbf{v}_2 = \begin{bmatrix} -14 \\ 11 \end{bmatrix}; \quad \mathbf{v}_3 = \mathbf{v}_5 = \begin{bmatrix} -1 \\ 1 \end{bmatrix}; \quad \mathbf{v}_4 = \mathbf{v}_6 = \begin{bmatrix} -2 \\ 3 \end{bmatrix}. \qquad (13)$$

Apply the iteration process (3) with starting matrix $\mathbf{Y}_0 = \mathbf{0}$ ($\mathbf{Y}_0 = \mathbf{0}$ implies that $\mathbf{Y}_{-1}$ is arbitrary).

To characterize the iteration process, in each step we computed the Euclidean norm $\|\mathbf{Y}_k - \mathbf{Y}_{k-1}\|$, the eigenvalues and eigenvectors of $\mathbf{Y}_k$. The eigenvectors are normed in the sense, that their first components should coincide with the first components of vectors in (13).

The iteration can be well illustrated by the following table:

k	$\|\mathbf{Y}_k - \mathbf{Y}_{k-1}\|$	λ_1	λ_2	$v_{1,2}$	$v_{2,2}$
10	$8 \cdot 10^{-1}$	1.000 138 76	1.888 006 85	21.000 157 2	10.857 265 6
15	$1 \cdot 10^{-1}$	1.000 000 51	1.985 508 40	21.000 000 6	10.980 706 2
20	$1 \cdot 10^{-2}$	1.000 000 00	1.998 082 00	21.000 000 0	10.997 432 4
25	$2 \cdot 10^{-3}$	1	1.999 746 81	21	10.999 660 9
30	$2 \cdot 10^{-4}$	1	1.999 966 63	21	10.999 955 3
35	$3 \cdot 10^{-5}$	1	1.999 995 61	21	10.999 994 1
40	$3 \cdot 10^{-6}$	1	1.999 999 42	21	10.999 999 2
45	$5 \cdot 10^{-7}$	1	1.999 999 92	21	10.999 999 9
50	$8 \cdot 10^{-8}$	1	1.999 999 99	21	11.000 000 0

References

1. Popper, Gy.—Ferenczi, M.: Numerical Method for Solving Eigenvalue Problems of Linear Vibration Systems of Finite Degrees of Freedom. *Acta Techn. Hung.* **84** (1977), 85—96
2. Tarnai, T.—Popper, Gy.: Solution of Flexural-Torsional Problem of Beams by Series Expansion in Eigenfunctions of Quadratic Operator Pencils. *Acta Techn. Hung.* **89** (1979), 237—254
3. Lancaster, P.: Lambda-Matrices and Vibrating Systems. Pergamon Press, Oxford, 1966
4. Ralston, A.: A First Course in Numerical Analysis. McGraw-Hill, 1965:
5. Lancaster, P.: A Fundamental Theorem on Lambda-Matrices with Applications. II. Difference Equations with Constant Coefficients. *Linear Algebra and Its Applications* **18,** 213—222 (1977)
6. Гашпар, Ж.—Поппер, Г.: Решение алгебраической проблемы собственных значений разбиением на клетки. Журнал вычислительной математики и математической физики. **21** (1981), 263—270

Acta Technica Academiae Scientiarum Hungaricae, 94 (3—4), pp. 111–122 (1982)

MEASUREMENT OF BOTH PORE AIR AND PORE WATER PRESSURE IN TRIAXIAL TESTING

Á. KÉZDI, GY. HORVÁTH*

[Received: 7 April, 1983]

Soils having secondary porosity display both pore air and pore water pressures which influence the shear strength and the behaviour of such systems. Authors constructed a device which can be used to measure — in the first phase of the compression — the pore air pressure in an open system, and, in the second phase, when the soil became quasi-saturated, the pore water pressure. Two test results are given: in the first, the load increased gradually, the critical state and the pore pressures have been determined; in the second, real conditions of dumping have been simulated.

Introduction

In the course of the construction of earthworks, there are periods, when the excavated earth material arrives to the site in bigger or smaller clods, it will be deposited and spread there. Later, these layers will or will not be compacted, a compression will come either due to an artifical compaction, or to the own weight of the material. It the stage between spreading and compaction, the earth has a special structure: the individual clods have the structure of the original material, before excavation, it constans solid grains and small voids filled by air and/or water; this is the primary structure, between the clods however, there are voids which are much larger than the individual solid particles and form, with the clods together, the so-called secondary structure. Even when compacted, the blocks and lumps cannot be brought into tight contact. Dams before and after compaction, loosely dumped heaps or so-called tips are typical representatives of this type of earthworks. The latters serve for the disposal of the spoil in open pit mining, the loose material will arrange itself according to its own laws, compaction usually will not follow. The material has — in the case of cohesive soils — typical secondary structure.

Since the behaviour of soils having both primary and secondary structure will be highly influenced by the stresses which arise in the pores, the knowledge of the pore water and pore air pressures, respectively, is a very important problem. This paper describes both a device and a method which serves to the independent measurement of

* Civ. Engr. Research Assistant. Budapest, H-1521, Műegyetem rkp. 3. Hungary

these pressures. First, we investigate some properties of soils having both primary and secondary pores.

In the spoil tips of the open pit mines in Hungary, the clay clods of medium plasticity ($I_p = 30 - 50$ per/cent) represent a substantial quantity. These soils cannot be dewatered by gravitation before excavation, in the original condition they are usually saturated, i.e. the "primary" pores contain only water, and this is the case also in the tip. During excavation and transport the clods become disintegrated, according to the conditions of weather and of the excavation method and they arrive in this state to the tip. The individual clods have a rather high compressive strength, their consistency is stiff to rigid. In thoroughly remoulded condition, the strength is usually much smaller, by one order of magnitude. We want to express numerically the phase composition of these materials.

Primary and secondary void ratios

Usually, the phase composition of a soil sample can be represented by a triangular diagram (Fig. 1.) (relative volume percentages of the solid, liquid and air particles s, v, and a). These values are calculated by using the respective masses (m) and density values (ρ). (Fig. 1.) The phase composition can be represented by a point (P) in the triangular diagram. (Kézdi, 1974.) This method is very useful in the practice.

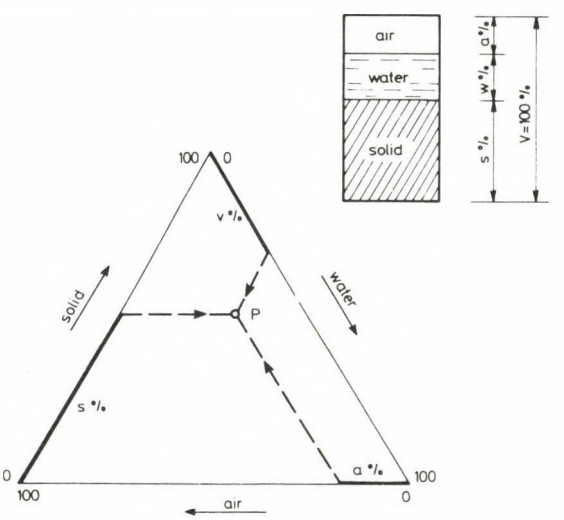

$$s\ \% = \frac{m_d}{V \cdot \rho_s} \cdot 100 = \frac{\rho_d}{\rho_s} \cdot 100$$

$$w\ \% = \frac{m_w - m_d}{V \cdot \rho_w} \cdot 100 = \frac{\rho_b - \rho_d}{\rho_w} \cdot 100$$

$$a\ \% = 100 - (s\ \% + w\ \%)$$

Fig. 1. Phase composition of soil in triangle diagram

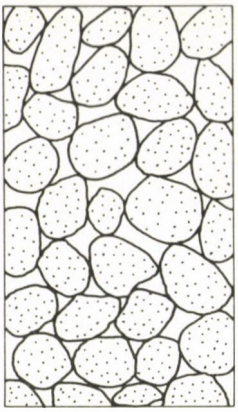

Fig. 2. Soil sample containing primary and secondary pores

The here discussed materials have primary voids within the individual clods and secondary ones between them (Fig. 2.) The phase composition can be characterized only by the introduction of certain new characteristics.

If the secondary voids contain only air, the unit volume in Fig. 3.a. can be divided into two parts: air and the soil containing only primary voids (Fig. 3.b) The phase composition in this case is shown in Fig. 3.c. from which the **s′ a′, s, v** and **a** quantities can be determined. Since the mass related to the unit volume is always identical, we get

$$\rho_b = v \cdot \rho_w + s \cdot \rho_s$$

$$a' + s' = a + v + s \tag{1}$$

$$\rho_b = s'\rho_r; \quad \rho d = s\rho_s;$$

from which it follows that

$$s' = \frac{\rho_b}{\rho_r}; \quad a' = 1 - s'$$

$$s = \frac{\rho_d}{\rho_s}; \quad v = \frac{\rho_b - s \cdot \rho_s}{\rho_w} = \frac{\rho_b - \rho_d}{\rho_w}, \tag{2}$$

$$a = 1 - (s + v)$$

ρ_s — density of the solid grains; (gr/cm^3)
ρ_w — density of water; (gr/cm^3)
ρ_b — wet bulk density of the soil containing both primary and secondary voids (gr/cm^3)
ρ_d — the same under dry conditions; (gr/cm^3)
ρ_c — natural wet bulk density of the clods; (gr/cm^3)
ρ_{cd} — the dry bulk density of the clods. (gr/cm^3)

If the secondary voids contain both air and water, the unit volume will look like Fig. 4.

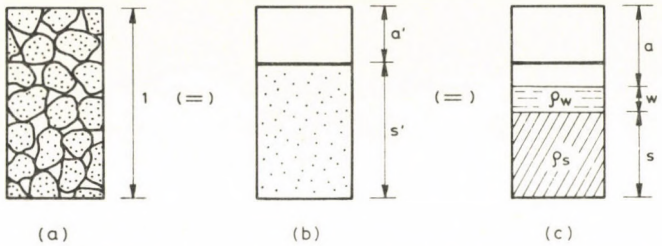

Fig. 3. Phase composition of a lump if the secondary voids contain only air

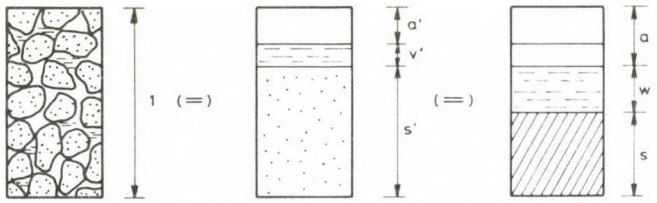

Fig. 4. Phase composition of a lump if the secondary voids contain air and water

In order to characterize the secondary structure, the following ratio may be introduced

$$\eta = \frac{1-s}{1-s'} \tag{3}$$

If $\eta > 0{,}05$, then the importance of the secondary voids is quite considerable.

The secondary porosity is:

$$n' = 1 - s' \tag{4}$$

Methods of determination of the secondary structure are given in Kézdi, 1980; along with numerical examples.

State of stress in the tip

The tip represents a loose three- phase unconsolidated mass. The stresses in this are mainly caused by its own weight; these stresses in the case of a growing tip, increse in time. The vertical stress is given by $\sigma_z = h\gamma$.

In the inside of the tip, the state of stress corresponds to the "earth pressure at rest" condition. The value of the horizontal stress

$$\sigma_x = K_0 \cdot \sigma_z = K_0 h\gamma . \tag{5}$$

The loose material suffers first, in the continuously dumped tip, a considerable compression. The original structure of the lumps is still stable, in the pores only air is

moving (the pore air pressure, $u_a > 0$), — this is possible in the large secondary pores however — the water is still fixed, due to capillary forces or to weak surface bonds. In this case, the state of stress can be considered as an anisotropic consolidation in an open system ($\sigma_2 = \sigma_3 = K_0\sigma_1$; $\varepsilon_1 \neq 0, \varepsilon_2 = \varepsilon_3 = 0$), since the phase movements, due to the pressures, are not hindered therein. The compression presses out a certain amount of the air contained in the secondary pores. In the course of the further compression, the small voids will become saturated, the air collects in the large pores or will partly be dissolved in the water. The compression caused by air movement keeps on, until the degree of saturation reaches a critical state, where independent movement of the gaseous phase stops, the enclosed air bubbles can move along the water only, since the inital air canals of the loose material became closed. The soil becomes quasi-saturated, the air does not make a continuous phase, the voids are filled with a compressible mixture of air and water ($u_a > u_w > 0$), where the air exists in a finely distributed or a dissolved state. After having reached this critical state, the pressure squeeze this mixture out of the tip or of the upper parts thereof. The inner part of the tip behaves then in the quasi-saturated state as a closed system, where the movement of the liquid and gaseus phases is hindered. If this air and water cannot leave the pores, they remain under pressure, and since these stresses are neutral, the shear strength will be radically decreased, slides and subsidences will occur in the tips or a liquifaction comes about. These phenomena are very important from practical point of view because they may cause disasters and endanger human lives. (Bishop, A. W., 1973.) In the frame of investigations connected with open-pit mining in Hungary, the stability of tips was of a major concern, therefore, the Soil Mechanics Laboratory of the Department of Geotechnique (Budapest Technical University) constructed a measuring device and worked out a method to measure pore water and pore air pressures in soils having secondary porosity.

Method of investigation

One of the important conditions to determine the shear strength of tip materials is to model precisely the loading process and the consolidation. Another important factor is the time coefficient, the rate of loading. Whether the tip forms, under the influence of the increasing load, an open, or a closed system, will depend on the rate of loading. At a relatively high rate of loading, the totally open system cannot be completely developed at the beginning of the anisotropic compression, since one part of the air canals will be closed by some plastic lumps. In these enclosed air-bubbles considerable pore-air pressure may develop, even in the initial phase.

Description of the measuring device

At the beginning of loading, as stated before, air will be pressed out in an open system from the soil having secondary porosity. After having reached a critical saturation, water will be squeezed out, which contains finely distributed and/or dissolved air. The investigation was made with a triaxial compression chamber equipped with a device for pore water pressure measurements. The triaxial chamber has been somewhat modified for the purpose of these tests. (For a detailed description of the modified apparatus see Kézdi, Á., Horváth, Gy., 1983.) It is possible to perform tests in axially symmetrical stress state, following different stress paths, at different loading rates. The data which can be measured are the following:

— the principal stresses (σ_1 ; $\sigma_2 = \sigma_3$)
— the pore water pressure,
— deformations,
— volume change,
— pore air pressure.

The latter can be measured by using the device illustrated on Fig. 5. It is measured at the beginning of the test only, before reaching the critical saturation, which indicates that the sample became quasisaturated. In this moment, the device is switched to measure pore water pressure, and it furnishes the u_w values, in closed system.

Fig. 5 shows also base plate of the triaxial chamber (B); the new device (A) is coupled here to the chamber and mounted on valve *4*. Pipes *8* to *10* are filled with water. The free water surfaces in pipe *9* and container *10* are under atmospheric pressure.

If the soil sample is exposed to an anisotropic compression which corresponds to the state of stresses in the "at rest" condition, in the way, that valve 4. will be opened and the air from one part of the secondary pores can be squeezed out. The escaped air will displace the water level in tube 8. In order to determine the exact volume of the air pressed out at the athmospheric pressure, we move container *10* downwards, until the water levels in the tubes 8., 9. and 10 will become indentical. (Pipe 9 serves to measure the exact volume of the air.) Now, we know the amount of air pressed out from the sample in unit of time and the vertical compression (volume change) of the sample, and making use of the Boyle-Mariotte equation, the pore-air pressure in the closed pores of the sample can be exactly calculated, even in open system.

$$u_a = \frac{[(V_a - \Delta V) + V_p] \cdot p_1}{V_a - \Delta V} \tag{6}$$

In this equation:

V_a — air volume (cm^3)
ΔV — volume decrease, measured under anisotropic consolidation, due to the vertical compression of the sample (cm^3)
V_p — air-volume, remained in the sample (cm^3)
p_1 — athmospheric pressure (100 kPa)

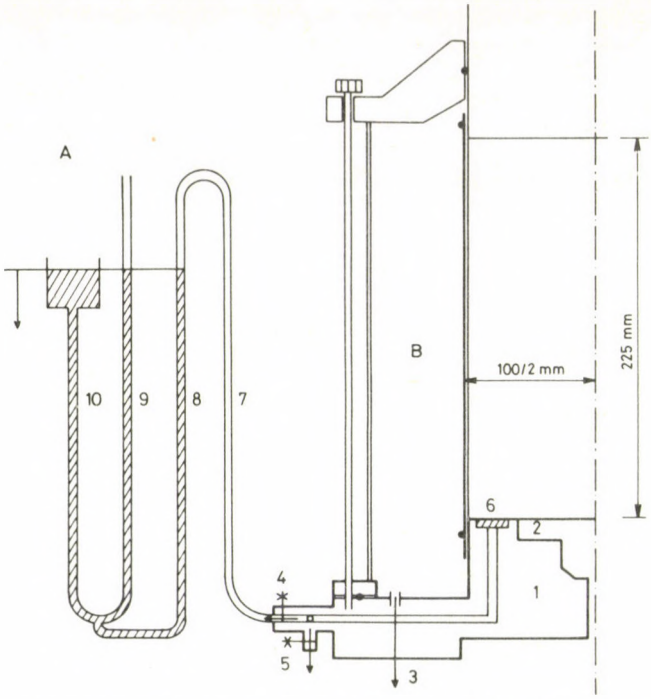

Fig. 5. Device to measure the pore-water — and pore-air pressures (*A*; *B* — triaxial cell). *1* — base of the cell; *2* — cell to measure the vertical principal stress; *3* — miniature cell to measure the third principal stress; *4* — valve connecting the pore-air pressure measuring device; *5* valve connecting the pore-water pressure measuring device; *6* — filter stone ring; *7 – 10* — device to measure the pore air pressure indirectly

The measurement is continued until the critical saturation is reached, when there is pressure also in the pore water. The interconnected air canals will be closed, water is squeezed out from the sample and water enters into the system of the measuring device. In this moment, valve *4* is closed and valve *5* opened, where a small pressure cell serves to measure further the pressure of water in the voids of the lumps and of the pressure of the water-air matrix in closed system.

Test results

The results of a test are given on Fig. 6. The height of the sample was 22,5 cm, its diameter 10 cm. The clay which was composed of lumps having the original, primary porosity, has been loosely filled into a mould and then lightly tamped. The characteristics of the soil and the test results are given in Table 1. The soil has a secondary porosity. The load was applied at the constant rate of 4 kPa/min. This rate corresponds in Hungary approximately to the usual rate in tip forming. The first principal stress, which is identical with the pressure due to the ownweight, increases

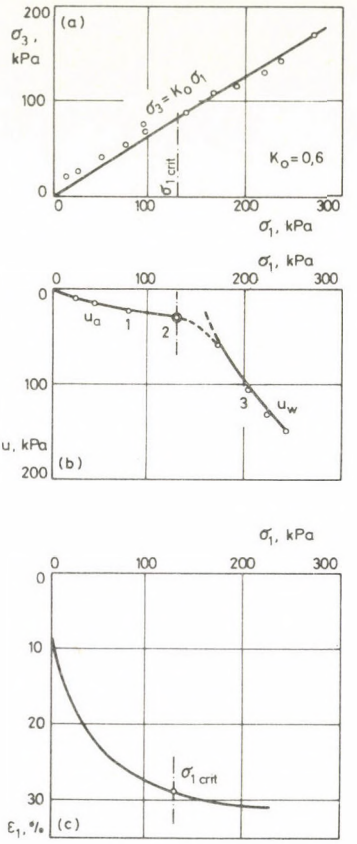

Fig. 6. Test results. *a* — values of the uniformly increasing principal stresses; *b* — pore air and pore water pressures vs. the first principal stress; *c* — specific compression, vs. the first principal stress

thus linearly in time; also, the third principal stress increases uniformly, according to the formula

$$\sigma_3 = K_0 \sigma_1 \,. \tag{7}$$

In the test, the ratio of the principal stresses was (at $\varepsilon_3 = 0$) $\sigma_3/\sigma_1 = 0{,}6$ Fig. 6 a shows the relationship between σ_1 and σ_3; however, since the rate of loading is constant the diagram can be regarded as representing the increase of the load in time. Fig. 6b presents the measured values of the neutral stresses. Before reaching the criticial state, the system is, as shown, open, the air can freely escape. The phase composition of the sample, at the beginning of the test, is shown on Fig. 7. Fig. 7a symbolizes the total volume; 7b represents the volume of the original sample (having primary pores only) and the total volume of the secondary pores. Finally, Fig. 7c gives the volume of the different phases. This is then, the composition of the sample at the beginning of the test. At increasing σ_1 the specific compression also increased (see Fig. 6c); at point *1* — before reaching the critical state —, after pressing out a certain volume of air and

Table 1

Results of triaxial test

σ_1 kPa	σ_3 kPa	Δh mm	ε_1 %	ρ_d (gr/cm^3)	s %	w %	a %	S	u kPa
**				1.36	48.6	48.3	3.1	0.94	0
0	0	0	0	0.84	30.0	29.8	40.2	0.43	0
7.3	10	33.8	15	0.99	35.4	35.1	29.5	0.54	7
23.7	27	41.9	18.6	1.03	36.8	36.6	26.6	0.58	14
48.7	39	50.4	22.4	1.08	38.6	38.3	23.1	0.62	23
100	63	60.1	26.7	1.14	40.7	40.5	18.8	0.68	29
134.6*	81	64.6	28.7	1.18	42.1	41.8	16.1	0.73	34
149.4	91	66.4	29.5	1.19	42.5	42.2	15.3	0.74	25
169.1	105	67.5	30.0	1.20	42.9	42.6	14.5	0.75	55.6
192.6	118	68.9	30.6	1.21	43.2	43.0	14.0	0.76	89.4
213.6	130	69.5	30.9	1.21	43.4	43.1	13.5	0.76	113.8
235.8	145	69.8	31.0	1.22	43.6	43.2	13.2	0.77	140.0
259.3	163	70.0	31.1	1.22	43.8	43.3	12.9	0.77	158

Soil type: yellow clay; $I_p = 42$ percent
*critical pressure
**one lump

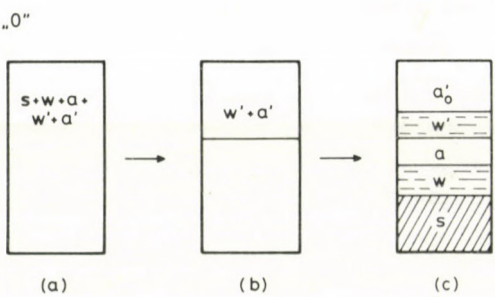

Fig. 7. The soil sample having secondary porosity at the beginning of the test (at point "*O*"). *a* — total soil sample; *b* — the original soil and the secondary pores, filled partly with air, partly with water

compressing the sample, the phase composition will be represented by Fig. 8. The phase composition will be similar in the critical state, where the water starts to escape. The system will be closed here, and the load increased; thus volume of the sample remains from here principally unchanged. However, a slight change will occur (Fig. 6c) since the air-water mixture, which is enclosed into the secondary pores, is not incompressible. The values of the pore-water pressures $\mathbf{u_w}$ after having passed the critical state, are given on Fig. 6b. At point *3* the phase composition will be as it is given on Fig. 8, since the volume will slightly change and this change is due to the compression of the air-water mixture, and not the squeezing out of the same.

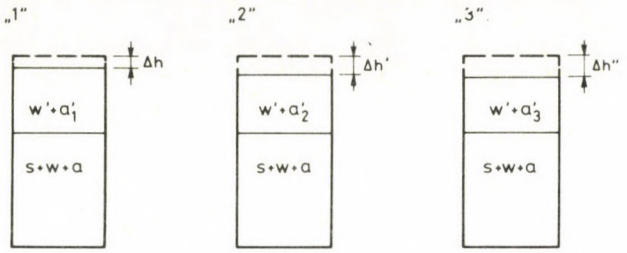

Fig. 8. Composition of the sample at points *1*, *2* (critical) and *3*

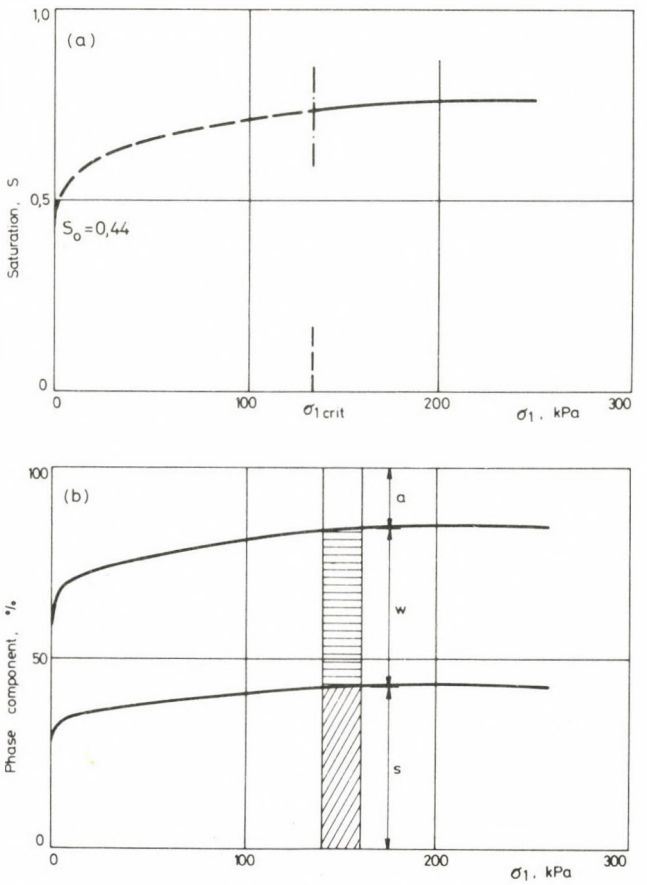

Fig. 9. Variation of *a* — the degree of saturation and *b* — of the phase composition respectively, vs. the first principal stress

The change in the degree of saturation (S) of the sample is given on Fig. 9a, vs. σ_1 . There is indeed a very slight change over the critical state. Fig. 9b illustrates the change of the phase composition.

In the following another example is given: the investigation of the aelotropic consolidation of a clay tip ($\mathbf{K}_0$ condition). The soil is composed of lumps, and it shows a considerable secondary porosity. The load was increased — in order to simulate real conditions — according to Fig. 10 (curve *a*); the specific compression is shown in Fig. 10 (curve *b*). The measured values of the pore — air, and pore — water pressures, respectively, are also given on Fig. 10 (curve *c*), vs. the specific compression. The test furnished important numerical data to visualize the stress state, the deformations and volume changes in the tip, which help to judge its comportment.

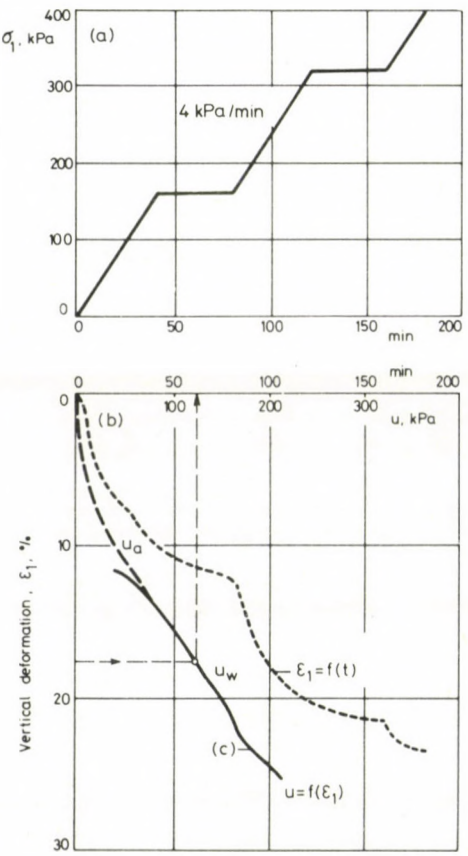

Fig. 10. Variation of the pore-air and pore-water pressures, respectively, due to the loading rate shown in *a*; *b* — specific compression; *c* — pore pressures vs. specific compression

References

Kézdi, Á. (1973): Handbuch der Bodenmechanik. Vol. 3. Verlag für Bauwesen, Berlin.

Kézdi, Á.—Horváth, Gy. (1977): Stresses and Strains in Sand in Axially Symmetrical Case. Proc. 9th. Int. Conf. Soil Mech. Found Engg., Vol. 1. pp. 161–164. Tokyo.

Kézdi, Á.—Horváth, Gy. Triaxial Pressure Cell for Precise Testing (in print)

Bishop, A. W. (1973): The Stability of Tips and Spoil Heaps. The Quarterly Journal of Engineering Geology; Vol. 6, nos. 3. 4. pp. 335–376. London and Edinburgh.

Acta Technica Academiae Scientiarum Hungaricae, 94 (3—4), pp. 123–131 (1982)

TRIAXIAL PRESSURE CELL FOR PRECISE TESTING

Á. KÉZDI, GY. HORVÁTH*

Using a specially transformed triaxial testing device with large sample which can be used to work along prescribed stress path (either stress or strain control), tests were performed to investigate the strains and volume changes in loose and dense sands. A given homogeneous inital condition has been established with a prescribed phase composition. The rate of loading was the same for all test. After establishing and measuring the coefficient of earth pressure at rest (K_0) strains, volume changes were measured during loading, and the character of the variations in the different stages of the test observed. The critical density can therefore be defined not only from point of view of the sign of volume change but also of the kind of the failure mechanism. It has been proved that the different stress paths do not influence the shear strength parameters neither the critical states of stresses occurring during the failure process.

Introduction

The triaxial pressure cell is generally known as a device which furnishes the relatively most reliable values of the shearing strength parameters of soil. The cells of different makes allow to apply to the sample a combined state of stress ($\sigma_1 \geq \sigma_2 = \sigma_3$) to measure the pore stresses, the vertical displacements and the volume changes. If the stresses are continuously changed, definite stress paths can be followed, it is possible to investigate the effect of the different stress paths and of turning of the principal planes. A few characteristic stress paths are given on Fig. 1; Fig. 2 shows the determination of shearing strength, by following different stress paths.

The differences found in test results due to these effects are generally small so they cannot be detected by using the customary equipment and testing methods. Therefore, the Geotechnical Laboratory of the Technical University of Budapest substantially modified a triaxial testing device of the make of Wykeham Farrance Engg. Ltd. making it suitable for the precise investigation of failure mechanism and thus increased the accuracy of the measurements. The modified device is suitable to produce any axially symmetrical state of stress and to follow any stress paths. In order to increase the accuracy of the measurements the device has been equipped with electric sensors and automatic registrating instruments. The original equipment was also suitable to carry out tests in different axial symmetrical stressed states, in open or in closed system, along different stress paths, with different loading rates. In the following the paper discusses the modified equipment and presents some test results.

* **Horváth, György**, Civil Engineer, Department of Geotechnique, Technical University, Budapest

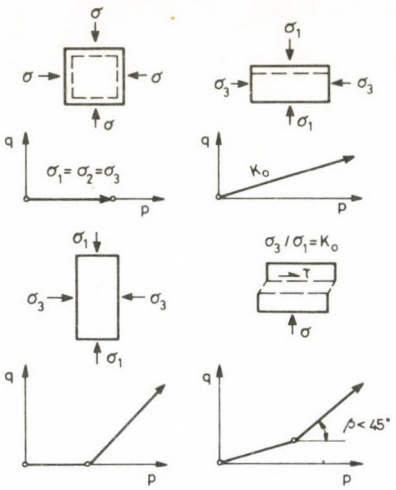

Fig. 1. Typical stress paths [$p=(\sigma_1+\sigma_3)/2$; $q=(\sigma_1-\sigma_3)/2$]

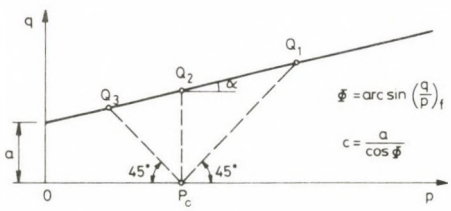

Fig. 2. Determining the shearing strength with triaxial test; applying different stress paths

Modification of the triaxial equipment

The block diagram of the modified triaxial equipment is given on Fig. 3. The end surfaces of the sample in the cell (*1*) having a diameter of 10 cm are loaded by pistons (*2*) of the same diameter and by the cell base. The loading piston and the cell base (*3*) have two different forms, as they are shown on the left hand side and the right hand side of Fig. 3. (Variants *a* and *b*.) It depends on the desired type of the test, which piston and which cell base are used, according to the diagram, so that stress σ_1 can be registered also by pressure cell (*4*). The sample is covered, as usual, by a rubber membrane; the fluid pressure σ_3 acts on the lateral surface of the same. σ_1 and σ_3 can be varied in any stage of the test, independently of each other.

In the course of the test, the separately mounted motor of the loading device pushes the cell with its base (*5*) upwards. The vertical load which acts on the sample will be displayed, besides the pressure cells (*4*), having a diameter of 7 cm, are also indirectly

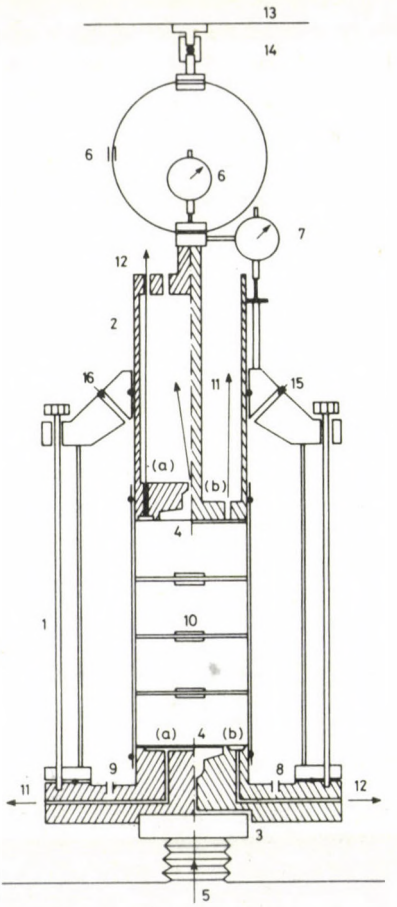

Fig. 3. The block diagram of the modified triaxial testing equipment. *1* — triaxial cell; *2* — pistons, ∅ 10 cm diam; *3* — cell base; *4* — pressure cells, ∅ 7 cm diam.; *5* — loading plate; *6* — pressure gauge; *7* — electric strain gauge; *8* — miniature cell to measure lateral pressure; *9* — connection to the volume change measuring device; *10* — bands to measure the changes in perimeter; *11* and *12* — measurement of pore pressures; *13* — stiff yoke; *14* — loading lever; *15* — deairing valve; *16* — oil valve

measured by the pressure gauge (*6*); at the same time, the glued strain gauges serve for automatic registration of the stresses. The velocity of vertical deformation can be varied between wide limits. Its exact value can be measured by an electric strain gauge (*7*). The prescribed $\sigma_3 = \text{const.}$ fluid pressure can be set by a mercury stress stabilizer through value (*8*). Its value is measured by a miniature pressure cell mounted on value *8*. The volume change will be obtained either a by measuring device mounted directly on value (*9*), or it is calculated using the readings taken on the precision perimeter measuring bands (*10*). These bands register the changes of the sample perimeter with an exactitude of two per mill. Slow deformations are measured by direct reading, fast ones by taking pictures. The pore water pressure is measured either manually by a

manometer fixed on valve (*11*), by using a null indicator and a regulating pump; or by a miniature cell (of the make Kyowa, Japan) connected through valve (*12*), with continuous registration. In soils having three phases — solids, water and air —, then there acts also a pore air pressure in the pores. These can be measured by using a device constructed on the basis of Boyle-Mariotte's Law (Kézdi, Á.—Horváth, Gy., 1979). This apparatus can be connected through valve (*12*).

For a test in open system, both the air and the water may leave through valves (*11*) and (*12*) to the open air.

The equipment has a motor drive and thus allows a loading with uniform displacement velocity ("*stress-control*"-*method*). The sample which is pushed upwards through the piston and the pressuremeter, is supported by a stiff yoke.

If, between the stiff yoke (*13*) and the pressuremeter (*6*) a one-armed loading lever (*14*) is installed, having a gear ratio 1 : 10, with a water container on the end of it, then, applying a load increase by filling the container uniformly by water, a "*strain-controlled*" test can also be performed. End switches on the one-armed lever ensure the uniform transmission of the load to the sample through piston (*2*).

The measuring elements (*4*), (*6*), (*7*), (*8*) and (*12*) allow to measure and register electrically the stresses and deformations. The signs go through an amplifier and to the registrating device having several canals and to the plotter. The results are evaluated by a Hewlett-Packard computer.

The complete equipment with the multicanalplotter is shown on Fig. 4.

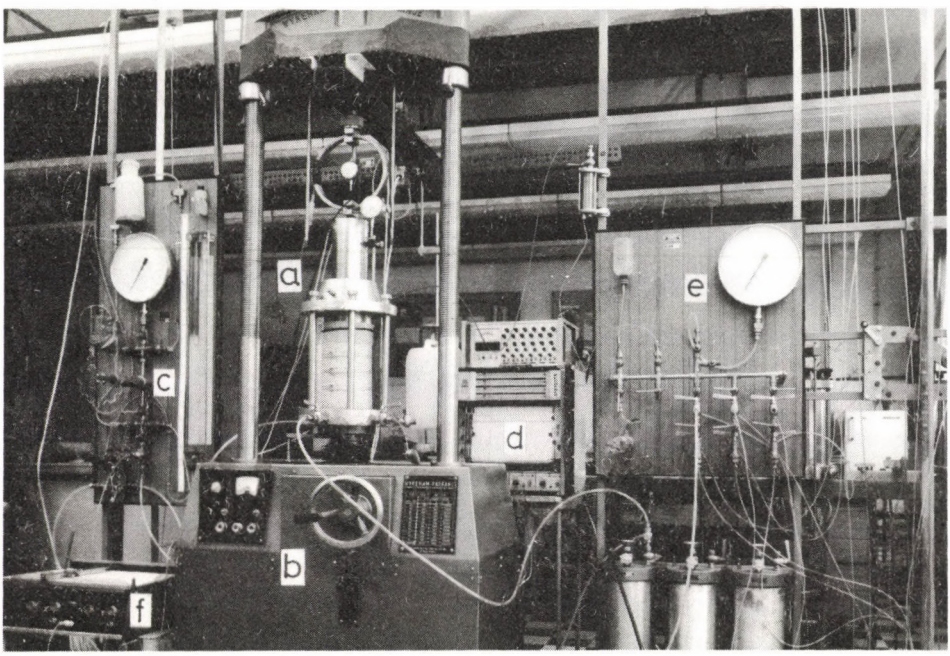

Fig. 4. Photo of the equipment

Tests with the modified equipment

a) Shearing strength of sand

For this test, a sand with the grain size distribution curve shown on Fig. 5 was used, in dense and loose state, having the physical characteristics in Table 1. It has to be mentioned that the density in the loose state was smaller than the critical one, in the dense state, it was greater than that, in the stress range used. The stress paths, the deformations, the volume changes have been determined and the shearing strength parameters in the failure state obtained. The sample was acted first by the principal stresses which corresponded to the "*at-rest*" state, then loaded by increasing the vertical stress up to the failure. Fig. 6 shows the stress paths and the failure line in the coordinate system in the loose and the dense state of the sand as well.

Further shearing strength results are given in the paper Kézdi, Á. and Horváth, Gy. (1977). It was an important result of the investigations that the angle of internal friction was independent of the stress path applied, in this axial symmetrical stressed state, for this sand.

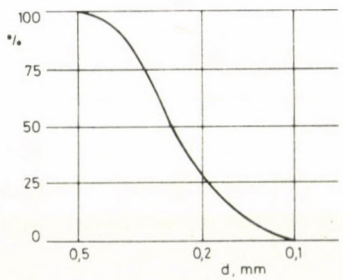

Fig. 5. Grain size distribution curve of the soil tested

Table 1

Physical characteristics of the soils tested

Physical characteristics	Dimension	Dense *a*	Loose *b*
Dry density γ_0	kN/m^3	15.9	14.0
Volume percentage of solids	$s\%_0$	60	53
Volume percentage of water	$v\%_0$	8	7
Volume percentage of air	$a\%_0$	32	40
Void ratio	e	0.67	0.89
Water content	$w\%_0$	5	

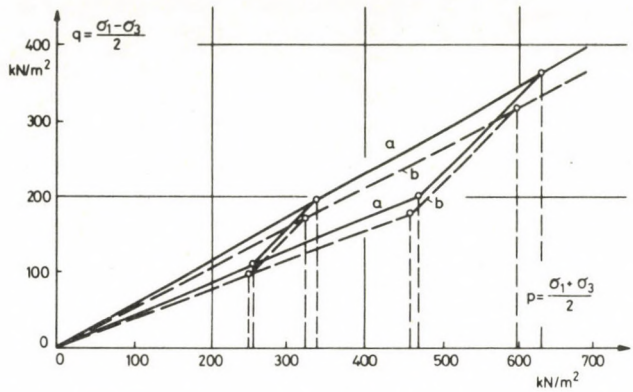

Fig. 6. Stress paths and failure lines of the tests (*a* — dense; *b* — loose)

b) Determination of the coefficient of earth pressure at rest

The coefficient of earth pressure at rest (K_0) in axial symmetrical stressed state is usually determined by performing the triaxial test at different σ_1 values and evaluating the σ_3 value at which the lateral displacement of the sample is zero. The modified equipment offers another method with a greater accuracy. The sample and the piston having both 10 cm diameter are surrounded by water. This water transmits the principal stress σ_3 on the sample. If we keep the amount of this water constant, then, at the load exerting by the piston the pressure σ_1 on the sample, if the water is deaired and the cell perfectly sealed, the pressure σ_3 in the closed cell space will necessarily correspond to the state of the earth pressure at rest. The sealings were checked before testing in the stress range used.

c) Measurements of the deformations

The vertical and radial displacements which occurred during the run of the previously given stress path are given on Fig. 7*a*; Fig. 7b shows the values of the specific volume change. On the latter diagram, the stress $\Delta\sigma_1$ has been plotted, which means the pressure increment applied after the "*at-rest*" stressed state has been reached. The volume change which occurred up to this point was proportional to the principal stresses. The volume change was a decrease first also in the dense state, then the process of failure starts which is accompanied by a loosening; finally, the soil fails and plastic deformations occur. (Section *3–4*.) The loose sand passes through alternating densification and loosening processes, no definite sliding surface is formed, only local slides occur. The failure mechanism for the dense sand and for the loose sand is different; this is particularly well displayed by the formation of the volume changes.

The Mohr's circles of the stressed states which were formed during the failure process and can be called as critical, are shown on Fig. 8. The "*at-rest*" state (*1*), the limit

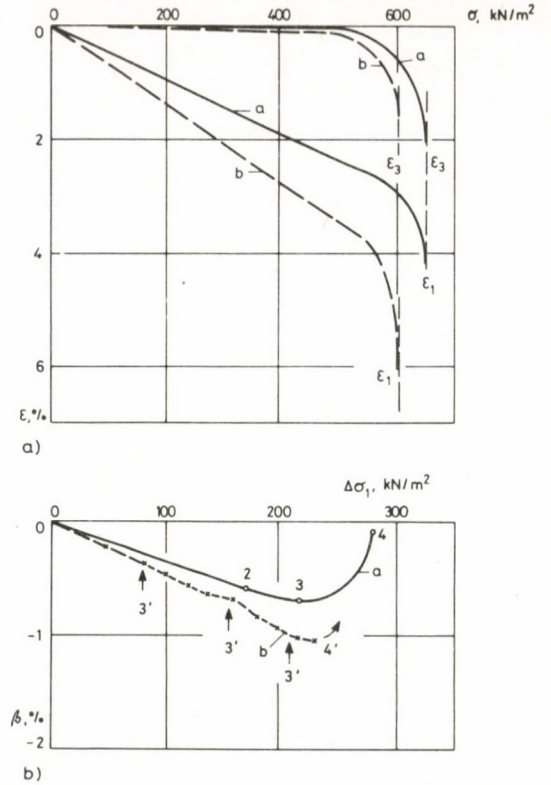

Fig. 7. a — specific displacements; *b* — volume changes

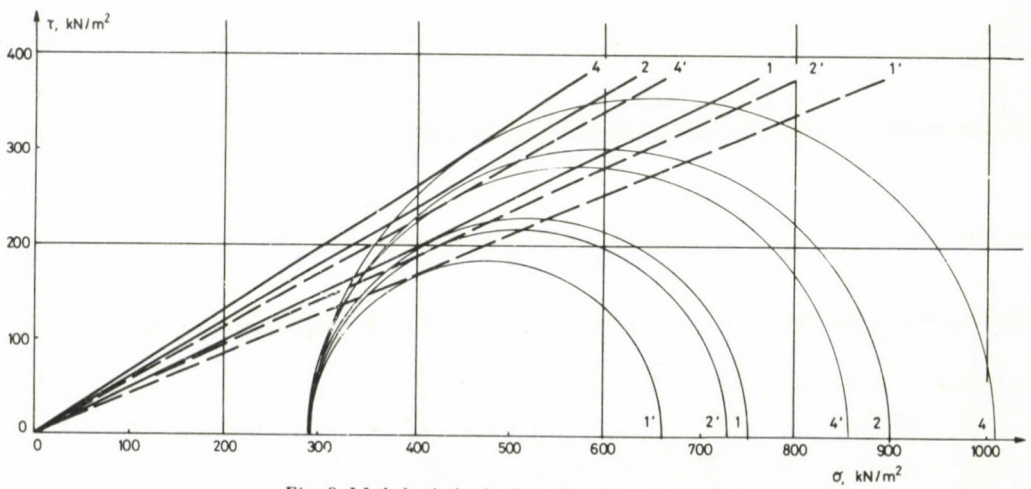

Fig. 8. Mohr's circles in the critical stressed states

of linearity (*2*) and the failure state (*4*) are given. The inclination of the tangents to the circles, the Φ_0 and Φ values respectively can be found in Table 2. In the initial state, the inclination of the tangent to this circle, being $(\sigma_1 - \sigma_0)/(\sigma_1 + \sigma_0)$; based on this the coefficient of the earth pressure at rest can be calculated. The values Φ, Φ_0 and K_0 are summarized in Table 2.

The precision bands fastened on the surface of the cylindrical sample like tyres, allowed to measure the lateral — radial — displacements in several cross sections. Results of such a measurement are given on Fig. 9 for loose and dense sand. It can be seen that the deformations of a dense sand are represented in every cross section by a smooth curve. The value of the pressure increment where the failure process starts, can

Table 2

Inclination of the tangents to Mohr's circles for critical stressed states

Data	Dense *a*	Loose *b*
e	0.67	0.89
Point *1.* (Earth pressure at rest)	26.6^0	23.3^0
Point *2.* (Limit of linearity)	31.0^0	25.4^0
Point *4.* (Failure)	33.4^0	29.8^0
K_0	0.39	0.44

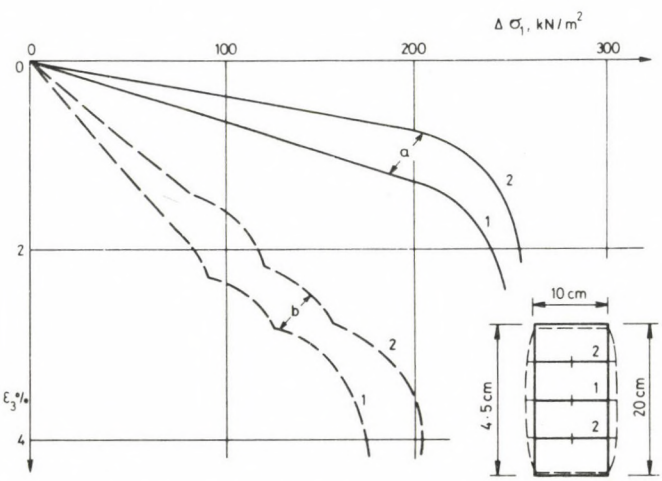

Fig. 9. Lateral displacements at different heights

be clearly determined. The smooth curves suggest the formation of an individual sliding surface which is initiated in the inside of the sample it then propagates and covers the whole sample. The bands located symmetrically on both sides of the sample, furnished identical results. In the same way, like the line of the volume change on Fig. 8, a loose sample gets into the failure state through alternating densification and loosening processes, through the formation of local sliding surfaces. The critical density can therefore be defined not only from point of view of the sign of volume change but also of the kind of the failure mechanism. Samples denser than the critical fail through progressive loosening and the forming of an individual sliding surface. Looser samples fail through a process of alternating loosenings and densifications, reaching a plastic state. It has been proved that the different stress paths do not influence the shear strength parameters neither the critical states of stresses occurring during the failure process.

References

Kézdi, Á.: Handbook of Soil Mechanics. Vol. 1 and 3. Elsevier Scientific Publishing Co. Amsterdam, London, New York (1974, 1979)

Kézdi, Á.—Horváth Gy.: Stresses and strains in sand in axially symmetrical case. Proc. 9th Int. Conf. Soil Mech. Found. Engg. (1977) Vol. I. pp. 161–164. Tokyo

Kézdi, Á.—Horváth, Gy.: Measurement of pore air and pore water pressure in triaxial testing. (1979)

Acta Technica Academiae Scientiarum Hungaricae, 94 (3—4), pp. 133–141 (1982)

CONTINUUM EQUATIONS OF TIMBER LATTICE SHELLS

L. KOLLÁR*

[Received: 28 August, 1982]

Lattice shells, consisting of timber laths running in two directions, are, due to their simple method of erection, advantageous for covering large areas. The paper derives continuum differential equations suitable for calculating internal forces and deformations of such lattice shells, both during erection and in the final state under arbitrary vertical loading.

Introduction

An advantageous solution for covering large areas is the lattice shell, mostly made of timber [2]. This is constructed in such a way that a grid of square (or rectangular) meshes is assembled of continuous laths by loose bolts on the ground (Fig. 1). It is lifted into the surface of desired shape, and in this position it is fastened to the edge girder (Fig. 2). The laths undergo during this operation, as a rule, bending in two directions and torsion, and the originally right angles subtended by them become distorted.

In the following we intend to set up the continuum differential equations describing the internal forces and the deformations of the lattice shell.

Assumptions

The individual laths are continuous; they are connected to each other in the joints by bolts which allow unhindered relative rotation of the two laths in the tangential plane of the shell.

The principal directions of the lath cross sections are perpendicular and parallel to the tangential plane of the shell surface at the point in question.

The elongation of the laths is negligible.

The surface of the lattice shell can be considered as sufficiently shallow as to make the approximations of the shallow-shell theory valid. Consequently, the network, originally rectangular in ground plan, remains (approximately) rectangular on the shell surface as well.

* Dr. Kollár L., Karap u. 9., H-1122 Budapest, Hungary

Fig. 1.

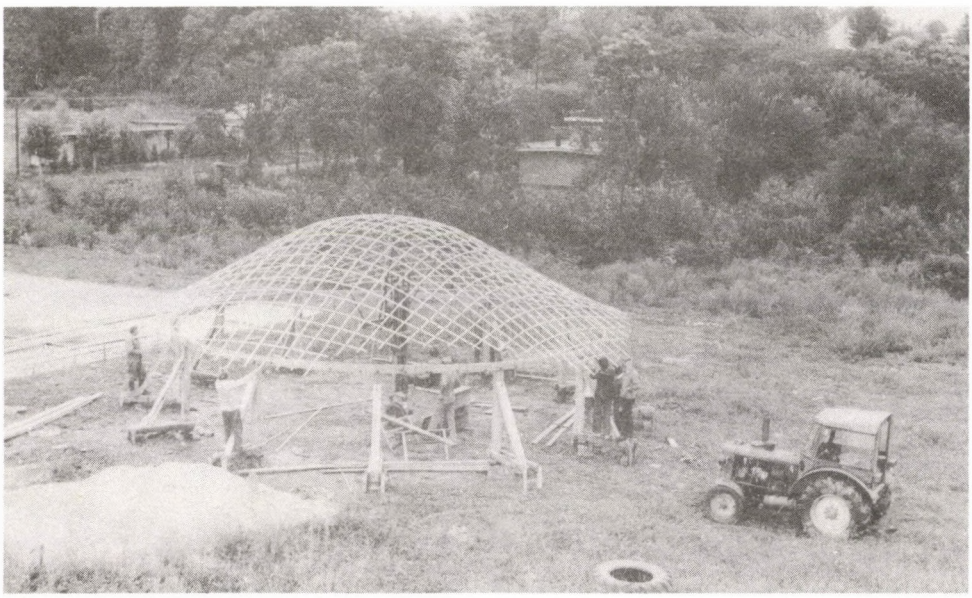

Fig. 2.

The laths are placed densely enough in order to allow us to describe the internal forces of the lattice shell by those of a continuum. To this purpose we have to divide the forces or moments arising in one lath by the distance b_x (or b_y) perpendicular to this lath, in order to obtain specific forces or moments. The well-foundedness of this assumption has been clarified in [4].

Poisson's ratio of the continuum will be taken equal to zero ($\nu = 0$).

The structure is only acted upon by a vertical load p_z.

Equilibrium equations

In the lattice shell the internal forces shown in Figs 3a, 4a and 5 arise. Of these forces those depicted in Figs 3a and 4a have equivalents in the continuous, bent shallow shell (Figs 3b and 4b). However, the internal forces of Fig. 5 have no equivalents in the continuous shell, so that the equivalent continuum of the lattice shell has to be a generalized (multipolar) continuum, in which also the equivalents of the forces of Fig. 5 exist.

Of the forces in Fig. 3 we have to remark that in the lattice shell no forces equivalent to the membrane shearing forces n_{xy} of the continuous shell develop, since the individual squares of the lattice have no shear resistance in themselves. This is the reason why in Fig. 3b $n_{xy} = n_{yx} = 0$ appears. Although the shearing forces $T_{z,x}$ and $T_{z,y}$ of Fig. 5 seemingly correspond to the forces n_{xy} and n_{yx} of the continuous shell, actually a fundamental difference exists between them. $T_{z,x}$ and $T_{z,y}$ are the shearing forces of the laths as individual beams bent in the tangential plane of the shell, and are not connected to each other by a relation similar to $n_{xy} = n_{yx}$, because they arise in two independent beams, and they are balanced by the variation of the bending moments of these beams.

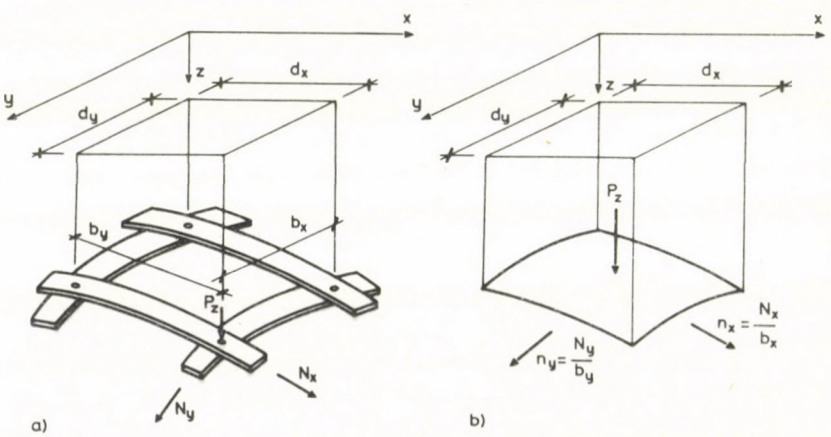

Fig. 3.

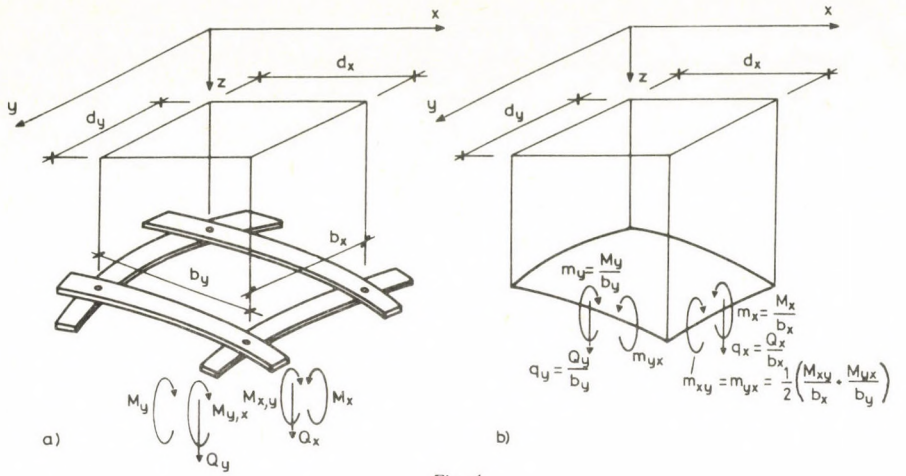

Fig. 4.

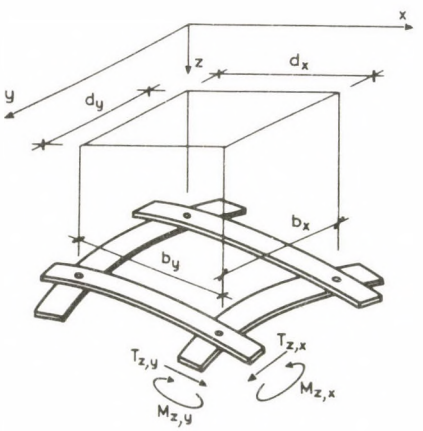

Fig. 5.

This property of the lattice shell can also be formulated as follows. The lattice shell has no shear rigidity proper: the deformation shown in Fig. 6a ($\gamma = \text{const}$) can develop without any resistance. On the other hand, it resists the deformation in Fig. 6b, which is, in fact, the variation of γ. This resistance is the bending stiffness of the beam in the tangential plane of the shell, which is connected to the internal forces shown in Fig. 5.

The shearing forces $T_{z,x}$ and $T_{z,y}$ are directly connected with the normal forces of the perpendicular laths: the normal force N_y (or N_x) increases in a joint to the same amounts as $T_{z,x}$ (or $T_{z,y}$) decreases.

Taking all these into account, the following equilibrium equations can be set up for the equivalent continuum of the lattice shell in a rectangular co-ordinate system,

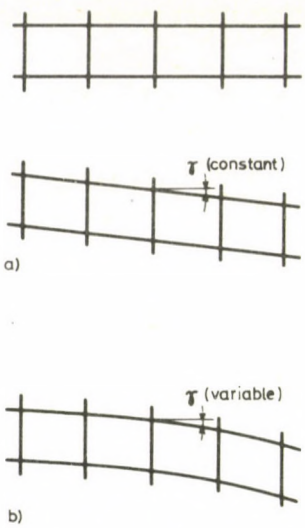

Fig. 6.

using the notations

$$' = \partial/\partial x$$

$$\dot{} = \partial/\partial y:$$

Projection equilibrium in the directions x and y:

$$\frac{T_{z,y}\dot{}}{b_y} = n'_x, \tag{1}$$

$$\frac{T_{z,x}{}'}{b_x} = n_y\dot{}. \tag{2}$$

The equation for the equilibrium in the z direction can be written on the basis of the shallow-shell theory [1], [1a] (considering that in our case $n_{xy}=0$):

$$n_x(z'' + w'') + n_y(z\ddot{} + w\ddot{}) + q'_x + q_y\dot{} + p_z = 0. \tag{3}$$

In this equation

z is the ordinate of the small surface, measured from the plane xy, in unloaded state ("erection shape"):
w is the displacement perpendicular to the shell surface:

The equilibrium of moments turning around the axes y and x can also be taken from the shallow-shell theory:

$$m'_x + m_{xy}\dot{} - q_x = 0, \tag{4}$$

$$m'_{xy} + m_y\dot{} - q_y = 0. \tag{5}$$

Finally, the moment equilibrium around axis z is ensured by the relations $T_{z,x}=M'_{z,x}$ and $T_{z,y}=M_{z,y}^{\cdot}$, valid for the individual laths as beams bent in the tangential plane of the shell, so that there is no need to set up the sixth equation.

In Eq. (3) we let appear in the expressions for the curvatures, in addition to z, also the derivatives of w, that is we wrote down this equation for the surface changed due to the loading, rather than for the "original" shape defined by z, i.e. we used the "large-deflection theory". If we content ourselves to use the "small-deflection theory", we can cancel the two w-derivatives.

Expressing the internal forces by the displacements

Denoting the displacements in the x and y directions by u and v respectively, the internal forces of the continuous laths, as beams bent in the tangential plane, can be expressed by the usual formulas:

$$v''=-\frac{M_{z,x}}{EI_{z,x}}, \tag{6a}$$

$$v'''=-\frac{T_{z,x}}{EI_{z,x}}, \tag{6b}$$

$$v''''=-\frac{T'_{z,x}}{EI_{z,x}}, \tag{6c}$$

$$u''=-\frac{M_{z,y}}{EI_{z,y}}, \tag{7a}$$

$$u'''=-\frac{T_{z,y}}{EI_{z,y}}, \tag{7b}$$

$$u''''=-\frac{T_{z,y}^{\cdot}}{EI_{z,y}}. \tag{7c}$$

In these relations $EI_{z,x}$ and $EI_{z,y}$ are the bending stiffnesses, effective against bending in the tangential plane of the shell (i.e. referred to the axis z), of the lath-beams running in the x and y directions respectively.

In the following we shall denote by u_0 and v_0 the x and y directed displacements coming about during erection, and by u and v those developing under external loads.

The specific "plate" moments appearing in Eqs (4) and (5) can be expressed by the curvatures and twist of the shell surface z and by the displacement w perpendicular to the surface:

$$m_x=-\frac{EI_x}{b_x}(z''+w''), \tag{8}$$

$$m_y=-\frac{EI_y}{b_y}(z''+w''), \tag{9}$$

$$m_{xy} = -\frac{1}{2}\left(\frac{GI_{tx}}{b_x} + \frac{GI_{ty}}{b_y}\right)(z'' + w''), \tag{10}$$

where EI_x and EI_y are the bending rigidities, valid in bending in the plane normal to the shell surface, of the lath-beams running in the x and y directions respectively, and GI_{tx} and GI_{ty} are the torsional rigidities of the same beams.

The second derivatives of z in Eqs (8) to (10) express the fact that one part of the moments in the laths are caused by distorting the lattice into the required erection shape, and the second derivatives of w show that the other part of the moments is due to the displacement w measured from the erection shape.

We still should express the normal forces n_x and n_y, appearing in Eqs (1) and (2), by the displacements parallel to the laths in which these forces arise. However, this cannot be done because of the assumed inextensionality of the laths. Instead, we can write the condition of inextensionality itself.

The condition of inextensionality during erection cannot be expressed by a simple equation, since the ordinate z of the erection shape can by no means considered as a "small" displacement. Hence, the fulfilment of this requirement has to be described by a method also valid for large displacements, as to be found e.g. in [3], which furnishes the displacements u_0 and v_0, pertaining to z.

The inextensional character of the deformation caused by external loads are expressed by the equations

$$u' - w(z'' + w'') = 0, \tag{11}$$

$$v^{\cdot} - w(z^{\cdot\cdot} + w^{\cdot\cdot}) = 0, \tag{12}$$

valid for small displacements, see e.g. in [6]. In most cases we can omit from these equations the terms w'' and $w^{\cdot\cdot}$, being small in comparison with the corresponding derivatives of z.

However, we can establish relations between the normal forces n_x, n_y and the displacements u, v of the perpendicular laths by expressing $T_{z,x}'$ and $T_{z,y}^{\cdot}$ from Eqs (6c) and (7c), and introducing them into (1) and (2), (separating u_0, v_0 from u, v):

$$n_x' = -\frac{EI_{z,y}}{b_y}(u_0^{\cdot\cdot\cdot\cdot} + u^{\cdot\cdot\cdot\cdot}), \tag{13}$$

$$n_y^{\cdot} = -\frac{EI_{z,x}}{b_x}(v_0'''' + v''''). \tag{14}$$

Writing the equations in terms of the displacements

Let us introduce (8), (9) and (10) into (4) and (5), express q_x and q_y and introduce them into (3):

$$n_x(z''+w'')+n_y(z^{\cdot\cdot}+w^{\cdot\cdot})-\frac{EI_x}{b_x}(z''''+w'''')-\left(\frac{GI_{tx}}{b_x}+\frac{GI_{ty}}{b_y}\right)(z''''+w'''')-$$

$$-\frac{EI_y}{b_y}(z^{\cdot\cdot\cdot\cdot}+w^{\cdot\cdot\cdot\cdot})+p_z=0. \tag{15}$$

We have, in addition the two equations of inextensionality (11) and (12), which have to be substituted for by the method to be found in [3] when investigating the erection shape.

We thus have three equations, for determining the three displacement functions. However, in (15) also n_x and n_y appear, and cannot be eliminated. Consequently, we have to add also Eqs (13) and (14), so that we finally have five equations for the five unknowns (u, v, n_x, n_y, and z or w).

Solution principle of the equation

We have to solve our equation system for two cases: for producing the erection shape and for the loading.

When looking for the *erection shape*, we have

$$u=v=w=0. \tag{16}$$

We assume the erection shape $z(x, y)$ required, expediently in the form of a series, compute the pertaining functions u_0, v_0 (e.g. on the basis of [3]), i.e. the horizontal displacements of the laths, and from these we determine n_x' and n_y' with the aid of (13) and (14). By integration we produce n_x and n_y, which should be introduced into (15). Thus we obtain an equation for z, in which two unknown functions resulting from the integration of n_x and n_y also appear. From this equation we determine z, and we repeat the procedure starting from this new z. The procedure can be repeated until the final z agrees with the initial z with the required accuracy.

The problem can be simplified by neglecting the own weight of the lattice shell ($p_z=0$). In this case we determine, in fact, the buckled shape of the lattice shell with large deformations.

If the erection shape is known and we are looking for the deformation and internal forces of the lattice shell *under a given load* p_z, the task becomes more complicated. We can proceed in several steps, and use approximations in the first steps.

So in the first step we may neglect u and v, i.e. we can consider the magnitudes of n_x and n_y as unchanged.

We intend to show the application of the method outlined above in the frame of a numerical example in a subsequent paper.

References

1. Flügge, W.: Statik und Dynamik der Schalen. 3. Aufl. Springer, Berlin/Göttingen/Heidelberg 1962
1a. Flügge, E.: Stresses in Shells. Springer, Berlin/Heidelberg/New York 1973
2. Happold, E.—Liddell, W. I.: Timber Lattice Roof for the Mannheim Bundesgartenschau. The Structural Engineer **53** (1975), 99—135
3. Hegedüs, I.: Computation of the Stretched Network Shape of Timber Lattice Shells. To be published in: Acta Techn. Hung.
4. Kollár, L.—Hegedüs, I.: Analysis and Design of Space Frames by the Continuum Method. Publ. House Hungarian Academy of Sciences, Budapest, and Elsevier Scientific Publ. Corp., Amsterdam; to be published in 1985
5. Love, A. E. H.: A Treatise on the Mathematical Theory of Elasticity. 4th Ed. Dover Publ. New York 1944
6. Timoshenko, S. P.—Gere, J. M.: Theory of Elastic Stability. McGraw—Hill, New York/Toronto/London, 1961

Acta Technica Academiae Scientiarum Hungaricae, 94 (3—4), pp. 143–155 (1982)

A RECENT METHOD FOR THE NUMERICAL SOLUTION OF ENGINEERING PROBLEMS PART II

E. BÉRES

[Received: 31 May 1982]

Computation error

The result of an approximate analysis can only be evaluated in knowledge of its accuracy, or else, of the computation error. Theoretically, this concept of an error is rather simple, it being understood as the difference between the computed and the true value. Only that in practice, this concept escapes quantification exactly when it would be a must. The approximate method is mostly applied in the absence of an exact solution possibility. Though, in that case, no error can be indicated, in more complex cases not even estimated. Namely, while in most problems, analysis can give an upper bound for the computation error, methods applied in several domains of physics — e.g. in elasticity — can give no such bounds, underlying the practice of qualifying these methods according to exactly solvable problems, permitting to confront approximate results with the exact solution. This yields fair conclusions on the method and its accuracy in general, without, however, yielding information on critical ranges of critical problems.

In several domains of physics — e.g. in elasticity — assignment is, however, in only one direction as complicated as to inhibit assignment of one group of variables to the other group, hence computation of the exact values. In the other direction the relationship is simple and exactly determinable. For instance, a common problem is to determine deformation and stress distribution under a given load, exceptional to be exactly solved. Though, load for a given deformation or stress distribution is rather simple to exactly compute.

Naturally follows the interpretation of another error. After having computed the approximate stress or deformation values for a given load, the load pertaining to this stress distribution (deformation) is to be computed, a rather simple computation theoretically yielding the exact load for a given stress distribution (deformation). Deviation between the given and the recalculated load is the computation error reflected to the load. This interpretation of the error may be countered by that it is in terms other than of stresses the solution is aimed at. But it is supported by the fact that in practice, load is always indicated at a — not too close — approximation. A further increase of the accuracy of the recalculated value within this range is about meaningless.

A number of computation methods relying on these error concepts have been developed, comprehensively recapitulated by Scharle [3]. Referring to the errors defined above, five "error principles" have been established, four among them may be conditions in practical computations. This clear-cut study discovers the drawback of these attempts by indicating the goal in p. 21 as "to a predetermined sense 'best' approximation". Namely there is an infinity of conditions to be assigned a solution best from the aspect of that condition. But it cannot be predicted, to what of these conditions the solutions best meeting the goal of the problem pertains. This predetermined sense is generally the extreme value of a scalar function. Now, to describe an error given by a multielement vector, a scalar is of limited use even if error vector elements are of the same unit. In elasticity problems, this convenience is restricted to special cases. The vector of errors generally contains also errors of the equilibrium conditions as well as of the dynamical and geometrical boundary conditions, with units [N], [N/m^2] and [m], resp., in the tridimensional case. No physical meaning can be attributed to the scalar value formed of the numerical values of these elements. As a matter of fact, extreme value of a fictious mathematical term is determined and assigned to the problem as solution. But this is not to mean the largeness of the computation, against the fact that the result is accepted without checking by resubstitution, while enhancing the extreme value character of the solution.

Essentially the best solution as defined above is to solve the redundant equation system after some weighting. Neither of the five error principles in [3] gives a more concrete solution than that.

The energetic method applied in the finite element method has, however, to be exempted from this general statement, namely that the extreme value of a concrete physical quantity in terms of a scalar gets determined. Obviously, extreme value of the error function does not refer to stresses of the minimum deviation from the real value obtained from a given function type.

This is one among items requiring exact and approximate methods to be definitely distinguished. Namely if the scalar value of the properly defined error function tends to zero then it is true that the solution tends to the exact one. It would be erroneous to conclude that where the error function of the approximate solution has an extreme value there is the best solution from every aspect. No such relationship exists!

To be precise, energy minimum of the approximate solution does not mean a minimum of errors. If the potential energy belonging to one of two given solutions is less than that of the other one it does not mean that the stress error maximum is the less in the same solution. Even the stress error in the solution with the lower energy minimum may be the multiple of that in the other one. All these hint to caution in evaluating the solution based on the principle of energy minimum.

Error calculation

Neither error principles nor variation methods are seen to suit error determination, let alone estimation. In the finite element method, equations for the equilibrium of each element and boundary conditions for each boundary point can though be written in terms of the calculated displacement and stress components, and their error applied to estimate calculation error, but on one hand, to write this equation system involves as much of work as that of the suggested method, thus the checking work demand is of the same order as that of the solution, on the other hand, errors obtained in checking the finite element method cannot be applied for correction. In the finite element method, an exact error calculation at an arbitrary point would only be possible if also the elements would be continuous to a properly high order, an impossibility under the actual circumstances except for extremely simple cases.

On the contrary, the suggested method permits both estimation and exact tracking of the error. This sharp distinction means that while even the exact error value is easy to obtain at any point (i.e. the error function can be produced,) equilibrium error of elements and error of boundary conditions for given nodes — mere error approximations — are just as important by helping the method to improve the result accuracy without increasing the number of terms of the approximate function, hence of the unknowns.

Error measured in terms of load or other starting data permits a relatively simple and exact error determination. The suggested method seems to be easier to understand via available results.

In the simplest case fulfilment of equilibrium conditions for a finite number of points is examined. Solution for a complete structure of finite elements accessible to exact analysis consists in determining the displacement of a finite number of points, its error being the difference between given nodal loads and loads that acting at the same poinst would produce exactly the calculated displacements. A typical example is the plane lattice subject to normal forces at nodes alone. Szabó [6] was the first to expound this method underlying also [8] by the Author. In this case all elements of the error vector being of the same unit, the complete calculation error is well described by a scalar value. The calculation accuracy is simplest improved in case of convergence to apply the load error with reversed sign, as load complement on the lattice. Thus, in case of a lattice, this way of error calculation suits, besides of calculation error estimation, also to increase the calculation accuracy.

The next important development of the method has been due to Szabó extending it to rope nets. The change consists essentially in assigning other than given rope lengths, rather than different nodal loads alone, to approximate nodal displacement values. Thus, calculating then resubstituting approximate rope net nodal displacement values will show not only loads at each node to differ from the given one but also rope lengths to differ from given rope lengths under calculated forces and at the given temperature. All these deviations should be contained in the error vector that thus will

have elements of different units. As a conclusion, no unique physical concept can be defined for error principles in [3] let alone tridimensional continua and more complex technical problems. Szabó [6], [7] has found a rather ingenious way to eliminate these difficulties in the case of rope nets. Nodal loads and rope lengths in the approximate solution are determined by resubstitution and the closeness of the solution is examined in terms of the physical reality corresponding to the errors rather than of the single scalar formed of them. In case of a rope net the recalculated nodal load values are required to be within the specified load accuracy range, while rope length errors are reckoned with in terms of the compensating temperature, rather than of the original unit (m). Namely, the length difference gives little hint of the resulting further force effects in the rope, affected also by the rope length and cross section. Though, converting the length error to e.g. stress partly makes the assignent more complex, and partly it will be less illustrative and perceptible than in terms of temperature. Error expressed in terms of temperature has the further advantage that practically also temperature is only known at a given accuracy. If the length error in terms of temperature is inside this range, a further refinement of the calculation would be meaningless in this respect.

Now, let us point out differences in handling continuum problems compared to the earlier procedure. First, for finite models, after having eliminated the errors, the solution accuracy could be arbitrarily improved, while in a continuum problem the type of the assumed approximate function (in the case of e.g. a polynomial its power and number of its terms) does not permit to reduce the calculation error below a given specific limit. This statement is obvious from the consideration that the error cannot be reduced below an arbitrary low limit else than by arbitrarily incresing the number of terms in the function series. Limitation of the number of terms in the function series involves the approximation error not to decrease beyond all bounds. In this case the best solution tends to another limiting condition rather than to the exact solution.

The continuum character and the approximation in form of finite series have another consequence. Rather than the exact error function, only the conditions of equilibrium for finite size elements, and boundary conditions for a finite number of nodes can be used for correcting the solution. Namely the solution process involves only these equations, the error function serving exclusively for exactly expressing the errors.

Let us see now, how to extend the principle developed for lattices and rope nets to continuum problems.

Remind that in the outlined method there are more equations than unknowns, and also that these equations are independent for normally assumed elements and edge nodes. Thus, substituting the solution with the minimum error square sum into given equations these are only met at some error, that are thus present already in the equilibrium and boundary condition equations. They are advantageous, however, by being no pure numerical values but physical magnitudes in units corresponding to the

given case, susceptible to realistic evaluation. How to utilize this approximate error value to improve accuracy will be seen in the subsequent item.

The error is made accessible to exact analysis by applying approximate functions continuous over the complete domain and differentiable as many times as required. Thereby solution functions can be substituted into differential equations and boundary conditions of the problem, and the rate of unfulfilment, to be considered error of the solution in a sense, can be determined at any point of the domain.

For instance, in the tridimensional case, error f_σ^i of the equilibrium differential equation

$$\sigma_{,j}^{ij}+\rho x^i=0$$

is obtained from:

$$f_\sigma^i=\sigma_{,j}^{ij}+\rho x^i$$

So are errors f_p^i and f_u^i of dynamical and geometrical boundary conditions, from formulae

$$f_p^i=\sigma^{ij}n_j-p^i\,,$$

and

$$f_u^i=u^i-u_0^i$$

respectively, where

σ^{ij} j-th element $\sigma^{ij}=\sigma^{ji}$ of the i-th row of the stress tensor;
ρ density;
p i-th coordinate of the mass force;
n_j j-th component of the surface normal;
u^i i-th displacement component.

$$\sigma_{,j}^{ij}=\sum_{j=1}^{3}\frac{\partial\sigma^{ij}}{\partial x^j}$$

Stress tensor $\mathbf{T}=[\sigma^{ij}]$ and deformation tensor $\mathbf{D}=[\varepsilon^{ij}]$ being related by:

$$\mathbf{T}=2G\{\mathbf{D}+\frac{\nu}{1-2\nu}I_1(\mathbf{D})\mathbf{E}\}$$

where G is the modulus of elasticity in shear, ν is the Poisson's ratio; $I_1(\mathbf{D})$ the first scalar invariant of tensor $\mathbf{D}$, $I_1(\mathbf{D})=\varepsilon_{11}$ and $\mathbf{E}$ a third-order unit matrix, further,

$$\mathbf{D}=\frac{1}{2}(\mathbf{u}\nabla^x+\nabla\mathbf{u}^x)$$

is the deformation tensor in terms of displacement, ∇ being a symbolic vector

$$\mathbf{V} = \begin{bmatrix} \dfrac{\partial}{\partial x_1} \\ \dfrac{\partial}{\partial x_2} \\ \dfrac{\partial}{\partial x_3} \end{bmatrix}$$

equilibrium equations in terms of displacement components are seen in final account to contain their second derivatives. Thus, in the finite element method, the error can only be exactly computed if the elements are continuously fitted even in the second derivative, a rather intricate, still unsolved problem in the general case, but even the theoretical solution would involve much more unknowns in the equation system than does the suggested method. The number of unknowns would increase by orders of magnitude upon requiring — for the given division — the continuity of elements to the desired order. Of course, practical hindrances of fitting to the desired order refer only to the general case. In special cases such as that in [4], fitting to the desired order is possible, the more so in checking a plate problem or in evaluating its solution. The plate equation is in a convenient form:

$$D\left(\frac{\partial^4 w}{\partial x^4} + 2\frac{\partial^4 w}{\partial x^2 \partial y^2} + \frac{\partial^4 w}{\partial y^4}\right) = p$$

where $p[\mathrm{N/m^2}]$ is load intensity and

$$D = \frac{Eh^3}{12(1-\nu^2)};$$

E is the modulus of elasticity, h the plate thickness and ν the Poisson's ratio. Substituting into this formula the calculated function w yields load $\tilde{p}[\mathrm{N/m^2}]$ in the form given by function w. Deviation of this value from that given at any point of the plate is the computation error in terms of load. Error of the geometrical boundary condition is directly given by the difference between the computed and the measured deflection. Of course, a similar computation may yield the error of another boundary condition — e.g. boundary moment. The formula shows such an error computation for a plate to be only possible if elements are continuous to at least order C^4.

Solution correction

According to the terminology in [3], the redundant equation system is a solution based on the error principle, comprised in the condition of minimum error square sum. But just as different solutions belong to different error principles, conditions of different solutions may be considered as different error principles. In this meaning, in solving a

redundant equation system, a new error principle is not only to minimize e.g. the sum of absolute values or other powers rather than the error square sum, but also to multiply each equation by a different constant. All the obtained solutions are "best approximations to a predefined sense". Unfortunately, these predefined senses cannot be ranked with respect to the final goal, it cannot be predicted, according to which to calculate to obtain the best solution from the aspect of the problem as a whole. Each of these solutions is the best from a given — purely mathematical — aspect, and it cannot be predicted which aspect would coincide with the solution closest approximating the physical reality.

The method of writing equilibrium conditions for finite elements, and boundary conditions for nodes at the edge or for part domains, and to determine the solution with the minimum error square sum for the obtained redundant equation is in fact a computation method on error principle itself, with all its uncertainties. Its essential advantage over others is to permit fast and rather simple computation of the error of each equation, hence fast estimation of load and boundary condition errors. Even, beyond helping evaluation, result appreciation, equation errors give a direct hint on what equations have the greatest errors. Though, reduction of greatest errors improves the solution.

In a redundant equation system, the error of any equation is rather simple to reduce. Namely multiplying the given equation by more than unity, hence increasing its weight compared to the other ones reduces the absolute numerical value of the equation error in terms of the given unit. With increasing the multiplier the error is reduced, with multiplier tending to infinity the error tends to zero.

Thereupon, for a given function type, the available redundant equation system can be applied to improve the computation results as follows:

Equations in the system are written multiplied by the proper constants, providing partly for coefficients in the equation system to belong to the domain of manageable numbers, and partly for the absence of differences by orders of magnitude between equations in terms of different units.

Eventual different orders of magnitude between numerical values of the physical magnitudes of each equation dependent on its type are easy to understand. For instance, be the element a cube with 10 cm sides; stress unit is N/m^2, then the numerical value of components in N of the resultant of forces acting on the element are by two orders less than that of the stresses. The proportion between equations of equilibrium and of dynamical boundary conditions will be the right one either upon dividing boundary condition equations, or upon multiplying equilibrium equations by 100. The balanced equation system will not only be started from, but also errors are calculated on its basis. Correction of the solution comprises the following steps:

— Solution of the equation system with the minimum error square sum is determined.

— The solution is resubstituted into the equation system, error of each equation determined and evaluated with respect to its unit.

— Equations featuring excessive errors are multiplied by a number depending on the relative magnitude of the error. (A possible way to choose the multiplier is shown in Example 2.)

— The reweighted equation system is solved.

— The result is substituted into the original equation system and evaluated as above.

— It is examined whether the error with the greatest absolute value is less or not than that of the former solution.

— If yes, then the computation goes on by changing again the equation weights taking the greatest errors into consideration, and solving the equation system. But if not, this result is rejected and the former taken as the best solution.

This is a rather unusual procedure. The effect of changes is only known in certain limits, or better, only its tendency. But it cannot be predicted whether it furthers the desired improvement or not, just as for any error principle. As a matter of fact, the result is improved by the checking computation deciding over the acceptance or refusal of the correction step.

Errors of the highest absolute value can practically always be reduced by reweighting, since, although theoretically there is a limit where any change of the weight increases the maximum error, but since this limit value is not the same as the exact solution of the probelm, the strive to a highly close approximation beyond practical requirements is useless. The numerical example shows a rather slight change of the weights to significantly alter the results. Thus, often this procedure is the only useful means to increase the accuracy, the number of iterations is, however, to be reasonably restricted.

Computation of composite domains

To now the simplest case of approximating the displacement by a single, continuous function valid for the entire domain has been concerned with. In most problems, treatment as a single domain is self-intended, but the method is valid also for part domains making up the domain.

Theoretically, displacement components in any domain can be approximated by a continuous function each, valid over the entire domain. Though, in certain cases an excessive insistence on it would hamper or even prevent practical realization, but at least it would be unreasonable. It seems self-intended to consider the plate of the plan seen in Fig. 1 as to consist of two part-domains, special equations providing for their connection.

For a complex domain, the computation starts by dividing the entire domain to part domains proper to its geometry. Displacement components are approximated by a different function (polynomial) in each part domain. Part domain boundaries are marked so as to cross nodes where function values for both parts, and also derivatives up to the specified order are required to be equal.

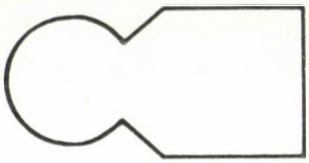

Fig. 1

Just as all boundary conditions are written as linear equations and are all incorporated into the equation system, also connection conditions of part domains are expressed by linear equations to share the redundant equation system. Conditions of connection add to the number of equations rather than to that of the unknowns. Parts of the equation system for a part domain each contain only terms for the unknowns occurring in the given part domain, connected exactly by the equations of connection condition.

The mentioned possibility to reduce the error in, or even to prescribe exactness of single equations of the redundant equation system is equally of importance. However desirable it would be to fit part domains in the due order, this condition must not be excessively insisted on in approximate calculation. Just as fulfilment of boundary conditions for the boundary of a complete domain is required at an accuracy fitting the circumstances, the same refers to part domain connections.

It is decidedly advantageous to have a possibility to connect in the due order. In general, however, fulfilment of the connection conditions at a moderate accuracy has to be made up with. Exact fulfilment of boundary and connection conditions is often renounced of, even if a possibility exists, but fulfilment of the condition would impair the computation as a whole by more than the benefit from exactly meeting this condition.

Numerical examples

Two problems have been solved as practical applications of the method. The first problem is that of a diaphragm, solved, in addition to the presented method, also by the finite element method. The second problem refers to a plate where also correction steps have been applied.

Both problems are bidimensional, hence displacement components are two-variable functions. While, however, the first problem comprises two displacement component functions, the second one, i.e. the plate problem has a single one.

The first problem has been illustrated in Fig. 2 where part b) shows division to elements according to the presented method.

Taking symmetry of the problem into consideration, displacement functions are:

$$u = a_1 x + a_2 xy + a_3 x^3 + a_4 xy^2 + a_5 x^3 y + a_6 xy^3 + \ldots + a_{26} x^7 y^3 + \\ + a_{27} x^5 y^5 + a_{28} x^3 y^7$$

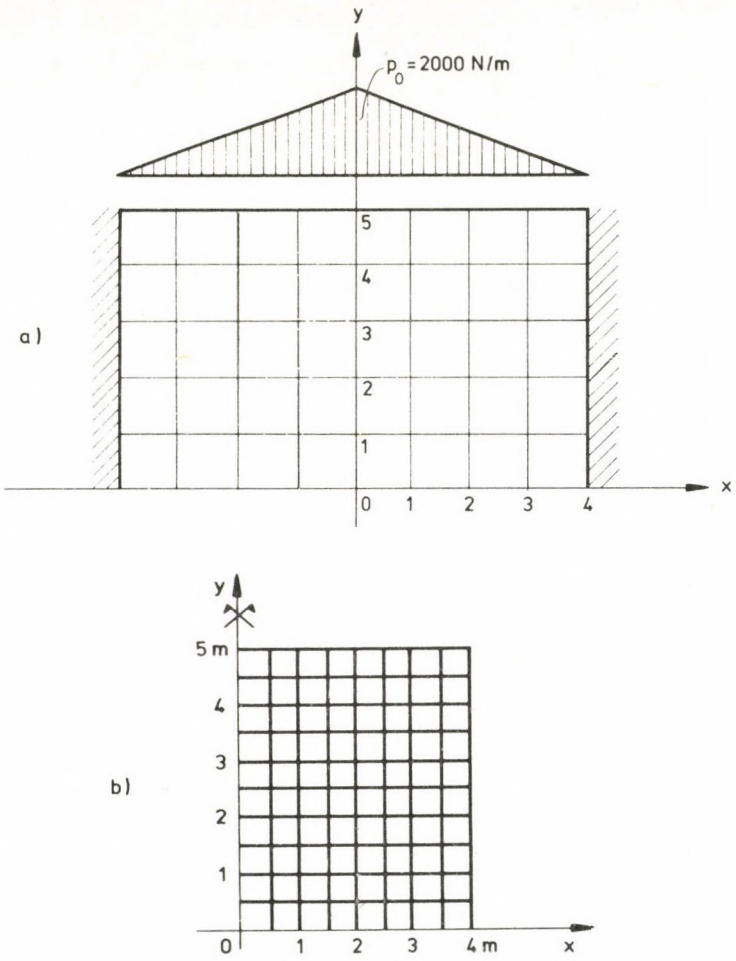

Fig. 2

$$v = b_1 y + b_2 x^2 + b_3 y^2 + b_4 x^2 y + b_5 y^3 + b_6 x^4 + \ldots + b_{29} x^8 y^2 + b_{30} x^6 y^4 + \\ + b_{31} x^4 y^6 + b_{32} x^2 y^8 .$$

A solution exactly meeting geometrical boundary conditions along boundary $x = 4$ is wanted.

Equilibrium errors have been determined for elements with 1 m sides also the finite element method has been applied on.

Equally weighting equilibrium and dynamical boundary condition equations, the maximum error of equilibrium is 236.3 N, while the hundredfold weight of boundary conditions at boundaries $y = 0$ and $y = 5$ increases the maximum error or equilibrium to 604.2 N at a reduction of the error of dynamical boundary conditions.

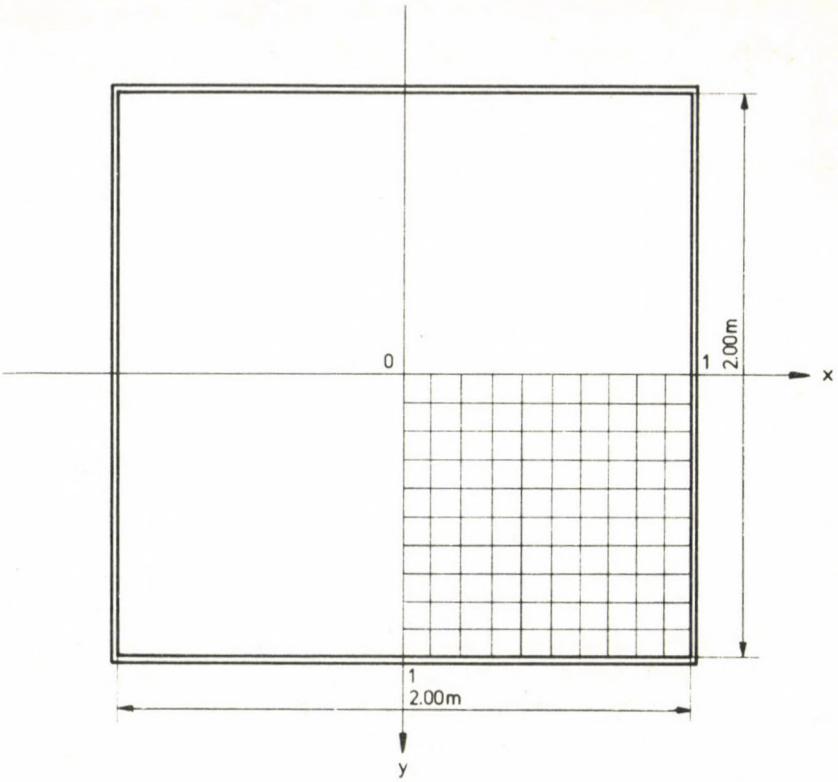

Fig. 3

At the same time the finite element method yields a maximum equilibrium error of 1050.6 N.

The second problem is that of a plate with 2.00 m sides, simply supported edges, subject to uniform load. Symmetry of the problem permits to reduce the computation to a quarter of the plate, still symmetry can be reckoned with inside it. The applied coordinate system and division of the quarter-plate to elements are seen in Fig. 3. The deflection function has been assumed as:

$$w = a_1 + a_2(x^2 + y^2) + a_3(x^4 + y^4) + a_4 x^2 y^2 + \ldots +$$
$$+ a_{37}(x^{20}y^2 + x^2 y^{20}) + a_{38}(x^{18}y^4 + x^4 y^{18}) +$$
$$+ a_{39}(x^{16}y^6 + x^6 y^{16}) + a_{40}(x^{14}y^8 + x^8 y^{14}) +$$
$$+ a_{41}(x^{12}y^{10} + x^{10}y^{12}).$$

A solution meeting geometrical boundary conditions at every point hence $w = 0$ all the boundary is wanted.

Dynamical boundary conditions specify zero moment at edge nodes.

Two alternative solutions have been developed. In one case only force-equilibrium equations, numbering 77 make up the equilibrium equations, in the other case also equations for the moment equilibria of the elements have been written, 177 in number. In both cases, there are 41 unknowns.

Correction steps have only been made in the second case. For the successive solutions, equation weights have been changed according to instruction

$$s_{inew} = \left[\frac{|h_i|}{h_a}\right] + s_i - 1$$

where h_i is error of the i-th equation; h_a the average of the error absolute values; and s_i the weight of the i-th equation.

Let us present some results picked out at random. For a uniform load intensity q, maximum moment, shear force and deflection values are

$$M = \alpha q a^2 \qquad Q = \beta q a \qquad w = \frac{\gamma q a^4}{D}$$

respectively, various solutions yield the tabulated α, β, γ values. First row of the table contains values for the solution with pure force equilibrium equations. The second row shows results where equilibrium equations comprise also those for moments, and equations are equally weighted. The third row is that for results after three reweightings, where the greatest weight is 4 applied only for two equations but even 3 is the multiplier for only seven equations. This weighting offered the best solution. Finally, the fourth row contains exact values by Timoshenko [9].

Table I

α	β	γ
0.04778	0.3388	0.004053
0.04775	0.3372	0.004055
0.04798	0.3365	0.004067
0.0479	0.338	0.00406

Particulars, evaluation, and conclusions drawn from the solutions and results of both problems are found in [10].

References

1. Huebner, K. H.: The Finite Element Method for Engineers. John Wiley and Sons New York–London–Sydney–Toronto 1975
2. Rothe, R.: Höhere Mathematik für Mathematiker, Physiker, Ingenieure. 6. T. von István Szabó Stuttgart, Teubner 1958

3. Scharle, P.: Numerical Analysis of Engineering Problems of Continua.* ÉTI Tudományos Közlemények **84,** Budapest 1976
4. Herpai, B. B.—Páczelt, I.: Analysis of Axisymmetrically Deformed Shells by the Finite Element Displacement Method. Acta Techn. *Hung.* **85** (1977), 93–122
5. Collatz, L.: The Numerical Treatment of Differential Equations. Springer Verlag, Berlin–Göttingen–Heidelberg 1960
6. Szabó, J.: Spatial Grid Equations.* ÉTI Tudományos Közlemények **34,** Budapest 1964
7. Szabó, J.—Kollár, L.: Structural Deseign of Cable-Suspended Roofs. Akadémiai kiadó, Budapest 1984
8. Béres, E.: Calculation of Grid Systems.* ÉTI Tudományos Közlemények **62,** Budapest, 1967
9. Timoshenko, S.—Woinowsky—Krieger: Theory of Plates and Shells. McGraw–Hill, New York–London–Toronto 1959
10. Béres, E.: Numerical Solution of Technical Problems.* SZIKKTI Tudományos Közlemények **65,** Budapest 1981

*** In Hungarian.**

Acta Technica Academiae Scientiarum Hungaricae, 94 (3—4), pp. 157–162 (1982)

DISPERSION OF A SOLUTE IN A CHANNEL FLOW OF NONLOCAL FLUIDS

GOODARZ AHMADI**

Department of Physics

The dispersion of a solute in a nonlocal channel flow is studied. The possibility of nonlocal mass diffusion is discussed. For the case where the regular Fick's law governs the diffusion process, it is shown that the solute is dispersed relative to a plane moving with the mean speed of the flow with an effective Taylor diffusivity which is a strong function of nonlocality of ıe fluid.

Introduction

In a series of papers Taylor [1, 2, 3] discussed the dispersion of soluble matter in the incompressible flow of a viscous fluid in a circular pipe. His method was applied to more complex fluids by other authors. The dispersion of a solute in a non-Newtonian fluid flow in a circular pipe was considered by Fan and Hwang [4]. Dispersion in hydro-magnetic channel flows has been investigated by Gupta and Chaterjee [5], Soundalgekar [6] and Ahmadi [7]. Soundalgekar [8, 9] studied dispersion in micropolar and couple stress fluid channel flows. The dispersion of soluble matter in the micropolar pipe flow was investigated by Ahmadi [10]. The theory of nonlocal media was developed by Eringen and Edelen [11] and Eringen [12]. The velocity distribution of a nonlocal fluid in a channel flow is also derived by Eringen [12].

In the present work, the diffusion of soluble matter in a nonlocal fluid is first discussed and a generalized Fick's law is proposed. In Section 3, a regular Fick's law is assumed and the dispersion of a solute in the laminar channel flow of a nonlocal fluid with respect to a plane moving with the mean speed of the flow is studied. Partial equilibrium is assumed and the effective Taylor diffusivity is obtained which is shown to be a strong function of nonlocality of the fluid. The results are tabulated and discussed. The paper is concluded by a few remarks in Section 4.

Nonlocal diffusion

The theory of nonlocal media as developed by Krőner [13], Eringen and Edelen [11], Edelen and Law [14] and Eringen [12] takes the nonlocal interatomic forces into consideration and hence nonlocal residuals appear in the equations of balance. The constitutive laws are also generalized and usually consist of a local classical part and a

* Goodarz Ahmadi, Department of Mechanical Engineering, Clarkson University, Potsdam, NY, USA and School of Engineering, Shiraz University, Shiraz, Iran

nonlocal part. These considerations have been discussed in [11–14] in detail. A similar generalization for mass diffusion seems to be in order. The classical diffusion theory is the well known Fick's law

$$\mathbf{q}_c = -D\nabla c \tag{1}$$

where $\mathbf{q}_c$ is the mass flux, c is concentration and D is the molecular diffusion. Equation (1) is a local equation and indicates that a local concentration gradient implies a mass flux with a coefficient of proportionality D. When the media is nonlocal and long range intermolecular forces affect the macroscopic process following [11–14], we propose the following generalized constitutive equation

$$\mathbf{q}_c = -D\nabla c - \int_{\mathbf{x}'} D'(|\,\mathbf{x}-\mathbf{x}'\,|)\nabla' c'\,\mathrm{d}\mathbf{x}' \tag{2}$$

where $\nabla' c'$ is ∇c evaluated at $\mathbf{x}'$. The second term in equation (2) is the nonlocal mass diffusion and expresses the mass flux at point $\mathbf{x}$ due to the concentration gradient at all the points of the body. The nonlocal diffusivity $D'(|\,\mathbf{x}-\mathbf{x}'\,|)$ is space dependent and usually is assumed to be a rapidly decaying function of its argument.

In the subsequent sections we assume that although the fluid is nonlocal, the diffusion process is governed by Fick's law as given by equation (1) and the nonlocal diffusion is absent.

Dispersion in channel flow

The expression for the velocity profile in a fully developed channel flow of a nonlocal fluid as derived by Eringen [12] is given by

$$\frac{u}{u_1} = -1-\eta^2+\alpha\left[1-|\,\eta\,|+\frac{1}{m}(e^{-m}-e^{-m|\eta|})\right] \tag{3}$$

where

$$u_1 = -\frac{h^2}{\mu(2+m\alpha)}\frac{\mathrm{d}P}{\mathrm{d}x}, \qquad \alpha = \frac{2\mu_0'}{km\mu}$$

$$\eta = y/h, \qquad m = (k+\mu_0'/\mu)h\,. \tag{4}$$

Here u_1 is a velocity scale, $2h$ is the thickness of the channel and $\mathrm{d}P/\mathrm{d}x$ is pressure gradient along the channel. μ is the coefficient viscosity and μ_0' and k are constants specifying the nonlocal viscosity of fluid. In the derivation of equation (3) Eringen [12] assumed the following nonlocal constitutive equation for the shear stress t_{21},

$$t_{21} = \mu\frac{\mathrm{d}u}{\mathrm{d}y} + \int_0^y \mu_v'(|\,y-\eta\,|)\frac{\mathrm{d}v(\eta)}{\mathrm{d}\eta} \tag{5}$$

with

$$\mu_v'(y) = \begin{cases} \mu_0' e^{-k|y|} & y \geq 0 \\ 0 & y < 0 \end{cases}. \tag{6}$$

Restricting ourselves to the Fick's law (1) the concentration c of a solute diffusing in a fluid moving in x-direction is given by

$$\frac{\partial c}{\partial t} + u\frac{\partial c}{\partial x} = D\left(\frac{\partial^2 c}{\partial x^2} + \frac{\partial^2 c}{\partial y^2}\right). \tag{7}$$

Following Taylor [1–3] we assume that the axial diffusion is much smaller than the diffusion normal to the flow direction, i.e.

$$\frac{\partial^2 c}{\partial x^2} \ll \frac{\partial^2 c}{\partial y^2}. \tag{8}$$

Using the dimensionless quantities

$$\xi = (x - \bar{u}t)/L, \qquad \theta = t\bar{u}/L \tag{9}$$

the diffusion (7) in a frame moving with the average velocity $\bar{u}$ becomes

$$\frac{\bar{u}}{L}\frac{\partial c}{\partial \theta} + \frac{W}{L}\frac{\partial c}{\partial \xi} = \frac{D}{h^2}\frac{\partial^2 c}{\partial \eta^2} \tag{10}$$

where L is a given length along the flow direction and

$$W = u - \bar{u}. \tag{11}$$

The average velocity $\bar{u}$ is given by

$$\bar{u}/u_1 = \frac{1}{h}\int_0^h \frac{u}{u_1}\,\mathrm{d}y = \frac{2}{3} + \alpha\left[\frac{1}{2} + \frac{e^{-m}}{m}(1 + 1/m) - 1/m^2\right]. \tag{12}$$

The relative velocity W then becomes

$$W/u_1 = \frac{1}{3} - \eta^2 + \alpha\left[\frac{1}{2} - |\eta| + \frac{1}{m^2}(1 - e^{-m} - me^{-m|\eta|})\right]. \tag{13}$$

If Taylor's limiting condition is valid for the present problem, then the partial equilibrium may be assumed in any cross section of the channel, thus $\partial c/\partial\theta$ can be neglected and equation (10) becomes

$$\frac{\partial^2 c}{\partial \eta^2} = \frac{h^2}{DL} W \frac{\partial c}{\partial \xi}. \tag{14}$$

Substituting for W from (13) and integrating twice we find

$$c = \frac{h^2 u_1}{DL}\left\{\frac{\eta^2}{6} - \frac{\eta^4}{12} + \alpha\left[\frac{\eta^2}{4} - \frac{|\eta|^3}{6} + \right.\right.$$

$$\left.\left. + \frac{1}{m^2}\left[(1 - e^{-m})\frac{\eta^2}{2} + \frac{1}{m}(1 - e^{-m|\eta|}) - |\eta|\right]\right]\right\}\frac{\partial c}{\partial \xi} + c_0 \tag{15}$$

where c satisfies the non-reacting wall boundary condition

$$\frac{\partial c}{\partial \eta} = 0 \qquad \text{at} \qquad \eta = \pm 1 \tag{16}$$

and c_0 is a constant which must be determined from the entry condition.

Now the volume rate of the transport of the solute across a section of the pipe is given by

$$Q = \int_h^h c W \mathrm{d}y \,. \tag{17}$$

Inserting the expression for c and W from (15) and (13) after integration we find

$$\begin{aligned} Q = \frac{2h^3 u_1}{DL} \Bigg\{ & -\frac{8}{945} + \alpha \Bigg[-\frac{1}{60} + \frac{1}{m^2}\left(\frac{7}{90} - \frac{2}{3m^2} + \frac{4}{m^4}\right) + \\ & + \frac{4e^{-m}}{m^2}\left(\frac{1}{45} - \frac{1}{3m^2} - \frac{1}{m^3} - \frac{1}{m^4}\right)\Bigg] + \\ & + \alpha^2 \Bigg[-\frac{1}{120} + \frac{1}{m^2}\left(\frac{1}{12} - \frac{4}{3m^2} + \frac{7}{2m^3} - \frac{2}{m^4}\right) + \\ & + \frac{e^{-m}}{m^2}\left(\frac{1}{12} - \frac{7}{3m^2} - \frac{2}{m^3} + \frac{4}{m^4}\right) - \\ & - \frac{e^{-2m}}{m}\left(\frac{1}{3} + \frac{3}{2m} + \frac{2}{m^2}\right)\Bigg]\Bigg\} \frac{\partial c}{\partial \xi} \,. \end{aligned} \tag{18}$$

Dividing (18) by $2h$ and comparing the resulting equation with the Fick's law (1) we find that the solute is dispersed relative to a plane moving with the mean speed of the flow with an effective Taylor diffusion coefficient D^* given by

$$D^* = \frac{h^2 u_1^2}{D} F(\alpha, m) \tag{19}$$

where

$$\begin{aligned} F(\alpha, m) = \frac{8}{945} & + \alpha \Bigg[\frac{1}{60} + \frac{1}{m^2}\left(-\frac{7}{90} + \frac{2}{3m^2} - \frac{4}{m^4}\right) + \\ & + \frac{4e^{-m}}{m^2}\left(-\frac{1}{45} + \frac{1}{3m^2} + \frac{1}{m^3} + \frac{1}{m^4}\right)\Bigg] + \\ & + \alpha^2 \Bigg[\frac{1}{120} + \frac{1}{m^2}\left(-\frac{1}{12} + \frac{4}{3m^2} - \frac{7}{2m^3} + \frac{2}{m^4}\right) + \\ & + \frac{e^{-m}}{m^2}\left(-\frac{1}{12} + \frac{7}{3m^2} + \frac{2}{m^3} - \frac{4}{m^4}\right)\Bigg] + \\ & + \frac{e^{-2m}}{m}\left(\frac{1}{3} + \frac{3}{2m} + \frac{2}{m^2}\right). \end{aligned} \tag{20}$$

Table I

Values of $F(\alpha, m)$

α/m	50	10	5	2	1	0.5	0.2	0.1
0.01	0.0086	0.0086	0.0086	0.0085	0.0085	0.0094	0.059	0.9
0.05	0.0094	0.0093	0.0092	0.0090	0.0097	0.033	1.28	22.57
0.1	0.010	0.010	0.010	0.097	0.013	0.11	5.12	90.37
0.2	0.013	0.013	0.012	0.011	0.025	0.39	20.47	361.68
0.5	0.020	0.019	0.017	0.016	0.104	2.44	127.92	2261.0
1.0	0.037	0.036	0.033	0.034	0.38	9.72	511.68	9046.0
2.0	0.091	0.087	0.078	0.091	1.51	38.85	2046.0	36186.0

The numerical values of $F(\alpha, m)$ for several values of α and m are given in Table I. It is observed that $F(\alpha, m)$ is an increasing function of α and decreases rapidly with an increase in m for small values of m and reaches a minimum and increases slightly with further increase of m.

In order to compare the Taylor diffusivity in a nonlocal fluid with that of a local viscous fluid with the same conditions and equal pressure gradient from (19) and (4) we obtain

$$\frac{D^*}{D_l^*} = \frac{F(\alpha, m)}{\frac{8}{945}(1+md/2)^2} \tag{21}$$

where D_l^* is the Taylor diffusivity of a regular viscous fluid. For small values of α and relatively large values of m which is usually valid from (2) and (21) we find

$$\frac{D^*}{D_l^*} \simeq 1+\alpha\left(\frac{63}{32}-m\right)\ldots \quad \text{for} \quad \alpha \ll \frac{1}{m} < 1 \tag{22}$$

It is observed that in this limiting case Taylor diffusivity of nonlocal fluid is greater or less than that of the corresponding local fluid if m is less or greater than 63/32, respectively. Several other limiting cases could be considered but in general D^* could be calculated from (19).

Further remarks

In the present work the Taylor diffusion coefficient of a solute dispersing in a laminar plane Poiseuille flow is calculated and it is shown to be strongly effected by the nonlocality of the fluid. The present work is limited to the validity of the Fick's law of diffusion given by equation (1). In principle it is possible to use the more suitable nonlocal form of Fick's law which is suggested by equation (2). Equations (7), (10) and (14) then become integro-differential equations. For instance instead of (14) we would have

$$\frac{\partial^2 c}{\partial \eta^2} + \frac{1}{D}\int_{\eta_1} \frac{\partial D'}{\partial \eta}(|\eta-\eta_1|)\frac{\partial c(\eta_1)}{\partial \eta_1}\,\mathrm{d}\eta_1 = \frac{h^2}{DL} w \frac{\partial c}{\partial \xi}. \tag{4.1}$$

For given $D'(|\eta-\eta_1|)$ it is possible in principle to solve the equation (4.1) for c and then following the steps similar to those of equations (17–19) the effective Taylor diffusivity could be calculated. The calculations are rather lengthy and we leave this for a future study.

Another important consideration is the effect of chemical reaction. In the present work it is assumed that the solutes are not chemically active. The effects of chemical reaction were investigated by Cleland and Wilhelm [15], Soloman and Hudson [16], Gupta and Gupta [17], Soundalgekar [18] and Soundalgekar and Gupta [19]. The study of coupling between nonlocality and chemical reaction is also left for a future communication.

Acknowledgements

The author would like to thank Dr. A. Hirose and Professor H. M. Skarsgard for their hospitality extended to him during the preparation of the present paper. This work is partially supported by the Ministry of science and Higher Education of Iran.

References

1. Taylor, G. I. Proc. Roy. Soc. *A219*, 186 (1953).
2. Taylor, G. I. Proc. Roy. Soc. *A223*, 446 (1954).
3. Taylor, G. I. Proc. Roy. Soc. *A225*, 473 (1954).
4. Fan, L. T.—Hwang, W. S.: Proc. Roy. Soc. *A283*, 576 (1965).
5. Gupta, A. S.—Chatterjee, A. S.: Proc. Camb. Phil. Soc. *64*, 1209 (1968).
6. Soundalgekar, V. M.: Phys. Fluids *14*, 2776 (1971).
7. Ahmadi, G. Pakistan: J. of Sci. and Indust. Res. (to appear).
8. Soundalgekar, V. M.: Rev. Roum. Phys. *15*, 805 (1970).
9. Soundalgekar, V. M.: Phys. Fluids *14*, 19 (1971).
10. Ahmadi, G.: Int. J. Multiphase Flow *1*, 487 (1974).
11. Eringen, A. C.—Edelen, D. G. B.: Int. J. Engng Sci. *10*, 233 (1972).
12. Eringen, A. C.: Int. J. Engng Sci. *10*, 561 (1972).
13. Kröner, E.: Int. J. Solids Struct. *3*, 731 (1967).
14. Edelen, D. G. B.—Law, N.: Arch. Rat. Mech. Anal. *34*, 283 (1969).
15. Cleland, F. A.—Wilhelm, R. H.: A. I. Ch. E. J. *2*, 489 (1956).
16. Soloman, R. L.—Hudson, J. L.: A. I. Ch. E. J. *13*, 545 (1967).
17. Gupta, P. S.—Gupta, A. S.: Proc. R. Soc. *A330*, 59 (1972).
18. Soundalgekar, V. M.: Int. J. Heat Mass Transfer *18*, 527 (1975).
19. Soundalgekar, V. M.—Gupta, S. K.: Int. J. Heat Mass Transfer *18*, 531 (1975).

Acta Technica Academiae Scientiarum Hungaricae, 94 (3—4), pp. 163–181 (1982)

BEITRAG ZU DEN METHODEN DER ÄQUIVALENTEN LINEARISIERUNG FÜR SCHWINGUNGSSYSTEME TEIL I.

GY. PATKÓ*

[Eingegangen: 22 Juli 1981]

Contribution to the construction of the equivalent linear vibrating systems — In the first part of the paper a generalisation of the Panovko type direct linearisation and the introduction of a linearisation method above the phase curve are shown. According to the latest a proposal is given to a definition of a measure of non-linearity. In the second part of the paper the character of transformation of the independent variable is analysed in the case of linearisation above the phase curve. It is shown, there are several methods for the analysis of non-linear oscillations having clear geometrical meaning.

Bezeichnungen

m	Masse
α	Eigenkreisfrequenz
Ω	Erregerkreisfrequenz
F	Amplitude der Erregerkraft
$g(x)$	nichtlineare Federkennlinie
$h(\dot{x})$	nichtlineare Dämpfungskennlinie
$f(x, \dot{x})$	nichtlineare Kennfläche
A	Integrationsgebiet
s	Phasenkurve
$\rho(x), \kappa(x, \dot{x})$	Gewichtsfunktionen

Andere Bezeichnungen werden im Text erklärt.

1. Einleitung

1.1. In früheren Jahrzehnten war man im Ingenieurwesen bestrebt, die Schwingungserscheinungen mit Hilfe von linearen dynamischen Modellen, deren Bewegungsgleichungen Systeme von linearen Differentialgleichungen sind, zu beschreiben. Die bei diesen Arbeiten gewonnenen Erfahrungen haben gezeigt, daß die in der Modellfindung unvermeidbaren kleineren bis größeren Vernachlässigungen und Näherungen auf vielen Gebieten der Praxis — mindestens in erster Näherung — gestattet sind.

Mit dem Ansteigen der Ansprüche bezüglich der Qualität von Maschinen und Konstruktionen ist es in zunehmendem Maße offensichtlich geworden, daß solche

* Patkó Gyula, Középszer u. 60. IV/3, H-3529 Miskolc, Ungarn.

dynamischen Modelle einen Teil der praktisch bedeutsamen Erscheinungen nicht beschreiben können. Deshalb ist es in der letzten Zeit immer notwendiger geworden, nichtlineare dynamische Modelle anzuwenden und die zu ihrer Untersuchung geeigneten mathematischen Methoden auszuarbeiten. In den letzten $2 \sim 3$ Jahrzehnten hat die Verbreitung moderner rechentechnischer Methoden die Behandlung der nichtlinearen Modelle in großem Maße gefördert.

Bei der Untersuchung der nichtlinearen Modelle ergeben sich große Schwierigkeiten aus dem Umstand, daß die ihre Eigenschaften beschreibende Theorie der nichtlinearen Differentialgleichungen auch im Falle der gewöhnlichen Differentialgleichungen zweiter Ordnung nicht vollständig ausgearbeitet ist, obschon viele wertvolle Teilergebnisse erschienen sind. Exakte Lösungen von geschlossener Form, die bei den linearen Differentialgleichungen mit konstanten Koeffizienten zur Verfügung stehen und über die Eigenschaften des Schwingungssystems einen schnellen und genauen Überblick ermöglichen, sind bei nichtlinearen Differentialgleichungen leider nur in Sonderfällen bekannt. Es ist möglich, die Lösungen mit Hilfe von unendlichen Reihen oder einer unendlichen Anzahl von Iterationsschritten aufzubauen, aber sie lassen die schnelle Übersehbarkeit, die dem Ingenieur notwendig ist, vermissen.

1.2. Die Praxis erhebt zwangsweise den Anspruch, daß zu entstehenden Problemen trotz der obenerwähnten Schwierigkeiten eine in der Technik akzeptable Lösung gefunden werden muß. Deswegen wurden die sogenannten Ingenieurmethoden überwiegend in den letzten Jahrzehnten entwickelt, ihre Wurzeln kann man aber bis auf die Arbeiten von Lagrange zurückführen. Weil die strenge mathematische Begründung dieser Ingenieurmethoden in manchen Fällen unvollkommen ist (vgl. [12], S. 115), wird hier die Frage der Kontrolle der Ergebnisse schärfer aufgeworfen, als es in anderen Fällen üblich ist.

1.3. Beim Überblicken der in der Praxis heutzutage gebräuchlichen Methoden kann man feststellen, daß sie sich größtenteils direkt oder indirekt auf schrittweise Näherungen gründen. Es ist wert, zwei solche Methoden gegenüberzustellen:

a) Heute stehen schon effektive Rechenprogramme zur numerischen Integration der Bewegungsgleichungen zur Verfügung, die zu festen Anfangsbedingungen die Lösung der nichtlinearen Differentialgleichung mit früher unvorstellbarer Genauigkeit erzeugen. Diese Methode hat neben ihren Vorteilen (z. B. hohe Genauigkeit) den Nachteil, daß sie nur zur Herstellung diskreter Lösungen geeignet und in vielen Fällen besonders bei Schwingungssystemen mit schwacher Dämpfung aufwendig ist [6].

b) In der Ingenieurpraxis braucht man oft Lösungen, aus denen die Abhängigkeit von technischen Parametern überblickt werden kann. Diese Aufgabe erfordert die Verwendung unendlicher Reihen für die erwähnten schrittweisen Näherungen. Dabei stößt man aber auf die allbekannten Schwierigkeiten. Trotzdem sind diese Methoden verbreitet, und es ergibt sich aus der praktischen Erfahrung, daß oft schon einige Schritte der Näherungen die Eigenschaften der dynamischen Erscheinungen klar machen, wobei meist sogar der erste Schritt die wichtigsten Informationen enthält.

1.4. Es gibt eine Gruppe der als analytisch bezeichneten Methoden, die nicht in die Kategorie der schrittweisen Näherungen eingeordnet werden kann. Sie heißen *Linearisierungsmethoden.* Sie erstreben nicht die genauen Lösungen sondern eine erste in der Praxis gut anwendbare Näherung dadurch, daß eine lineare im allgemeinen als äquivalent genannte Differentialgleichung durch irgendeine Überlegung der ursprünglichen nichtlinearen Differentialgleichung zugeordnet wird. Der Zweck der Zuordnung ist, die gesuchte Lösung der nichtlinearen Bewegungsgleichung durch eine Lösung der linearen Bewegungsgleichung möglichst gut zu approximieren. Bei der Durchführung der Linearisierung werden die von der Lage und Geschwindigkeit abhängigen nichtlinearen Funktionen der nichtlinearen Differentialgleichung durch lineare Funktionen ersetzt. Die Linearisierungsmethoden haben verschiedene Varianten (vgl.: [1], [4], [5], [16], [18], [23]).

Es ist bemerkenswert, daß unter den Methoden, die sich auf schrittweise Näherungen gründen, auch solche gefunden werden können, deren erster Schritt mit einer Linearisierung äquivalent ist, aber ihre Erklärung für Ingenieure im allgemeinen nicht unmittelbar anschaulich und manchmal schwer zu begreifen ist.

1.5. Die oben umrissenen Ingenieurmethoden haben von mathematischem Standpunkt aus wohl mehrere Mängel. Zwei davon sind:

a) In der Ingenieurpraxis werden periodische Lösungen in überwiegender Mehrheit untersucht, ohne daß die Bedingungen der Existenz der periodischen Lösungen auf theoretischem Weg überprüft werden. Der Ingenieur ersetzt diese Untersuchungen durch die aus der Praxis entnommenen Erfahrungen.

b) Im allgemeinen braucht man weitere Untersuchungen, um zu entscheiden, ob und in welchem Maße die gesuchte Lösung der ursprünglichen nichtlinearen Differentialgleichung durch die erhaltene Näherung approximiert wird. Fallweise stehen geeignete Methoden zur Fehlerabschätzung zur Verfügung (vgl.: [8], [13], [14], [21], [25]), in anderen Fällen sind sie noch mangelhaft. Häufig sieht es der Ingenieur nicht als seine Aufgabe an, solche mathematischen Methoden auszuarbeiten, sondern er begnügt sich damit, seine Näherungslösungen entweder direkt mit praktischen Erfahrungen, oder mit anderen in der Literatur als gut angenommenen Ergebnissen zu vergleichen.

1.6. Die vorliegende Arbeit gründet sich auf die von Panovko vorgeschlagene direkte Linearisierungsmethode. Diese Methode wurde im Jahre 1952 in russischer [15] später in englischer Sprache [1] veröffentlicht. Viele weitere Arbeiten (z. B.: [2], [3], [16], [17], [22], [23]), die einerseits über die mit dieser Methode erreichbaren Ergebnisse, andererseits über ihre Verbesserung berichten, zeigen, daß diese Methode bekannt und populär geworden ist. In Kenntnis der zitierten Arbeiten stellt es sich heraus, daß die Methode von Panovko neben den für die Ingenieure sympathischen Eigenschaften auch Mängel hat.

Die vorliegende Arbeit setzt sich zum Ziel, diese Methode zu verfeinern.

In der Literatur wird diese Methode zur Linearisierung von mathematisch getrennten Feder- und Dämpfungskennlinien benutzt. In dieser Arbeit wird sie für

solche Fälle verallgemeinert, bei denen die nichtlineare Kennfläche nicht aus einer nur von der Lage abhängigen Federkennlinie und aus einer von der Geschwindigkeit abhängigen Dämpfungskennlinie zusammengesetzt werden kann.

Bei der Verallgemeinerung erhebt sich die Frage, wie der Fehlerausgleich im allgemeinen Fall interpretiert werden soll. Dazu empfehlen sich mehrere Möglichkeiten. Ein möglicher Weg ist der in dieser Arbeit dargelegte Ausgleich über die Phasenkurve. Diese Methode wird im folgenden als Linearisierung über der Phasenkurve bezeichnet. Damit kann folgendes gezeigt werden:

— Die Methode gibt eine naheliegende und anschauliche Vorschrift zur Durchführung der Linearisierung, und die erhaltenen Ergebnisse stimmen mit den in der Literatur als gut anerkannten überein.

— Mit Hilfe dieses Verfahrens kann gezeigt werden, daß mehrere häufig angewandte Methoden auch eine anschauliche geometrische Deutung haben.

— Ein geometrisches Maß der Nichtlinearität kann eingeführt werden, das allgemeiner ist, als das aus der Literatur bekannte und mit der Erfahrung besser in Einklang steht.

In dieser Arbeit wird die Linearisierung über der Phasenkurve nur in Verbindung mit mechanischen Systemen von einem Freiheitsgrad behandelt, aber sie kann auch für Systeme mit mehreren Freiheitsgraden angewandt werden.

2. Über die direkte Linearisierungsmethode von Panovko

2.1. Die direkte Linearisierungsmethode, die von Panovko vorgeschlagen wurde, ordnet der nichtlinearen Differentialgleichung

$$m\ddot{x}+g(x)=0 \tag{2.1}$$

eine lineare Differentialgleichung der Form

$$m\ddot{x}+cx+d=0 \tag{2.2}$$

zu. Der hier dargestellte Gedankengang dieser Methode weicht aus Zweckmäßigkeitsgründen für das Folgende von der üblichen Darstellung ab.

Mit der Bezeichnung $\alpha^2=c/m$ hat die allgemeine Lösung von (2.2) die Form

$$x=A_0+A_1\cos(\alpha t-\vartheta_1),$$

wobei die Größe A_0 aus der Gleichung

$$cA_0+d=0 \tag{2.3}$$

berechnet werden kann, A_1 und ϑ_1 sind durch die Anfangsbedingungen bestimmt.

Für die Größen c und d schreibt die Methode von Panovko vor, daß das Quadratintegral der Abweichung

$$r(x)=g(x)-(cx+d) \tag{2.4}$$

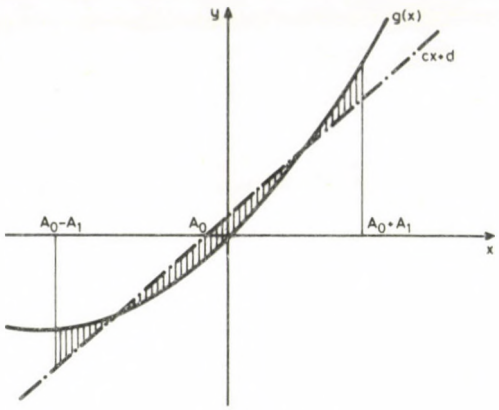

Bild 1

im Intervall $[A_0 - A_1;\ A_0 + A_1]$ minimal sei (Bild 1). So gelangt man aus

$$I_1 = \int_{A_0 - A_1}^{A_0 + A_1} [g(x) - (cx + d)]^2 \, dx \doteq \text{Minimum} \tag{2.5}$$

auf Grund der Beziehungen $\partial I_1 / \partial c = 0$, $\partial I_2 / \partial d = 0$ zu den Formeln

$$c = \frac{3}{2A_1^3} \int_{A_0 - A_1}^{A_0 + A_1} g(x) x \, dx - A_0 \int_{A_0 - A_1}^{A_0 + A_1} g(x) \, dx , \tag{2.6}$$

$$d = \frac{1}{2A_1} \left[\left(1 + 3 \frac{A_0^2}{A_1^2} \right) \int_{A_0 - A_1}^{A_0 + A_1} g(x) \, dx - 3 \frac{A_0}{A_1^2} \int_{A_0 - A_1}^{A_0 + A_1} g(x) x \, dx \right]. \tag{2.7}$$

Setzt man (2.6) und (2.7) in (2.3) ein, so ergibt sich, daß die Größen A_0 und A_1 die Gleichung

$$\int_{A_0 - A_1}^{A_0 + A_1} g(x) \, dx = 0 \tag{2.8}$$

erfüllen. Das bedeutet, daß das System (2.1) an den Stellen $A_0 - A_1$ und $A_0 + A_1$ dieselbe potentielle Energie hat. Berücksichtigt man (2.8) in (2.6) und (2.7), so können die Größen c und d aus

$$c = \frac{3}{2A_1^3} \int_{A_0 - A_1}^{A_0 + A_1} g(x) x \, dx \tag{2.9}$$

und

$$d = -cA_0 \tag{2.10}$$

berechnet werden.

2.2. Falls die Funktion $A_0 = A_0(A_1)$ nach (2.8) und die Größen c, d nach (2.9), (2.10) bestimmt werden, dann bekommt man erfahrungsgemäß für die Eigenfrequenz eine sehr ungenaue Gleichung. Deswegen wird in [15] vorgeschlagen, daß die Funktion $A_0 = A_0(A_1)$ auch ferner aus (2.8) berechnet wird, aber zur Bestimmung der Größen c und d nicht (2.5), sondern das Quadratintegral der gewichteten Abweichungen $r(x)\rho(x - A_0)$ zum Minimum gemacht wird, wobei $\rho(x)$ eine passend gewählte Gewichtsfunktion ist. So bringt die Methode gute Ergebnisse. Zum Beispiel erhält man die Schwingungsperiode des vorgespannten Duffingschen Systems bei der Wahl von $\rho(x) = x$ nach [3] mit einem Fehler, der kleiner als 5% ist.

In Kenntnis von $g(x)$ kann die Gewichtsfunktion $\rho(x)$ so gewählt werden, daß c in (2.2) optimal wird (vgl.: [17], [23]). In [23] ist gezeigt, daß die Ergebnisse aller bekannten Linearisierungsmethoden bei geeigneter Wahl der Gewichtsfunktion mittels der Methode von Panovko erhalten werden können. Deswegen wird diese Methode in [17] als die Verallgemeinerung von anderen Methoden angesehen.

2.3. Der Grundgedanke der direkten Linearisierungsmethode kann auch bei erregten Schwingungen, bei Schwingungen mit mehreren Freiheitsgraden (vgl.: [15]) und bei gedämpften Schwingungen mit einer Dämpfungskennlinie $h(\dot{x})$ (vgl.: [22]) benutzt werden.

Die direkte Linearisierungsmethode wird bei vielen technischen Aufgaben mit Erfolg angewendet [1], [17]. Ein großer Vorteil dieser Methode besteht darin, daß sie einfach ist, und eine anschauliche geometrische Deutung hat.

3. Die Verallgemeinerung der direkten Linearisierungsmethode von Panovko

3.1. In der Praxis treten nichtlineare Schwingungssysteme auf, bei denen die Nichtlinearität $f(x, \dot{x})$ nicht als Summe einer Federkennlinie $g(x)$ und einer Dämpferkennlinie $h(\dot{x})$ zusammengesetzt werden kann, das heißt

$$f(x, \dot{x}) \neq g(x) + h(\dot{x}) .$$

Im weiteren wird gezeigt, daß der Gedankengang der direkten Linearisierungsmethode von Panovko in solchen Fällen angewandt werden kann, aber die Formeln etwas allgemeiner aufgeschrieben werden müssen. Die Verallgemeinerung wird für harmonisch erregte Schwingungen dargestellt, sie ist jedoch auch bei freien Schwingungen anwendbar.

Betrachtet sei das nichtlineare Schwingungssystem, deren Bewegungsgleichung die Form

$$m\ddot{x} + f(x, \dot{x}) = F \cos \Omega t \tag{3.1}$$

hat. Zu (3.1) wird die Bewegungsgleichung

$$m\ddot{x} + b\dot{x} + cx + d = F \cos \Omega t \tag{3.2}$$

eines linearen Schwingungssystems zugeordnet. Die stationären Schwingungen von (3.2) haben die Form

$$x = a_0 + a_1 \cos(\Omega t - \vartheta_1), \tag{3.3}$$

wobei die Konstanten a_0, a_1, ϑ_1 bei Kenntnis von b, c, d bekanntlich nach den Formeln

$$a_0 = -\frac{d}{c}, \tag{3.4}$$

$$a_1 = \frac{F}{\sqrt{(c - m\Omega^2)^2 + (b\Omega)^2}}, \tag{3.5}$$

$$\tan \vartheta_1 = \frac{b\Omega}{c - m\Omega^2} \tag{3.6}$$

berechnet werden können. Auf Grund von (3.3) kann

$$\dot{x} = -a_1 \Omega \sin(\Omega t - \vartheta_1) \tag{3.7}$$

geschrieben werden, wobei $a_1 \Omega$ die Geschwindigkeitsamplitude ist.

Die in (3.2) vorkommenen Größen b, c, d werden so bestimmt, daß die Kennfläche $f(x, \dot{x})$ durch die Ebene $b\dot{x} + cx + d$ über das Gebiet $a_0 - a_1 \leqq x \leqq a_0 + a_1$, $-a_1 \Omega \leqq \dot{x} \leqq a_1 \Omega$ möglichst gut angenähert wird (Bild 2). Deswegen wird vorgeschrieben, daß das Quadratintegral der Differenz

$$q(x, \dot{x}) = f(x, \dot{x}) - (b\dot{x} + cx + d)$$

über das obenerwähnte Gebiet minimal sei. So bekommt man aus

$$I_2 = \int\int_{(A)} [f(x, \dot{x}) - (b\dot{x} + cx + d)]^2 \, dx \, d\dot{x} \doteq \text{Minimum}$$

auf Grund der Beziehungen $\partial I_2 / \partial b = 0$, $\partial I_2 / \partial c = 0$, $\partial I_2 / \partial d = 0$ die Formeln

$$b = \frac{3}{4a_1^4 \Omega^3} \int\int_{(A)} f(x, \dot{x}) \dot{x} \, dx \, d\dot{x}, \tag{3.8}$$

$$c = \frac{3}{4a_1^4 \Omega} \left[\int\int_{(A)} f(x, \dot{x}) x \, dx \, d\dot{x} - a_0 \int\int_{(A)} f(x, \dot{x}) \, dx \, d\dot{x} \right], \tag{3.9}$$

$$d = \frac{1}{4a_1^2 \Omega} \left[\left(1 + 3\frac{a_0^2}{a_1^2}\right) \int\int_{(A)} f(x, \dot{x}) \, dx \, d\dot{x} - 3\frac{a_0}{a_1^2} \int\int_{(A)} f(x, \dot{x}) x \, dx \, d\dot{x} \right]. \tag{3.10}$$

Setzt man (3.9) und (3.10) in (3.4) ein, so ergibt sich, daß die Konstanten a_0 und a_1 die Gleichung

$$\int_{x = a_0 - a_1}^{a_0 + a_1} \int_{\dot{x} = -a_1 \Omega}^{a_1 \Omega} f(x, \dot{x}) \, dx \, d\dot{x} = 0 \tag{3.11}$$

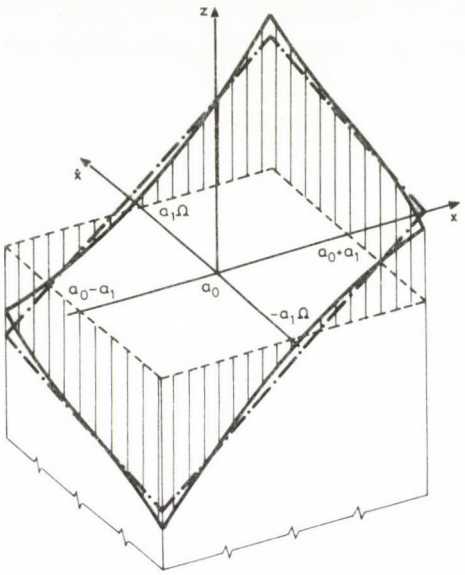

Bild 2

erfüllen. So können die Größen c und d anstatt über (3.9) und (3.10) aus den Formeln

$$c = \frac{3}{4a_1^4\Omega}\int\int_{(A)} f(x, \dot{x})x \, \mathrm{d}x \, \mathrm{d}\dot{x}\,, \tag{3.12}$$

$$d = -ca_0 \tag{3.13}$$

berechnet werden.

3.2. Falls für die Nichtlinearität $f(x, \dot{x}) = g(x)$ gilt, das heißt sie unabhängig von $\dot{x}$ ist, dann bekommt man aus (3.8) $b = 0$ und aus (3.9)—(3.13) die Formeln (2.6)—(2.10). Wenn die Nichtlinearität vom Typ

$$f(x, \dot{x}) = g(x) + h(\dot{x})$$

ist, das heißt sie aus einer Feder- und Dämpferkennlinie zusammengesetzt werden kann, dann erhält man im Fall

$$\int_{a_1\Omega}^{a_1\Omega} h(\dot{x})\,\mathrm{d}\dot{x} = 0 \tag{3.14}$$

aus (3.9)—(3.13) wieder die Formeln (2.6)—(2.10). Die Bedingung (3.14) bedeutet bei beliebigem $a_1\Omega$, daß $h(\dot{x})$ eine ungerade Funktion ist. In diesem Fall kann die Dämpfungskennlinie $h(\dot{x})$ auf Grund des im Punkt 2.1. beschriebenen Prinzips mit Hilfe einer Gerade angenähert werden, die durch den Anfangspunkt des Koordinatensystems geht.

3.3. Der Punkt 3.1. ist eine formale Verallgemeinerung der im Punkt 2.1. beschriebenen direkten Linearisierungsmethode. Weil die direkte Linearisierungsmethode in der im Punkt 2.1. beschriebenen Form, das heißt ohne Gewichtsfunktionen, sehr ungenaue Ergebnisse liefert, kann man dasselbe von der Verallgemeinerung erwarten.

Die im Punkt 2.2. erwähnten Gewichtsfunktionen können auf verschiedene Weise ausgewählt werden. Die Verallgemeinerung hat darüber hinaus eine weitere Willkür. Im Punkt 2.1. lag es auf der Hand, die Kennlinie $g(x)$ im Intervall $A_0 - A_1 \leqq x \leqq A_0 + A_1$ mit einer Gerade anzunähern. Im Punkt 3.1. wurde das Rechteck $a_0 - a_1 \leqq x \leqq a_0 + a_1$, $-a_1\Omega \leqq \dot{x} \leqq a_1\Omega$ zum Gebiet der Integration deswegen gewählt, weill sich so die Ergebnisse des Punktes 2.1. als Spezialfälle ergaben. Diese auf den ersten Blick vielleicht naheliegende Wahl gibt keine Garantie dafür, daß man eine gute Annäherung bekommt. So können die Ergebnisse der Verallgemeinerung auf zwei verschiedenen Wegen verbessert werden.

Die Ergebnisse des Punktes 3.1. können auf ähnliche Weise wie in Punkt 2.2. mit Hilfe von Gewichtsfunktionen modifiziert werden. In diesem Fall werden die Funktion $a_0 = a_0(a_1)$ und die Größe d auch ferner aus (3.11) und (3.13) berechnet, aber zur Bestimmung der Größen c und b wird das Quadratintegral der gewichteten Differenzen $q(x, \dot{x})\kappa(x - a_0, \dot{x})$ minimiert. Zur geeigneten Wahl der Gewichtsfunktion κ braucht man Erfahrung. Es ist zu betonen, daß der größte Vorteil dieser Linearisierung darin besteht, daß ihre Anwendung einfache Rechnungen mit sich bringt.

Eine andere Möglichkeit der Modifikation der Ergebnisse besteht darin, daß die Kennfläche $f(x, \dot{x})$ durch eine Ebene $b\dot{x} + cx + d$ über ein anderes Gebiet angenähert wird. Mit der Veränderung der Form und Größe des Integrationsgebietes verändern sich die Größen b, c, d. Dementsprechend kann man eventuell ein Integrationsgebiet finden, bei dem die zu den Größen b, c und d gehörende stationäre Lösung von (3.2) die beste Annäherung von (3.1) wird.

Man hat den Eindruck, daß diese Überlegungen ebenso, wie ein Teil der in der nichtlinearen Schwingungen üblichen Überlegungen, viel Willkür enthalten.

3.4. Im folgenden wird deshalb eine Methode, die bei der Bestimmung der Näherungsebene weniger Willkür enthält, vorgeschlagen. Bisher wurde die nichtlineare Kennfläche durch eine Ebene so angenähert, daß alle ihre über einem Gebiet A liegenden Punkte berücksichtigt wurden, obwohl nur die über der Phasenkurve liegenden Punkte der Kennfläche an einer konkreten periodischen Bewegung teilnehmen. Zwei unterschiedliche Schwingungssysteme, deren obenerwähnte Kurve gemeinsam ist, können sich bei passenden Anfangsbedingungen auf gleiche Weise bewegen. Das führt zum Gedanken, daß nur die über der Phasenkurve liegende Kurve der Kennfläche bei der Bestimmung der Näherungsebene berücksichtigt werden soll.

Weil die wirkliche Bewegung des Schwingungssystems (3.1) nicht bekannt ist, kann man von vornherein nur eine Näherung anwenden. Falls angenommen werden kann, daß die Phasenkurven der Bewegungsgleichungen (3.1) und (3.2) zueinander

nahe liegen, scheint es zulässig zu sein, daß man die mit (3.2) beschriebene äquivalente Bewegung statt der wirklichen Bewegung von (3.1) benutzt. Dementsprechend werden die Punkte der nichtlinearen Kennfläche, die über der Phasenkurve der äquivalenten Bewegung liegen, zur Bestimmung der Näherungsebene berücksichtigt. Es läßt sich zeigen, daß die auf diesem Weg erhaltenen Ergebnisse mit den Ergebnissen in Einklang stehen, die in der Literatur als gute Annäherungen bezeichnet sind. Der Vorteil dieser Methode besteht darin, daß die Bestimmung der Näherungsebene anschaulich ist.

Die Einzelheiten werden in den Punkten 4 und 5 behandelt.

4. Linearisierung über der Phasenkurve

4.1. Es werden die Bewegungsgleichungen (3.1) und (3.2) zugrunde gelegt. Wir wollen die Größen b, c, d in (3.2) so bestimmen, daß die Abweichungen zwischen den Flächen $f(x, \dot{x})$ und $b\dot{x}+cx+d$ über der Phasenkurve der Lösung von (3.2) klein sind.

Es wird die dimensionlose Zeit $\tau=\Omega t$ eingeführt. Dann können die Gleichungen (3.1) und (3.2) in der Form

$$m\Omega^2 x''+f(x, \Omega x')=F\cos\tau, \tag{4.1}$$

$$m\Omega^2 x''+b\Omega x'+cx+d=F\cos\tau \tag{4.2}$$

geschrieben werden, wobei der Strich die Ableitung nach τ bezeichnet. Die stationären Schwingungen von (4.2) haben die Form

$$x=a_0+a_1\cos(\tau-\vartheta_1), \tag{4.3}$$

wobei die Konstanten a_0, a_1, ϑ_1 bei Kenntnis von b, c und d aus den Beziehungen (3.4)—(3.6) berechnet werden können. Aus (4.3) ergibt sich:

$$x'=-a_1\sin(\tau-\vartheta_1). \tag{4.4}$$

Weil x und x' von derselben Maßeinheit sind, kann das Bogenelement auf der Phasenebene $x-x'$ definiert werden.

Im Bild 3 ist die Kennfläche $f(x, \Omega x')$ und die Näherungsebene $b\Omega x'+cx+d$ über der Phasenebene $x-x'$ dargestellt. Die den Formeln (4.3) und (4.4) entsprechende Phasenkurve ist ein Kreis mit dem Radius a_1 und dem Mittelpunkt $(a_0, 0)$. Der auf der Phasenkurve stehende Kreiszylinder schneidet die Kennfläche $f(x, \Omega x')$ in der durchgezogen gezeichneten Raumkurve, und die Ebene $b\Omega x'+cx+d$ schneidet sie in der strichpunktiert gezeichneten Ellipse. Bei festen Werten von a_0, a_1 und ϑ_1 werden die Größen b, c und d so bestimmt, daß die Raumkurve durch die Ellipse gut approximiert wird. Zur Approximation können verschiedene Kriterien gewählt werden. Hier wird nur eine Möglichkeit untersucht, bei der das Quadratintegral der auf Bild 3 schraffierten Abweichungen über der Phasenkurve des linearen Systems

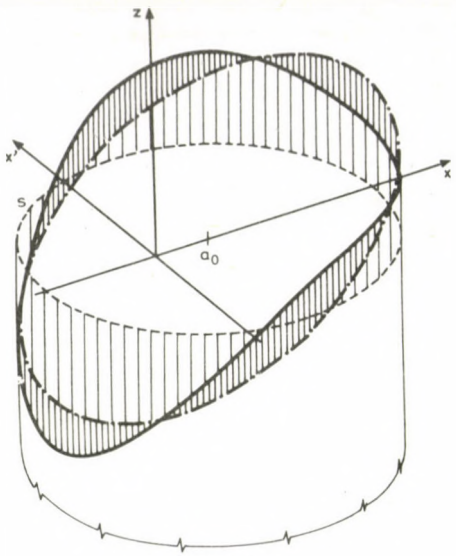

Bild 3

minimal wird, das heißt

$$J_1 = \oint_{(s)} [f(x, \Omega x') - (b\Omega x' + cx + d)]^2 \mathrm{d}s \doteq \text{Minimum.}$$

Wird die Abkürzung $\psi = \tau - \vartheta_1$ eingeführt, so erhält man das Bogenelement $\mathrm{d}s = a_1 \mathrm{d}\psi$. Auf Grund der Bedingungen

$$\frac{\partial J_1}{\partial b} = 0, \qquad \frac{\partial J_1}{\partial c} = 0, \qquad \frac{\partial J_1}{\partial d} = 0$$

ergeben sich die Formeln

$$b = -\frac{1}{\pi a_1 \Omega} \int_0^{2\pi} f(a_0 + a_1 \cos\psi;\ -a_1 \Omega \sin\psi) \sin\psi \mathrm{d}\psi, \tag{4.5}$$

$$c = \frac{1}{\pi a_1} \int_0^{2\pi} f(a_0 + a_1 \cos\psi;\ -a_1 \Omega \sin\psi) \cos\psi \mathrm{d}\psi, \tag{4.6}$$

$$d = \frac{1}{2\pi} \int_0^{2\pi} f(a_0 + a_1 \cos\psi;\ -a_1 \Omega \sin\psi) \mathrm{d}\psi -$$

$$- \frac{a_0}{a_1 \pi} \int_0^{2\pi} f(a_0 + a_1 \cos\psi;\ -a_1 \Omega \sin\psi) \cos\psi \mathrm{d}\psi. \tag{4.7}$$

Setzt man (4.6) und (4.7) in (3.4) ein, so bekommt man die Beziehung

$$\int_0^{2\pi} f(a_0 + a_1 \cos\psi;\ -a_0 \Omega \sin\psi) \mathrm{d}\psi = 0 \tag{4.8}$$

zwischen den Größen a_0 und a_1. Auf diese Weise kann der Wert von d aus der Beziehung $d = -ca_0$ berechnet werden.

Aus (4.8) kann die Funktion $a_0 = a_0(a_1, \Omega)$ bestimmt werden. Diese wird in (4.5) und (4.6) eingesetzt, und daraus können die Funktionen $b = b(a_1, \Omega)$ und $c = c(a_1, \Omega)$ berechnet werden. Durch Einsetzen der letzten in (3.5) ist der Amplituden-Frequenzgang $a_1 = a_1(\Omega)$ des nichtlinearen Schwingungssystems (3.1) näherungsweise berechenbar. Eine Näherung des Phasen-Frequenzganges des nichtlinearen Schwingungssystems (3.1) kann mit der Einsetzung der Funktionen $b(a_1, \Omega)$ und $c(a_1, \Omega)$ in (3.6) berechnet werden.

Oben wurde die Kennfläche $f(x, \Omega x')$ über der in der Phasenebene $x - x'$ dargestellten Phasenkurve des Schwingungssystems (4.2) durch die Ebene $b\Omega x' + cx + d$ angenähert. Es ist leicht einzusehen, daß die obigen Ergebnisse auch dann erhalten werden können, wenn die Kennfläche $f(x, \dot{x})$ über der in der Phasenebene $x - \frac{\dot{x}}{\Omega}$ dargestellten Phasenkurve des Schwingungssystems (3.2) durch die Ebene $b\dot{x} + cx + d$ angenähert wird.

4.2. Das im Punkt 4.1. beschriebene Verfahren kann zur Annäherung der periodischen Lösungen von autonomen Systemen benutzt werden. In diesem Fall wird der nichtlinearen Bewegungsgleichung

$$m\ddot{x} + f(x, \dot{x}) = 0 \tag{4.9}$$

die homogene lineare Differentialgleichung mit konstanten Koeffizienten

$$m\ddot{x} + b\dot{x} + cx + d = 0 \tag{4.10}$$

zugeordnet. (4.10) hat periodische Lösungen nur bei $b = 0$, es ist aber im weiteren zweckmäßig, b als Parameter zu behalten. Im Falle $b = 0$ hat die allgemeine Lösung von (4.10) die Form

$$x = a_0 + a_1 \cos(\alpha t - \vartheta_1), \tag{4.11}$$

wobei a_1 und ϑ_1 die von den Anfangswerten abhängigen Konstanten sind. Für a_0 gilt die Beziehung

$$ca_0 + d = 0. \tag{4.12}$$

Auf Grund von (4.9) und (4.10) kann die Eigenkreisfrequenz α der durch (4.9) beschriebenen nichtlinearen periodischen Schwingung näherungsweise aus der Beziehung

$$\alpha^2 = \frac{c}{m} \tag{4.13}$$

berechnet werden.

Es wird wiederum die dimensionlose Zeit $\tau = \alpha t$ eingeführt. So können die Differentialgleichungen (4.9) und (4.10) in der Form

$$\alpha^2 m x'' + f(x, \alpha x') = 0, \tag{4.14}$$

$$\alpha^2 m x'' + b\alpha x' + cx + d = 0 \tag{4.15}$$

geschrieben werden, wobei der Strich die Ableitung nach τ bezeichnet. Auf Grund von (4.11) kann

$$x = a_0 + a_1 \cos(\tau - \vartheta_1) \tag{4.16}$$

und

$$x' = -a_1 \sin(\tau - \vartheta_1) \tag{4.17}$$

geschrieben werden. Die Kennfläche wird analog zu Punkt 4.1. über die Phasenebene $x - x'$ dargestellt (vgl.: Bild 3). Die in (4.10) und (4.15) vorkommenden Größen werden so bestimmt, daß das Quadratintegral

$$\oint_{(s)} [f(x, \alpha x') - (b\alpha x' + cx + d)]^2 \mathrm{d}s \tag{4.18}$$

über die zu (4.16) und (4.17) gehörende Phasenkurve s minimal wird. So erhält man die Beziehungen

$$b = -\frac{1}{\pi a_1 \alpha} \int_0^{2\pi} f(a_0 + a_1 \cos\psi;\ -a_1 \alpha \sin\psi) \sin\psi \mathrm{d}\psi, \tag{4.19}$$

$$c = \frac{1}{\pi a_1} \int_0^{2\pi} f(a_0 + a_1 \cos\psi;\ -a_1 \alpha \sin\psi) \cos\psi \mathrm{d}\psi, \tag{4.20}$$

$$d = \frac{1}{2\pi} \int_0^{2\pi} f(a_0 + a_1 \cos\psi;\ -a_1 \alpha \sin\psi) \mathrm{d}\psi -$$

$$- \frac{a_0}{a_1 \pi} \int_0^{2\pi} f(a_0 + a_1 \cos\psi;\ -a_1 \alpha \sin\psi) \cos\psi \mathrm{d}\psi. \tag{4.21}$$

Durch Einsetzen von (4.20) und (4.21) in (4.12) ergibt sich die Beziehung

$$\int_0^{2\pi} f(a_0 + a_1 \cos\psi;\ -a_1 \alpha \sin\psi) \mathrm{d}\psi = 0 \tag{4.22}$$

zwischen den Größen a_0 und a_1.

Aus (4.22) kann die Funktion $a_0 = a_0(a_1, \alpha)$ bestimmt und durch Einsetzen in (4.20) die Funktion der linearisierten Federsteifigkeiten $c = c(a_1, \alpha)$ berechnet werden. Wenn die letzte in (4.13) eingesetzt wird, so ergibt sich die Beziehung

$$m\alpha^2 = c(a_1, \alpha). \tag{4.23}$$

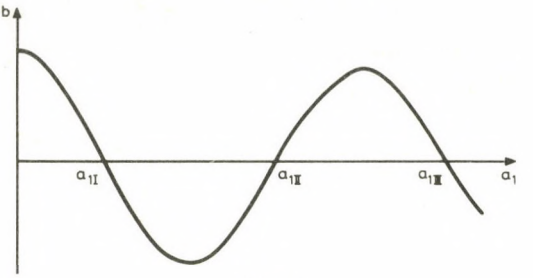

Bild 4

Weil sich periodische Lösungen nur bei $b=0$ ergeben, besteht auf Grund von (4.19)

$$\int_0^{2\pi} f(a_0+a_1\cos\psi;\ -a_1\alpha\sin\psi)\sin\psi\mathrm{d}\psi=0. \tag{4.24}$$

Aus den Gleichungen (4.22)—(4.24) können die Werte a_1 und α bestimmt werden, bei denen die Bewegungsgleichung (4.9) nach der obigen Näherung eine periodische Lösung oder auf der Phasenebene $x-x'$ einen Grenzzykel haben kann.

Durch Einsetzen der aus (4.23) bestimmbaren Funktion in (4.19) ergibt sich die Funktion mit einer Variablen $b=b(a_1)$ (Bild 4), deren Nullstellen die Amplituden der periodischen Lösungen angeben. Die Phasenkurve werde zur Bestimmung der Ausgleichsebene auch bei kleinen Werten von b durch den obigen Kreis mit dem Radius a_1 angenähert. So kann man dem Gedankengang von [20] folgend aus dem Verhalten der Funktion $b=b(a_1)$ auf die Stabilität der Grenzzykel schließen. Auf Grund von Bild 4 ist es leicht einzusehen, daß die Amplitude a_{1II} stabil ist. Falls die Ungleichheit $a_1>a_{1II}$ in der unmittelbaren Umgebung von a_{1II} besteht, dann ist der linearisierte Dämpfungswert positiv, und das führt in (4.9) zur Abnahme der Amplituden. Wenn $a_1<a_{1II}$, dann $b<0$ und das zieht die Zunahme der Amplituden nach sich. Auf gleiche Weise kann man einsehen, daß die periodischen Lösungen mit den Amplituden a_{1I} und a_{1III} instabil sind.

Falls (4.24) sich identisch erfüllt, dann erhält man aus (4.23) den Amplituden-Frequenzgang des Schwingungssystems (4.9).

4.3. In der Schwingungstechnik trifft man Nichtlinearitäten an, die antimetrisch sind, das heißt die Bedingung

$$f(x,\dot{x})=-f(-x,-\dot{x}) \tag{4.25}$$

erfüllen. Es ist leicht einzusehen, daß

$$a_0=0$$

eine Lösung von (4.8) ist, womit sich die Beziehungen (4.5)—(4.7) auf die Form

$$b=-\frac{1}{\pi a_1\Omega}\int_0^{2\pi} f(a_1\cos\psi;\ -a_1\Omega\sin\psi)\sin\psi\mathrm{d}\psi, \tag{4.26}$$

$$c=\frac{1}{\pi a_1}\int_0^{2\pi} f(a_1\cos\psi;\ -a_1\Omega\sin\psi)\cos\psi\,\mathrm{d}\psi, \tag{4.27}$$

$$d=0 \tag{4.28}$$

reduzieren.

Entsprechend dem Punkt 4.2. tritt α an die Stelle von Ω in (4.26) und (4.27) im Falle von autonomen Systemen.

Der auf der Phasenkurve s stehende Kreiszylinder schneidet die Kennfläche in einer Raumkurve, die nach dem obigen durch eine Ellipse angenähert werden kann, die in der durch den Koordinatenursprung gehenden Ebene liegt (Bild 5).

4.4. Als ein Maß der im Punkt 4.1. beschriebenen Näherung kann der quadratische Integralmittelwert der am Kreiszylinder gemessenen Abweichungen

$$M=\sqrt{\frac{1}{2\pi a_1}\oint_{(s)}[f(x,\Omega x')-(b\Omega x'+cx+d)]^2\,\mathrm{d}s} \tag{4.29}$$

dienen. Der zu diesem Integralmittelwert gehörende relative Fehler kann in der Form

$$e_r=\sqrt{\frac{\oint_{(s)}[f(x,\Omega x')-(b\Omega x'+cx+d)]^2\,\mathrm{d}s}{\oint_{(s)}f^2(x,\Omega x')\mathrm{d}s}} \tag{4.30}$$

geschrieben werden.

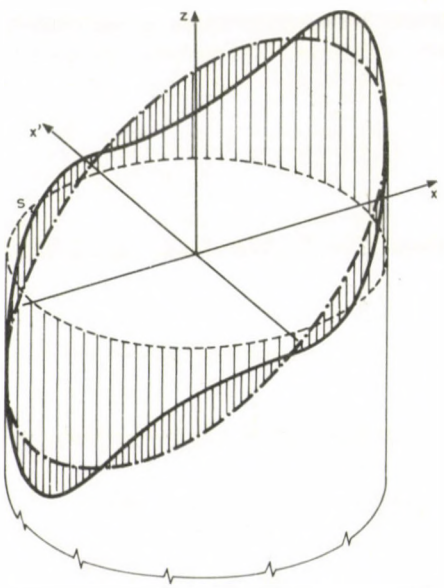

Bild 5

Im autonomen Fall tritt α anstatt Ω in den Formeln (4.29) und (4.30) auf.

Der Ausdruck (4.30) kann als ein geometrisches Maß der Nichtlinearität benutzt werden. Falls $f(x, \dot{x})$ linear ist, ist e_r Null. Bei einer schwach nichtlinearen Kennfläche $f(x, \dot{x})$ ist e_r offensichtlich ein in der Nähe von Null liegender Wert. In diesem Sinne kann man in Abhängigkeit der Größe von e_r Systeme als stark oder schwach nichtlinear interpretieren.

Es kommt vor, daß die nichtlineare Kennfläche in der Form

$$f(x, \dot{x}) = kx + \mu g(x, \dot{x}) \tag{4.31}$$

geschrieben werden kann, wobei k eine Konstante und μ ein dimensionloser Parameter ist. Man findet in der Literatur Angaben (vgl.: [11], S. 147), die μ als Maß der Nichtlinearität ansehen. Es ist wichtig, daß das mit (4.30) definierte Maß der Nichtlinearität auch dann benutzt werden kann, wenn die nichtlineare Kennfläche nicht eindeutig in der Form (4.31) aufgespaltet werden kann.

4.5. Als Beispiel wird untersucht, wie das Maß der Nichtlinearität sich bei der Duffingschen Gleichung

$$m\ddot{x} + kx + \varepsilon x^3 = 0 \tag{4.32}$$

verändert. Hier hängt die nichtlineare Funktion

$$f(x, \dot{x}) = kx + \varepsilon x^3 \tag{4.33}$$

nicht von $\dot{x}$ ab. (4.32) wird die lineare Bewegungsgleichung

$$m\ddot{x} + cx = 0 \tag{4.34}$$

zugeordnet. Mit der Transformation $\tau = \alpha t$ werden die Gleichungen (4.32) und (4.34) in

$$m\alpha^2 x'' + kx + \varepsilon x^3 = 0,$$

$$m\alpha^2 x'' + cx = 0$$

überführt. Hier wird durch Strich wieder die Ableitung nach τ bezeichnet. Die Lösungen der obigen Bewegungsgleichungen werden in der Form

$$x = a \cos \psi \tag{4.35}$$

gesucht, wobei $\psi = \tau - \vartheta_1$. Mit Hilfe von (4.27) ergibt sich

$$c = k + \frac{3}{4}\varepsilon a^2. \tag{4.36}$$

Durch Einsetzung der Formeln (4.33), (4.35), (4.36) in (4.30) erhält man

$$e_r = \frac{|\mu|}{\sqrt{2(8 + 12\mu + 5\mu^2)}}, \tag{4.37}$$

wobei die Bezeichnung

$$\mu = \frac{\varepsilon}{k} a^2$$

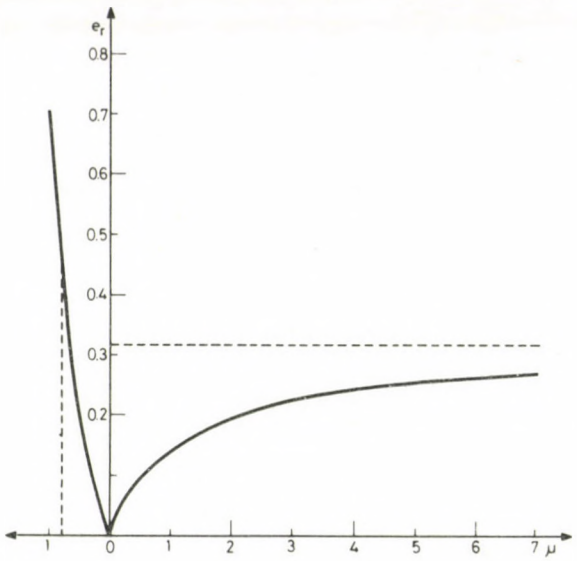

Bild 6

benutzt wurde. Die Funktion $e_r = e_r(\mu)$ ist auf Bild 6 dargestellt. Im Bild ist zu sehen, daß es bei Duffingschen Systemen, deren Differentialgleichungen sich nur im Vorzeichen von ε voneinander unterscheiden, das zu $\varepsilon < 0$ gehörende stärker nichtlinear ist als das zu $\varepsilon > 0$ gehörende.

Weigand (vgl.: [10], S. 43—50) erzielte beispielsweise bei der Untersuchung des Systems (4.32) das Resultat, daß die Lösung bei $\mu = 2$ einer cosinus Linie ähnlicher ist als die bei $\mu = -0.8$. Dieses Ergebnis stimmt mit der Aussage des in dieser Arbeit definierten Maßes der Nichtlinearität überein. Nach Bild 6 ist das System (4.32) bei $\mu = -0.8$ stärker nichtlinear, als bei $\mu = 2$.

4.6. Die Werte von b, c und d wurden in den Punkten 4.1. und 4.2. so bestimmt, daß die durch den Kreiszylinder ausgeschnittene Raumkurve durch die Ellipse gut angenähert wird. Deswegen wurde vorgeschrieben, daß das Quadratintegral der Abweichungen

$$f(x, \Omega x') - (b\Omega x' + cx + d) \tag{4.38}$$

über der Phasenkurve oder beim autonomen Fall (4.18), minimal wird.

Zur Annäherung der obigen Raumkurve können auch andere Bedingungen gestellt werden. Man könnte zum Beispiel vorschreiben, daß das Integral der *absoluten Werte* der Abweichungen (4.38) über der Phasenkurve minimal wird. Man könnte auch vorschreiben, daß der größte Absolutwert der Abweichungen über der Phasenkurve minimal wird. Es ist bemerkenswert, daß die Einführung der dimensionlosen Zeit in letzterem Fall nicht nötig ist. In diesen Fällen kann erwartet werden, daß man zu abweichenden Ergebnissen gegenüber den in den Punkten 4.1. und 4.2. erhaltenen gelangt.

Iwan und Patula [7] haben in Verbindung mit den obenerwähnten Methoden numerische Untersuchungen gemacht. Sie haben festgestellt, daß zwischen den mit unterschiedlichen Ausgleichsmethoden erhaltenen Ergebnissen keine wesentlichen Unterschiede bestehen. Die Rechnungsdurchführung ist jedoch dann am einfachsten, wenn das Quadratintegral der Abweichungen minimiert wird. Man kann für die in den Punkten 4.1. und 4.2. beschriebene Methode offensichtlich dasselbe Ergebnis erwarten.

Die in den Punkten 4.1. und 4.2. gewählte Annäherung hat außer der Einfachheit den Vorteil, daß eine anschauliche geometrische Deutung auch der anderen für die Untersuchung der nichtlinearen Systeme benutzten Methoden durch sie angegeben werden kann. Auf deren Untersuchung kommen wir in Punkt 6. zurück.

Schrifttum

1. Panovko, Ya. G.: A review of applications of the method of direct linearization, *Appl. Mech. Proc., XI. Int. Congr. Appl. Mech.*, Munich, 1964, pp. 167—171.
2. Panovko, Ya. G.: Elements of the applied theory of elastic vibration, Mir, Moscow, 1971.
3. Bapat, V. A., Srinivasan, P.: Effect of static deflection on natural frequency of non-linear spring mass system by direct linearization method, *Journal of Sound and Vibration*, (1969) **10,** (3), pp. 443—454.
4. Blaquière, A.: Une nouvelle méthode de linéarisation locale des opérateurs non-linéaires: approximation optimale. *2-nd Conf. Nonlinear Vibrations* (Warsaw, 1962), Warsaw, 1964.
5. Iwan, W.: On defining equivalent systems for certain ordinary nonlinear differential equations, *Int. J. Non-Linear Mechanics*, Vol. **4.** (1969), pp. 325—334.
6. Spanos, P.—T. D., Iwan, W.: Harmonic analysis of dynamic systems with non-symmetric nonlinearities, *J. Dynamic Systems, Measurement Control*, **101,** pp. 31—36. (1979).
7. Iwan, W., Patula, E. J.: The merit of different error minimization criteria in approximate analysis, *Journal of Applied Mechanics*, **39** (1972), pp. 257—262.
8. Iwan, W., Patula, E. J.: On the validity of equation difference minimization techniques, *Int. J. Non-Linear Mechanics*, Vol. **7.** (1972), pp. 1—17.
9. Lurje, A. I.: Einige nichtlineare Probleme aus der Theorie der selbsttätigen Regelung, Akademie Verlag, Berlin, 1957.
10. Weigand, A.: Einführung in die Berechnung mechanischer Schwingungen, Band I, VEB Verlag Technik, Berlin, 1959.
11. Andronow, A. A., Witt, S. E., Chaikin, S. E.: Theorie der Schwingungen, Teil II. Akademie Verlag, Berlin, 1962.
12. Forbat, N.: Analytische Mechanik der Schwingungen, VEB Deutscher Verlag der Wissenschaften, Berlin, 1966.
13. Sagirow, P.: Zur Frage der Fehlerabschätzung beim Verfahren der harmonischen Balance, *Zeitschrift für Angewandte Mathematik und Mechanik* **40.** (1960), S. 451—453.
14. Urabe, M.: Galerkin's procedure for nonlinear periodic systems, *Archive for Rational Mechanics and Analysis*, **20,** (1965), pp. 120—152.
15. Пановко, Я. Г.: Способ прямой линеаризации в нелинейных задачах теории упругих колебаний, *Инженерный сборник*, том **XIII.** (1952) с. 113—122.
16. Вибрации в технике, Справочник в 6. томах, том 2.: Блехман, И. И.: Колебания нелинейных механических систем, Машиностроение, Москва, 1979.
17. Вибрации в техгике, Справочник в 6. томах, том. 3.: Диментберг, Ф. М. Колесников, К. С.: Колебания машин, конструкций и их элементов, Машиностроение, Москва, 1980.
18. Попов, Е. П., Пальтов, И. П.: Приближенные методы исследования нелинейных автоматических систем, физматгиз, Москва, 1960.
19. Градштейн, И. С., Рыжик, И. М.: Таблицы интегралов, сумм, рядов и произведений, физматгиз, Москва, 1963.

20. Боголюбов, Н. Н., Митропольский, Ю. А.: Асимптотические методы в теории неличейных колебаний, Наука, Москва, 1974.
21. Розенвассер, Е. Н.: Колебания нелинейных систем, Наука, Москва, 1969.
22. Лойцянский, Л. Г.: Свободные и вынуждённые колебаныя при наличии квадратического и промежуточного между линейным и квадратичным законов сопротивления, *Инженерный сборник*, том **XYIII.** (1954) с. 139—148.
23. Карабан, В. Н. Дубовицкий, А. Ю.: О способах линеаризации при расчетах свободных колебаний нелинейных систем, В кн.: *Теория механизмов и машин*, вып. **23.** Харьков, Вища школа, (1977) с. 35—39.
24. Проскуряков, А. П.: Сравнение периодических решений квазилинейных систем, построенных методом Пуанкаре и методом Крылова-Боголюбова, *Прикладная математика и механика*, том **28.** вып. 4. (1964) с. 765—770.
25. Гарбер, Е. Д. Оценка погрешности метода гармонического баланса, *Автоматика и телемеханика*, Том **XXIY** (1963) с 482—492.

ZUSAMMENFASSUNG

Im ersten Teil der Arbeit wird eine Verallgemeinerung der direkten Linearisierungsmethode von Panovko vorgestellt, und es wird die Methode der Linearisierung über der Phasenkurve eingeführt. Auf Grund der letzten Methode wird eine Definition des Maßes der Nichtlinearität vorgeschlagen. Im zweiten Teil der Arbeit wird die Bedeutung der Transformation der unabhängigen Variablen bei der Linearisierung über der Phasenkurve untersucht. Es wird gezeigt, daß mehrere zur Untersuchung der nichtlinearen Schwingungssysteme angewandten Methoden eine anschauliche geometrische Deutung haben.

Acta Technica Academiae Scientiarum Hungaricae, 94 (3—4), pp. 183–195 (1982)

PRACTICAL TESTING OF COHERENCY BASED DYNAMIC EQUIVALENTS

G. HORNIÁK*, A. Y. SALIB

[Received: 5 May, 1982]

The coherency analysis procedure is one of the useful approaches to power system dynamic equivalents. Practical testing of different methods of coherency recognition is presented. The computational requirements for the identification of coherent generators and the accuracy of the dynamic equivalents are considered. A necessary condition for increasing the accuracy of some methods is discussed.

Introduction

Dynamic equivalents are commonly used for interconnected power systems to allow transient studies to be made with limited computer time and memory resources. Several techniques [15, 16] have been advanced for such a purpose. Coherency analysis procedure is one of the practical approaches to power system dynamic equivalents. Different methods [1—13] have been proposed for the identification of groups of coherent generators, which is the essential step for constructing coherency based dynamic equivalents.

This paper describes practical testing of coherency based dynamic equivalents. Two important factors are considered: the computational requirements for coherency recognition and the agreement of the results of the simplified models with the performance of the real system. Coherency recognition methods have been evaluated using a real system, and the computational requirements are presented. Coherency based reduction is made for identified groups and dynamic equivalents are formed. Comparisons of swing curves of internal system generators of the full system and reduced order models are shown. For better measuring of the accuracy of the different methods, an accuracy measure is proposed. The necessary condition for increasing the accuracy of some methods is discussed.

Coherency recognition

Six methods of coherency recognition have been applied to the 16-machine system shown in Fig. 1. The network is divided into a study system, containing generators at buses 2, 5, 6, 14 and associated transmission network, and an external system. The generators are represented by constant voltage behind transient reactance.

* G. Horniák, Villamosenergiaipari Kutató Intézet Zrínyi u. 1. H-1051 Budapest, Hungary

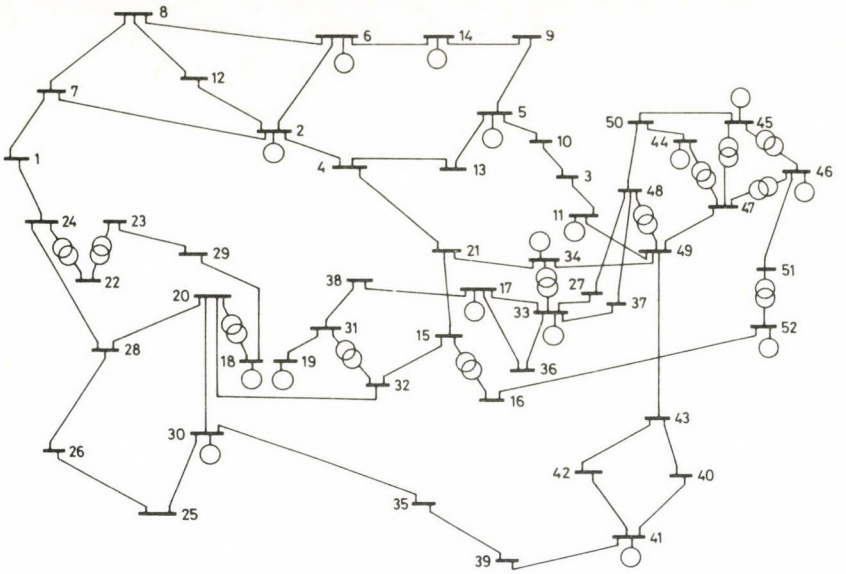

Fig. 1. The 16 machine system

For all methods, with the exception of the 3rd method, the fault selected for the evaluation is 0.1 Sec. three-phase short circuit at the terminal bus of generator 14. For the 3rd method the disturbance is assumed to be a zero mean, independent, of the disturbances at all other buses, and identically distributed step disturbance in mechanical input power (ZMIID). The coherent groups identified from the methods are given in Table II for two levels of specified tolerance given in Table I. The CPU time and core size requirements, for IBM/360 system, are given in Table III. The evaluated methods are:

The relaxed definition of coherency

Two generators i and j are defined as coherent if

$$\delta_i(t) - \delta_j(t) \leq \varepsilon \qquad 0 \leq t \leq T \tag{1}$$

where

δ internal rotor angle, degrees
ε specified tolerance
T transient period, Sec.

Recognition of coherent groups from this definition requires a base case transient stability study [1]. Large computational effort can be achieved using simulation of a simplified linear model [5]. If the power system is divided into some areas and assuming that the definition (1) is satisfied for generators within each area, network structural procedure [2—4] may be used to form dynamic equivalents.

In this paper, the linear simulation has been used to identify groups of coherent generators from this definition.

The max—min coherency measure

The max—min coherency measure [6] between generator internal buses i and j is

$$C_{ij} = \max_{0 \le t \le T} \{\delta_i(t) - \delta_j(t)\} - \min_{0 \le t \le T} \{\delta_i(t) - \delta_j(t)\}. \tag{2}$$

This measure requires a base case transient stability study to obtain the time-angle response of each generator.

The RMS coherency measure

The RMS coherency measure between generator internal buses i and j based on the uncertain description of disturbances is

$$C_{ij} = \sqrt{\hat{\mathbf{e}}_{ij}^T \hat{\mathbf{S}}_x(T) \hat{\mathbf{e}}_{ij}}, \tag{3}$$

where $\hat{\mathbf{S}}_x(T)$ is a $(n-1)$ square matrix and $\hat{\mathbf{e}}_{ij}$ is a $(n-1)$ dimensional vector; n is the number of system generators.

The matrix $\mathbf{S}_x(T)$ has been derived in reference [6]. As T approaches infinity and when the disturbance in mechanical input power is ZMIID, $\hat{\mathbf{S}}_x$ will take the form [7]

$$\hat{\mathbf{S}}_x(\infty) = [(\mathbf{MT})^{-1}\mathbf{M}]\,[(\mathbf{MT})^{-1}\mathbf{M}]^T. \tag{4}$$

In this case the RMS coherency measure is a function of system structure only. The matrices $\mathbf{M}$ and $\mathbf{T}$, and the vector $\hat{\mathbf{e}}_{ij}$ have been defined in references [6, 7].

Weighted eigenvectors method

The linearized power system state space model has been derived [9] as

$$\dot{\mathbf{x}} = \mathbf{Ax} + \mathbf{Bu}, \qquad 0 < t < t_c, \qquad \mathbf{x}(0) = 0, \tag{5}$$

$$\dot{\mathbf{x}} = \mathbf{Ax}, \qquad t \ge t_c, \qquad \mathbf{x}(t_c) = \mathbf{x}_c, \tag{6}$$

where

t_c fault clearing time
$\mathbf{x}_c$ state of the system at t_c, evaluated from (5)

equations (5) and (6) refer to faulted state and post-fault state, respectively. The eigen system approach (eigenvalues, eigenvectors and reciprocal eigenvectors) of $\mathbf{A}$ together with $\mathbf{x}_c$ determine the post-fault solution of (6) as

$$\mathbf{x}_{pf} = \mathbf{Sz}_s(t) \tag{7}$$

where $\mathbf{z}_s$ is the vector of modes of $\mathbf{A}$. Then $\mathbf{S}$ depends on both $\mathbf{x}_c$ and the eigen system.

Row properties of S are then used to determine coherency; thus, generators i and j are coherent if

$$h_{ij} = \frac{\|\mathbf{r}_i - \mathbf{r}_j\|}{\max \|\mathbf{r}_k\|} < \varepsilon, \qquad k = 1, 2, \ldots, n-1 \tag{8}$$

where $\mathbf{r}_i$ and $\mathbf{r}_j$ are the i-th and j-th rows of S. The matrices and vectors of equations (5), (6) and (7) have been defined in reference [9].

The pattern recognition method

Coherency recognition is made [10] by the examination of the three factors

$$r_1 = \left| \frac{\max\limits_i a_i - \min\limits_i a_i}{\max\limits_i a_i} \right| \tag{9}$$

$$r_2 = \frac{\min\limits_{i \in C} \min\limits_{\substack{j \in C \\ j \neq i}} Y_{ij}}{\max\limits_{i \in C} \max\limits_{k \in \Phi} Y_{ik}} \tag{10}$$

$$r_3 = \frac{\max\limits_i M_i - \min\limits_i M_i}{\max\limits_i M_i} \tag{11}$$

where

Φ set of generators in the area of disturbance
C set of generators considered for coherency
a_i acceleration of generator i during fault
M_i inertia constant of generator i
Y_{ij} magnitude of transfer admittance between generators i and j

The singular points method

Two generators i and j are defined as coherent if the following condition is satisfied [11]

$$|(\delta^s_{in} - \delta^0_{in}) - (\delta^s_{jn} - \delta^0_{jn})| \leq \varepsilon \tag{12}$$

where δ^s_{in} and δ^0_{in} $i = 1, 2, \ldots, n-1$ are, respectively, the angle coordinates of the stable operating point and the singular point which corresponds to the expected system instability.

Table I

Specified tolerances or thresholds

Method	Relaxed	Max—Min	RMS	Eigenvectors	Pattern	S. Points
Tight Criteria	5°	10°	0.5	0.05	$r_1 \leq 30\%$ $r_2 \geq 3.0$ $r_3 \leq 90\%$	2°
Loose Criteria	10°	20°	0.7	0.10	$r_1 \leq 50\%$ $r_2 \geq 0.68$ $r_3 \leq 90\%$	5°

Table II

Identified Coherent Groups

Method	Generator Numbers	
	Tight Criteria	Loose Criteria
Relaxed	45, 44, 34 33, 19, 17	45, 44, 41, 34, 11 33, 19, 18, 17
Max—Min	46, 44 41, 30 19, 17	46, 44 41, 34, 30, 11 33, 19, 18, 17
RMS	52, 46, 45 33, 17 30, 18	52, 46, 45, 44 33, 30, 19, 18, 17
Eigenvectors	46, 45, 44 33, 17	52, 46, 45, 44 34, 33, 17 30, 19, 18
Pattern	30, 18 52, 46 34, 33	46, 45, 44, 41, 34 30, 18 19, 17 33, 11
S. Points	44, 34 33, 18, 11 19, 17	46, 45 44, 34 33, 19, 17 30, 18, 11

Table III

Computational Requirements

Method	Relaxed	Max—Min	RMS	Eigenvectors	Pattern	S. Points
CPU time [s]	16.80	36.94	28.40	12.66	3.52*	3.86
Core size [Kbyte]	100	62	118	122	58	64

* The algorithm is repeated for tight and loose tolerances

Dynamic equivalents

The REI approach [14] is applied to each coherent group to establish the magnitude and initial angle of the internal voltage of the equivalent generator, and its connection to the network. The load buses are reduced using Gaussian elimination. A simple transient stability study, for the sake of simplicity, is carried out for each of the reduced order models. The fault selected for this evaluation is 0.1 Sec three-phase short circuit at the terminal bus of generator 14 for a transient period of 2 seconds. Comparisons of swing curves, of generator 14, of the full system and reduced order models are shown in Figures 2 through 7.

Discussion

All the methods appear to give satisfactory results for the particular fault studied, although the groups of coherent generators are not identical. However, to compare the methods it is interesting to introduce a certain factor which may give better indication of the accuracy of the methods. The root mean square of the rotor angle deviation of the faulted generator, over the transient period, from the base case simulation is proposed as an accuracy measure. These accuracy measures are given in Table IV.

It is worthwhile to note that, for the methods which use certain factors for coherency recognition the identified coherent groups must be inspected carefully to insure that there is no large deviation between the initial rotor angles of generators in the group. For this purpose, the following formula can be used

$$\max_i \delta_i^0 - \min_i \delta_i^0 \leq \varepsilon_0 \tag{13}$$

where

δ_i^0 initial rotor angle of generator i in a group
ε_0 specified tolerance ($\varepsilon_0 < 20^\circ$ is proposed)

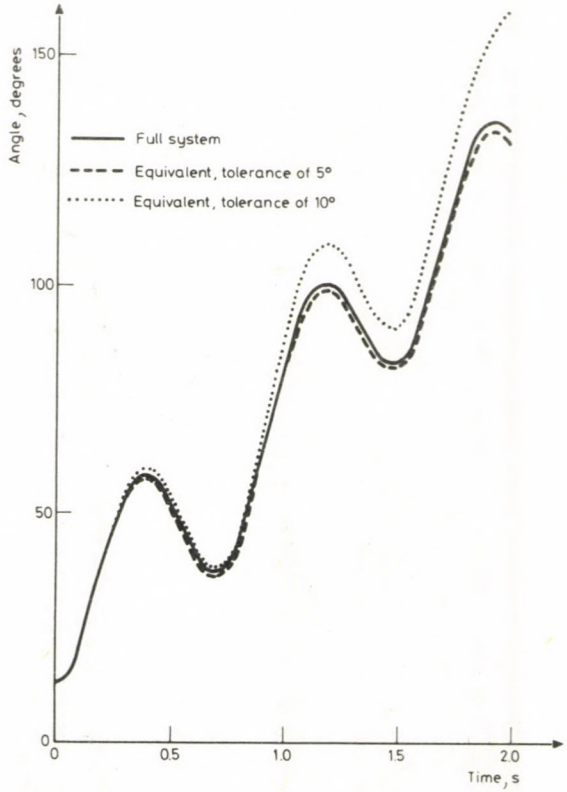

Fig. 2. Comparison of swing curves of Generator 14 with coherent groups identified from the relaxed definition

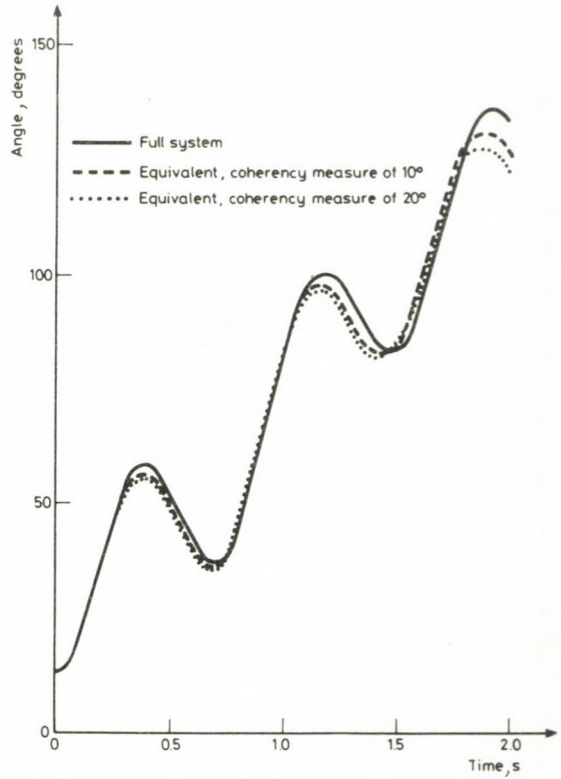

Fig. 3. Comparison of swing curves of Generator 14 with coherent groups identified from the max—min coherency measure

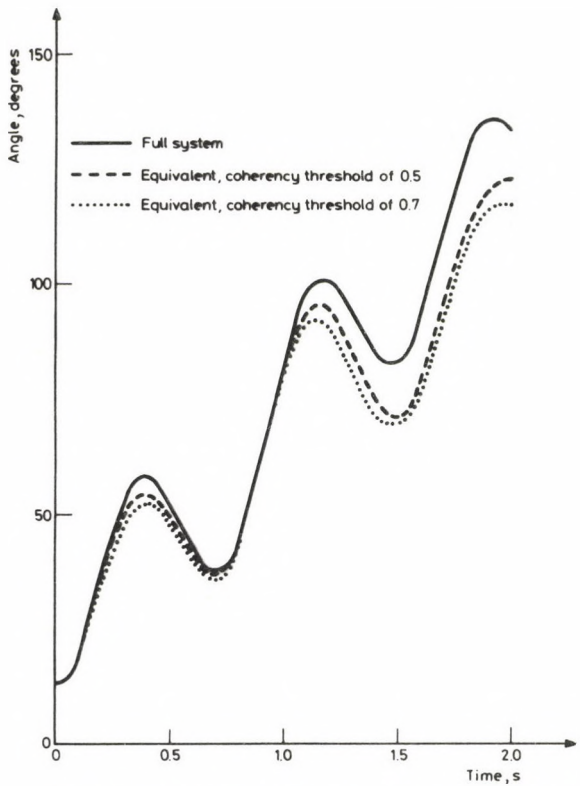

Fig. 4. Comparison of swing curves of Generator 14 with coherent groups identified from the RMS coherency measure

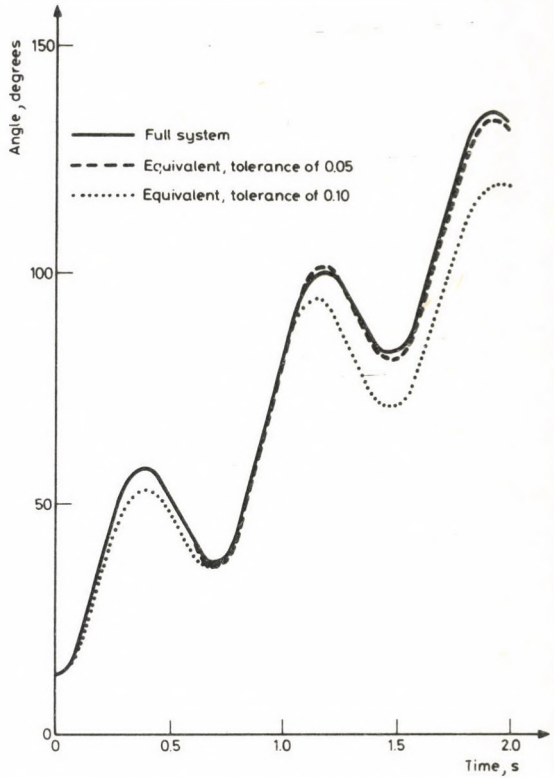

Fig. 5. Comparison of swing curves of Generator 14 with coherent groups identified from the weighted eigenvectors method

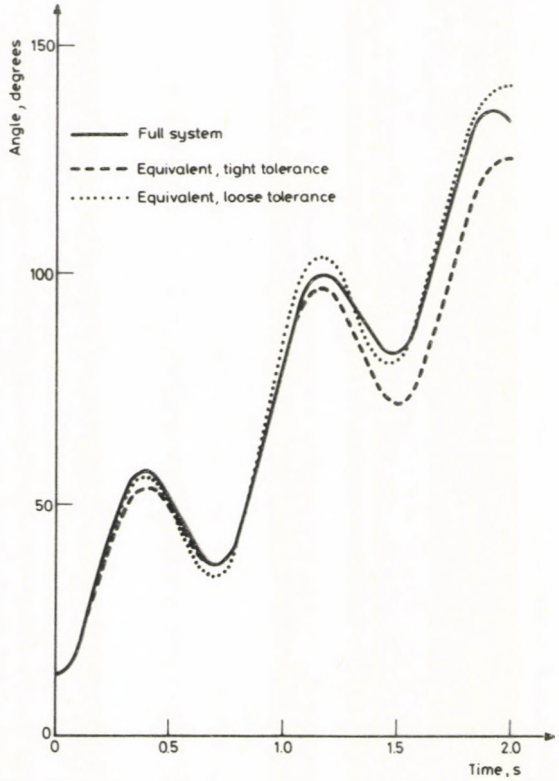

Fig. 6. Comparison of swing curves of Generator 14 with coherent groups identified from the pattern recognition method

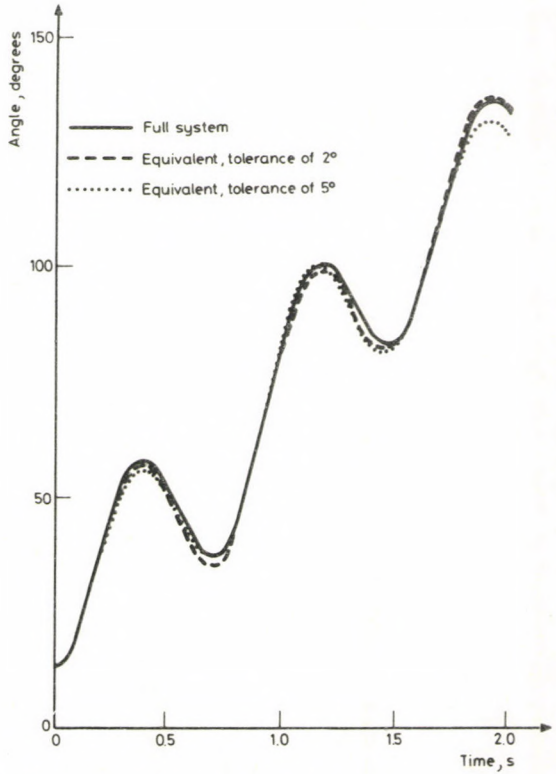

Fig. 7. Comparison of swing curves of Generator 14 with coherent groups identified from the singular points method

Table IV

Accuracy Measures in Degrees

Method	Relaxed	Max—Min	RMS	Eigenvectors	Pattern	S. Points
Tight Criteria	1.417	3.115	9.041	1.215	7.962	1.125
Loose Criteria	8.631	3.850	10.968	9.293	2.192	1.784

Table V

Accuracy measures in degrees, with generator 52 excluded from coherent groups

Method	Relaxed	Max—Min	RMS	Eigenvectors	Pattern	S. Points
Tight Criteria	1.417	3.115	1.317	1.215	1.814	1.125
Loose Criteria	8.631	3.850	2.267	1.563	2.192	1.784

The above check (13) will produce dynamic equivalents with higher accuracy. This will be seen by excluding generator 52 from coherent groups given in Table II. Comparisons of swing curves of generator 14 under this condition are shown in Figures 8 through 10, and the accuracy measures are given in Table V.

Conclusions

The practical testing of coherency based dynamic equivalents has been mentioned. Two important factors are considered:

(1) The computational requirements. For the particular system studied, identification of coherent groups from the pattern recognition method requires the smaller computer time and core size. For large interconnected power systems this method and the relaxed definition, as used with the linear simulation of the power system model, are the more practical methods. This fact is due to the smaller computational effort required for these methods.

(2) The agreement of the results of the dynamic equivalents with the performance of the original system. If we consider the lower order dynamic equivalents (9-machine system), the dynamic equivalent obtained from the pattern recognition method produces greater accuracy.

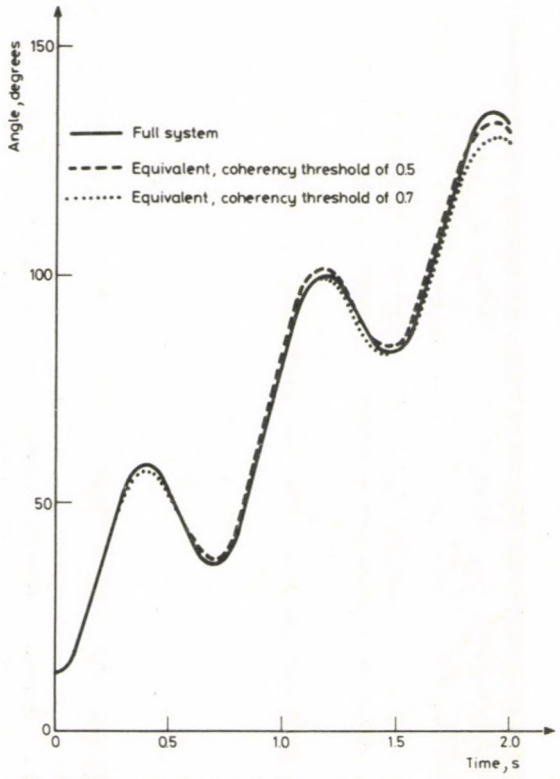

Fig. 8. Comparison of swing curves of Generator 14 with coherent groups identified from the RMS coherency measure, generator "52" excluded

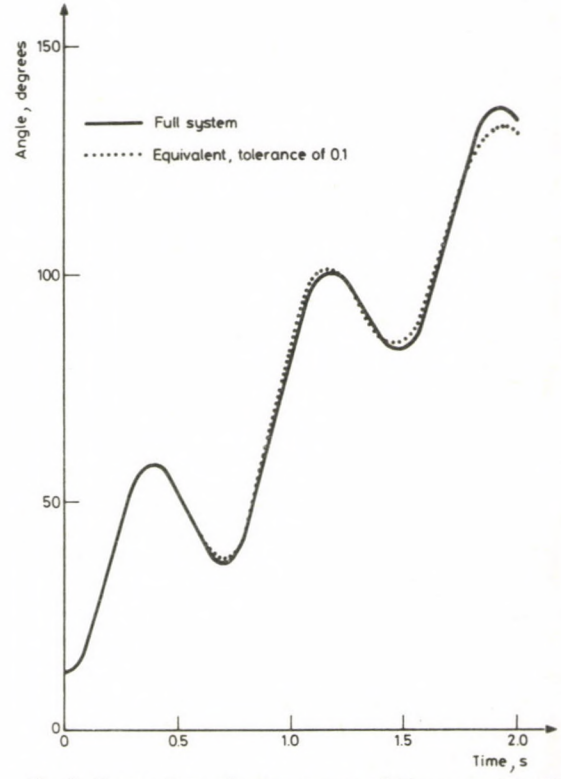

Fig. 9. Comparison of swing curves of Generator 14 with coherent groups identified from the weighted eigenvectors method, generator "52" excluded

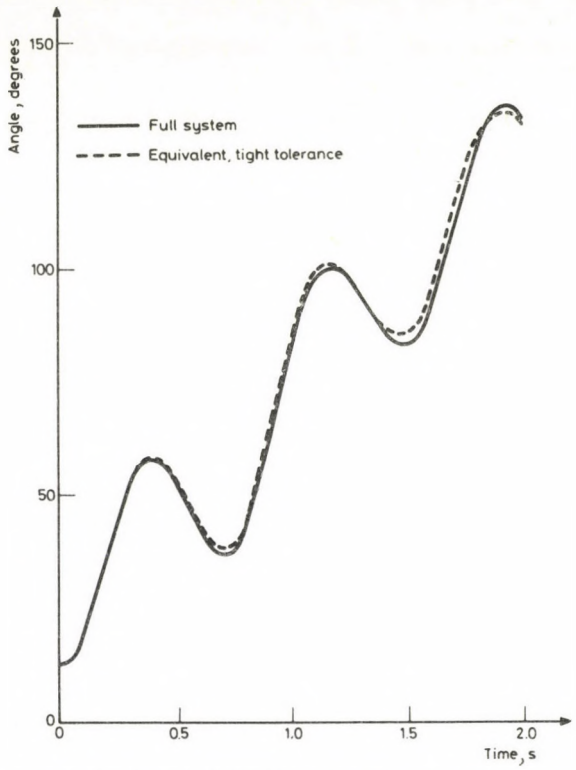

Fig. 10. Comparison of swing curves of Generator 14 with coherent groups identified from the pattern recognition method, generator "52" excluded

For some methods, which use certain factors for coherency recognition, the identified coherent groups can be checked to insure that there is no large deviation between the initial rotor angles of generators in the group. By this checking the accuracy of the dynamic equivalents can be increased.

References

1. Chang, A.—Adibi, M. M.: Power System Dynamic Equivalents. IEEE Trans., PAS-**89**, No. 8 Nov./Dec. (1970), 1737—1744
2. Saccomanno, F.: Development and Evaluation of Simplified Models for Multimachine Electric Power Systems. PSCC (1972), Paper No. 3.1/22
3. Saccomanno, F.: Dynamic Modelling of Multimachine Electric Power System. 2nd FORMATOR Symposium on Mathematical Methods for the Analysis of Large Systems. Praga, 18—21 June (1974)
4. Di Caprio, U.—Marconato, R.: A Novel Criterion for the Development of Multi-Area Simplified Models Oriented to the On-Line Evaluation of Power System Dynamic Security. PSCC (1975), Paper No. 3.2/3
5. Podmore, R.: Identification of Coherent Generators for Dynamic Equivalents. IEEE Trans., PAS-**97**, No. 4 July/August (1978), 1344—1354

6. Schlueter, R. A.—Akhtar, H.—Modir, H.: An RMS Coherency Measure: A Basis for Unification of Coherency and Modal Analysis Model Aggregation Techniques. Paper No. A 78 533-2, IEEE PES Summer Meeting (1978)
7. Lawler, J.—Schlueter, R. A.: Modal-Coherent Equivalents Derived from an RMS Coherency Measure. IEEE Trans., PAS-**99,** No. 4 July/Aug. (1980), 1415—1425
8. Schlueter, R. A.—Akhtar, H.: A Transient Coherency Measure and its Use to Analyze System Transient Response. Paper No. A 79 480-5, IEEE PES Summer Meeting (1979)
9. Pai, M. A.—Adgaonkar, R. P.: Identification of Coherent Generators Using Weighted Eigenvectors. Paper No. A 79 022-5, IEEE PES Winter Meeting (1979)
10. Lee, S. T. Y.—Schweppe, F. C.: Distance Measures and Coherency Recognition for Transient Stability Equivalents. IEEE Trans., PAS-**92,** No. 5 Sept./Oct. (1973), 1550—1557
11. Spalding, B. D.—Yee, H.—Goudi, D. B.: Coherency Recognition for Transient Stability Studies Using Singular Points. IEEE Trans., PAS-**96,** No. 4 July/August (1977) 1368—1375
12. Ohsawa, Y.—Hayashi, M.: Coherency Recognition for Transient Stability Equivalents Using Lyapunov Function. PSCC (1978), 815—818
13. Winkelman, J. R. et al.: An Analysis of Interarea Dynamics of Multi-Machine Systems. IEEE Trans., PAS-**100,** No. 2 Feb. (1981), 754—763
14. Tinney, W. F.—Powell, W. L.: The REI Approach to Power Network Equivalents. IEEE PICA Conf. Proc. (1977), 314—320
15. Salib, A. Y.: A Survey of Simplified Power System Dynamic Models. Internal Report No. 52.81-016-2, Institute for Electrical Power Research, Budapest — Hungary, October 1981
16. Horniák, G.—Salib, A. Y.: Power System Dynamic Equivalents — A Survey. Acta Techn. Hung. **94** (1982), 81—90

Acta Technica Academiae Scientiarum Hungaricae, 94 (3—4), pp. 197–214 (1982)

THE SUPPORTING EFFECT OF THE FABRIC OF TENT STRUCTURES STRECHED ONTO AN ARCH ROW ON THE LATERAL STABILITY OF THE ARCHES

L. KOLLÁR*

[Received: 28 August, 1982]

The arches of prestressed tent structures are laterally restrained against buckling by the fabric. The paper presents a method by which, in the case of tent structures stretched onto arch rows, this restraining effect can be simply computed. In knowledge of these data the lateral stability analysis of the arches can be performed by the usual methods.

1. Introduction

One of the most frequently used forms of tent structures is that streched onto an arch row (Fig. 1). Its arches can be economically designed if the elastic supporting effect of the fabric against their lateral-torsional buckling is also taken into account.

In the following we set as an aim to develop a method, also suitable for practical use, for taking the elastic supporting effect of the fabric into account.

2. Assumptions and approximations

The problem of lateral stability of elastically supported arches has been solved only for the case when the stiffness of the lateral support is constant all along the length of the arch [4], [5]. Hence we take some "average" value of this stiffness, and assume that this is constant along the arch axis.

We consider the fabric as a linearly elastic and orthotropic material, and we compute its stiffnesses on the basis of its original geometric shape (small-deflection theory), i.e. we neglect the influence of the change in shape of the fabric on its rigidities. Consequently, we need not consider the vertical excess loads, due to the supporting effect of the fabric, acting on the arches, and also not the change of rigidity of the fabric caused by the external loads. For the same reason we can consider the relation between the supporting force, arising when the arch deforms, and the displacement of the arch as linear.

* Dr. L. Kollár, Karap u. 9. H-1122 Budapest, Hungary

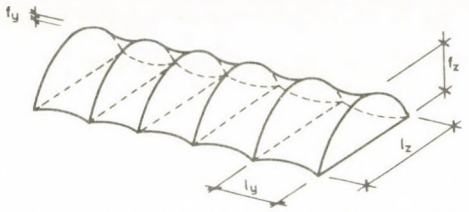

Fig. 1. Tent structure stretched onto an arch row

We stipulate that the fabric is appropriately fastened to the arches, and it is sufficiently stressed in order to take both tension and compression necessary for supporting the arch.

The fabrics used in practice are mostly coated on both sides by a plastic film. The fabric itself has considerable tensile stiffnesses in the directions of both threads perpendicular to each other, but has no shear stiffness at all. The plastic coating has tensile and shear stiffnesses as well, but these are small in comparison to the tensile stiffnesses of the fabric. Hence the coated fabric has a comparatively high tensile and a comparatively low shear rigidity.

We shall separately consider these two kinds of rigidities in our paper. In Sect. 3 we only take its two tensile stiffnesses into account. To this purpose we can adequately model the fabric by a cable net with cables running in the directions of the threads. We suppose that these two directions are parallel and perpendicular, respectively, to the projections of the arches onto the ground plan. We further stipulate that both sets of cables consist of shallow arcs, so that the pertaining approximations can be applied.

The shear stiffness of the coated fabric will be taken into account in Sect. 4.

We shall consider the stiffnesses of the intermediate fabric sections as equal to each other, but the stiffnesses of the extreme fabric sections (connecting the last arch with the earth) may be different.

We stipulate that every arch has the same cross section, and that they are loaded totally with the same load intensity. (This latter assumption mostly means a deviation to the safe side for the extreme arches.) Since all arches must buckle simultaneously due to their elastic interconnections, it follows from the foregoing that the buckling shapes of all arches are identical.

3. Taking into account the tensile stiffness of the coated fabric

3.1 The stiffness of one fabric section

The tensile stiffness of a fabric section which can be modelled by a cable net can be simply computed by using the assumption that we consider two strips of unit width, crossing each other, treat them as "representative" cables, and suppose that all other cables develop the same cable force as the representative cable which is parallel to them.

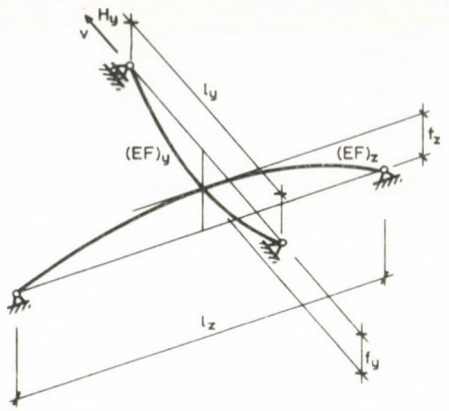

Fig. 2. Two cables representing a doubly-curved canvas section

By so doing we obtain, according to the investigations made on cable nets [6], a good approximation, as a rule.

Let us consider the two cables, crossing each other, shown in Fig. 2 as the representative strips of the fabric section between two arches (Fig. 1). Let us compute the y directed v displacement of one end point of the y directed cable due to a force H_y, also acting at this end point in the y direction.

The displacement v of the y directed cable consists of two parts. First we have to consider the displacement due to the elongation caused by H_y:

$$v_H = \frac{H_y l_y}{(EA)_y}, \tag{1}$$

(the notations are shown in Fig. 2; (EA) is the tensile stiffness of the cable). The second part is due to the deflection arising from the elongation of the cables running in the other direction. In order to compute this effect, we first have to determine the load p, considered as uniform, transmitted from the y directed cables to the z directed ones:

$$H_y = \frac{p l_y^2}{8 f_y},$$

thus

$$p = \frac{8 f_y H_y}{l_y^2}. \tag{2}$$

From this we obtain the central deflection of the z directed cable [6]:

$$w_z = \frac{3 p l_z^4}{128 f_z^2 (EA)_z}. \tag{3}$$

The y directed cable undergoes a deflection of the same magnitude, due to which a horizontal displacement

$$v_w = \frac{16 f_y}{3 l_y} w_z \tag{4}$$

comes about at the end point where H_y acts [6].

Introducing (2) and (3) into (4):

$$v_w = \frac{f_y^2}{f_z^2} \frac{l_z^4}{l_y^3 (EA)_z} H_y. \tag{5}$$

The "spring constant" c of the fabric section, i.e. its stiffness, can be obtained by dividing H_y by the total displacement v, consisting of the sum of (1) and (5):

$$c = \frac{H_y}{v_H + v_w} = \frac{1}{\dfrac{l_y}{(EA)_y} + \dfrac{f_y^2}{f_z^2} \dfrac{l_z^4}{l_y^3 (EA)_z}}. \tag{6}$$

This spring constant is valid in the middle of the arc. At other points it is greater, since the assumed uniform load p causes deflections of the shape shown in Fig. 3 in the cables, i.e. the largest one at the centre, and smaller ones at other places. However we commit an error to the benefit of safety if we consider the central spring constant as overall valid.

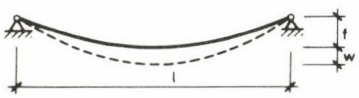

Fig. 3. Deflection of the cable due to uniformly distributed load

The derivation shown has the condition of validity that the z-directed prestressing cables displace outwards (or inwards) all along their lengths. This corresponds to the buckling of the arches in one half wave. In the cases of buckling in two or more half waves a different situation arises (Fig. 4). From Fig. 4 we can immediately see that the y-directed cables would undergo elongation and compression along the one and the other half length of the arch, respectively, but the antisymmetric deformation of the z-directed cables allows the y directed ones to follow these displacements by the changes of their sags, without any elongation. Hence this deformation of the cable net needs no forces at all, so that the spring constant of the cable net becomes zero for this deformation.

A more detailed investigation would probably show that the y-directed cables undergo some stretching too. However, we certainly commit an error to the benefit of safety if we neglect the rigidity due to this elongation. We shall do this in the following.

Consequently, in the case of buckling in two or more half waves only the shear rigidity of the coated fabric, not treated so far, supports the arches, see in Sect. 4.

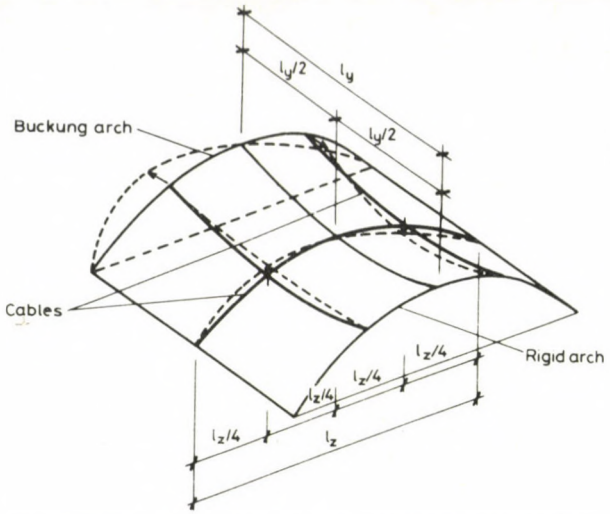

Fig. 4. "Inextensional deformation" of the cable net in the case of buckling in two half waves

3.2 The spring force supporting the individual arches

Knowing the spring constants of each fabric section, the "effective" spring constant c_{eff}, which supports the individual arches, can be determined as follows:

The whole structure can be modelled as shown in Fig. 5a or b. We shall denote the stiffness of the springs, referred to unit arch length, in the intermediate fields by c_i, and in the extreme fields by c_e. We stipulate that neither c_i, nor c_e is equal to zero or infinity.

Since the loading and rigidity of each arch is identical, and, due to their elastic interconnection, they can only buckle simultaneously, their lateral displacements y have to assume values which give rise to identical spring constants c_{eff} for every arch, i.e. the sum of the spring forces acting on one arch divided by its displacement y should be the same for all arches.

It can be seen by inspection that all arches have to buckle in the same direction, since it is this way that the springs exert the least total resistance. It is also obvious that the arches which are in the middle part of the structure have to develop larger displacements y than the extreme ones, since otherwise the springs were not able to support them. Finally it can also be seen that the magnitudes of the displacements y of the various arches should have a distribution symmetric with respect to the axis of symmetry of the whole structure, while the magnitude of the spring forces have to vary antisymmetrically. Consequently, in the centre of the structure (at its axis of symmetry) no spring force can develop, so that here the structure can be cut into two parts. (If there is an arch on the symmetry line, we have to cut it into two half arches, each having half

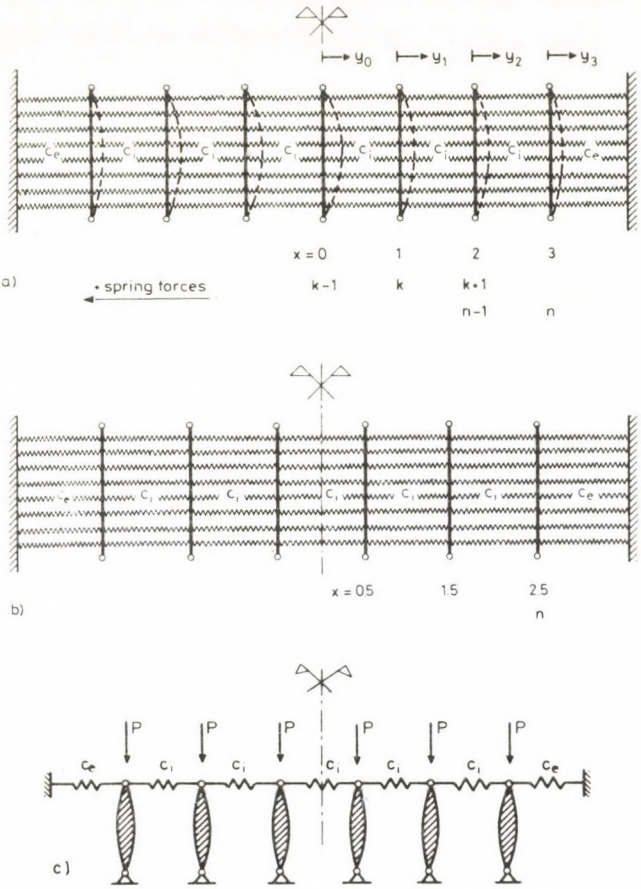

Fig. 5. Modelling the structure for computing the restraining effect due to the tensile stiffness of the canvas sections

a — structure containing arches of uneven number
b — structure containing arches of even number
c — pendulum row coupled by springs

the rigidities of the original one. By so doing no forces arise in the connection between the two half arches, so that we again arrive at two independent half structures.)

The most characteristic features of the arch row connected by springs can also be demonstrated on the pendulum row coupled by springs, shown in Fig. 5c. The pendulum columns have no own rigidities, and are only connected with each other by one spring each, so that the system is much simpler than the arch row of Figs 5a, b. Nevertheless, even this simple model clearly shows the influence of springs.

The following derivation is equally valid for both the pendulum row and the arch row.

In the derivation we apply the usual notations of the finite difference calculus. We begin the numbering of the arches in the middle of the structure. If there is an arch here (Fig. 5a), then for this arch $x=0$, further $x=1; 2$; etc., so that an interval becomes $\Delta x=1$. If, however, there is a spring in the middle of the structure (Fig. 5b), then for the first arch $x=0.5$, further $x=1.5, 2.5$; etc., but the interval remains $\Delta x=1$ also in this case.

Taking all these into consideration, we can write the following relations (see also [3]):

The spring forces acting upon an intermediate arch k are (taking the positive signs of forces as indicated in Fig. 5a):

from the left: $-c_i(y_{k-1}-y_k)$;

from the right: $+c_i(y_k-y_{k+1})$;

summing up: $$-c_i[(y_{k+1}-y_k)-(y_k-y_{k-1})]=-c_i\Delta^2 y_k; \tag{7}$$

i.e. the resultant of the spring forces acting on an arch is proportional to the second difference quotient of the lateral displacement y. (We omitted Δx and $\Delta^2 x$, respectively, in the denominator, since $\Delta x=1$.)

The effective spring constant is the quotient of the spring force and the displacement:

$$c_{\text{eff}}=-c_i\frac{\Delta^2 y_k}{y_k}. \tag{8}$$

The value of c_{eff} has to be the same for every arch, so that (8) represents a linear, homogeneous difference equation with constant coefficients:

$$\Delta^2 y+\frac{c_{\text{eff}}}{c_i}y=0. \tag{9}$$

It has the solution:

$$y=A\cos(\lambda x)+B\sin(\lambda x), \tag{10}$$

with

$$\lambda=\sqrt{\frac{c_{\text{eff}}}{c_i}}, \tag{11a}$$

or

$$c_{\text{eff}}=\lambda^2 c_i. \tag{11b}$$

Due to the aforementioned symmetric distribution of the displacements y it is sufficient to keep only the symmetric part of (10), so that

$$y=A\cos(\lambda x). \tag{12}$$

The boundary condition is furnished by the n^{th} (extreme) arch. The spring forces acting upon it are:

from the left: $-c_i(y_{n-1}-y_n)$;

from the right: $+c_e y_n$:

summing up: $$-c_i(y_{n-1}-y_n)+c_e y_n. \tag{13}$$

The spring constant becomes:

$$c_e - c_i \frac{y_{n-1}-y_n}{y_n} \tag{14}$$

The spring constant also has to be equal to c_{eff}, valid for the intermediate arches, which can be expressed, according to (11b), with the aid of λ. We thus arrive at the following relation:

$$c_e + c_i \frac{y_n - y_{n-1}}{y_n} = c_i \lambda^2, \tag{15a}$$

or

$$\frac{c_e}{c_i} + 1 - \lambda^2 - \frac{y_{n-1}}{y_n} = 0. \tag{15b}$$

The numerator of the fourth term is, according to (12), equal to $A \cos \lambda(n-1)$, and its denominator to $A \cos \lambda n$. Hence we can write (15b) in the following form:

$$\frac{c_e}{c_i} + 1 - \lambda^2 - \frac{\cos \lambda(n-1)}{\cos \lambda n} = 0. \tag{16}$$

Thus the hitherto unknown λ, and, with the aid of (11), also c_{eff}, is arrived at by solving the transcendent equation (16). Since, according to (11), λ^2 is proportional to c_{eff}, consequently we have to use the smallest of the roots of (16), in order to obtain the smallest spring constant, i.e. the lowest critical force.

The coefficient A, which determines the magnitude of the displacements, remains unknown, like the buckling amplitudes in general in the frame of the linear theory.

In order to find the smallest root of Eq. (16) an orientation is given by the consideration that c_{eff} has to be smaller than the sum of the two extreme spring constants, divided by the total number of arches, i.e.

$$c_{\text{eff}} < \frac{2c_e}{2(n+0.5)}, \tag{17}$$

or, taking (11b) into account:

$$\lambda < \sqrt{\frac{c_e}{c_i(n+0.5)}}. \tag{18}$$

The explanation of relation (17) is that if the intermediate arches were connected to each other by springs of infinite stiffness, the inequality (17) would turn into equality. The finite stiffness of the intermediate springs obviously reduces the effective spring constant c_{eff} with respect to this case.

4. The role of the shear stiffness of the coated fabric

The rigidity of the fabric against shear deformation acts on the arch in the form of distributed moments (Fig. 6). Hence in the following we have to clarify some basic questions concerning distributed moment loads.

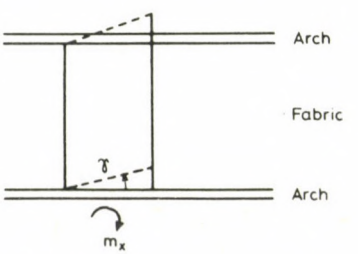

Fig. 6. Distributed moments exerted by the shear stiffness of the fabric

4.1 The kinds of distributed moments

Let us consider the simple beam on two supports, shown in Fig. 7, subjected to linearly varying distributed bending moments acting in the plane of the beam. Let us first investigate the case in which the distributed moments are transmitted to the beam in the form of couples parallel to the axis of the beam (e.g. as twisting moments of two-flanged trusses, joining the beam on its side, like purlins). Constructing the bending moment and shearing force diagrams according to the well-known rules of statics, we obtain those shown in Fig. 7a.

However, if we transmit the distributed moments by couples which are perpendicular to the axis of the beam (e.g. by bending moments of vertical bars that join our beam in its plane, perpendicularly to its axis, as in Fig. 7c, which is obtained by turning Fig. 7b by 90°), then these couples yield distributed forces q_y perpendicular to the axis of the beam, — as with the Kirchhoff forces arising from twisting moments acting along the simply supported boundaries of plates [7], — whose magnitude is equal to the first derivative of the distributed moments, so that in our case they will be uniformly distributed (Fig. 7b). From these forces q_y the same bending moment diagram as in Fig. 7a will be obtained, but the shearing force diagram differs.

At the right end of the beam, where the magnitude of the distributed moment is not zero, but it suddenly "ceases to exist", a concentrated force arises, corresponding to

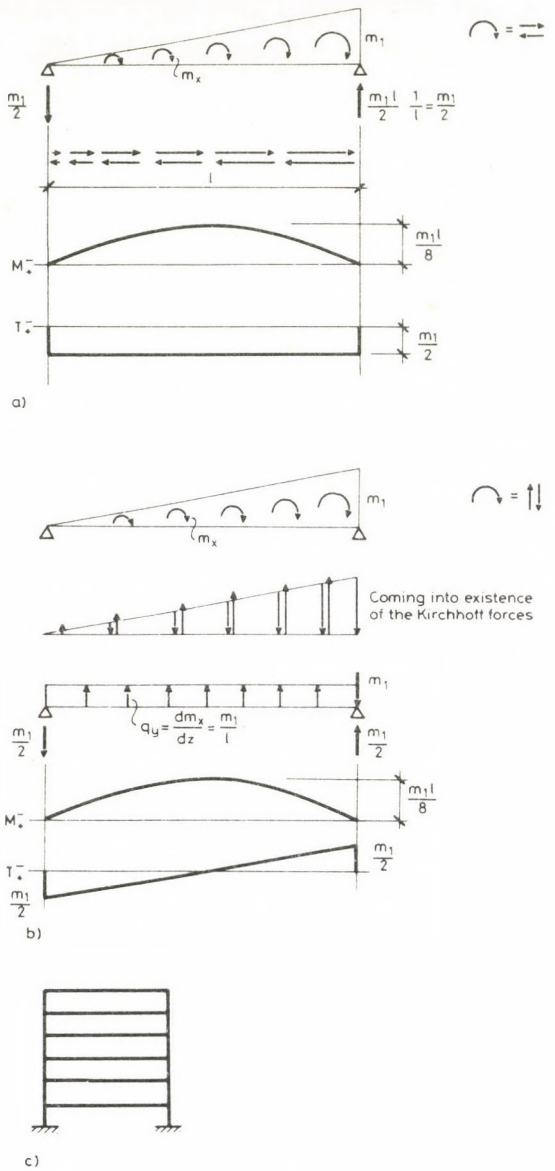

Fig. 7. Cases of transmitting the distributed moments
a— in the form of couples parallel to the beam axis
b— in the form of couples perpendicular to the beam axis
c— example for b.

this "derivative", as with the concentrated Kirchhoff force in the corners of simply supported rectangular plates.

Hence, as can be seen, the distributed moments transmitted in two different ways produce the same bending moment diagram, but yield different results with respect to the shearing force and the lateral load q_y. Hence we have to decide, on the basis of the static model of the structure, which way of transmitting the distributed bending moments is valid, and we have to determine the lateral load and the shearing force diagram accordingly.

4.2 The supporting effect of the shear rigidity of the coated fabric

For taking the shear rigidity into account, we shall model the fabric according to Fig. 8, i.e. we divide it perpendicularly to the arch axis into narrow strips of the width a, and we surround each of these strips by a hinged frame consisting of incompressible bars. The fabric is attached to the cross section of the arch at point G. Consequently, the shearing forces necessary to produce angular distortion $\gamma = dv_G/ds$ of the strip are transmitted from the arch by a couple $P_1 a$ and by the tangential force P_{t1}, as shown in the figure. Hence the arch is subjected to distributed axial forces P_{t1}/a and to distributed couples $P_1 a/a = P_1$; on the other hand, the fabric obtains all these forces as tangential ones. (With v_G we denoted the y-directed displacement of the point of attachement of the fabric.)

Since a fabric section of the width l_y joins two arches, the force

$$P_1 = \tau\delta \frac{l_y}{2} = G\delta\gamma \frac{l_y}{2} = G\delta \frac{l_y}{2} \frac{dv_G}{ds} \tag{19}$$

has to act from one arch to the fabric to produce the angular distortion γ. (Here δ denotes the thickness and G the modulus of shear of the coated fabric.)

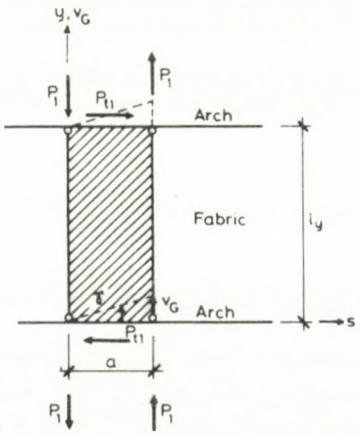

Fig. 8. Modelling the canvas for computing the restraining effect due to shear stiffness

The distributed moments are transmitted to the arch by couples perpendicular to the arch axis. Hence, according to what was said in Sect. 4.1, a lateral force q_{y1}, equal to the derivative of these moments, will act on the arch:

$$q_{y1} = \frac{\mathrm{d}P_1}{\mathrm{d}s} = G\delta \frac{l_y}{2} \frac{\mathrm{d}\gamma}{\mathrm{d}s} = G\delta \frac{l_y}{2} \frac{\mathrm{d}^2 v_G}{\mathrm{d}s} = g_1 \frac{\mathrm{d}^2 v_G}{\mathrm{d}s^2}, \tag{20a}$$

where

$$g_1 = G\delta l_y/2 . \tag{20b}$$

Since the fabric is mostly attached to the arch at a point different from the shear centre, the aforementioned lateral forces q_{y1} also cause distributed twisting moments.

In addition, the distributed axial force

$$\frac{P_{t1}}{a} = \frac{\tau\delta a}{a} = G\delta\gamma = G\delta \frac{\mathrm{d}v_G}{\mathrm{d}s} \tag{21}$$

also acts on the arch.

All the above data give the supporting forces exerted by one fabric section onto one arch. The subscripts 1 refer to this circumstance. Since, however, one arch is in most cases supported by two fabric sections, we accordingly have to take twice these values into account. Hence on one arch the force

$$q_y = g \frac{\mathrm{d}^2 v_G}{\mathrm{d}s^2} \tag{22a}$$

acts, where

$$g = 2g_1 = G\delta l_y . \tag{22b}$$

It should be remarked that we also could obtain the above results with the aid of the elementary theory of strength of materials: considering the two arches together with the intermediate fabric section as an I-beam, the shear distortion of the web can be computed from the formula

$$\frac{\mathrm{d}v_G}{\mathrm{d}s} = \frac{T}{G\delta l_y} . \tag{23a}$$

Since

$$q_y = (-)\frac{\mathrm{d}T}{\mathrm{d}s},$$

we arrive at the relation (22), giving the total shear rigidity of one fabric section, exerted on two arches.

The curvedness of the fabric does not change the shear rigidity computed for the plane fabric, since the assumed pure shear stress state can equally develop in curved surfaces (cf. the twisting of thin-walled closed sections). The only reason why the shear rigidity of curved fabric sections may be different from that of plane sections is that the arc length of the curved section is longer than l_y. However, this deviation is negligibly small in our treatment, due to the assumption concerning the shallowness of the fabric.

5. Lateral stability analysis of the arches

5.1 Analysis neglecting the shear rigidity of the fabric

If we only consider the tensile stiffness of the fabric, we have to perform the stability analysis, according to what has been said in Sect. 3, in such a way that, after computing c_{eff} from Eqs. (16) and (11), we determine the critical compressive force of the arch supported elastically in the lateral direction, taking one half wave as the buckling shape (first, symmetric buckling mode), from the formulas given in [4] or [1], depending on the end support conditions. In addition, we have to compute the critical force of the unsupported arch with two half waves (second, antisymmetric buckling mode). The lower value of the two gives the most onerous critical load.

5.2 Taking into account both the tensile and shear rigidities of the fabric

If we consider both kinds of rigidities of the fabric, then, in performing the stability analysis, according to what has been said in Sect. 5.1, we have to consider both the tensile and shear rigidities when investigating the first, symmetric buckling mode, as described in [5] and [1]; and to take only shear rigidity into account when computing the second, antisymmetric mode (i.e. by setting $c_{\text{eff}}=0$ in the equations).

Obviously, both the tensile and shear stiffnesses of the fabric increase the critical load of the arch.

6. Numerical examples

6.1 Controlling example

Let us compute the spring constant c_{eff}, supporting each arch of the tent structure consisting of six arches, shown in Fig. 9. The stiffnesses of the extreme and intermediate springs be equal ($c_e=c_i=c$). Let us perform the computation by the method outlined in this paper and also by directly solving the equations written for each arch (exact method).

6.1.1 Method outlined in the paper. For the extreme arch: $n=2.5$ (cf. Fig. 5b). Eq. (16):

$$1+1-\lambda^2-\frac{\cos 1.5\lambda}{\cos 2.5\lambda}=0$$

According to (18):

$$\lambda<\sqrt{\frac{1}{2.5+0.5}}=0.58\,.$$

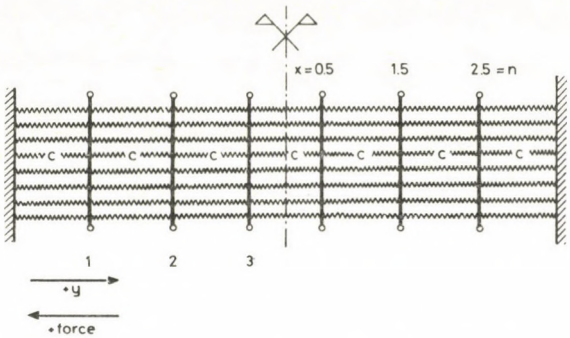

Fig. 9. Model of the structure of the controlling example

By trial and error we find.

$$\lambda = 0.448\,,$$

or, according to (11b):

$$c_{\text{eff}} = 0.201c\,.$$

6.1.2 Directly solving the equations. The serial numbers of the arches would become, according to Fig. 5b, broken numbers. Hence, for simplification, we number the arches on the left-hand side of the structure with whole numbers from 1 on, and write the equations accordingly. We denote the displacements of the arches by y. The spring forces acting on the individual arches are:

Arch 1: $cy_1 - c(y_2 - y_1)$;

Arch 2: $c(y_2 - y_1) - c(y_3 - y_2)$;

Arch 3: $c(y_3 - y_2)$ (since in the central spring no force arises).

We obtain the spring constant c_{eff}, valid for each arch, by dividing these forces by the corresponding displacements y. Since c_{eff} has to be equal for all arches, we can write:

$$c_{\text{eff}} = \frac{c(2y_1 - y_2)}{y_1} = \frac{c(2y_2 - y_1 - y_3)}{y_2} = c_{\text{eff}}\,, \tag{a}$$

and

$$\frac{c(2y_2 - y_1 - y_3)}{y_2} = \frac{c(y_3 - y_2)}{y_3} = c_{\text{eff}}\,. \tag{b}$$

From Eq. (a):

$$y_2 = \sqrt{y_1^2 + y_1 y_3}\,. \tag{c}$$

Introducing (c) into (b), we arrive at the following equation of the fourth order for $\eta_3 = y_3/y_1$:

$$\eta_3^2 - \eta_3\sqrt{1+\eta_3} - 1 = 0\,.$$

By trial and error:

$$\eta_3 = 2.5 ,$$

i.e.

$$y_3 = 2.5 y_1 ,$$

and, from Eq. (c):

$$y_2 = 1.80 y_1 .$$

The spring constant c_{eff} can be obtained either from (a), or from (b):

$$c_{\text{eff}} = 0.200 c ,$$

i.e. practically identical with that yielded by the method outlined in this paper.

6.2 Analysis of an erected tent structure

Let us determine the effective tensile and shear rigidities of the fabric of the tent structure shown in Fig. 10. The data not explained in the figure are:

The tensile and shear stiffnesses of a strip of 1 m width of the fabric are, on the basis of [2]:

$$(EA)_y = E_y \delta = 737.7 \text{ kN/m} ;$$

$$(EA)_z = E_z \delta = 257.7 \text{ kN/m} ;$$

$$G\delta = 24.0 \text{ kN/m} .$$

The tensile stiffness of an intermediate fabric section is, according to (6):

$$c_i = \frac{1}{\dfrac{9}{737.7} + \dfrac{1.5^2}{6^2}\,\dfrac{18^4}{9^3(257.7)}} = 21 \text{ kN/m}^2 .$$

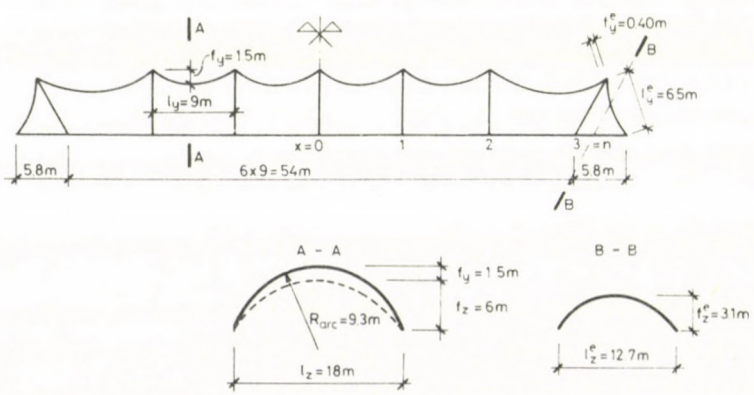

Fig. 10. Geometric data of the erected tent structure

The stiffness of the extreme, slanting section of the fabric is to be computed on the basis of the section $B-B$ of Fig. 10. Using Eq. (6) we obtain:

$$c_e^{\text{slanting}} = \frac{1}{\frac{6.5}{737.7} + \frac{0.40^2}{3.1^2}\,\frac{12.7^4}{6.5^3 \times 257.7}} = 67.0\ \text{kN/m}^2 .$$

From this value we have to compute the spring force due to the horizontal displacement $\Delta^{\text{horiz}} = 1$ of the extreme arch (Fig. 11).

Since $$\Delta^{\text{horiz}} = \Delta \sin \alpha = 0.872 \Delta ,$$

and $$\Delta^e = \Delta \sin (\alpha + \beta) = 0.731 \Delta ,$$

consequently $\Delta^e = \dfrac{0.731}{0.872}\,\Delta^{\text{horiz}} = 0.838\,\Delta^{\text{horiz}}$.

Hence, due to $\Delta^{\text{horiz}} = 1$ a spring force

$$c_e^{\text{horiz}} = 0.838 \times 67.0 = 56.1\ \text{kN/m}^2$$

arises, so that the spring constant of the extreme section to be considered is:

$$c_e = 56.1\ \text{kN/m}^2 .$$

Since the structure contains seven arches, we have for the extreme arch, according to Fig. 5a, $n = 3$.
Eq. (16) becomes:

$$2.671 + 1 - \lambda^2 - \frac{\cos 2\lambda}{\cos 3\lambda} = 0$$

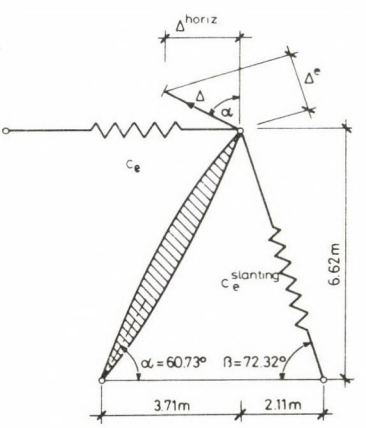

Fig. 11. Converting the slanting spring constant into a horizontal one

On the basis of (18):

$$\lambda < \sqrt{\frac{56.1}{21(3+0.5)}} = 0.874 .$$

By trial and error (16) yields:

$$\lambda = 0.465 ,$$

and, according to (11b):

$$c_{\text{eff}} = 4.54 \text{ kN/m}^2 .$$

The shear stiffness of one fabric section gives rise to a distributed force

$$q_{y1} = 24.0 \frac{9}{2} \frac{\mathrm{d}^2 v_G}{\mathrm{d}s^2} = 108 \frac{\mathrm{d}^2 v_G}{\mathrm{d}s^2} \text{ kN/m} ,$$

so that twice this value acts on one arch:

$$q_y = 216 \frac{\mathrm{d}^2 v_G}{\mathrm{d}s^2} \text{ kN/m} ,$$

or, according to (22):

$$g = 216 \text{ kN} .$$

Although the two rigidity characteristics (c_{eff} and g) cannot be directly compared due to their different units, their numerical values show that the comparatively high tensile stiffness of the fabric results in a low c_{eff}, while the comparatively low shear stiffness of the fabric yields a high g. We can explain this phenomenon by considering, on the one hand, that c_{eff} decreases with the increasing number of arches, according to the explanation given to Eqs. (17) and (18), and that c_{eff} is inversely proportional to the lengths of the fabric sections. On the other hand, g is independent of the number of arches, since each arch is stiffened by the neighbouring fabric sections, and, according to our assumption made in Sect. 4.2, the magnitude of g is directly proportional to the lengths of the fabric sections.

We omit the computation of the axial force P_t, since it gives a term small of the second order in the stability analysis, so that it is to be neglected in comparison with other, first-order terms.

With these data we shall perform the stability analysis of the arch in [5], according to the principles described in Sect. 5.

References

1. Bódi, I.: Lateral Buckling of Arches with Built-in Ends, Elastically Supported against Lateral Displacement and Rotation. To be published in the Acta Techn. Hung.
2. Harnach, R.—Hartmann, B.—Niemann, H.—J.: Stresses and Deformations of Pneumatic Structures under Wind Load and Internal Pressure. Paper presented at the IASS Symposium on Shell and Spatial Structures: The Development of Form. Morgantown, 1978. — See also in: Research Report. IASS Working Group of Pneumatic Structures (Chairman: Y. Tsuboi). Yokohama National University, Japan, 1978, pp. 125–150
3. Kármán, Th. von—Biot, M. A.: Mathematical Methods in Engineering. McGraw-Hill, New York/London, 1940
4. Kollár, L.—Gyurkó, J.: Lateral Buckling of Elastically Supported Arches. Acta Techn. Hung. **94** (1982), pp. 37—45.
5. Kollár, L.—Bódi, I.: Lateral Buckling of Arches Elastically Supported against Lateral Displacement and Rotation. To be published in the Acta Techn. Hung. **95** (1982), 99—106.
6. Szabó, J.—Kollár, L.: Structural Design of Cable-Suspended Roofs. Ellis Horwood, Chichester — Publ. House of the Hung. Academy of Sciences, Budapest, 1984.
7. Timoshenko, S.—Woinowsky-Krieger, S.: Theory of Plates and Shells. 2nd Ed. McGraw-Hill, New York/Toronto/London 1959

Acta Technica Academiae Scientiarum Hungaricae, 94 (3—4), pp. 215–221 (1982)

BOUNDS FOR THE FLEXIBILITY OF CIRCULAR PLATES OF VARIABLE THICKNESS

I. ECSEDI*

[Received: 29 November, 1982]

The paper deals with circular plates of variable thickness made of elastic material. The proof of the bounds relating to the coefficient of flexibility defined by the formula (2.1) is based on the two minimum-theorems of the elastostatics. Applications of the inequality relations (3.3) and (4.2) are demonstrated by an example.

The following symbols of major significance are used in this paper:

r, φ, z	polar coordinates,
E	Young's modulus,
ν	Poissons ratio,
$h = h(r)$	plate thickness,
D	bending stiffness of plate,
$w = w(r)$	deflection of plate middle surface,
F	force,
U	energy of deformation,
C	flexibility (coefficient of flexibility),
R	stiffness,
$g = g(r)$	auxiliary function,
M_r, M_φ	moments with respect to unit length of radial and tangential direction respectively,
Q_r	radial shear force with respect to the unit length,
$V = V(r)$	auxiliary function,
π	potential energy,
K	complementary energy
$A = A(r)$	auxiliary function.

The problem to be solved

The homogeneous, isotropic, circular plate of variable thickness and linearly elastic material is bounded in the radial direction by a cylindrical surface having a radius $r = a$. The thickness of the plate is a given function of the radial coordinate r: $h = h(r)$. The plane designated with the coordinate $z = 0$ is the middle plane of the plate, and at the same time, its symmetry plane. The plate is freely supported at its external edge and is subjected to the force F at its centre.

The paper makes use of the customary assumptions of Kirchhoff's theory of plates.

The conclusion of Kirchhoff's theory of plates is that the relation between force F and the displacement $w(0)$ of its point of application is homogeneously linear (Fig. 1), that is:

$$w(0) = CF\,. \tag{2.1}$$

* Dr. I. Ecsedi, Vászonfehérítő u. 24., H-3531 Miskolc, Hungary

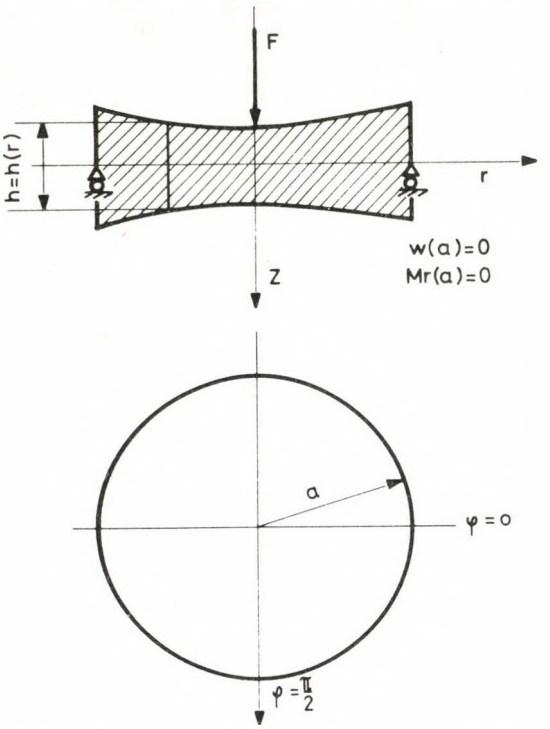

Fig. 1. Circular plate of variable thickness

The quantity C entering in the above formula is referred to as the flexibility of the plate of variable thickness (i.e. its flexibility coefficient). The inverse of flexibility C is called the stiffness of the circular plate:

$$R = \frac{1}{C} = \frac{F}{w(0)}. \tag{2.2}$$

In the case with $h = \text{constant}$ one obtains the result for flexibility C:

$$C = \frac{(3+\nu)a^2}{16\pi(1+\nu)D} \tag{2.3}$$

wherein

$$D = \frac{Eh^3}{12(1-\nu)^2}. \tag{2.4}$$

The correctness of the formula (2.3) directly ensues from formula (88) to be found on page 70 of the work [1].

In case with $h \neq \text{constant}$, for the determination of the exact (strict) value of flexibility C a fourth order, inhomogeneous linear differential equation of variable coefficient should be solved, the explicit solution of which is, in a great many instances,

unknown. That is because such methods and principles are of very high significance, through the application of which the lower and upper bounds can be produced to the flexibility of a circular plate of variable thickness defined by formula (2.1).

Lower bound

Proposition. With the function $g=g(r)$ nonidentically equal to zero, being in the open interval $0<r<a$ twice, and in the closed interval $0\leq r\leq a$ once, continuously differentiable, and satisfying the homogeneous boundary conditions

$$g'(0)=0, \qquad g(a)=0 \tag{3.1), (3.2}$$

the inequality relation

$$C\geq \frac{[g(0)]^2}{2\pi D_0 \int_0^a \left[H\left(\frac{\mathrm{d}^2 g}{\mathrm{d}r^2}+\frac{1}{r}\frac{\mathrm{d}g}{\mathrm{d}r}\right)^2-2(1-\nu)\frac{1}{r}\frac{\mathrm{d}g}{\mathrm{d}r}\frac{\mathrm{d}^2 g}{\mathrm{d}r^2}\right] r\,\mathrm{d}r} \tag{3.3}$$

is valid wherein:

$$D_0=\frac{Eh_0^3}{12(1-\nu)^2}, \qquad H=\left(\frac{h(r)}{h_0}\right)^3, \tag{3.4), (3.5}$$

$$h_0=h(0)\,.$$

Demonstration. Proving takes place by the application of the minimum theorem connected to the potential energy functional.

The value of the potential energy associated to the kinematically possible field of displacement satisfying the homogeneous kinematic boundary conditions

$$\tilde{w}'(0)=0 \qquad \tilde{w}(a)=0 \tag{3.6), (3.7}$$

can be determined on the basis of formula [1]:

$$\pi(\tilde{w})=D_0\pi\int_0^a H\left[\left(\frac{\mathrm{d}^2\tilde{w}}{\mathrm{d}r^2}+\frac{1}{r}\frac{\mathrm{d}\tilde{w}}{\mathrm{d}r}\right)^2-\right.$$

$$\left.-2(1-\nu)\frac{1}{r}\frac{\mathrm{d}\tilde{w}}{\mathrm{d}r}\frac{\mathrm{d}^2\tilde{w}}{\mathrm{d}r^2}\right] r\,\mathrm{d}r-F\tilde{w}(0) \tag{3.8}$$

The value of the potential energy associated with the exact solution $w=w(r)$ may also be expressed by the work W of force F:

$$\pi(w)=-\frac{1}{2}W=-\frac{1}{2}Fw(0)\,. \tag{3.9}$$

Let us have

$$\tilde{w} = F\lambda g(r)\,. \tag{3.10}$$

In formula (3.10) the symbol λ so far denoted a voluntary real parameter.

It is evident that

$$g'(0) = 0, \qquad g(a) = 0\,. \tag{3.11), (3.12}$$

Considering the relationships (3.8), (3.9), (3.10) and the minimum theorem associated with the potential energy functional

$$\pi(w) \leq \pi(\tilde{w}) \tag{3.13}$$

it can be written that

$$C \geq \lambda^2 \left(-2D_0\pi \int_0^a H \left[\left(\frac{\mathrm{d}^2 g}{\mathrm{d}r^2} + \frac{1}{r}\frac{\mathrm{d}g}{\mathrm{d}r} \right)^2 - \right.\right.$$

$$\left.\left. -2(1-\nu)\frac{1}{r}\frac{\mathrm{d}g}{\mathrm{d}r}\frac{\mathrm{d}^2 g}{\mathrm{d}r^2} \right] r\,\mathrm{d}r \right) + 2\lambda g(0)\,. \tag{3.14}$$

The relation (3.14) is valid for any value of variable λ.

At the point

$$\lambda = \frac{g(0)}{2\pi D_0 \int_0^a H \left[\left(\frac{\mathrm{d}^2 g}{\mathrm{d}r^2} + \frac{1}{r}\frac{\mathrm{d}g}{\mathrm{d}r} \right)^2 - 2(1-\nu)\frac{1}{r}\frac{\mathrm{d}g}{\mathrm{d}r}\frac{\mathrm{d}^2 g}{\mathrm{d}r^2} \right] r\,\mathrm{d}r} \tag{3.15}$$

the expression at the right-hand side of the inequality (3.14) has an absolute maximum. On the basis of the value of the maximum in question it may be written:

$$C \geq \frac{[g(0)]^2}{2\pi D_0 \int_0^a H \left[\left(\frac{\mathrm{d}^2 g}{\mathrm{d}r^2} + \frac{1}{r}\frac{\mathrm{d}g}{\mathrm{d}r} \right)^2 - 2(1-\nu)\frac{1}{r}\frac{\mathrm{d}g}{\mathrm{d}r}\frac{\mathrm{d}^2 g}{\mathrm{d}r^2} \right] r\,\mathrm{d}r}\,. \tag{3.16}$$

The formula (3.16) is always true in that case where the function $g = g(r)$ which satisfies the continuity and differentiability conditions, is non-identically constant, because, the expression of the specific energy of deformation is, in such cases, positive.

Upper bound

Proposition. With any one-variable function $A = A(r)$ which is continuous in the closed interval $0 \leq r \leq a$ and continuously differentiable in the open interval $0 < r < a$, satisfying the boundary condition

$$A(a)=\frac{a}{2\pi}, \tag{4.1}$$

the inequality relation

$$C\leq \frac{2\pi}{D_0(1-\nu^2)}\int_0^a \frac{1}{H}\left[\left(\frac{A}{r}+\frac{\mathrm{d}A}{\mathrm{d}r}-\frac{1}{2\pi}\right)^2-\right.$$

$$\left.-2(1+\nu)\left(\frac{A}{r}-\frac{1}{2\pi}\right)\frac{\mathrm{d}A}{\mathrm{d}r}\right]r\,\mathrm{d}r \tag{4.2}$$

is valid.

Demonstration. Proving is based upon the minimum theorem associated with the complementary energy functional K.

The expression of the complementary energy associated to the statically potential fields of moments $\tilde{M}_r=\tilde{M}_r(r)$ and $\tilde{M}_\varphi=\tilde{M}_\varphi(r)$ satisfying the equilibrium conditions

$$\tilde{M}_r+r\frac{\mathrm{d}\tilde{M}_r}{\mathrm{d}r}-\tilde{M}_\varphi-rQ_r=0 \qquad 0<r<a\,, \tag{4.3}$$

$$\tilde{M}_r(a)=0 \tag{4.4}$$

is, by taking as basis the formula (8.55) on page 162 of [2]:

$$K(\tilde{M}_r,\tilde{M}_\varphi)=\frac{\pi}{D_0(1-\nu)^2}\int_0^a\frac{1}{H}\left[(\tilde{M}_r+\tilde{M}_\varphi)^2-\right.$$

$$\left.-2(1+\nu)\tilde{M}_r\tilde{M}_\varphi\right]r\,\mathrm{d}r \tag{4.5}$$

The quantities of positive signs $\tilde{M}_r$, $\tilde{M}_\varphi$, Q_r are shown in *Fig. 2.*

The value of the complementary energy belonging to the fields $M_r=M_r(r)$ and $M_\varphi=M_\varphi(r)$ satisfying all conditions relating to the plate problem, including the compatibility and equilibrium conditions, is $K(M_r, M_\varphi)$. Taking for basis the minimum theorem associated with the complementary energy functional, the following may be written:

$$K(M_r,M_\varphi)\leq K(\tilde{M}_r,\tilde{M}_\varphi)\,. \tag{4.6}$$

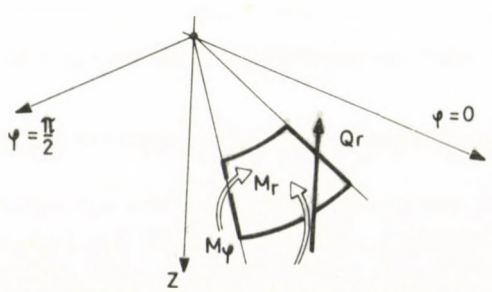

Fig. 2. Interpretation of the signs of M_r, M_φ, Q_r

Let us have

$$\tilde{M}_r = Fm_r, \qquad \tilde{M}_\varphi = Fm_\varphi \tag{4.7), (4.8}$$

$$rQ_r = -F\frac{\mathrm{d}V}{\mathrm{d}r} \tag{4.9}$$

Combination of (4.3), (4.7), (4.8), (4.9) yields the equation

$$\frac{\mathrm{d}}{\mathrm{d}r}(rm_r - V) = m_\varphi \tag{4.10}$$

Be given

$$m_r = \frac{A}{r} + \frac{V}{r} \tag{4.11}$$

wherein $A = A(r)$ is a one-variable function, at least once continuously differentiable. Then, on the basis of (4.10) it may be written that of necessity

$$m_\varphi = \frac{\mathrm{d}A}{\mathrm{d}r}. \tag{4.12}$$

By an elementary train of thoughts it may be pointed out that in the present problem ([1] p. 62)

$$Q_r = \frac{F}{2\pi r} \tag{4.13}$$

By combining (4.9) and (4.13) one finds

$$V = -\frac{1}{2\pi}r \tag{4.14}$$

The exact value of the work W of force F is the same as that of the complementary energy:

$$K(M_r, M_\varphi) = \frac{1}{2}Fw(0) = \frac{1}{2}CF^2 \tag{4.15}$$

Combination of the formulae (4.5), (4.6), (4.7), (4.8), (4.11), (4.12), (4.14) and (4.15) yields the inequality relation (4.2) to be proved if one takes equation

$$A(a) = \frac{a}{2\pi} \tag{4.16}$$

resulting from the boundary condition (4.4) into account.

Example

5.1. Fig. 3 represents a plate of linearly variable thickness. The *Young's* modulus and *Poisson*'s ratio of the material of the disc are as follows respectively:

$$E = 2 \cdot 10^5 \ \mathrm{Nmm}^{-2}, \qquad \nu = 0.25\,.$$

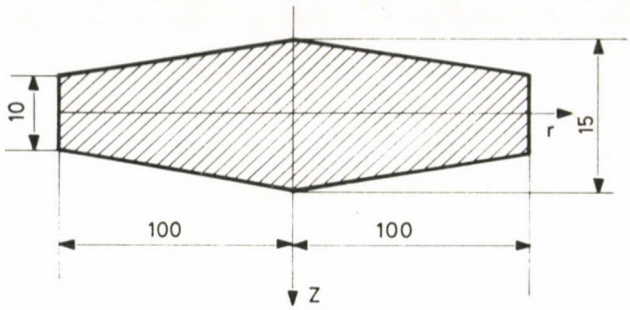

Fig. 3. Circular plate of linearly changeable thickness

Application of the inequality relation (3.3) to the function

$$g(r)=r^2-a^2 \tag{5.1}$$

yields the lower bound

$$C=1.38\cdot 10^{-5}\,\mathrm{mmN}^{-1} \tag{5.2}$$

5.2. The upper bound with respect to the flexibility C of the plate investigated in the preceding example is obtained from the inequality relation (4.2) with the help of the function

$$A(r)=r^2\left(\ln\frac{r}{a}+\frac{1}{2\pi a}\right) \tag{5.3}$$

$$C\leq 1.421\cdot 10^{-5}\,\mathrm{mm}\cdot\mathrm{N}^{-1}. \tag{5.4}$$

References

1. Timoshenko, S.—Woinowsky–Krieger, S.: Theory of Plates and Shells. Műszaki Könyvkiadó. Budapest 1966
2. Washizu, K.: Variational Methods in Elasticity and Plasticity. First edition. Pergamon Press. Oxford–London–New York–Toronto 1963

Acta Technica Academiae Scientiarum Hungaricae, 94 (3—4), pp. 223–233 (1982)

INVESTIGATION OF THE ENGAGEMENT OF HARMONIC DRIVES — PART II

J. PÉTER*

[Received: April 12, 1982]

In engaging of a pair of toothed gears consisting of a circular spline and a flexspline of a great number of teeth and small difference in number of teeth, those which are simultaneously meshing, may be significantly higher than those calculated. The present paper investigates this phenomenon in the harmonic drives.

1. Introduction

In the late 50s C. W. Musser, an American engineer, surprised the technicians engaged in the problems of gearings: he integrated in the drive a flexible toothed wheel, the flexspline. During running, the flexspline is deformed in a wave-like way.

The present paper deals with this particular case of meshing of toothed wheels and continues the author's work began in [1]. Part I [1] summarizes the symbols and concepts needed for the investigations and simplifies the problem to the engagement of a normal circular spline and a spur gear of a centre of rotation displaced as compared to its centre. Each of the pairs of teeth are engaged, similarly to the cylindrical gears, along the tooth profiles.

In the harmonic drives, a pair of gears, i.e., a circular spline and a spur gear of high tooth number ($z_2 = 100 \ldots 800$) and a slight difference in tooth number (in general, $z_3 - z_2 = 2$) are included. The teeth of both gears of greathly similar profiles are, beyond the theoretical bounds of the involute engagement so near to each other that the backlash between them, in consequence of the flexible deformation of the drive elements (and, first of all, the flexspline) and due to the rearrangement of the clearances, will be suppressed. Then, in theory, the engagement takes place between the crest edge of one of the wheels (in practice the part of the tooth flank near the crest edge) and the tooth flank of the other wheel.

Beyond the theoretical bounds of the involute engagement, the number of teeth being engaged simultaneously, non-correctly in an edge-like way, is the function of the construction parameters and loading of the drive, as is to be seen in Fig. 1 [3, 4].

* Péter J., Derkovits u. 54, I. 3, H-3529 Miskolc, Hungary

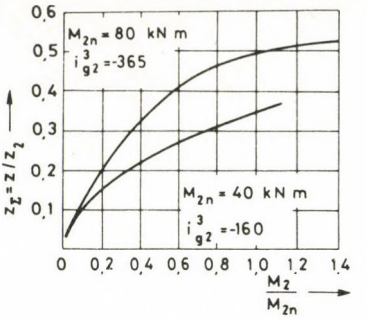

Fig. 1. Change of the ratio ($z_\Sigma = z/z_2$) of the number of the simultaneously meshing teeth (z) and the tooth number (z_2) of the flexspline, depending on the ratio between the torque (M_2) actuating the slowly rotating axle and the nominal torque (M_{2n}) acting on the slowly rotating axle

2. Engagement beyond the theoretical bounds of the involute engagement

The teeth of the harmonic drive are engaging beyond the bounds of the involute engagement, in case where the backlash is

$$j \leq cm\,, \tag{2.1}$$

wherein c is a coefficient depending on the loading and the construction parameters of the drive and its value may be, according to experiments, in case of nominal loading and drives of light design 0.06 and for drives of heavier design 0.04; m, being the module.

The investigations are carried out in the plane of the wave generator, in the system of coordinates established to the generator. It was examined how the backlash changed depending on the rotation of the flexspline in relation to the principal deformation axis. It was assumed that where (2.1) is true, the teeth are engaging. Thereafter, the momentary transmission ratio [1] and the velocity of slip should be determined.

2.1. The engagement between the crest edge of the flexspline and the tooth flank of the circular spline

2.1.1. Definition of the backlash.

Let us investigate how the backlash changes depending on the rotation φ_2 of the flexspline in relation to the principal deformation axis (Fig. 2):

$$j = (\mu + \varphi_3 + \sigma_3 - \tan \alpha'_{t2}) \frac{z_3 m \cos \alpha_0}{2}\,, \tag{2.1.1.1}$$

wherein:

z_3 = tooth number of circular spline;
m = module;
α_0 = angle of standard rack.

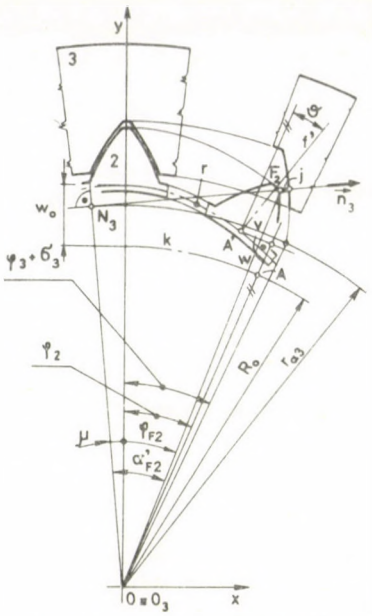

Fig. 2. Backlash between the tooth edge of the flexspline and the tooth flank of the circular spline

Between the radii O_3N_3, O_3F_2 the formulae

$$\alpha'_{F2} = \arccos \frac{z_3 m \cos \alpha_0}{2\,\overline{O_3F_2}}, \qquad ((2.1.1.2)$$

$$\overline{OF_2} = \sqrt{S}$$

with

$$S = \left(R_0 + w + h_{02} \cos \vartheta - \frac{s_{f2}}{2} \sin \vartheta\right)^2 +$$

$$+ \left(v + h_{02} \sin \vartheta + \frac{s_{f2}}{2} \cos \vartheta\right)^2, \qquad (2.1.1.3)$$

are valid.

Herein:

R_0 = radius of the middle line k;

$w = f(\varphi_2)$, $v = f(\varphi_2)$, $\vartheta = f(\varphi_2)$ = a displacement of point A of the middle line in the radial and tangential direction, and the rotation of the cross section, respectively;

h_{02} = distance between middle line (middle circle) and addendum circle;

s_{f2} = width of tooth top of wheel 2.

Between the radius O_3N_3 and the principal deformation axis it is valid that

$$\mu = \alpha'_{F2} - \varphi_{F2}\,. \qquad (2.1.1.4)$$

wherein

$$\varphi_{F2}=\varphi_2+\arctan\frac{v+h_{02}\sin\vartheta+\frac{s_{f2}}{2}\cos\vartheta}{R_0+w+h_{02}\cos\vartheta-\frac{s_{f2}}{2}\sin\vartheta}. \tag{2.1.1.5}$$

In case where the flexspline rotates at an angle φ_2 as compared with the deformation principal-axis, the rotation of the circular spline, with the knowledge of the tooth number, is:

$$\varphi_3=\frac{1}{i_{23}^{g}}\varphi_2=\frac{z_2}{z_3}\varphi_2\,. \tag{2.1.1.6}$$

The central angle corresponding to the half width of the tooth groove of the standard rack of wheel *3* is

$$\sigma_3=\text{inv}\,\alpha_0+\frac{w_{03}}{z_3 m}, \tag{2.1.1.7}$$

wherein the width of the tooth groove on the pitch circle

$$w_{03}=\frac{\pi m}{2}+2x_3 m\tan\alpha_0\,, \tag{2.1.1.8}$$

and x_3 is the coefficient of tool supply.

2.1.2. The momentary transmission ratio

Let us assume that the backlash calculated at some angle φ_2 is smaller than that given by (2.1), i.e., the tooth pair is in engagement (Fig. 3). In this case we have

$$(\dot{v}_2'-\dot{v}_3)\dot{n}_3=0$$

or

$$(\rho'+h_{02})\omega_{2'g}\cos\left(\mu+\varphi_2+\frac{s_{f2}}{2(\rho'+h_{02})}+\vartheta\right)=$$

$$=\omega_{3g}\overline{O_3F_2}\cos\alpha_{F2}'\,, \tag{2.1.2.1}$$

where $\omega_{2'g}$ and ω_{3g} are the angular velocities of the tooth of the wheel *2* investigated and wheel *3*, respectively, as compared with the generator.

By making use of Eq. (2.1.2.1) for the momentary transmission ratio one obtains

$$i_{2'3}^{g}=\frac{\omega_{2'g}}{\omega_{3g}}=\frac{\overline{O_3F_2}\cos\alpha_{F2}'}{(\rho'+h_{02})\cos\left[\mu+\varphi_2+\frac{s_{f2}}{2(\rho'+h_{02})}+\vartheta\right)}. \tag{2.1.2.2}$$

$\overline{O_3F_2}$, α_{F2}' and μ entering in the relationship (2.1.2.2) are to be calculated with the aid of relationships (2.1.1.3), (2.1.1.2) and (2.1.1.4) respectively. $\rho'=f(\varphi_2)$ is the radius of curvature at point A' of the flexible line.

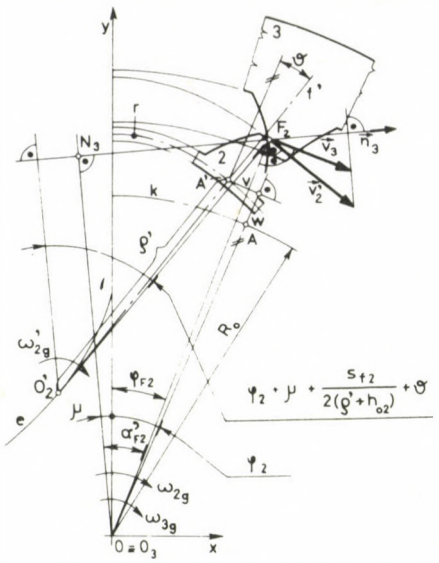

Fig. 3. The slip velocity between the tooth edge of the flexspline and the tooth flank of the circular spline

2.1.3. The velocity of slip

Let us investigate how much the velocity of slip is in case where the engagement of the teeth has an edge-pattern. Using the symbols of Fig. 3 yields

$$v_{t2'3} = \omega_{2'g}(\rho' + h_{02}) \sin\left[\mu + \varphi_2 + \frac{s_{f2}}{2(\rho' + h_{02})} + \vartheta\right] - \\ - \omega_{3g}\overline{O_3 F_2} \sin \alpha'_{F2} \,. \tag{2.1.3.1}$$

In relationship (2.1.3.1) $\omega_{2'g} = \omega_{2'} - \omega_g$, $\omega_{3g} = \omega_3 - \omega_g$, $\omega_{2'}$, ω_3 and ω_g are the angular velocities of the tooth investigated of wheel *2*, wheel *3* and the generator *g*, respectively, in relation to the casing.

Let us introduce the designations $i_{2'g} = \omega_2/\omega_g$, $i_{3g} = \omega_3/\omega_g$. After transformation we have

$$v_{t2'3} = \omega_g \left\{(i_{2'g} - 1)(\rho' + h_{02}) \sin\left[\mu + \varphi_2 + \frac{s_{f2}}{2(\rho' + h_{02})} + \vartheta\right]\right. \\ \left. - (i_{3g} - 1)\frac{z_3 m \cos \alpha_0}{2} \tan \alpha'_{F2}\right\}. \tag{2.1.3.2}$$

From the relationship (2.1.3.2) in case of one degree of freedom (if $\omega_3 = 0$), the direction of the drive is $g \rightarrow 2$, one obtains

$$v_{t2'3} = \omega_g \left\{ \frac{z_3 m \cos \alpha_0}{2} \tan \alpha'_{F2} - \right.$$

$$\left. - i^g_{2'3} (\rho' + h_{02}) \sin \left[\mu + \varphi_2 + \frac{s_{f2}}{2(\rho' + h_{02})} + \vartheta \right] \right\} \tag{2.1.3.3}$$

If $\omega_2 = 0$, the direction of the drive is $g \to 3$,

$$v_{t2'3} = \omega_g \left\{ \frac{1}{i^g_{2'3}} \frac{z_3 m \cos \alpha_0}{2} \tan \alpha'_{F2} - \right.$$

$$\left. - (\rho' + h_{02}) \sin \left[\mu + \varphi_2 + \frac{s_{f2}}{2(\rho' + h_{02})} + \vartheta \right] \right\}. \tag{2.1.3.4}$$

2.2. Engagement between the crest edge of the circular spline and the tooth flank of the flexspline

2.2.1. Determination of the backlash

Making use of the symbols of Fig. 4 and following the train of thought of Chapter 2.1.1 the backlash may be calculated with the following relationship

$$j = (\tan \alpha'_{F3} - \varphi'_A - \sigma_2) \frac{z_2 m \cos \alpha_0}{2}, \tag{2.2.1.1}$$

wherein z_2 is the tooth number of the teeth of the flexspline,

$$\alpha'_{F3} = \frac{z_2 m \cos \alpha_0}{2 \overline{O_2 F_3}}; \tag{2.2.1.2}$$

$$\overline{O_2 F_3} = \sqrt{\overline{O_2 O_3^2} + r_{f3}^2 - 2 \overline{O_2 O_3} r_{f3} \cos (\delta + \varphi_{F3})} \tag{2.2.1.3}$$

$$\overline{O_2 O_3} = \sqrt{\overline{O_3 A'^2} + R_0^2 - 2 \overline{O_3 A'} R_0 \cos \vartheta'}; \tag{2.2.1.4}$$

$$\overline{O_3 A'} = \sqrt{(R_0 + w)^2 + v^2}; \tag{2.2.1.5}$$

$$\vartheta' = \vartheta - \arctan \frac{v}{R_0 + w}; \tag{2.2.1.6}$$

$$\delta = \arcsin \frac{R_0 \sin \vartheta'}{\overline{O_2 O_3}} - \varphi_2 - \arctan \frac{v}{R_0 + w}; \tag{2.2.1.7}$$

$$\varphi_{F3} = \varphi_3 - \frac{w_{f3}}{2 r_{f3}}; \tag{2.2.1.8}$$

the width of the tooth groove on the addendum circle of radius r_{f3} is

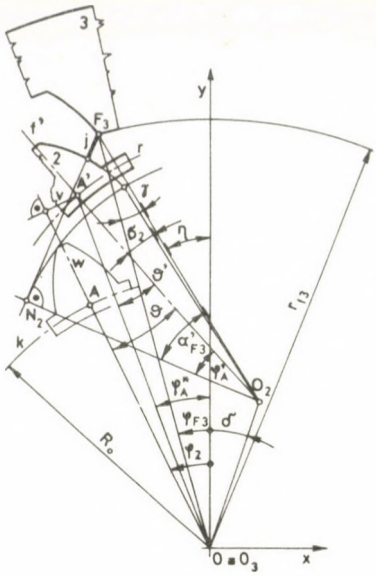

Fig. 4. Backlash between the tooth edge of the circular spline and the tooth flank of the flexspline

$$w_{f3} = m \frac{\cos \alpha_0}{\cos \alpha_{f3}} \left[\frac{\pi}{2} + 2x_3 \tan \alpha_0 + z_3 (\text{inv}\, \alpha_0 - \text{inv}\, \alpha_{f3}) \right], \tag{2.2.1.9}$$

wherein

φ_3 should be calculated with the aid of Formula (2.1.1.6) and
α_{f3} profile angle on the addendum circle of radius r_{f3}.

2.2.2. The momentary transmission ratio

Similarly to (2.1.2.1), on the basis of Fig. 5, the condition of the engagement is

$$\omega_{2'g} \overline{O'_2 F}_3 \cos \alpha^*_{F3} = \omega_{3g} r_{f3} \cos (\alpha^*_{F3} + \gamma'). \tag{2.2.2.1}$$

This, after transformation gives the momentary transmission ratio

$$i^g_{2'3} = \frac{\omega_{2'g}}{\omega_{3g}} = \frac{r_{f3} \cos (\alpha^*_{F3} + \gamma')}{\overline{O'_2 F}_3 \cos \alpha^*_{F3}},$$

or

$$i^g_{2'3} = \frac{r_{f3} \cos (\alpha'_{F3} + \gamma')}{\overline{O'_2 F}_3 \cos (\alpha'_{F3} + \gamma - \gamma')}, \tag{2.2.2.2}$$

where

r_{f3} = the addendum circle of wheel *3* and
α'_{F3} = may be calculated with the aid of relationship (2.2.1.2),

$$\gamma = \arcsin \frac{\overline{O_2 O}_3 \sin (\delta + \varphi_{F3})}{\overline{O_2 F}_3}, \tag{2.2.2.3}$$

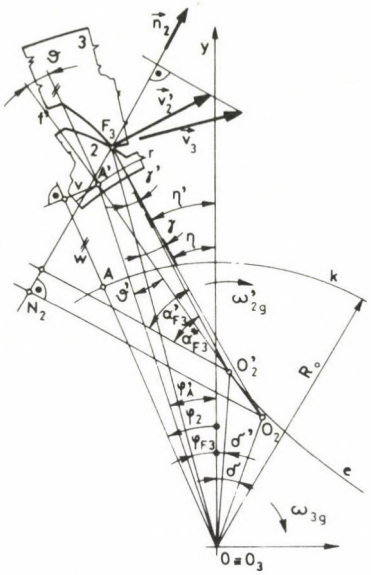

Fig. 5. The slip velocity between the tooth edge of the circular spline and the tooth flank of the flexspline

$$\overline{O_2O_3} = \sqrt{\overline{O_3A'^2} + R_0^2 - 2\overline{O_3A'}\,R_0 \cos \vartheta'}\,, \tag{2.2.2.4}$$

the values of δ, φ_{F3}, $\overline{O_2F_3}$, $\overline{O_3A'}$ and ϑ' may be found with the aid of relationships (2.2.1.7), (2.2.1.8), (2.2.1.3), (2.2.1.5) and (2.2.1.6) respectively,

$$\gamma' = \arcsin \frac{\overline{O_2'O_3} \sin(\varphi_{F3} + \delta')}{\overline{O_2'F_3}}; \tag{2.2.2.5}$$

$$\overline{O_2'O_3} = \sqrt{\overline{O_3A'^2} + \rho'^2 - 2\overline{O_3A'}\,\rho' \cos \vartheta'}\,; \tag{2.2.2.6}$$

$$\overline{O_2'F_3} = \sqrt{r_{f3}^2 + \overline{O_2'O_3^2} - 2\overline{O_2'O_3}\,r_{f3} \cos(\varphi_{F3} + \delta')}\,; \tag{2.2.2.7}$$

$$\delta' = \arcsin \frac{\rho' \sin \vartheta'}{\overline{O_2'O_3}} - \varphi_3 + \frac{w_{f3}}{2r_{f3}}. \tag{2.2.2.8}$$

2.2.3. Slip velocity

Developing the idea of Chapter 2.1.3 and making use of Fig. 5 we have

$$v_{t2'3} = \omega_g[(i_{2'g} - 1)\,\overline{O_2'F_3} \sin \alpha_{F3}^* - (i_{3g} - 1) r_{f3} \sin(\alpha_{F3}^* + \gamma')]\,. \tag{2.2.3.1}$$

If $\omega_3 = 0$, the direction of the drive is $g \to 2$,

$$v_{t2'3} = \omega_g[r_{f3} \sin(\alpha_{F3}' + \gamma) - i_{2'3}^g\,\overline{O_2'F_3} \sin(\alpha_{F3}' + \gamma - \gamma')]\,. \tag{2.2.3.2}$$

wherein α'_{F3}, γ, $i^g_{2'3}$, $\overline{O'_2F_3}$, γ' may be calculated with the aid of relationships (2.2.1.2), (2.2.2.3), (2.2.2.2), (2.2.2.7) and (2.2.2.5), respectively.

If $\omega_2 = 0$, $g \to 3$.

$$v_{t2'3} = \omega_g \left[\frac{1}{i^g_{2'3}} r_{f3} \sin(\alpha'_{F3} + \gamma) - \overline{O'_2F_3} \sin(\alpha'_{F3} + \gamma - \gamma') \right]. \tag{2.2.3.3}$$

3. Number of teeth engaging simultaneously

By making use of the relationships (2.1.1.1) and (2.2.1.1), in case where $j = cm$ the angle $\varphi_2 = \varphi_{2F2}$ and $\varphi_2 = \varphi_{2F3}$ may be determined at which the edge-like engagement begins and ends.

The pitch of the flexspline being $\tau_2 = 2\pi/z_2$, so within the interval $\langle \varphi_{2F2}; \varphi_{2F3} \rangle$ in each engagement zone simultaneously

$$\frac{z}{2} = \frac{\varphi_{2F2} - \varphi_{2F3}}{\tau_2} \tag{3.1}$$

teeth will be engaged (in case where the number of the deformation waves is 2).

The ratio of the tooth number simultaneously engagingand that of the flexspline *(Fig. 1)* is:

$$z_\Sigma = \frac{z}{z_2} \tag{3.2}$$

4. Example

Let us continue the investigation begun in Chapter [1] 5. The significant characteristics of the drive are: $z_2 = 190$; $z_3 = 192$; $m = 1$ mm; $\alpha_0 = 20^0$; $w_0 = 1.2$ mm; $R_0 = 97.1$ mm; $r_{f2} = 100.1$ mm; $r_{f3} = 99.95$ mm; $\tau_2 = 1.89474^\circ$.

To describe the flexible line the relationships recommended in [2] are used.

Let us assume that under the effect of the loading the radial displacement w_0 (Fig. 2) will be reduced from 1.2 mm to 1.0 mm and increasing the loading of the drive, w_0 decreases to 0.9, further, the teeth will be meshed in case where the value of the backlash calculated with the aid of the relationships (2.1.1.1) and (2.2.1.1) is $j \leq 0.06m$.

For $w_0/m = 1.0$ (Fig. 6.a) at each zone of meshing $z/2 \approx 18$ teeth will be meshed simultaneously. In such cases $z_\Sigma = z/z_2 \approx 0.19$. The value of the backlash determined by photographs magnified twenty times (Fig. 6b) and the change of loading (measured with strain gauges) acting on a tooth of the circular spline measured as the function of the rotation of the wave generator (Fig. 6.c) are in agreement with the results of the calculations.

For $w_0/m = 0.9$ (Figs. 6.d, 6.e, 6.f) $z/2 \approx 31$, $z_\Sigma \approx 0.33$. The calculated backlash increases after the beginning of the meshing, then decreases, and subsequently rapidly

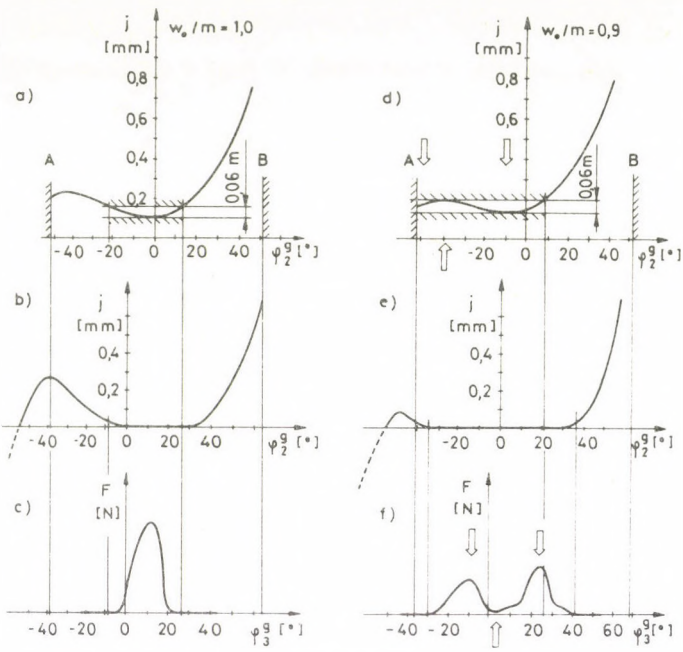

Fig. 6. Comparison of the calculated (Figs. 6.a, 6.d) and measured (Figs. 6.b, 6.e) values of the backlash as well as the tooth load measured (Figs. 6.c, 6.f)

increases. The tooth loading increases after meshing begins, then decreases (where the calculated backlash increased) which is followed by a new peak load. The characteristic points of the backlash calculated and the tooth load measured (which are marked with arrows) do not cover correctly the defectivenesses of the relationships [2] describing the flexible line.

Let us now see how the momentary transmission ratio of the pair of teeth meshing edge-like (2.1.2.2), (2.2.2.2) and the slip velocity (2.1.3.3), (2.2.3.2) in dependence of the deflection of the flexspline as compared with the principal deformation axis.

If the teeth are meshing at $j \leq 0.06m$, so simultaneously $z/2 \approx 14$ pairs of teeth are meshing within each engagement zone. In this case, the transmission ratio of the pair of teeth meshing edge-like changes between the limits $i_{2'3}^g = 1.033\,876 \ldots 1.043\,342$.

If the wave generator, in agreement with Figs. 3 and 5, rotates with an r.p.m. $n_g = 1500$ counter clockwise and $\omega_3 = 0$, $g \to 2$, the slip velocity varies between the values $v_{t2'3} = -182 \ldots 136$ mm s^{-1}.

5. Summary

The number of teeth of harmonic drives engaging simultaneously depends on the loading and construction parameters of the drive. Under the effect of the loading the elements (essentially the flexspline) will be flexibly deformed and displaced as

compared with their theoretical position defined, in consequence of which the teeth of the gear pair will be engaged beyond the theoretical bounds of the involute engagement doing that in an improper, edge-like way. It is assumed that where the backlash theoretically defined is smaller than the value determined experimentally depending on the construction parameters and loading of the drive, the teeth are meshing.

With the knowledge of the momentary value of the transmission ratio of the gear pair meshing the slip velocity may be determined in case of any arbitrary drive direction.

References

1. Péter, J.: Investigation of the Engagement of Harmonic Drives — Part I
2. Шувалов, С. А.—Волков, А. Д.: Деформация гибкого колеса волновой передачи двумя дисками. Известия ВУЗов. Машиностроение (1971) 10. 44/49.
3. Ступаков, А. А.: Выбор рациональных параметров зацепления волновой зубчатой передачи с учетом деформации ее звенев. Вест. маш. **54** (1974), 7. 17—21.
4. Волков, Д. П., Маргулис, М. В.—Крайнев, А. Ф.: Исследование редукторов с высокомоментной волновой передачей для поворотного механизма роторного экскаватора. В сб.: «Строительные и дорожные машины. Экскаваторы и стреловые краны». Вып. 2. Москва ЦНИИТЭ строймаш, 1972. 24/29.

BOOK REVIEWS

Á. BOSZNAY (Editor): *Bracketing of eigenfrequencies of continuous structures*, Akadémiai Kiadó, Budapest 1980

Organized by the Department of the Technical Sciences of the Hungarian Academy of Sciences, and technically arranged by the Structural Engineering Departmental Research Party, the 112th EUROMECH Colloquium was held in Mátrafüred from 21st to 23rd February 1979.

At the Conference of high scientific standard 59 participants assisted from 11 countries. The concluding proceedings of the Colloquium contain most of the verbal lectures or papers admitted subsequently, on 670 pages.

The papers deal with the following subjects associated with the group of processes designated by the title of the Colloquium:

1. the recent variants, developments and new applications of the Poincaré-Rayleigh-Ritz-method, the method of the intermediate operators, recent variants of Fichera's method of the orthogonal nonvariants or other procedures serving for the same purposes,
2. optimizations in connection with the eigenvalues,
3. procedures with the purpose to determine all of the eigenvalues in a given region.

The number of participants and, in general, the objective of the EUROMECH permitted to realize the programme of the Colloquium in a single section.

In the proceedings, the papers are arranged in the alphabetical order according to the authors' names. Their scientific value is outstanding; in the field of the given subject the recent results of the research investigations are reported. The high scientific level is warranted also by the names of the authors. The works of mathematicians, engineers of theoretical cast of mind and physicists, engineers skilled in measuring practice give starting points to further research work. All of these circumstances show that it was timely to assure such a forum for summarizing the results attained in the subject standing in the foreground of scientific interest having also practical significance, and to assure due development on this field.

Most of the 38 manuscripts produced by using the "camera ready" technique are of proper presentation, the figures and tables are easy to survey, clearly arranged. It is to be seen that the authors brought great care to bear upon the lucidity in formulating the mathematical expressions and here and there did not take due care of the forms of characters and indices. Nevertheless, all in all, it can be stated that the exterior appearance of the book equals its high internal professional value. The neat and careful work of the Publishing House of the Hungarian Academy of Sciences has to be especially emphasized.

Gy. Czeglédi

FRANZ, G. (Schriftleiter): *Beton-Kalender 1983.* Taschenbuch für Beton-, Stahlbeton- und Spannbetonbau sowie die verwandten Fächer. 72. Jahrgang, Verlag von Wilhelm Ernst u. Sohn, Berlin—München. Teil I: S. 872, Teil II: S. 1006.

Dieses Taschenbuch ist seit 72 Jahren ein wertvolles Handbuch des Beton- und Stahlbetonfaches, dessen Erscheinung von Jahr zu Jahr — selbst über den Grenzen der BRD — mit lebhaftem Interesse erwartet wird. In diesem mit jährlich veränderlichem Inhalt erscheinenden Werk sind die neuesten Ergebnisse der Wissenschaft und Praxis in kurzgefaßter aber leicht verständlicher Form aufzufinden, sowie jene Kenntnisse gesammelt, die zur zeitgemäßen, sicheren und wirtschaftlichen Ausführung der Beton- und Stahlbetonbauten nötig sind.

Im *1. Teil* des Werkes behandelt Prof. J. BONZEL die Eigenschaften, das Herstellen und Bearbeiten des Betons. D. BERTRAM berichtet

über Baustähle, Stahlerzeugnisse, Betonstahl und Betoneinlagen. Prof. K. MÖHLER befaßt sich mit Bauholz, Holzwerkstoffen und Schalungen. K. STIGLAT—H. WIPPEL behandeln Fragen von der Bemessung verschiedenartig belasteter und gestützter massiver Platten. Prof. E. GASSER gibt Anweisungen zur Bemessung der Stahlbetonteile für Biegung mit Längskraft, Schub und Torsion. Von Prof. K. KORDINA und Prof. U. QUAST wird die Bemessung der schlanken Bauteile eingehend besprochen, sowie auch Tragverhalten schlanker Druckglieder und verschiedene Knicksicherheitsfragen. Die Anwendungsbeispiele, Diagramme und Tafeln erleichtern die Anwendung der Vorgetragenen. Prof. H. KUPFER beschäftigt sich mit der Bemessung der Stahlbetonbauteile, sowie mit den Fragen der teilweisen Vorspannung. Hier wird unter anderen der Nachweis der Gebrauchsfähigkeit eingehend erörtert. Der I. Teil endet mit Angaben der Niederländischen Stahlbetonbestimmungen.

Im *II. Teil* des Werkes berichtet H. GOFFIN über die in der BRD gültigen Bestimmungen, Normen, Richtlinien, und Erlasse. Dieses Kapitel umfasst mehr als 500 Seiten und ist für den praktizierenden Fachmann unentbehrlich und äußerst nützlich. H. BECHER berichtet über verschiedene Fragen bezüglich der Massivbrücken. W. SCHLEEH beschäftigt sich mit Bauteilen (Scheiben), die sich in zweiachsigem Spannungszustand befinden. Ausser der klassischen analytischen Verfahren werden auch vereinfachte Rechnungsmethoden mitgeteilt, sowie Versuchsverfahren zur Bestimmung von Scheibenspannungen. Im letzten Kapitel berichtet Prof. W. SCHÜLE über Wärme- und Feuchteschutzfragen und Prof. K. GÖSELE erörtert verschiedene Probleme des Schallschutzes.

Es kann festgestellt werden, dass der neueste Jahrgang des Beton-Kalenders, den früheren Jahrgängen entsprechend, einen weiten Überblick vom neuesten Stand der Betonwissenschaft und der aktuellen Fragen dieses Faches bietet. Die Verfasser der einzelnen Kapitel sind anerkannte Fachmänner ihres Faches die unter der Leitung des weitbekannten erfahrenen Schriftleiters, Prof. Dr.-Ing. e.h. G. FRANZ alles mögliche geleistet haben damit dieses Taschenbuch mit seinem reichen Inhalt und wertvollen Wissensmaterial ein treues, verläßliches Hilfsmittel der Fachkreise bleibe.

P. Csonka

LIPKA, I.: *Theoretical Investigation of the Precision of Metal Cutting Machine-Tools (geometric and processing accuracies)*. Akadémiai Kiadó, Budapest, 1982. 286 pages.

The Author of the book, the contents of which is comprehensively expressed by the title, is a mathematician, Anyhow, it is very difficult to find a mathematician who does not spare any trouble in order to become absorbed in the details of the machine-building technology for trying to find models with the aid of the solution and evaluation of which renders help to the design engineer of the up-to-date machine-tools.

The Author of the book who earned the scientific degree of Doctor of Technical Sciences, became a few decades ago a research officer of the Institute of the Development of the Hungarian Machine-Tool works, where in possession of the knowledge in applied mathematics fostered the work of the developing, designing and researching engineers.

The Author and the publisher Akadémiai Kiadó acted right on summarizing and completing on uniform bases the numerous papers (the Author refers to 23 papers of his own) and publishing them in form of a book of general interest.

The book is divided into three parts. Part one and two try to find the theoretical relationships between the accuracy of the processed work-piece and the factors influencing the precision of the work of the machine-tools to the technologies using single-edged and multi-edged cutting tools respectively. The third part (i.e., the annexe) presents the mathematical methods applied.

In investigating the accuracy of shape of the circular-cylinder surfaces processed with a single-edged cutting tool, the cylindrical inaccuracy is analysed in case of processing by tool feed, i.e., by work-piece feed. The cylindrical or positioning inaccuracies occurring in fine boring are separately treated. Part one is concluded by the failure analysis of the jig-borer, further by the circular inaccuracy of shape of the circular-cylinder surfaces processed with single-edged cutting tool.

In the geometrical accuracy of the circular-cylinder surfaces processed with multi-edged cutting tool, the theory of the envelopes of the set of surfaces and curves plays a decisive part. Therefore, the book investigates in detail the cross-sectional curves of the work pieces, the envelope of the set of circles described by the abrasive disc, their singularities, the characteristics, cylindrical inaccuracy of the profiles

of the work pieces ground with grinding wheels of large diameter. This part is ended by the analysis of the accuracy of the centreless grinder, the optical shape grinder, the shape and position and that of the drilling-milling machine of horizontal and vertical spindle.

From the annex, the theory of the envelope of the sets of curves and the surfaces is to be mentioned in particular (as well as the definition, and the deduction of the set of the parametric equations of the envelope).

The simplified mathematical treatment and the 70 linear explanatory figures help to easily read and understand the book.

Z. Terplán

BOLOTIN, V. V.: *Wahrscheinlichkeitsmethoden zur Berechnung von Konstruktionen (Methods of the Theory of Probability in the Calculation of Constructions)* 567 pages, 272 figures, 5 tables

The book published in 1965 and 1971 has been translated from Russian by a collective consisting of German experts, under the leadership of the scientific editor Albert Duda. The work is, as a matter of fact, an enlarged re-edition of the handbook written in Russian also by Bolodin: "Statistical Methods in the Mechanics of Construction" published in 1961.

The book consists of three parts, from which the first one gives a recapitulation on the theory of probability; in particular, the first head chapter deals with the elements of the theory of the calculation of probabilities, while the second one with those of the stochastic processes. Both head chapters treat of the parts of the theoretical mathematics which are necessary in the dimensioning of constructions as well as in their static and dynamic examination. The first head chapter consists of nineteen, and the second one of eleven chapters.

Part two discusses the statistical methods of the dynamics of constructions. Chapter three is titled: "Statistical Methods and Problems". The head chapter comprises 12 chapters. Head chapter 4 which is composed of nine chapters, treats by making use of the statements of the preceding head chapter of the dimensioning and the stability problems of beams on elastic foundation. Head chapter five describes the dynamic dimensioning of structures, as a matter of course, by utilizing methods of the theory of probability. The head chapter in question consisting of thirteen chapters details the application of stochastic processes and systems to the dynamic dimensioning.

The third main part of the book deals with the reliability of constructions. Head chapter six bears the superscription "Theory of the Reliability and Durability of Bearing Structures". The head chapter consisting of eighteen chapters deals not only with bearing constructions but also with the problems of oscillating systems. The subject of head chapter seven is the statistical ultimate design-theory. This head chapter containing eleven chapters uses for the description of strength the second lower extremes (Weibull's) distribution. It also treats of the theoretical fundaments of the accumulation of damages. Head chapter eight discusses the theoretical bases of the dimensioning of bearing structures according to the prescriptions on the subject. The head chapter consisting of six chapters details the different formulations of the problem of safety.

The work may be utilized as a very useful handbook by the civil engineers, architects and mechanical engineers, and is an indispensable aid for engineers being engaged in structural dimensioning.

E. Misléth

MAJOR, S.: *Dynamics in Civil Engineering*, Vol. I: 320 pp., Vol. II: 302 pp., Vol. III: 291 pp., Vol. IV: 306 pp. Akadémiai Kiadó, Budapest 1980.

This book of four volumes in English is a natural successor of the first edition in Hungarian, and the second one in German. The recent, abrupt development imposed to spend as much as four volumes on the most crucial problems. This work assists both theoreticians and practicing engineers by offering a wealth of numerical examples and references. Chapter subjects are the following:

Volume I focussed on theory reflects the idea of its Author to present practically proven, useful theoretical results in addition to latest test results. Completing data in previous editions by latest results, a detailed discussion is spent on the theoretical deduction and methods of damping. Problems of shock effects and of systems with several, up to six, degrees of freedom are investigated. In classifying machine foundations, kinds of spring-supported machine foundations and great many general cases and conditions of designing machine foundations are presented. Problems of fatigue of building materials and of determining moduli of elasticity are scrutinized. The data set compiled in tables and diagrams is of utmost importance in design, permitting researchers to take the optimum from among alternatives of dynamic force effects on soils.

The scope of *Volume II* relies on theoretical and practical fundamentals in Volume I. It devotes a

uniform discussion to technology and foundation problems of machines of impact action, low r.p.m., or of special destination, including foundations for machine tools set directly on the floor. A detailed examination is spent on vibration damping problems, including spring-damping interaction. A detailed analysis is given of steel and rubber springs and of their comparison, advantages and drawbacks. All these are illustrated on recent numerical examples. Thereafter mechanical methods aiming at reducing or avoiding vibrations inside the machine itself are discussed, including problems of the critical number of revolutions, of machine balancing, antivibrators and amortizers. At last, elastic couplings are presented, with their latest, most up-to-date types, omitting outdated ones. Essential modifications have been suggested for the design of hammer foundations.

Volume III has been concerned with foundations for high r.p.m. machines, involving technology problems of these latter. Theoretical matter in this volume relies on fundamentals in Volume I. Chapter 1 refers to classification of machines and their arrangement, points out the trend of development, ways of load assumption, data for material consumption and for economically favourable arrangement outdoors or in part outdoors are being considered, in particular, for thermal and nuclear power stations. Chapter 2 imparts theoretical fundamentals together with different computation methods. Resonance, amplitude and combined methods are discussed according to a new system matching practice of the recent decade.

First part of *Volume IV* has been concerned with overall dynamic problems of constructions and industrial structures, including wind effects, seismic effects and explosions. The second part is devoted to dynamic problems of hydraulic engineering structures and objects, including dynamic effects on dams, pressure oscillations in pipelines, dynamic effects in hydraulic power stations and pumping stations. Also vibration problems of floating structures and pumping stations have been considered, including ship vibrations, extending to elastic foundations for ship-borne machines. Third part of the volume has been concerned with dynamic problems of bridges, classifies them according to span from the aspect of dynamics, describes theoretical and field vibration measurements on bridges, including determination of the dynamic factor in course of internationally organized experiments. Particular consideration is given to dynamic problems of large-span suspended bridges and short-span, mainly pipe aqueducts, relying on theoretical considerations and test results.

This new book of four volumes by Prof. Major is a significant item in the Hungarian and international special literature, counting, just as hitherto, on the acknowledgement of English-speaking specialists, in particular, by treating subjects — skyscrapers, earthquakes, seaside power stations — extending beyond Hungarian practice. Both English and Russian publications are referred to, compared and evaluated, and up-to-date computer facilities are widely taken into account.

O. Halász

NEWS

THE INDIAN CONCRETE INSTITUTE

We have been asked for anouncing that a new Scientific Centre — The Indian Concrete Institute — has been formed. Its headquaters are at the Structural Engineering Research Centre, CSIR Campus, TTTI — Pharamani PO, Madras 600113. President of the Institute is Ramaiah, M. (Structural Engineering Research Centre, CSIR Compus, Madras-600113, Vice president is Chakravarti S. K. (Tata Iron and Steel Co. Limited, Jamshedpur — 831001).

The membership is open to all those, who are interested in the development of concrete construction technology.

ERRATA

In Volume 93 of this periodical on page 93 in P. Csonka's paper: "Elliptic Plate with Clamped Edge" the well-known formulas of the moments were misprinted. The correct formulas are:

$$m_x = -K\left(\frac{\partial w^2}{\partial x^2} + \mu \frac{\partial w^2}{\partial y^2}\right),$$

$$m_{xy} = K(1-\mu)\frac{\partial^2 w}{\partial x\, \partial y},$$

$$m_y = -K\left(\frac{\partial w^2}{\partial y^2} + \mu \frac{\partial w^2}{\partial x^2}\right).$$

PRINTED IN HUNGARY
Akadémiai Kiadó és Nyomda, Budapest

NOTICE TO CONTRIBUTORS

Papers in English * are accepted to the condition that they have not been previously published or accepted for publication.

Manuscripts in two copies (the original type-written copy plus a clear duplicate one) complete with figures, tables, and references should be sent to the Editor.

Acta Technica
Münnich F. u. 7. I. 111A
Budapest, Hungary
H-1051

Although every effort will be made to guard against loss, it is advised that authors retain copies of all material which they submit. The editorial board reserves the right to make editorial changes.

Manuscripts should be typed double-spaced on one side of good quality paper with proper margins and bear the title of the paper and the name(s) of the author(s). The full postal address(es) of the author(s) should be given in a footnote on the first page. An abstract of 50 to 100 words should precede the text of the paper. The paper should not exceed 25 pages including tables and references. The approximate location of the tables and figures should be indicated on the margin. An additional copy of the abstract is needed. Russian words and names should be transliterated into English.

References. Only papers closely related to the author's work should be referred to. The citations should include the name of the author and/or the reference number in brackets. A list of numbered references should follow the end of the manuscript.

References to periodicals should mention: (1) name(s) and initials of the author(s); (2) title of the paper; (3) name of the periodical; (4) volume; (5) year of publication in parentheses; (6) number of the first page. Thus: 5. Winokur, A., Gluck, J.: Ultimate strength analysis of coupled shear walls. American Concrete Institute Journal 65 (1968), 1029.

References to books should include: (1) author(s)' name; (2) title; (3) publisher; (4) place and year of publication. Thus: Timoshenko, S., Gere, J.: Theory of Elastic Stability. McGraw-Hill Company, New York, Toronto, London 1961.

Illustrations should be selected carefully and only up to the necessary quantity. Black-and-white photographs should be in the form of glossy prints. The author's name and the title of the paper together with the serial number of the figure should be written on the back of each print. Legends should be brief and attached on a separate sheet. Tables, each bearing a title, should be self-explanatory and numbered consecutively.

Authors will receive proofs which must be sent back by return mail.

Authors are entitled to 50 reprints free of charge.

* Hungarian authors should submit their paper also in Hungarian.

Periodicals of the Hungarian Academy of Sciences are obtainable at the following addresses:

AUSTRALIA
C.B.D. LIBRARY AND SUBSCRIPTION SERVICE
Box 4886, G.P.O., *Sydney N.S.W. 2001*
COSMOS BOOKSHOP, 145 Ackland Street
St. Kilda (Melbourne), Victoria 3182

AUSTRIA
GLOBUS, Höchstädtplatz 3, *1206 Wien XX*

BELGIUM
OFFICE INTERNATIONAL DE LIBRAIRIE
30 Avenue Marnix, *1050 Bruxelles*
LIBRAIRIE DU MONDE ENTIER
162 rue du Midi, *1000 Bruxelles*

BULGARIA
HEMUS, Bulvar Ruszki 6, *Sofia*

CANADA
PANNONIA BOOKS, P.O. Box 1017
Postal Station "B", *Toronto, Ontario M5T 2T8*

CHINA
CNPICOR, Periodical Department, P.O. Box 50
Peking

CZECHOSLOVAKIA
MAD'ARSKÁ KULTURA, Národní třida 22
115 66 Praha
PNS DOVOZ TISKU, Vinohradská 46, *Praha 2*
PNS DOVOZ TLAČE, *Bratislava 2*

DENMARK
EJNAR MUNKSGAARD, Norregade 6
1165 Copenhagen K

FEDERAL REPUBLIC OF GERMANY
KUNST UND WISSEN ERICH BIEBER
Postfach 46, *7000 Stuttgart 1*

FINLAND
AKATEEMINEN KIRJAKAUPPA, P.O. Box 128
SF-00101 Helsinki 10

FRANCE
DAWSON-FRANCE S. A., B. P. 40, *91121 Palaiseau*
EUROPÉRIODIQUES S. A., 31 Avenue de Versailles, *78170 La Celle St. Cloud*
OFFICE INTERNATIONAL DE DOCUMENTATION ET LIBRAIRIE, 48 rue Gay-Lussac
75240 Paris Cedex 05

GERMAN DEMOCRATIC REPUBLIC
HAUS DER UNGARISCHEN KULTUR
Karl Liebknecht-Straße 9, *DDR-102 Berlin*
DEUTSCHE POST ZEITUNGSVERTRIEBSAMT
Sraße der Pariser Kommüne 3–4, *DDR-104 Berlin*

GREAT BRITAIN
BLACKWELL'S PERIODICALS DIVISION
Hythe Bridge Street, *Oxford OX1 2ET*
BUMPUS, HALDANE AND MAXWELL LTD.
Cowper Works, *Olney, Bucks MK46 4BN*
COLLET'S HOLDINGS LTD., Denington Estate
Wellingborough, Northants NN8 2QT
WM. DAWSON AND SONS LTD., Cannon House
Folkstone, Kent CT19 5EE
H. K. LEWIS AND CO., 136 Gower Street
London WC1E 6BS

GREECE
KOSTARAKIS BROTHERS INTERNATIONAL BOOKSELLERS, 2 Hippokratous Street, *Athens-143*

HOLLAND
MEULENHOFF-BRUNA B.V., Beulingstraat 2,
Amsterdam
MARTINUS NIJHOFF B.V.
Lange Voorhout 9–11, *Den Haag*

SWETS SUBSCRIPTION SERVICE
347b Heereweg, *Lisse*

INDIA
ALLIED PUBLISHING PRIVATE LTD., 13/14
Asaf Ali Road, *New Delhi 110001*
150 B-6 Mount Road, *Madras 600002*
INTERNATIONAL BOOK HOUSE PVT. LTD.
Madame Cama Road, *Bombay 400039*
THE STATE TRADING CORPORATION OF INDIA LTD., Books Import Division, Chandralok
36 Janpath, *New Delhi 110001*

ITALY
INTERSCIENTIA, Via Mazzé 28, *10149 Torino*
LIBRERIA COMMISSIONARIA SANSONI, Via Lamarmora 45, *50121 Firenze*
SANTO VANASIA, Via M. Macchi 58
20124 Milano
D. E. A., Via Lima 28, *00198 Roma*

JAPAN
KINOKUNIYA BOOK-STORE CO. LTD.
17-7 Shinjuku 3 chome, Shinjuku-ku, *Tokyo 160-91*
MARUZEN COMPANY LTD., Book Department,
P.O. Box 5050 Tokyo International, *Tokyo 100-31*
NAUKA LTD. IMPORT DEPARTMENT
2-30-19 Minami Ikebukuro, Toshima-ku, *Tokyo 171*

KOREA
CHULPANMUL, *Phenjan*

NORWAY
TANUM-TIDSKRIFT-SENTRALEN A.S., Karl Johansgatan 41–43, *1000 Oslo*

POLAND
WĘGIERSKI INSTYTUT KULTURY, Marszałkowska 80, *00-517 Warszawa*
CKP I W, ul. Towarowa 28, *00-958 Warszawa*

ROUMANIA
D. E. P., *Bucureşti*
ILEXIM, Calea Grivitei 64–66, *Bucureşti*

SOVIET UNION
SOJUZPECHAT – IMPORT, *Moscow*
and the post offices in each town
MEZHDUNARODNAYA KNIGA, *Moscow G-200*

SPAIN
DIAZ DE SANTOS, Lagasca 95, *Madrid 6*

SWEDEN
ALMQVIST AND WIKSELL, Gamla Brogatan 26
101 20 Stockholm
GUMPERTS UNIVERSITETSBOKHANDEL AB
Box 346, *401 25 Göteborg 1*

SWITZERLAND
KARGER LIBRI AG, Petersgraben 31, *4011 Basel*

USA
EBSCO SUBSCRIPTION SERVICES
P.O. Box 1943, *Birmingham, Alabama 35201*
F. W. FAXON COMPANY, INC.
15 Southwest Park, *Westwood Mass. 02090*
THE MOORE-COTTRELL SUBSCRIPTION AGENCIES, *North Cohocton, N. Y. 14868*
READ-MORE PUBLICATIONS, INC.
140 Cedar Street, *New York, N. Y. 10006*
STECHERT-MACMILLAN, INC.
7250 Westfield Avenue, *Pennsauken N. J. 08110*

YUGOSLAVIA
JUGOSLOVENSKA KNJIGA, Terazije 27, *Beograd*
FORUM, Vojvode Mišića 1, *21000 Novi Sad*

HU ISSN 0001—7035

Index: 26.025